CONFINEMENT OF RECTANGULAR REINFORCED CONCRETE COLUMN WITH NON-SEISMIC DETAILING

CHUNG YUK MING WILSON

Ph.D

The Hong Kong

Polytechnic University

2010

THE HONG KONG POLYTECHIC UNIVERSITY

DEPARTMENT OF CIVIL & STRUCTURAL ENGINEERING

CONFINEMENT OF RECTANGULAR REINFORCED CONCRETE COLUMN WITH NON-SEISMIC DETAILING

CHUNG YUK MING WILSON

A THESIS SUBMITTED IN PARTIAL FULFILMENT OF THE REQUIREMENTS

FOR THE DEGREE OF DOCTOR OF PHILSOPHY

August 2009

Certificate of Originality

I hereby declare that this thesis is my own work and that, to the best of my knowledge and belief, it reproduces no material previously published or written, nor material that has been accepted for the award of any other degree or diploma, except where due acknowledgement has been made in the text

____________________(Signed)

Chung Yuk Ming Wilson (Name of student)

Abstract

In Hong Kong, reinforced concrete structures are traditionally designed without seismic provisions. In particular, one commonly used local detailing for columns allows large spacing of transverse reinforcements, use of 90º hooks and transverse reinforcements not necessary tied to the main reinforcements. By end of the last century, Hong Kong has been classified as a region with moderate seismic hazard. There is in need of assessing structural behavior of columns with local detailing when subjected to cyclic loading. Reinforced concrete columns are normally designed in a ductile manner to resist seismic load. It is necessary to assess the confinement action provided by transverse reinforcements based on local detailing. Objectives of this study are to assess the seismic resistance of and to develop mathematical models for a class of columns with local detailing. In order to achieve the above, (a) confinement action of transverse reinforcements under axial load; and (b) hysteresis behavior of columns with local detailing were examined experimentally.

Confinement of columns with local detailing was assessed by conducting axial loading tests on 12 ¼-scaled specimens. Detailing of transverse reinforcements consisted of reinforcement hoops with 90º end hooks, long crossties and short crossties. This is a common type of local detailing for columns. The test results indicated that columns with local detailing have limited confinement action with up to 80% reduction in load carrying capacity. Stress-strain behavior of confined concrete with local detailing is developed by performing statistical analysis on the test results. In particular, ascending branch of stress-strain relationship of confined concrete is similar to Propovics' model while descending branch assumes a linear relationship similar to Hoshikuma's model.

Hysteretic response of columns with local detailing was investigated by conducting cyclic-loading tests on 12 0.4-scaled specimens. Test parameters include volumetric transverse reinforcement ratio, axial load ratio and type of details. Specimens with high and low volumetric transverse reinforcement ratio failed distinctively, namely by flexural-shear mechanism and shear failure respectively. A hysteresis model is proposed based on the test results to predict the cyclic behavior of columns with local detailing. A shear damage model related to the lateral displacement of column is developed. It is recommended to limit the spacing of transverse reinforcements to 160mm and to apply the local detail when axial load ratio is very small and ductility demand is less than 4.

Publications arising from the thesis

Chung W.Y.M. and Lam E.S.S. (2004) “Confinement of Columns with Non-seismic Detailing”, Proceedings of 2004 Annual Meeting Networking of Youth Earthquake Engineering Researchers and Professionals, Hanolulu, Hawaii.

Chung W.Y.M., Lam E.S.S., Wu B. and Wong. Y.L. (2006), “Stress-strain Behavior of Concrete with Non-seismic Detailing”, Proceedings of the 2nd fib Congress, June 5-8, 2006 Naples, Italy, 13.44, (CD-Rom).

Chung W.Y.M., Lam E.S.S. and Wong Y.L. (2006) “Confinement action of Reinforced Concrete Column with Non-seismic Detailing”, Proceedings of 4th International Conference on Earthquake Engineering, Taipei, Taiwan, October 12-13,2006, No.304 (CD-Rom).

Chung W.Y.M., Lam E.S.S., Wu B. and Wong Y.L. (2007) “Hysteretic Behavior of Rectangular Reinforced Concrete Columns with Non-seismic detailing”, Proceedings of Structural Congress 2007, ASCE, Long Beach, May 17-19 (CD-Rom)

Chung W.Y.M., Lam E.S.S., Wu B. and Wong Y.L. (2007) “Cyclic Behavior of Rectangular Reinforced Concrete Columns with Non-seismic Detailing”, 2007 Ancer Meeting, Paper No. 50, CD-Rom

Chung W.Y.M., Lam S.S.E., Wu B., Wong Y.L. and Ho I.F.Y. (2009), “Cyclic Response of Rectangular RC Columns with Non-Seismic Detailing”, Proccedings of the ANCER Conference, Illinois, USA

Chung T.S.K., Lam S.S.E., B. Wu, W.L. Xu and Chung W.Y.M. (2009), “Experimental and Numerical Verification of Hydraulic Displacement Amplification Damping System”, accepted for publication in Structural Engineering and Mechanics

Lam S.S.E., Chan T.H.T., Wong T.C.S., Wong C.Y.K., Mok K.W.K., Chung T.S.K. and Chung W.Y.M. (2008), Vibrations induced by household activities on structural members in high-rise buildings, in the process of seeking approval from client – CEDD, to be submitted to Journal of Infrastructure Systems

Chung T.S.K., Lam S.S.E., Wu B., Xu W.L. and Chung W.Y.M. (2008), "Influence of Hydraulic Displacement Amplification Damping System on Cyclic Response of RC Beam-column Joints", submitted to Journal of Structural Engineering, ASCE

Lam E.S.S., Wu B., Liu Q. and Chung W.Y.M. (2008), Stress-Strain Relationship for High Strength Concrete with Polypropylene Fiber at Elevated Temperatures, submitted to Engineering Structures

Wu B., Lam E.S.S., Liu Q. and Chung W.Y.M. (2008), Creep behaviour of High Strength Concrete with Polypropylene Fiber at Elevated Temperatures, submitted to ACI Material Journal

Chung W.Y.M., Lam E.S.S., Wu B. and Wong Y.L. (2008), "Stress-strain Relationship of Confined Concrete with Non-Seismic Detailing", submitted to Structural Engineering and Mechanics

Chung W.Y.M., Lam S.S.E., Wu B., Wong Y.L. and Ho I.F.Y. (2009), "Cyclic Response of Rectangular RC Columns with Non-Seismic Detailing", submitted to ACI Structural Journal

Acknowledgement

The authors would like to thank for the sincere support from the supervisors Dr Eddie S.S. Lam, Dr Y. L. Wong and Prof B. Wu from South China University of Technology, China. The report is based on the efforts of the technical staff in particular, Mr. M.C. Ng, Mr. K.H. Wong, Mr. W.C. Chan and Mr. W.K. Tung from the Department of Civil and Structural Engineering of the Hong Kong Polytechnic University. Their invaluable contribution is gratefully acknowledged.

I would like to thank my friends for their contribution on my study, especially, Mr. C.S. Chan, Dr. S.K. Chung and Dr. H.C. Ho who gave a sincere support in this study.

I would also like to thank my family and my girl friend Ms. Esther Lee in supporting me for the study.

Content

List of Figure

List of Table

Notation

A_{cc}	Area of confined concrete
A_g	Gross sectional area of concrete
A_o	Strain energy in the reinforced concrete member subjected to monotonic loading
A_n	Strain energy of reinforced concrete column reminding after n^{th} cycle of lateral loading
A_{shy}	Transverse reinforcement area parallel to y- direction
A_{st}	Area of main reinforcement
A_{uc}	Area of unconfined concrete
A_{sv}	Area of transverse reinforcement
$A_{sv,c}$	Area of transverse reinforcements required by ACI-318
$A_{sv,w}$	Area of transverse reinforcement proposed by Wehbe (1996)
C_{fy}	Correction factor on yield strength of main reinforcement
C_s	Correction factor on slenderness ratio
C_{SC}	Correction factor on shear capacity
C_{type}	Coefficient for configurations of transverse reinforcements in damage model
D	Damage index
D_{ana}	Damage index calculated from modified model
D_d	Displacement part of damage index
D_e	Energy dissipation part of damage index

D_{exp}	Damage index identified during experiment
D_{KJ}	Damage index proposed by Kunnath and Jenne (1994)
D_n	Damage at the n^{th}-times cycle of reinforced concrete column in cyclic loading test
D_p	Damage index proposed by Khashee (2005)
D_{PARK}	Damage index calculated from Park and Ang's model
$DI_{compressive}$	Damage index in compressive state
$DI_{tensile}$	Damage index in tensile stage
E	Hysteretic energy
E_{con}	Young's Modulus of confined concrete
E_{des}	Modulus of descending branch
E_{sec}	Secant Modulus of confined concrete
E_{usec}	Secant Modulus of unconfined concrete
E_s	Modulus of Elasticity of transverse reinforcement
EG_{cc}	Strain energy of confined concrete at peak strain
EG_{85}	Strain energy of confined concrete at post peak strain at 85% peak strength
F_y	Lateral yield load
G_{eq}	Shear modulus of concrete
I	Second moment of area
I_{e50}	Effective confinement index of ultimate strain
I_e'	Effective confinement index at peak strength
I_g	Gross sectional area of moment
K_d	Three times diameter of main reinforcement
K_{conf}	Confinement strength index

$K_{d,bou}$	Strain increment ratio proposed by Bousalem and Chikh (2007)
$K_{des,Shah}$	Descending branch ratio proposed by Shah (1985)
K_e	Effective confinement index
$K_{e,mo}$	Elastic stiffness in moment curvature relationship
$K_{re,mo}$	Reloading stiffness with pinching region
$K_{re,mo}^{+}$	Reloading stiffness with pinching in positive direction
$K_{re,pin,mo}$	Reloading stiffness without pinching
K_s	Flexural stiffness
$K_{s,bou}$	Strength increment ratio proposed by Bousalem and Chikh (2007)
$K_{s,\ Park}$	Strength increment ratio proposed by Park (1982)
$K_{s,Saat}$	Strength increment ratio proposed by Saatcioglu and Razvi (1992)
K_{sec}	Secant stiffness at maximum excursion in cyclic loading
$K_{sh,mo}$	Strain hardening stiffness in moment curvature relationship
$E_{soft,bou}$	Softening energy ratio proposed by Bousalem and Chikh (2007)
$K_{str\ SKEIKH}$	Strength increment of confined concrete from Seikh (1982)
K_{un}	Unloading lateral stiffness
$K_{un,mo}$	Unloading stiffness in moment curvature relationship
$K_{v,45}$	Shear stiffness
L	Height of reinforced concrete specimen
$L_{9,7,3,1}$	Width between point 9 and point 3
L_p	Plastic hinge length
M	Moment
M_{max}	Maximum moment throughout the loading history
M_f	Failure moment

$M_{f,i}$	Failure moment at curvature i
M_i	Moment at curvature i
M_m	Moment at maximum curvature excursion
$M_{m,pin}$	Moment at maximum curvature excursion point without pinching
M_n^+	Moment with no pinching effect in positive direction
M_o^+	Projected moment from M_m^+ to the strain hardening line in positive direction
M_o^-	Projected moment from M_m^- to the strain hardening line in negative direction
M_{pin}^+	Moment after pinching
M_{ratio}	Moment ratio
M_y	Moment corresponding to yielding of main reinforcement
M'_m	Reduced moment during the cycle
N_{fi}	Number of complete cycle causing failure at a particular drift ratio i
N_{2fc}	Number of complete cycles to failure for concrete
N_{2fr}	Number of complete cycles to failure for reinforcing bars
P	Compressive force of reinforced concrete column
P_o	Axial load carrying out capacity of reinforced concrete column
P_{occ}	Axial load supported by confined concrete section
Type	Type of configuration of transverse reinforcement
V	Shear force
V_f	Flexural strength capacity
V_s	Shear strength capacity
V_y	Shear force in yield stage

a_{EY}	Coefficient of damage proposed by Erduran and Yakut (2007)
a_{tf}	Reduction factor of concrete area
b_c	Length of reinforcement hoops measured from centerline
b_{EY}	Coefficient of damage proposed by Erduran and Yakut (2007)
c	Distance between neutral axis and external compressive side of concrete section
c_{EY}	Coefficient of damage proposed by Erduran and Yakut (2007)
c_i	Clear spacing of legs in transverse reinforcement
d	Effective depth of concrete section
d_{31}	Distance between point 1 and point 3
d_s	Depth of specimen
f_2	Active hydrostatic pressure
$f_{b,e}$	Bond strength of reinforcements in elastic stage
$f_{b,p}$	Bond strength of reinforcements in plastic stage
f_{by}	Bond strength of reinforcements in yield stage
f_c	Unconfined concrete strength
$f_{c,n}$	Reference unconfined concrete strength
f_{cco}	Confined concrete stress
f_{cc}	Confined concrete strength
f_{cu}	Cube strength of concrete
f_{cult}	Strength corresponding to ultimate strain
f_{cy}	Concrete yield strength
f_l	Average confinement stress provided by transverse reinforcement
f_{le}	Effective confinement stress

f_s	Main reinforcement stress
$f_{s,n}$	Reference yield strength of main reinforcement
f_t	Transverse reinforcement stress at peak strength of confined concrete
f_{t1}	Lateral stress under tri-axial state
f_{t2}	Vertical stress under tri-axial state
$f_{u,2}$	Vertical stress under uni-axial state
f_{uc}	Unconfined concrete stress
f_y	Yield strength of main reinforcement
f_{yt}	Yield strength of transverse reinforcement
h	Width of reinforced concrete column
h_c	Width of reinforcement hoops measured from centerline
h_o	Width of reinforcement hoop measured from outermost dimension
h_{lu}	Height of lugs on main reinforcement
k_1	Effective index for conversion to circular transverse reinforcement
k_2	Effective index on confinement action of rectangular transverse reinforcement
k_{1P}	Effective confinement index 1 proposed by (Paultre 2003)
k_{2P}	Effective confinement index 2 proposed by (Paultre 2003)
$k_{i,j}^{+}$	Stiffness of a specimen cycled to failure to curvature i
$k_{i,ave}^{+}$	Average stiffness of a specimen cycled to failure at curvature i
l	Length of transverse reinforcements interval
l_{bp}	Anchorage length in plastic stage
l_{by}	Anchorage length in yield condition
l_{bc}	Length of pull out zone

l_d	Development length of main reinforcements
l_e	Bond length of main reinforcements in elastic stage
l_u	Ultimate length of transverse reinforcements after testing
n	Axial load capacity ratio
n_{hfi}	Number of half completed cycle at a particular drift ratio in the cyclic loading
n_i	Number of clear space in transverse reinforcements
n_i^+	Number of cycle reaching curvature in positive loading direction
n_i^-	Number of cycle reaching curvature in negative loading direction
nos	Number of cycle
r	Modulus of elasticity ratio of confined concrete
r_y	Radius of gyration in weak axis
r_{unstr}	Ratio of unconfined concrete strength
s	Spacing of transverse reinforcements
s'	Clear spacing of transverse reinforcements
s_l	Horizontal spacing of the laterally restrained main reinforcements
s_k	Strength incremental factor between confined concrete (f_{cc}) and unconfined concrete (f_{co})
s_{lu}	Spacing of lugs on main reinforcements
u_m	Displacement at maximum excursion point
u_t	Bond slip of main reinforcements
u_y	Yield displacement
w_i^+	Weighting coefficient on damage at curvature i in positive direction
w_i^-	Weighting coefficient on damage at curvature i in negative direction

x	Ratio of confined concrete strain to peak strain of confined concrete
z	Distance measured from tip of reinforced concrete column to the calculated point
ΔM	Differential moment between strain hardening moment and M_f
Δ_{flex}	Flexural deflection
Δ_{fe}	Flexural deflection in elastic stage
Δ_{fy}	Yield flexural deflection
Δ_m	Displacement at maximum excursion point during cyclic load
Δ_{max}	Deflection at peak lateral load
Δ_p	Plastic deflection in each cycle
Δ_r	Reloading target displacement
Δ_{r1}	Deformation of previous pointed peak
Δ_{r2}	Increased deformation of pointed peak
Δ_p	Plastic deflection
Δ_{shear}	Shear deflection
$\Delta_{shear,y}$	Shear deflection in yield stage
Δ_{slip}	Bond slip deflection due to bond slip of main reinforcements
Δ	Deflection of speicemen
Δ_u	Ultimate displacement under later load
Δ_y	Yield displacement under lateral load
α	Unloading stiffness ratio
α_{area}	Effective confinement area ratio
α_{conf}	Effective ratio for configurations of transverse reinforcements
α_{stress}	Peak strength index for different configuration ratio

α_{Dd}	Coefficient related to the displacement
α_p	Parameter of drift ratio at maximum excursion point
α_v	Stiffness degradation relating to shear span depth ratio
β_{Kim}	Material constant, equal to 0.0588
β_{Park}	Degradation parameter defined by Park and Ang
β_p	Parameter of sum of plastic drift ratio
β_{re}	Reloading displacement factor
β_{strain}	Index ratio of strain of confined concrete
β_{De}	Coefficient related to energy dissipation
γ_{ult}	Index of ultimate strain of confined concrete with different configuration
δ_3	Vertical displacement measured from transducer
ε_{31}	Strain located at the mid-point of transducer 3 and 1
ε_{50cc}	Confined concrete strain corresponding to 50% of confined concrete strength
ε_{50uc}	Unconfined concrete strain corresponding to 50% of confined concrete strength
ε_{ap}	Average plastic strain on both minimum and maximum strain by number of cycle
ε_c	Confined concrete strain
ε_{cs}	Compressive strain in the analysis
ε_{cu}	Ultimate confined concrete strain
ε_{cy}	Yield strain of confined concrete
ε_{cc}	Peak strain of confined concrete
$\varepsilon_{cc,80}$	Post peak strain at 80% of peak strength of confined concrete

ε_{ho}	Reinforcement hoop strain
$\varepsilon_{l\ cro}$	Long crosstie strain
ε_{min}	Minimum strain by number of cycle
ε_{max}	Maximum strain by number of cycle
ε_{s}	Main reinforcement strain
ε_{s1}	First peak strain of confined concrete
ε_{s2}	Second peak strain of confined concrete
ε_{s85}	Post peak strain corresponding to 85% peak strength of confined concrete
$\varepsilon_{s\ cro}$	Short crosstie strain
ε_{sm}	Ultimate strain of transverse reinforcements
ε_{ts}	Tensile strain at the analysis
ε_{tu}	Ultimate tensile strain of reinforcements
ε_{uc}	Peak strain of unconfined concrete
ε_{uuc}	Ultimate strain of unconfined concrete
ε_{lult}	Ultimate elongation of reinforcements
ε_{uc85}	Post peak strain at 85% strength level of unconfined concrete
ε_{y}	Main reinforcement yield strain
κ	Ratio of unconfined concrete strength to transverse reinforcement stress
λ	Shear span depth ratio
μ_{m}	Displacement ductility at maximum excursion point
μ_{u}	Ultimate displacement ductility
μ_{φ}	Curvature ductility of reinforced concrete column
μ_{Δ}	Displacement ductility of reinforced concrete column
ν	Poisson's ratio

ϕ_{main}	Diameter of main reinforcements
$\phi_{transverse}$	Diameter of transverse reinforcements
θ_c	Angle of tangential line of confinement action to transverse reinforcements
θ_s	Angle of diagonal crossties to reinforcement hoop
θ_{slip}	Slippage rotation at the base of reinforced concrete column
φ	Curvature of reinforced concrete column along height
φ_f	Failure curvature under monotonic loading
φ_i^+	Curvature of column at the i^{th} positive direction
φ_{i-1}^+	Curvature of column at the $i\text{-}1^{th}$ positive direction
$\varphi_{m,pin}$	Maximum curvature excursion point without considering pinching effect
φ_m^+	Maximum curvature excursion point in positive direction
φ_n^+	Intersection point between the elastic stiffness and reloading stiffness with no pinching
$\varphi_{n,s}$	Intersection point between the elastic stiffness and reloading stiffness without pinching but considered shear effect
φ_o^+	curvature corresponding to M_o^+
φ_o^-	curvature corresponding to M_o^-
φ_{pin}^+	Curvature after pinching
φ_r^+	Reloading curvature in positive loading including strain hardening coefficient
φ_r^-	Reloading curvature in negative loading including strain hardening coefficient
φ_y	Yield curvature
φ_u	Ultimate curvature

$\varphi_{9,7,3,1}$	Curvature of transducers between points 9,7 and 3,1
θ_i	Drift ratio of reinforced concrete member
ρ_{cc}	Ratio of main reinforcement area to enclosed area of reinforcement hoop
ρ_{main}	Main reinforcement ratio
ρ_s	Volumetric transverse reinforcement ratio
ρ_{sey}	Effectively transverse reinforcement ratio
χ	Strain hardening ratio
χ_r	Stiffness degradation index
$\int dE$	Total hysteretic energy dissipated during cyclic load

1. Introduction

1.1 Background

In Hong Kong, reinforced concrete structures are traditionally designed without seismic provision. Researchers found that Hong Kong is subjected to moderate seismic hazards (Lee et al 1996, Chau et al 1998, Wong et al 1998 a & b and Chandler and Lam 2002), for instance, see the seismic intensity map as shown in Figure 1-1. There is a lot of reclaimed land in Hong Kong. The soil condition amplifies seismic action. According to the Chinese Zonation map, the peak ground acceleration of the earthquake that would occur in Hong Kong for a return period of 475 years is around 0.1-0.15g. Meanwhile, our high rise buildings consist of transfer structure to allow more space in the lower stories. The soft storey will be subjected to large amount of seismic force due to heavy mass of the transfer plate. So it may severely damage the reinforced concrete columns below transfer plate. It is necessary to examine the response of reinforced concrete columns with local detailing under seismic action (Lam et al 2002).

In the past, reinforced concrete buildings were designed in Hong Kong according to Code of Practice for Structural Use of Concrete in 1987. Seismic action is not considered in this code and the buildings are designed to resist high wind load.

There are a large number of residential buildings built between 1960s and 1980s. They are normally between 10 and 30 stories. The buildings are more susceptible to seismic action than wind load. Columns in this class of building usually have high axial load ratio, high main reinforcement ratio, low shear span depth ratio and non-seismic detailing. In addition, major function of transverse reinforcements is to resist buckling of main reinforcements and design of columns is controlled by strength only. Previous studies have indicated that this class of columns has limited ductility (Lam et al 2003). In this study, seismic performance of this class of columns was examined, columns with local detailing were tested and mathematical model is developed to predict the behavior under seismic attack.

Figure 1-2 shows some typical detailing of columns in Hong Kong. Firstly, end hooks of the transverse reinforcements are at 90º rather than 135º. Benefits in using 90º end hook is that transverse reinforcements can be fixed easily but main drawback of this arrangement is that the end hooks may not be able to restrain the main reinforcements. Current design practice, i.e. based on Code of Practice for Structural Use of Concrete 2004 and Kwan (2006), specifies that hooks in the transverse reinforcements in column must be at 135º hook. This provides proper anchor to transverse reinforcements in reinforced concrete column. When compressive stress increases in concrete section, there is a progressive increase in the lateral strain. The concrete tends to expand laterally with formation of micro-cracks. The transverse reinforcements interact and provide passive pressure to confine lateral expansion and to prevent further cracking of concrete. Strength and ductility of concrete are then increased. Therefore, closely spaced transverse reinforcements with 135º hooks are specified in the seismic detailing.

Secondly, according to the Code of Practice for the Structural Use of Concrete - 1987, “transverse reinforcements should be secured to the main reinforcements and the ends of such transverse reinforcements shall be properly anchored”. There is no elaboration on how to anchor the transverse reinforcements to the main reinforcements. To facilitate concreting, transverse reinforcements may not be secured to main reinforcements. They may be tied to the perpendicular transverse reinforcements at one ends rather than to the main reinforcements. As a result, stress-strain relationship of the confined concrete with local detailing is different from that predicted by Mander *et al* (1988), Saatcioglu (1992) and El-Dash (2004).

The occurrence of large earthquake is less frequent than the smaller ones. It would be economical in designing structure to resist large earthquake force in a ductile manner. This reduces size of members because large amount of energy is consumed in inelastic behavior of members. Comparison between strength and ductile design is shown in Figure 1-3. In particular, ductility of reinforced concrete column is enhanced by reducing spacing of transverse reinforcements, proper configuration of detailing, such as using 135º hook, and high volumetric transverse reinforcements ratio.

It is necessary to develop the stress-strain relationship of confined concrete in reinforced concrete column with non-seismic detailing to predict the moment curvature relationship of a column section. Relationship between lateral force and deflection is a critical issue in seismic design. Deflection of reinforced concrete columns subjected to lateral force consists of three components. They are flexural deflection, bond-slip rotation and shear deflections. Flexural deflection is obtained from the moment curvature relationship. Bond slip rotation and shear deflection is obtained from experimental data. Hysteresis behavior of reinforced concrete columns is also very important in seismic design. It influences damping characteristics of building and can be analyzed by two approaches. First approach is to analyze cyclic behavior based on stress-strain relationship of confined concrete by finite element method (Bazant and Bhat 1977, Palermo and Vecchio 2007). Second approach considers macroscopic stiffness method (Takeda et al 1970, Saiidi 1982 and Ibrra et al 2005). The first approach is complicated and time consuming. The second approach is simple and can be used easily by engineers.

In this study, damage model is proposed for reinforced concrete columns. It quantifies the damage in relation to number of cycles, maximum attainable displacement and energy dissipation. Parameters in damage model include volumetric transverse reinforcement ratio, strength of concrete and steel, aspect ratio and axial load ratio.

1.2 Research Significance

Although Hong Kong is situated in a moderate seismic hazard zone, reinforced concrete structures do not have any seismic provision. In particular, there are lots of high rise buildings with transfer structures. Large seismic force will be induced when subjected to earthquake action due to the mass of the transfer plate. Therefore, columns under a transfer structure are critical elements.

The transverse reinforcement detailing traditionally need in Hong Kong is different from those applied to severe seismic zone. It is necessary to study confinement action of reinforced concrete column with this type of detailing. This can quantify the resistant of existing reinforced concrete column when subjected to moderate seismic attack. Stress-strain relationship of confined concrete is also investigated to predict the response of reinforced concrete column.

This study assists the investigation of reinforced concrete structure with local detailing when subjected to seismic attack. In this study, a lateral force-deflection model is proposed to describe the hysteresis behavior of reinforced concrete column. The lateral force deflection model can be incorporated in a non-linear time history analysis model or static pushover analysis model to investigate response of a reinforced concrete building when subjected to moderate seismic action. Alternatively, an interstorey drift ratio is proposed in this study. It can assist in determining the interstorey shear force.

Lastly, a damage model is proposed to assist engineers to quantify the damage of reinforced concrete column after analyzing the column by non-linear time history analysis. The damage index quantifies the damage and provides justification for engineers to decide the proper means strengthening reinforced concrete columns.

1.3 Objective

Recent studies have indicated that Hong Kong is located an area of moderate seismic risk (Lee et al 1996). As buildings in Hong Kong are not designed to seismic provision, an imminent hazard exists when local buildings are subjected to seismic attack. It is the objective of proposed investigation to examine the response of reinforced concrete columns with local transverse reinforcement detailing when subjected to seismic loading.

Tests were carried to assess the confinement action of reinforced concrete column with different transverse reinforcement detailing. The test results are analyzed and mathematical model representing the stress-strain relationship of confined concrete in reinforced concrete columns with local detailing is developed.

Cyclic behaviour of reinforced concrete columns with local detailing is also examined by conducting cyclic loading tests on test specimens. Hysteresis model and damage model are developed based on the test data.

1.4 Organization

In Chapter 2, mathematical model in describing stress-strain relationship of confined concrete in reinforced concrete columns is discussed. Behavior of reinforced concrete columns under cyclic loading and unilateral movement is discussed. Damage models are also reviewed.

Tests on reinforced concrete columns when subjected to uni-axial loading are reported in Chapter 3. Parameters considered in the tests include volumetric transverse reinforcement ratio and configuration of detailing. The tests results are presented in Chapter 4. Mathematical model is developed statistically from the test results.

Besides axial loading tests, cyclic behavior of reinforced concrete columns is examined in Chapter 5. Cyclic loading tests on reinforced concrete columns with local detailing were conducted for specimens with different axial load ratio, volumetric transverse reinforcement ratio and configuration of local detailing (Type L and M). Test results of cyclic loading tests are discussed in Chapter 6. Performance of specimens with different volumetric transverse reinforcement ratio and axial load ratio is critically assessed.

A hysteretic model of reinforced concrete columns is proposed. The hysteretic model consists of elastic stiffness, strain hardening stiffness, unloading stiffness and reloading stiffness. Elastic stiffness and strain hardening stiffness are discussed in Chapter 7 while the unloading and reloading stiffness are presented in Chapter 8. Damage model for quantifying the damage of reinforced concrete columns is presented in Chapter 9.

Finally, summary and conclusion of the study and recommendation are presented in Chapter 10.

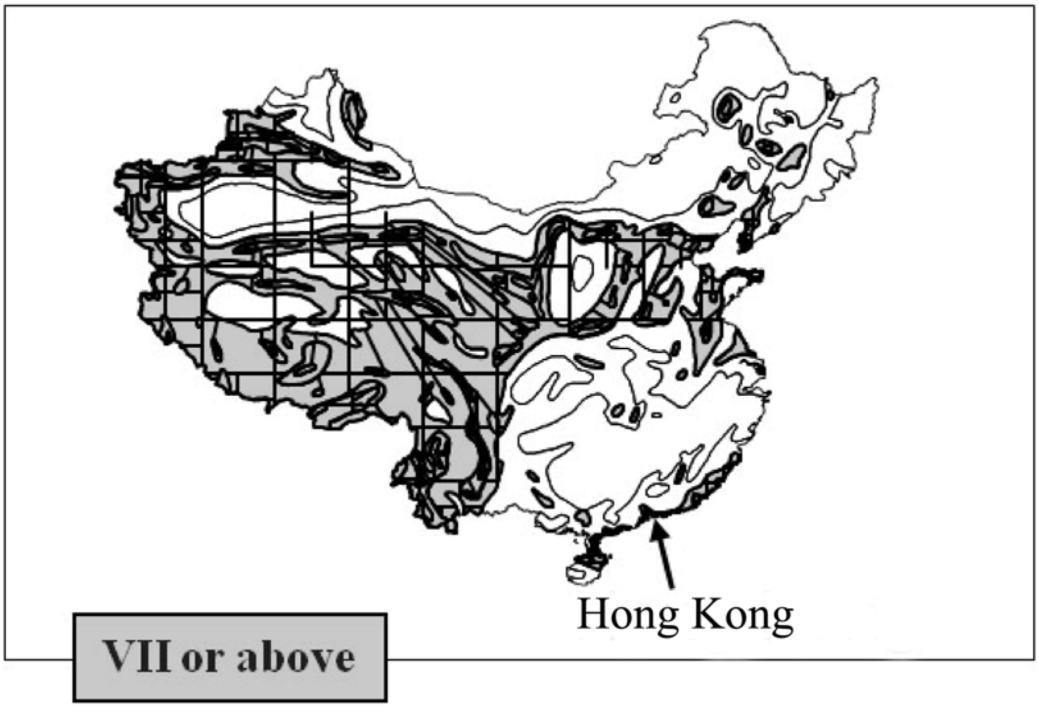

Figure 1-1 Zonation Map of China Showing Seismic Intensity Larger Than 7

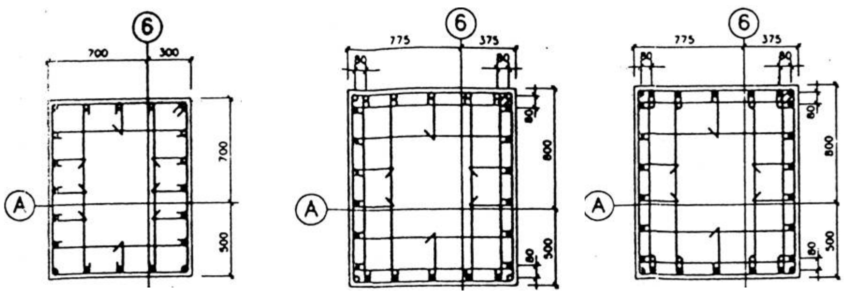

Figure 1-2 Some Typical Detailing of Columns in Hong Kong (Extracted from Drawings Showing Design of Local Building)

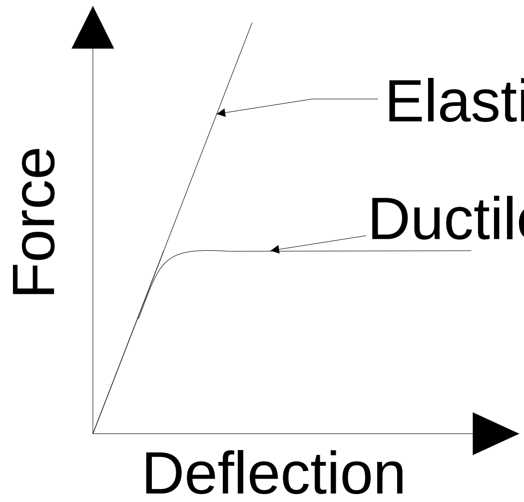

Figure 1-3 Comparison between Strength and Ductile Design Principle

2. Literature Review

2.1 Introduction

The occurrence of seismic attack has been increased in previous years, such as, Wenchuan earthquake in China (12^{th} May, 2008), Lincolnshire earthquake in England (27^{th} February 2008), Hokkaido earthquake in Japan (25^{th} September, 2003), Java earthquake in Indonesia (17^{th} July, 2006) & L'Aquila earthquake in Italy (6^{th} April, 2009) (UGCS Webpage). Such seismic attack has led to great deal of economic loss. Therefore, it is necessary to review the seismic hazard in Hong Kong.

Hong Kong is specified as having a moderate seismic hazard according to the China Code for Seismic Design in Building (GB50011-2001). Many Researchers have suggested that Hong Kong is an area with moderate seismic hazard (Chau et al 1998). As a result, there is increasing concern on our structures being designed according to local code of practice, as to whether it will survive under seismic attack.

In Hong Kong, design of reinforced concrete structure (i.e. before 2005) was according to "Code of Practice on Structural Use of Concrete 1987" and "Structural Use of Concrete" (BS8110). Both standards do not have seismic consideration. So local building may not have sufficient seismic resistance. For the vast number of tall buildings in Hong Kong, typical structural system is wall-frames supported by transfer plate. Below the transfer plate are frames at large spacing to provide open space at the lower floors. The drawback of the system is that abrupt change in stiffness occurs below the transfer plate (i.e. a soft storey). Local columns, however, are not provided with sufficiently transverse reinforcements to confine the concrete and to resist the shear force. If there is a moderate seismic attack in Hong Kong, the buildings may be substantially damaged or collapse at the soft storey.

In the meantime, many local researchers conducted and are conducting researches to investigate the structural behaviour of reinforced concrete structures when subjected to seismic action, just to name a few of the published work: reinforced concrete beam (Pam et al 2001a, Pam et al 2001b, Ho et al 2005, Au et al 2005, Kwan et al 2006, Au and Bai 2007, Bai and Au 2007, Lam et al 2008 and Zhu et al 2009), reinforced concrete column (Ho et al 2000, Kuang and Wong 2001, Pam and Ho 2001, Pam and Ho 2002, Ho and Pam 2003, Lam et al 2003, Ho and Pam 2004 and Kuang and Wong 2005) and reinforced concrete building (Chen et al 2002, Chan and Zou 2004, Atanda and Kuang 2004, Kuang and Atanda 2005a and b, Li et al 2006, Li et al 2008, Su et al 2008, Su 2008 and Zhu and Su 2008)

On the other hand, many design standards have incorporated seismic provision. In particular, the European Code 8: Design Provisions for Earthquake Resistance of Structure, Chinese Code: Code for Seismic Design of Buildings (GB 50011-2002), Japanese Code: AIJ Structural Design Guidelines for Reinforced Concrete Buildings and New Zealand Code: Concrete Structures Standards provide additional design guidance for buildings in moderate seismic zone. However, there is in lack of literature and research studies on the discussion of confinement action of local detailing.

2.2 Seismic Design Principle

The principle adopted in seismic design can be categorized into three limit states (Paulay and Priestley 1992):

i. Serviceability limit state is to ensure that main functions of the buildings are unaffected. At this limit state, cracking of concrete is acceptable if repair is not needed.
ii. Damage control limit state allows repairable damage, including spalling of concrete and formation of wide cracks.
iii. Survival limit state is considered in an extreme event earthquake, where severe and possibly irreparable damage may occur, but collapse and loss of life is avoided.

Seismic design can be divided into two types (Paulay and Priestley 1992):

i. Elastic Design – the structure should provide enough strength to remain elastic when subjected to seismic loading. This scheme is uneconomical and requires massive structural system.
ii. Inelastic Design – the structure may respond inelastically when subjected to severe seismic loading. Some structural elements will be in the plastic range and ductile to absorb part of the seismic energy. Member size will be

reduced as compared with elastic design. Inelastic design also enhances damping ratio of the structure, and reduces the seismic response. Modern seismic design provision applies inelastic design, such as the Chinese code (GB50011-2001). The drawback of this scheme, however, is that large deformation will cause discomfort to the occupants and substantial damage of non-structural elements. The commonest form of reinforced concrete structure in inelastic design is “the strong column weak beam” scheme. This scheme requires the column to be in the ductile range.

2.3 Unconfined Concrete

Concrete is strong in compression but brittle in nature. The stress-strain relationship of concrete is that the stress is initially parabolic and reduces linearly to zero. Typical stress-strain relationship of concrete is shown in Figure 2-1. The strain corresponding to the maximum stress is about 0.002 (Kent and Park 1971). Slope of descending branch depends on the cylinder strength of concrete and becomes steeper when concrete strength increases. Initial stiffness of concrete depends on the concrete strength. Characteristic of unconfined concrete is that compressive strength of concrete increases with the strain rate. Strain of concrete at spalling is about 0.004. In the design code, it is assumed that concrete stress increases parabolically to maximum strength with corresponding strain approximately to 0.002 and remains constant to ultimate strain (0.0035). The corresponding design curve is shown in Figure 2-3.

When a unreinforced concrete column is compressed, it will expanded laterally. Cracks appear on concrete column when the lateral stress is larger than the tensile strength of concrete. The concrete then fails with extensive spalling. The mechanism is shown in Figure 2-2.

Reinforced concrete is classified as unconfined when there is insufficient transverse reinforcements or transverse reinforcements are not closely spaced. In general, concrete surrounding the main reinforcements and concrete cover are unconfined. Unconfined concrete spalls off when spalling strain is reached. An unreinforced concrete column fails by buckling of main reinforcements and/or crushing of concrete due to spalling. When the main reinforcements buckle, force is transferred from the reinforcements to the concrete core and the column is then collapse.

2.4 Steel

Concrete is strong in compression but weak in tension. Reinforcements are added to resist tension, and increase the flexural strength of reinforced concrete element and provide ductility (high yield deformed bars). Yield strength and corresponding strain of reinforcements used in Hong Kong are 460MPa and 0.0023 respectively. Modulus of elasticity is about 200GPa. Main characteristic of reinforcements is that it has large yield plateau and gradual increase in strain hardening. Typical stress-strain relationship of reinforcements is shown in Figure 2-4.

Although reinforcements increase the flexural strength, they are limited to about 2.6% (GB50011-2001) for a section under flexural. This is because at high reinforcement ratio, concrete may fail before yielding of the reinforcements. In such case, the section fails in a brittle manner i.e. an over-reinforced section.

Transverse reinforcements are very important. It prevents the main reinforcements from buckling, and increases shear capacity strength and ductility.

2.5 Confined Concrete

Strength and ductility of concrete are increased when it is loaded tri-axially, (Richart 1928), that is subjected to uni-axial load as well as hydrostatically loaded in the lateral directions. This hydrostatic pressure is active confined pressure. Similarly, closely spaced transverse reinforcements provide passive confined pressure to core concrete. When concrete is loaded to its maximum compression, it expands laterally due to the Poisson's effect. Vertical internal cracking is induced when tensile strain in lateral direction exceeds cracking strain. Transverse reinforcements react against expansion of concrete and the concrete is said to be confined. The ultimate strain of confined concrete can be defined as the strain corresponding to fracture of the first transverse reinforcements or premature buckling of main reinforcements.

According to Richart (1928), uni-axial strength of concrete is related to active confined pressure. The expression of the model is as follows,

$$f_{cc}=f_c+4.1f_2 \tag{2-1}$$

where f_{cc} is confined concrete strength, f_c is unconfined concrete strength and f_2 is active confined stress.

2.5.1 Park's Model (1971)

When core concrete of a column is confined by transverse reinforcements, ultimate strain of columns is increased. Kent and Park (1971) assumed that concrete stress increases parabolically and then deforms gently as compared to those in unconfined concrete. It was observed that strain in confined concrete corresponding to 50% of peak strength in the descending branch is related to the one in unconfined concrete and volumetric transverse reinforcement ratio. Details of the Park's Model are as shown in Figure 2-5 and Eq (2-2).

$$\varepsilon_{50cc}=\varepsilon_{50uc}+0.75\rho_s(b_c/s)^{0.5} \qquad (2\text{-}2)$$

where ε_{50cc} is strain at 50% of confined concrete strength, ε_{50uc} is strain at 50% of unconfined concrete strength, ρ_s is volumetric transverse reinforcement ratio, b_c is width of transverse reinforcement measured from centreline and s is spacing of transverse reinforcement.

2.5.2 Skeikh's Model (1982)

When a reinforced concrete column is subjected to compressive load, response of concrete is separated into two different zones. Firstly, concrete cover and ineffectively confined zone, which is termed as unconfined concrete, deforms in accordance with plain concrete and is brittle in nature. It spalls off after concrete attaining the spalling strain.

Secondly, for concrete inside the effectively confined concrete zone, it deforms in a more ductile manner and achieves a higher strength than that in unconfined concrete. The effectively confined concrete area is smaller than the area enclosed by the reinforcement hoops. Lateral expansion in confined concrete is resisted by axial stiffness of transverse reinforcements. In fact, action of transverse reinforcements is similar to arch mechanism. The arch is assumed to be parabolic with a tangential angle (θ_c) at intersection point of the transverse reinforcements. The angle is about 45 degrees. Effective confined concrete area is given in Eq (2-3) and shown in Figure 2-6 and 2-7. Parameter a_{tf} in Eq (2-3) is 5.5 (Skeikh and Uzumeri 1982). This is based on the result obtained from statistical analysis.

$$A_{cc} = A_g \left(1 - \frac{\sum_{i-1}^{n} c_i^2}{a_{tf}} \right) \left(1 - \frac{0.5s}{b_c} \tan\theta_c \right) \left(1 - \frac{0.5s}{h_c} \tan\theta_c \right) \qquad (2\text{-}3)$$

where A_{cc} is effectively confined concrete area, A_g is enclosed area of transverse reinforcement measured from centreline of transverse reinforcement, w_i is horizontal spacing of transverse reinforcement among crossties, s is vertical spacing of transverse spacing, b_c is width of transverse reinforcement hoop along the centreline, h_c is depth of transverse reinforcement hoop along the centreline, θ_c is angle of tangential line of confinement action to transverse reinforcement and a_{tf}=5.5 is reduction factor of concrete area.

Skeikh's model is different from other stress-strain relationships. Stress is assumed to increase with strain parabolically to maximum stress. The maximum stress in confined concrete is larger than the one in unconfined concrete due to tensile resistance from transverse reinforcements. The stress remains constant along the concrete strain, from ε_{s1} to ε_{s2}. Stress is then reduced in a gentle slope similar to Park's model but strain at 85% of maximum stress in descending branch is used to define the slope of the descending branch. Strength increment $K_{str\ SKEIKH,}$, ε_{s1}, ε_{s2} and ε_{s85} are defined by following equations. The stress-strain relationship is as shown in Figure 2-8,

$$K_{str,SKEIKH} = 1 + \frac{b_c^{\ 2}}{140P_{occ}}\left[\left(1 - \frac{\Sigma c_i^2}{5.5b_c^{\ 2}}\right)\left(1 - \frac{s}{2b_c}\right)^2\right]\sqrt{\rho_s f_{yt}} \qquad (2\text{-}4)$$

$$\varepsilon_{s1} = 80K_{str,SKEIKH} f_c x 10^{-6} \qquad (2\text{-}5)$$

$$\frac{\varepsilon_{s2}}{\varepsilon_{uc}} = 1 + \frac{248}{c_i'}\left[1 - 5\left(\frac{s}{2b_c}\right)^2\right]\frac{\rho_s f_{yt}}{\sqrt{f_{cc}}} \qquad (2\text{-}6)$$

$$\varepsilon_{s85} = 0.225\rho_s\sqrt{\frac{b_c}{s}} + \varepsilon_{s2} \qquad (2\text{-}7)$$

where $K_{str\ SKEIKH}$ is strength increment of confined concrete proposed by Skeikh (1982), b_c is width of transverse reinforcement hoop measured on centreline, P_{occ} is confined concrete load, c_i is spacing of transverse reinforcement,, s is vertical spacing of transverse reinforcement, ρ_s is volumetric transverse reinforcement ratio, f_{yt} is yield strength of transverse reinforcement, f_{cc} is confined concrete strength, ε_{ucv} is peak strain of unconfined concrete, ε_{s1} is peak strain of confined concrete, ε_{s2} is peak strain of confined concrete and ε_{s85} is strain corresponding to 15% strength reduction of confined concrete.

As demonstrated in above equations, volumetric transverse reinforcement ratio in reinforced concrete column increases axial strength by providing confinement action to resist lateral expansion of concrete. The increased compressive strength in confined concrete compensates the loss of concrete strength from spalling of unconfined concrete.

2.5.3 Modified Park's Model (1982)

Strength increment ratio K is introduced according to the amount of transverse reinforcements. Strain at maximum stress in confined concrete is increased with the factor K, the strength increment ratio. Ultimate strain is defined as the first fracture of transverse reinforcements, and is related empirically to transverse reinforcement ratio. Strength of the confined concrete increases as strain rate is increased. However, descending branch of stress-strain relationship of confined concrete becomes steeper.

$$f_{cco} = K_{s,Park}\, f_c \left[\frac{2\varepsilon_c}{0.002K_{s,Park}} - \left(\frac{\varepsilon_c}{0.002K_{s,Park}} \right)^2 \right] \tag{2-8}$$

$$f_{cco}=K_{s,Park}f_c[1-Z_m(f_c-0.002K_{s,Park})] \tag{2-9}$$

$$K_{s,Park} = 1 + \frac{\rho_s f_{yt}}{f_c} \tag{2-10}$$

$$Z_m = \frac{0.5}{\dfrac{3+0.29f_c}{145f_c-1000} + \dfrac{3}{4}\rho_s\sqrt{\dfrac{h_o}{s}} + 0.002K_{s,Park}} \tag{2-11}$$

$$\varepsilon_{cu} = 0.004 + 0.9\rho_s\left[\frac{f_{yt}}{300}\right] \tag{2-12}$$

where f_c is unconfined concrete strength, $K_{s,Park}$ is strength increment ratio proposed by Park (1982), f_{cco} is confined concrete stress, ε_c is confined concrete strain, Z_m is descending branch of confined concrete proposed by Park (1982), ρ_s is volumetric transverse reinforcement ratio, f_{yt} is yield strength of transverse reinforcement, h_o is width of transverse reinforcement measured from outside dimension, s is vertical centre to centre spacing and ε_{cu} is ultimate strain of reinforced concrete column.

2.5.4 Shah's Model (1985)

Strength of concrete core increases with the amount of volumetric transverse reinforcement ratio. The latter is used to define the extent of confinement action in reinforced concrete column. For rectangular reinforced concrete column, confinement action is related to inscribed diameter in enclosed area of reinforcement hoops. Shah's model describes stress-stain relationship of confined concrete by two different curves to define ascending and descending branches in confined concrete respectively. The confined concrete of Shah is as shown in Figure 2-9. Detailed description of the curves is referred to Fafitis and Shah (1985).

For ascending branch

$$f_{cco} = f_c\left[1-\left(1-\frac{\varepsilon}{\varepsilon_{cc}}\right)^{r_{unstr}}\right] \tag{2-13}$$

For descending branch

$$f_{cco} = f_c \exp\left[-k\left(\varepsilon_c-\varepsilon_{cc}\right)^{1.15}\right] \tag{2-14}$$

$$r_{unstr} = \frac{E_{con}\varepsilon_{uc}}{f_c} \tag{2-15}$$

$$K_{des,Shah} = 0.17 f_c \exp(-0.01 f_l) \tag{2-16}$$

$$f_{cc} = f_c + \left(1.15 + \frac{21}{f_c}\right) f_l \tag{2-17}$$

$$\varepsilon_{cc} = 1.48915\times10^{-5} f_c + 0.0296\frac{f_l}{f_c} + 0.00195 \tag{2-18}$$

$$f_l = \frac{A_{sh} f_{yt}}{\phi_{transverse} s} \tag{2-19}$$

where f_c is unconfined concrete strength, f_{cco} is concrete stress, ε is concrete strain, ε_{uc} is unconfined concrete peak strain, ε_{cc} is confined concrete peak strain, f_l is average confinement stress of transverse reinforcement, $\phi_{transverse}$ is diameter of transverse reinforcement, s is spacing of transverse reinforcement, f_{cc} is confined concrete peak strength, f_{yt} is yield strength of transverse reinforcement, A_{sh} is area of transverse reinforcement, r_{unstr} is ratio of unconfined concrete strength and $K_{des,Shah}$ is descending branch ratio proposed by Shah (1985).

2.5.5 Mander's model (1984)

When concrete is confined by transverse reinforcements, compressive strength of concrete is increased. However, rectangular reinforcement hoops are less effective than that in circular ones. Circular column is confined by hoop stress provided by axial stiffness in circular reinforcement hoops while rectangular column is confined by axial strength of transverse reinforcements located at the intersection point of two transverse reinforcements. The reaction from lateral expansion is resisted by arch action. The angle of arch action is assumed to be 45 degrees, similar to Skeikh's model. However, area of confined curve in (Eq. 2-4) is 6, being calculated from area of parabolic curve, rather than 5.5, being from empirical formula.

Peak stress in confined concrete is related to the plasticity model and is correlated to tri-axially loaded experimental result, of which the model is defined by William and Warnke (1975). Strain on peak stress in confined concrete is empirically related to peak stress increment factors as shown in (Eq. 2-20).

The ultimate confined concrete strain is related to fracture strain in transverse reinforcements. The additional strain energy in core concrete is provided from energy stored in transverse reinforcements. The total input energy is from uni-axial load and is related to strain energy stored in unconfined concrete in concrete cover, confined concrete, main reinforcements and transverse reinforcements.

Mander's model is different from previous models in that the stress-strain relationship is based on Popovics's model (1973). Popovics's model is used in describing the stress-strain relationship in unconfined concrete. The stress-strain relationship of confined concrete defined by Mander's model is shown in Figure 2-9 and given by the following equations.

$$f_c = \frac{f_{cc} x r}{r - 1 + x^r} \tag{2-20}$$

$$x = \frac{\varepsilon}{\varepsilon_{cc}} \tag{2-21}$$

$$f_{cc} = f_c\left(-1.254 + 2.254\sqrt{1+\frac{7.94 f_l}{f_c}} - \frac{2 f_l}{f_c}\right) \tag{2-22}$$

$$\varepsilon_{cc}=0.002[1+5(f_{cc}/f_c-1)] \tag{2-23}$$

$$f_l=K_e\rho_x f_{yh} \tag{2-24}$$

$$\alpha_{area} = \left(1-\frac{\sum_{i-1}^{n} c_i^2}{6b_c h_c}\right)\left(1-\frac{0.5s'}{b_c}\right)\left(1-\frac{0.5s'}{h_c}\right) \tag{2-25}$$

$$K_e = \frac{\alpha_{area}}{(1-\rho_{cc})} \tag{2-26}$$

$$\rho_x=A_{sv}/sb_c \tag{2-27}$$

$$r = \frac{E_c}{E_c - E_{\sec}} \tag{2-28}$$

$$E_{sec}=f_{cc}/\varepsilon_{cc} \tag{2-29}$$

where f_c is confined concrete stress, f_{cc} is confined concrete strength, x is strain ratio of confined concrete, r is ratio of modulus of confined concrete to secant modulus of confined concrete, ε is confined concrete strain, ε_{cc} is confined concrete strain confined concrete peak strain, f_{co} is unconfined concrete strength, f_l is average confinement stress provided by transverse reinforcement, α_{area} is effective confinement area ratio, K_e is strength increment ratio, ρ_s is volumetric transverse reinforcement ratio, ρ_{cc} is ratio of main reinforcement area to enclosed area of transverse reinforcement hoop, A_{sv} is area of transverse reinforcement, b_c is width transverse reinforcement hoop measured from centreline, E_c is Young's modulus of concrete and E_{sec} is secant modulus of confined concrete.

2.5.6 Meyer's model (1983)

Peak stress in confined concrete is larger than that in unconfined concrete because transverse reinforcements restrain lateral expansion in confined concrete. This increases peak stress, peak strain and also ductility of concrete. Stress-strain relationship in confined concrete is simplified by a tri-linear model. The curve is shown in Figure 2-11 and defined by the following equations.

$$f_{cy}=2/3\, f_c\ ;\ \varepsilon_{cy}=2/3\varepsilon_{uc} \tag{2-30}$$

$$f_{cc}=(1+10\rho_s)\, f_c\ ;\ \varepsilon_{cc}=(1+10\varepsilon_s)\varepsilon_{uc} \tag{2-31}$$

$$f_{cult}=0.2\, f_c;\ \varepsilon_{cu}=(2+600\rho_s)\varepsilon_{uuc} \tag{2-32}$$

$$\rho_s=\frac{2\left(b_c+d_c\right)A_{sv}}{b_c d_c s} \tag{2-33}$$

where f_{cy} is concrete yield strength, f_c is unconfined concrete strength, f_{cc} is confined concrete strength, f_{cult} is strength corresponding to ultimate strain yield strain in confined concrete, ε_{cy} is peak strain of unconfined concrete, ε_{uc} is peak strain in confined concrete, ε_c is confined concrete strain, ε_{cu} is ultimate strain of confined concrete, ε_{uuc} is ultimate strain of unconfined concrete, ρ_s is volumetric transverse reinforcement, A_{sv} is area of transverse reinforcement, b_c is width of transverse reinforcement measured from centreline, d_c is depth of transverse reinforcement and s is spacing of transverse reinforcement.

2.5.7 Saatcioglu's model (1999)

Saatcioglu (1992) proposed an alternative stress-strain relation of confined concrete. When concrete is subjected to axial load, lateral strain is expanded due to the Poisson's effect. Transverse reinforcements counteract movement in resisting concrete expansion. When the lateral stress acts on concrete, concrete is under a tri-axial state of stress. This increases the uni-axial capacity of concrete due to restraint of lateral strain because the lateral strain in confined concrete is resisted by transverse reinforcements in a reinforced concrete column.

$$-\frac{\nu f_{u2}}{E_{con}} = \frac{f_{t1} - \nu(f_{t2} + f_{t1})}{E_{con}} \tag{2-34}$$

$$f_{t2} = f_{u2} + \frac{(1-\nu) f_{t1}}{\nu} \tag{2-35}$$

where $f_{u,2}$ is vertical stress under uni-axial state, f_{t1} is lateral stress under tri-axial state, f_{t2} is vertical stress under tri-axial state, ν is Poisson's ratio and E_{con} is Young's modulus of concrete.

Lateral stress in concrete due to restraint is non-uniform and stress-strain behaviour is non-linear. Poisson ratio of concrete varies according to state of stress. It may cause difficulty in defining confinement action in reinforced concrete. When concrete stress is at peak strength, the Poisson ratio also increases to its maximum value. It would be better to formulate maximum stress similar to Eq. (2-1) as proposed by Richart (1928).

Lateral stress acted on circular column is assumed to be under uniform pressure. The confining pressure is proportional to elastic rigidity of the transverse reinforcements until the yield point. There is also an additional restraining force acted on the concrete when the steel is under strain hardening stage. Rectangular column is different from the circular one because the lateral stiffness of the hoops is not uniform. The corner bar has a higher restraining force than the other bars located away from the corner because the axial stiffness of the tie is much higher than the flexural stiffness of the tie. The equivalent pressure can be found by the following equations,

$$f_{le} = k_2 f_l \tag{2-36}$$

$$f_l = \frac{\sum A_s f_{yt} \sin\theta_s}{s b_c} \tag{2-37}$$

$$k_1 = 6.7(f_{le})^{-0.17}$$

(2-38)

$$k_2 = 0.26\sqrt{\left(\frac{b_c}{s}\right)\left(\frac{b_c}{s_l}\right)\left(\frac{1}{f_l}\right)} \le 1.0 \tag{2-39}$$

where f_{yt} is yield strength of transverse reinforcement, f_{le} is effective confinement stress, f_l is average confinement stress, k_1 is effective index for conversion to circular transverse reinforcement, k_2 is effective index on confinement action of rectangular transverse reinforcement, b_c is width of transverse reinforcement hoop measured from centreline, s is spacing of transverse reinforcement, s_l is horizontal spacing of the laterally restrained main reinforcement and θ_s is angle of diagonal crossties to transverse reinforcement hoop.

Saatcioglu also found that there is a higher axial strength in transverse reinforcements when larger bar size and/or, higher strength reinforcements are used. As a result, stress concentration will be increased and the equivalent lateral stress is reduced. The stress-strain relationship of the confined concrete is similar to the Mander's model. The Popovics's curve is used as ascending branch in stress-strain relationship on confined concrete until the maximum stress is reached. By then, the stress-strain relationship will decline linearly. The confined concrete strain is defined as follows,

$$\varepsilon_{cc} = \varepsilon_{uc}(1+5K_{s,saat}) \tag{2-40}$$

$$K_{s,saat} = \frac{k_1 f_{le}}{f_c} \tag{2-41}$$

where ε_{cc} is peak strain in confined concrete, ε_{uc} is peak strain in unconfined concrete, $K_{s,saat}$ is strength increment factor proposed by (Saatcioglu and Razvi 1992), k_1 is effective index for conversion to circular transverse reinforcement, f_{le} is effective lateral stress in transverse reinforcement and f_c is unconfined concrete strength.

Regression analysis of test data, (Saatcioglu 1992), indicates that the following expression could be used to establish the strain at 85% strength level and beyond the peak stress of confined concrete ε_{85}

$$\varepsilon_{s85} = 260\rho_s\varepsilon_{cc}+\varepsilon_{uc85} \tag{2-42}$$

$$\rho_s = \frac{\sum A_{sv}}{s(b_c+d_c)} \tag{2-43}$$

where ε_{s85} is post peak strain at 85% strength of confined concrete, ε_{uc85} is post peak strain at 85% strength of unconfined concrete, ρ_s is volumetric transverse reinforcement ratio,

A_{sv} is transverse reinforcement area, s is spacing of transverse reinforcement, b_c is width of transverse reinforcement along the centreline and d_c is depth of transverse reinforcement along the centreline. In addition, ultimate strain should be determined under the same rate of loading used for the confined concrete.

Stress-strain relationship of confined concrete is identical to that proposed by Hognestad (1951) for unconfined concrete, of which the concrete has no transverse reinforcement and confinement action. The model has a parabolic shape ascending branch and a linear descending branch. The model is as follows,

$$f_c = \frac{f_{cc} x r}{r - 1 + x^r} \tag{2-44}$$

where f_c is confined concrete strength, f_{cc} is confined concrete strength, x is strain ratio which is strain to peak confined concrete strain, r is stiffness ratio of transverse reinforcement.

2.5.8 Paultre's model (2003)

Many previous models have assumed that the transverse reinforcements yield when confined concrete is at maximum stress. This is not true if high yield steel bars are used as the transverse reinforcements or if volumetric transverse reinforcement ratio is low. If the amount of transverse reinforcements is low, this cannot effectively confine lateral expansion from compression of concrete. When strength of transverse reinforcements is increased, yield strain of transverse reinforcements is also increased. The transverse reinforcements in reinforced concrete may not yield at peak strength of confined concrete. However, the transverse reinforcements without reaching yielding will increase its stress until fracture when confined concrete strain is further increased. Higher yield strength in transverse reinforcements increases ductility of confined concrete. The spacing in transverse reinforcements is also another factor that can increase confinement action in reinforced concrete column.

As transverse reinforcements may remain elastic at maximum stress of confined concrete, an empirical formula is proposed and represented by the following equations.

$$f_t = f_{yt} \qquad \text{if } \kappa \le 10 \tag{2-45}$$

$$f_t = \frac{0.25 f_{cc}}{\rho_{sey}\left(\kappa - 10\right)} \ge 0.43\varepsilon_{uc}E_s \le f_{yt} \qquad \text{if } \kappa > 10 \tag{2-46}$$

$$\kappa = \frac{f_c}{\rho_{sey}E_s\varepsilon_{uc}} \tag{2-47}$$

$$\rho_{sey} = K_e \frac{A_{shy}}{sc} \tag{2-48}$$

K_e is the same as that defined in Mander's model, Eq.(2-26).

Stress-strain relationship in confined concrete is defined by two different curves. The ascending branch is similar to Mander's model while the descending branch of the model is according to Fafitis and Shah (1985). Paultre's model is different from Shah's model.

$$f_{cco} = f_{cc}\exp\left[k_{1P}\left(\varepsilon_c - \varepsilon_{cc}\right)^{k_{2P}}\right] \tag{2-49}$$

$$k_{1P} = \frac{\ln 0.5}{\left(\varepsilon_{50cc} - \varepsilon_{cc}\right)^{k_{2P}}} \tag{2-50}$$

$$k_{2P} = 1 + 25\left(I_{e50}\right)^2 \quad (2\text{-}51)$$

$$\frac{f_{cc}}{f_c} = 1 + 2.4\left(I'_e\right)^{0.7} \quad (2\text{-}52)$$

$$\frac{\varepsilon_{cc}}{\varepsilon_{uc}} = 1 + 35\left(I'_e\right)^{1.2} \quad (2\text{-}53)$$

$$I'_e = \frac{K_e A_{shy} f_t}{s d_c f_c} \quad (2\text{-}54)$$

$$I_{e50} = \frac{K_e A_{shy} f_{yt}}{s d_c f_c} \quad (2\text{-}55)$$

$$\frac{\varepsilon_{50cc}}{\varepsilon_{50uc}} = 1 + 60 I_{e50} \quad (2\text{-}56)$$

where f_t is transverse reinforcement stress at peak strength of confined concrete, f_{yt} is stress in transverse reinforcement, f_c is unconfined concrete strength, ρ_{sey} is effectively transverse reinforcement ratio, κ is ratio of unconfined concrete strength to transverse reinforcement stress, E_s is Young's modulus of transverse reinforcement, ε_c is confined concrete strain, A_{shy} is transverse reinforcement area parallel to y- direction, d_c is width of transverse reinforcement measured from centreline, ε_{cc} is peak strain in confined concrete, k_{1P} is effective confinement index 1 proposed by Paultre (2003), k_{2P} is effective confinement index 2 proposed by Paultre (2003), ε_{50cc} is post peak strain corresponding to 50% of confined concrete strength, I_e' is effective confinement index at peak strength and I_{e50} is effective confinement index of ultimate strain.

2.5.9 Kinugasa et al's Model (2004)

Strain energy stored in confined concrete comprises strain energy stored in unconfined concrete and transverse reinforcements. Peak strain and post peak strain corresponding to 85% of peak strength of confined concrete are defined from strain energy of confined concrete and stress-strain relationship of confined concrete. The above are defined by the following equation in

for $\varepsilon_{cc} \leq \varepsilon_{uuc}$

$$EG_{cc} = 0.44 \times \left(\rho_s f_{yt} / f_c \right) \tag{2-57}$$

$$EG_{85} = 2.18 \times \left(\rho_s f_{yt} / f_c \right) \tag{2-58}$$

$$\varepsilon_{cc} = \left[-\left(f_{cc} - f_c \right) + \sqrt{\left(f_{cc} - f_c \right)^2 + 8 E_c EG_{cc}} \right] / 2E_c + \varepsilon_{uc} \tag{2-59}$$

$$\varepsilon_{s85} = \left[-\left(1.85 f_{cc} - 2 f_c \right) + \sqrt{\left(1.85 f_{cc} - 2 f_c \right)^2 + 4 E_{usec} \left[\varepsilon_{cc} \left(f_c - 0.85 f_{cc} \right) - 2EG_{85} \right]} \right] / 2E_{usec} + \varepsilon_{uc} \tag{2-60}$$

for $\varepsilon_{uuc} \leq \varepsilon_{cc}$

$$EG_{cc} = 5.8 \times \left(\rho_s f_{yt} / f_c \right) - 0.75 \tag{2-61}$$

$$EG_{85} = 10.9 \times \left(\rho_s f_{yt} / f_c \right) - 0.87 \tag{2-62}$$

$$\varepsilon_{cc} = \left[2EG_{cc} + \left(\varepsilon_{uuc} - \varepsilon_{uc} \right) f_c \right] / \left[f_c + f_{cc} \right] + \varepsilon_{uuc} \tag{2-63}$$

$$\varepsilon_{s85} = \left[2EG_{85} + \varepsilon_{uuc} f_c - \varepsilon_{cc} \left(f_c + f_{cc} \right) \right] / \left[1.85 f_{cc} \right] + \varepsilon_{uuc} + \varepsilon_{cc} \tag{2-64}$$

where f_c is unconfined concrete strength, f_{yt} is yield strength of transverse reinforcement, f_{cc} is peak strength of confined concrete, E_{usec} is secant modulus of unconfined concrete, ρ_s is volumetric transverse reinforcement ratio, ε_{uuc} is ultimate strain of unconfined concrete, ε_{cc} is peak strain of confined concrete, EG_{cc} is strain energy at peak strength stored in confined concrete and EG_{85} is strain energy at ultimate strain stored in confined concrete.

2.5.10 Bousalem and Chikh's Model (2007)

Normal strength reinforced concrete columns were tested to verify the ductile behaviour of reinforced concrete column. New parameters were proposed to increase the accuracy in predicting maximum strength and peak strain in the stress-strain relations. The stress-strain relationship consists of ascending and descending branches. In their model, the ascending branch is similar to the one used in Mander's model (1984) while the descending branch is assumed to be linearly related from peak strain to the ultimate strain. The ultimate strain is assumed to be the strain where the strength is dropped to 30% of peak strength in the descending branch. The parameters in describing the stress-strain relationships are as follows,

$$K_{s,bou} = 1 + 0.4\frac{K_e \rho_s f_{yt}}{\sqrt{f_c}} \tag{2-65}$$

$$K_{d,bou} = 1 + 2.7\frac{K_e \rho_s f_{yt}}{\sqrt{f_c}} \tag{2-66}$$

$$K_{soft,bou} = \frac{4 f_c^{\,2}}{K_e \rho_s f_{yt}} \tag{2-67}$$

where K_e is effective confinement action, ρ_s is volumetric transverse reinforcement ratio, f_{yt} is yield strength of transverse reinforcement, f_c is unconfined concrete strength, $K_{s,bou}$ is strength increment ratio proposed by Bousalem and Chikh (2007), $K_{d,bou}$ is strain increment ratio proposed by Bousalem and Chikh (2007), $E_{soft,bou}$ is softening energy ratio proposed by Bousalem and Chikh (2007).

The comparison of previous model proposed by researchers will be shown in Chapter 4.

2.6 Flexural Behaviour of Reinforced Concrete Columns

2.6.1 Previous Test in Investigating Flexural Behaviour of Reinforced Concrete Columns

The experiments may be divided into three types in investigating flexural behaviour of reinforced concrete columns. They are single cantilever model, double curvature and column with single stub as shown in Figure 2-14.

Single cantilever model is used to simulate the cyclic behaviour of reinforced concrete column in buildings or bridge column. In this arrangement, point of contraflexure of a column is assumed to be at mid-height of the column because equal and opposite force adds on floors above and below the columns when subjected to seismic action. This arrangement can minimize height constraint in the instrumentation, and is suitable for analyzing bridge columns, for example, Park and Paulay (1990), Saatcioglu and Ozcebc (1989) and Ho (2003).

For double curvature model, rigid beams are fixed on both sides of column specimens. This simulates a column between two floors subjected to seismic action. Scale of model is controlled by height constraints of the laboratory. This arrangement investigates the diagonal shear failure under cyclic loading. Horizontal load is applied by an actuator at the end of a moment arm frame while vertical load is added on the top of specimen, for example, Sakai et al 1990, Umebbra and Jira 1982, Sezen 2000 and Lam et al 2003.

For the column with stubs, concrete stubs are used to simulate the floors. Horizontal load is applied to the stubs. Horizontal reaction force is counterbalanced by triangular steel frame. Vertical load is added on top of the specimens. Point of contraflexure of reinforced concrete column is assumed to be at mid-height. The concrete floor is represented by providing relative stiffness on the column, but loading capacity of the column specimen should not be too large. Previous studies using this type of arrangement include Ang et al 1981, Soesianawati et al 1986 and Tanaka and Park (1990).

2.6.2 Flexural Behaviour of Reinforced Concrete Column

During the past 30 years, a large number of researches were carried out to investigate flexural behaviour of reinforced concrete columns. Main parameters in the investigations include axial load ratio, volumetric transverse reinforcement ratio, configurations of transverse reinforcements, main reinforcement ratio, concrete strength and yield strength of steel reinforcements. The following is a review of the related studies.

Sargin et al (1971) carried out flexural tests on reinforced concrete columns by adding eccentricity. Flexural behaviour, such as ductility and rotation capacity, of reinforced concrete column depends on type of configurations of transverse reinforcements, spacing and amount of transverse reinforcements. Curvature ductility of reinforced concrete column is predicted by the following equation.

$$\mu_{\varphi} = 1 + 3\left(1 + 5.4\alpha_{con}\right)\frac{L_p}{L}\left(2 - \frac{L_p}{L}\right) \quad (2\text{-}68)$$

where μ_{φ} is curvature ductility of reinforced concrete column, α_{con} is index of configurations of transverse reinforcements, L is height of reinforced concrete column and L_p is plastic hinge length.

Azizinamini et al (1992) carried out twelve flexural tests on reinforced concrete columns. The axial load ratio of the columns is between 0.2-0.4. Flexural strength increases with axial load. There is no difference on flexural behaviour of columns having the same volumetric transverse reinforcement ratio with different transverse reinforcement spacing. When transverse reinforcement ratio is dropped to 50% of that required in accordance with ACI 318 (1983), the columns behave in less ductile manner.

Lynn et al (1996) carried out eight full-scaled reinforced concrete columns to investigate flexural behaviour of the columns with different transverse reinforcement ratios. Ductility of concrete column reduces with transverse reinforcement ratio. Shear strength of the column is not related to displacement ductility demand. Vertical strength reduced sharply after loss of lateral resistance. Column with small amount of volumetric transverse reinforcement ratio would fail in shear manner. On the other hand, the column with high volumetric transverse reinforcement ratio would fail in a flexural manner with some degree of ductility.

Skeikh and Khory (1993) conducted tests on reinforced concrete columns subjected to cyclic lateral load and high axial load. The experimental results were compared with predicted value obtained from ACI-318 1983. The study revealed that maximum strength and ductility of reinforced concrete column increases with reducing spacing of transverse reinforcements and main reinforcements. The load capacity ratio of reinforced concrete column increases with peak strength but reduces the ductility. Parameters for required volumetric transverse reinforcement ratio to resist seismic action include spacing of transverse reinforcements, distribution of main reinforcements and also the load capacity ratio. They also suggested that the required transverse reinforcements in less severe seismic zone would be reduced.

Configurations of transverse reinforcements affect flexural behaviour of reinforced concrete column. Intermediate reinforcements benefit confined core concrete to resist buckling of main reinforcements. In addition, beam and slab provide restraint to enhance flexural strength of end section of reinforced concrete column. Flexural strength of reinforced concrete column reduces with span depth ratio.

ACI-318 (1989) did not consider the configurations of transverse reinforcements, load capacity and stub column effect. The required volumetric transverse reinforcement ratio according to ACI-318 may not be conservative to resist severe seismic action. The ACI-318 requirement was modified as follows,

$$A_{sv,c} = 0.45sd_c\left(\frac{A_g}{A_{cc}}-1\right)\frac{f_c}{f_{yt}} \geq 0.12sd_c\frac{f_c}{f_{yt}} \tag{2-69}$$

$$A_{sv} = \alpha_{con}\left[1+13\left(\frac{P}{P_o}\right)^5\right]\frac{\mu_\varphi^{1.15}}{29}A_{sv,c} \tag{2-70}$$

where $A_{sv,c}$ is required area of transverse reinforcement of ACI-318, A_{sv} is area of transverse reinforcement required in eq.(2-70), s is spacing of transverse reinforcement,

d_c is width of transverse reinforcement hoop measured from centreline, A_g is gross cross sectional area of concrete, A_{cc} is enclosed area of transverse reinforcement hoop, f_c is cylinder concrete strength, f_{yt} is yield strength of transverse reinforcement, P is axial load added on concrete column, P_o is axial load capacity, α_{con} is parameter of configuration of transverse reinforcement and μ_φ is curvature ductility.

Saatcioglu and Ozcebe (1989) carried out fourteen tests to investigate cyclic behaviour of reinforced concrete column. Axial load added to the reinforced concrete column deteriorates flexural behaviour. Closely spaced transverse reinforcements are effective to restrain the main reinforcements in reinforced concrete column. Flexural behaviour of reinforced concrete column can be increased with reduction of axial load. Biaxial lateral load added on reinforced concrete column specimen would reduce flexural strength of reinforced concrete column.

Wehbe et al (1999) conducted 4 experimental tests. The tests consisted of specimens with 40% to 60% volumetric transverse reinforcement ratio required according to American Association of State Highway and Transportation Officials *(*AASHTO). Axial load ratio added on specimens was relatively small, similar to loading capacity ratio of reinforced concrete column added on bridge structures (0.1 and 0.24 P/P_o). Volumetric transverse reinforcement ratio required in AASHTO is mainly designed to resist in severe seismic zone. The aim of Wehbe's project was to propose volumetric transverse reinforcement ratio required to resist in moderate seismic zone. The expression is given as follows,

$$A_{sv,w} = 0.1\mu_{\Delta}\sqrt{\frac{f_{c,n}}{f_c}}\left[0.12sd_c\frac{f_{c,n}}{f_c}\left(0.5+1.25\frac{P}{f_cA_g}\right)+0.13sd_c\left(\rho_{main}\frac{f_y}{f_{s,n}}-0.01\right)\right] \quad (2\text{-}71)$$

where $A_{sv,w}$ is required transverse reinforcement area proposed by Wehbe (1996), μ_{Δ} is displacement ductility, $f_{c,n}$=27.6MPa, f_c is concrete strength, s is spacing of transverse reinforcements, d_c is width of transverse reinforcements hoops measured from centreline of reinforcement hoops, P is axial load, A_g is gross area of reinforced concrete specimen, ρ_{main} is main reinforcement ratio, f_{yt} is yield strength of transverse reinforcements and $f_{s,n}$=414MPa.

Lam et al (2003) carried out nine tests to investigate shear span depth ratio, configuration of transverse reinforcements and high axial load ratio. Drift capacity of reinforced concrete column with 90º hooks of reinforcement hoops was reduced to 40% of specimens having reinforcement hoops with 135º hook.

Xiao and Zhang (2008) conducted fourteen reinforced concrete specimens with high axial load ratio to investigate the configuration of transverse reinforcements, volumetric transverse reinforcement ratio and shear span depth ratio. Increasing the axial load ratio increases shear capacity but reduces ductility of reinforced concrete specimens. Therefore, it is necessary to limit the axial load capacity ratio of reinforced concrete column for seismic resistance.

2.6.3 Plastic Hinge Length

Lateral deflection of reinforced concrete column consists of flexural deflection, bond slip rotation and shear deformation. Curvature distribution along a reinforced concrete column is shown in Figure 2-15. Flexural deflection can be calculated as the integration of curvature profile along height of column, but the assumption of plane section remains plane is not valid. This is attributed to an uneven distribution on flexural and shear cracks and plastic curvature near the base of column. When reinforcements in reinforced concrete column are subjected to cyclic loading, bonding between reinforcements and concrete deteriorated at the base of column. Slippage of reinforcements in reinforced concrete column induces base rotation along height of reinforced concrete column. Based on the above, it would be better to assume that the plastic deformation of reinforced concrete column was induced from plastic rotation along certain height from base of the column. Plastic deflection is defined by the following equation, see Figure 2-18.

$$\Delta_p=(\varphi_u-\varphi_y)L_p(L-0.5L_p) \qquad (2\text{-}72)$$

where Δ_p is plastic deflection, φ_u is ultimate curvature, φ_y is yield curvature, L_p is plastic hinge length and L is height of column.

Park et al (1982) assumed that the L_p was equal to 0.4h where h is the width of column. The plastic hinge length of reinforced concrete column was related to height of concrete column and diameter of main reinforcements, (Priestley and Park 1987). The equation is given as follows

$$L_p=0.08L+6\phi_{main} \qquad (2\text{-}73)$$

where L_p is plastic hinge length, L is height of column and ϕ_{main} is diameter of main reinforcements.

Plastic hinge length varies during the loading stage prior to reaching peak strength of column, see Figure 2-18, (Saatcioglu and Razvi 1999). Flexural strength of reinforced concrete column is reduced after reaching peak deflection. Curvature profile along height of the reinforced concrete column was reduced. Plastic hinge length remains constant after reaching peak deflection. It is defined as the height of column minus the height of column between point of contra-flexure and yield moment location along moment profile at peak moment stage.

Bae and Bayrak (2008) relates the plastic hinge length to axial load capacity ratio, area of tensile main reinforcements and shear span depth ratio by carrying out non-linear least square analysis. Plastic hinge length increases with axial load, shear-span depth ratio and area of tensile main reinforcements. A sectional analysis along height was conducted to compute moment curvature. Plastic hinge length is defined as the distance from 0.25h to the location that the compressive strain was equal to yield strain of main reinforcements in compression. It is assumed that 0.25h is the section with little damage due to stub column effect. Expression of plastic hinge length is shown below,

$$\frac{L_p}{h} = \left(\frac{0.3P}{P_o} + \frac{3A_{st}}{A_g} - 0.1 \right) \frac{L}{h} + 0.25 \geq 0.25 \qquad \text{(2-74)}$$

where L_p is plastic hinge length, h is width of reinforced concrete column section, P is axial load, P_o is axial load capacity, A_{st} is main reinforcements in tension, A_g is gross sectional area and L is height of reinforced concrete column.

2.6.4 Deflection of Reinforced Concrete Column

Reinforced concrete column subjected to lateral load consists of flexural, bond slip and shear behaviours. When reinforced concrete column is in the elastic stage, flexural deflection dominates the total deflection. When reinforced concrete column is in the post-peak range, plastic deflection induces from plastic rotation in plastic hinge region and bond slip from reinforcements and concrete. The expression is given as follows

$$\Delta=\Delta_y+\Delta_p \tag{2-75}$$

where Δ is deflection, Δ_y is yield deflection and Δ_p is plastic deflection.

2.6.4.1. Elastic Deflection

Response of reinforced concrete column when subjected to lateral loading consists of flexural, bond slip and shear behaviour. The expression is given as follows,

$$\Delta_y=\Delta_{fy}+\Delta_{by}+\Delta_{sy} \tag{2-76}$$

where Δ_y is yield deflection, Δ_{fy} is flexural yield deflection, Δ_{by} is bond slip yield deflection and Δ_{sy} is shear yield deflection.

Flexural deflection of reinforced concrete column is calculated by integrating curvature profile along the height of reinforced concrete column.

$$\Delta_{fe}=\int_0^L \varphi z dz=\frac{\varphi L^2}{3} \tag{2-77}$$

where Δ_{fe} is flexural deflection in elastic stage, φ is curvature of reinforced concrete column along height profile, z is distance measured from tip of reinforced concrete column to the calculated point and L is height of reinforced concrete column.

Bond slip of reinforced concrete column is related to slippage of reinforcements and extension of main reinforcements. For reinforced concrete column subjected to lateral force, only tensile reinforcements slip. Bond slip is related to diameter of reinforcements, concrete strength, stresses in main reinforcements. Bond strength between concrete and main reinforcements is referred to Calderone's model (Calderone et al 2000). Bond slip is calculated based on ratio of slippage of main reinforcements about neutral axis. Calculation of bond slip is given as follows,

$$L_{ae} = \frac{f_s \phi_{main}}{4 f_{be}} \tag{2-78}$$

$$f_{be} = \sqrt{f_c} \tag{2-79}$$

$$u_t = \int \varepsilon_s dz = \frac{\varepsilon_s L_{ae}}{2} \tag{2-80}$$

$$\theta_{slip} = \frac{u_t}{h-c} \tag{2-81}$$

$$\Delta_{slip} = \theta_{slip} L \tag{2-82}$$

where f_s is main reinforcements stress in the end section, ϕ_{main} is diameter of main reinforcements, f_{be} is bond strength, f_c is unconfined concrete strength, ε_s is main reinforcement strain, u_t is bond slip of main reinforcements, h is is effective depth of concrete section, c is the neutral axis of concrete section, L is height of reinforced concrete column, θ_{slip} is slippage rotation at the base of reinforced concrete column and Δ_{slip} is bond slip deflection due to bond slip of main reinforcements.

For short reinforced concrete column, shear deflection is critical component. Shear strain is related to shear modulus of concrete and shear area of reinforced concrete column, (Park 1975) When reinforced concrete column is in elastic stage, the shear deflection is calculated as follows,

$$\Delta_{sy} = \frac{VL}{0.4E_{con}0.74A_g} \quad (2\text{-}83)$$

where E_{con} is modulus of concrete column, A_g is gross sectional area, V is shear force, L is height of column, and Δ_{sy} is shear deflection.

2.6.4.2. Plastic deflection

Plastic deformation of reinforced concrete column can be determined in two ways. Some researchers (Park 1975, Priestley et al 1996) considered that plastic deflection in reinforced concrete members is due to formation of plastic rotation at the end section. The plastic rotation consists of plastic curvature along plastic hinge zone and bond slip rotation at the end section. Shear deflection is not included in the deflection of reinforced concrete column when shear span depth ratio is larger than 4. Flexural deflection in plastic stage is given as follows,

$$\Delta_{fp} = \left(\varphi_u - \varphi_y\right) L_p \left(L - \frac{L_p}{2}\right) \quad (2\text{-}84)$$

where Δ_{fp} is flexural plastic deflection, L_p is the equivalent plastic hinge length, L is length of the cantilever, φ_u is ultimate curvature and φ_y is yield curvature.

Paulay and Priestley (1992) proposed an empirical formula of plastic hinge length related to height of column, diameter of main reinforcements and yield strength of main reinforcements which is independent on the axial load level and amount of transverse reinforcements. The formulation is given as follows,

$$L_p=0.08L-0.022\phi_{main}f_y \tag{2-85}$$

where L_p is plastic hinge length, L is height of reinforced concrete column, ϕ_{main} is diameter of main reinforcements and f_y is the yield strength of reinforcements.

The calculated plastic hinge length is approximately equal to half the width of reinforced concrete column section (L_p=0.5h), where h is width of column.

Skeikh et al (1993), conducted experiments to study the cyclic behaviour of reinforced concrete columns. The plastic hinge length is equal to width of reinforced concrete section. It is independent on height of column, main reinforcement diameter, yield strength of main reinforcements and transverse reinforcements and concrete strength.

Baker and Amarkone (1964) proposed two different formulas for the plastic hinge length in reinforced concrete column with unconfined and confined concrete respectively. The formulas related to unconfined and confined concrete are given as follows,

For reinforced concrete column in unconfined concrete

$$L_p = k_{p1}k_{p2}k_{p3}\left(\frac{L}{d}\right)^{\frac{1}{4}} \tag{2-86}$$

For reinforced concrete column confined by transverse reinforcements

$$L_p = 0.8k_{p1}k_{p3}\left(\frac{L}{d}\right)c \tag{2-87}$$

where k_{p1} is 0.7 for mild steel and 0.9 is for cold drawn working steel. k_{p2}= 1+0.5P/P_o (2-88)

k_{p3}: 0.6 for f'_c is 35.2MPa and 0.9 for f'_c is 11.7MPa

where P is axial compression load, P_o is axial compressive strength of member under concentric load, d is effective depth of member, L is length of reinforced concrete column and c is the neutral axis depth at ultimate moment.

2.6.4.2.1 Flexural deflection

Razvi and Saatcioglu (1999) investigated continuous change in plastic deflection of reinforced concrete column subjected to lateral load. Plastic hinge length was related to flexural behaviour of reinforced concrete column and defined by the following expression;

$$L_p = \left(1 - \frac{M_y}{M}\right) L \qquad (2\text{-}89)$$

where L_p is plastic hinge length, M is applied moment, M_y is yield moment, and L is height of reinforced concrete column.

Determination of plastic hinge length is referred to Figures 2-17 and 2-18. Yield moment is defined as yielding of main reinforcements. Plastic hinge length is then defined as the ratio of yield moment to the first peak moment times the height of reinforced concrete column when the moment strength is increased in the post peak range.

Xiao and Zhang (2008) also proposed plastic hinge length of reinforced concrete column. They proposed that plastic hinge length is related to reinforced concrete column section and axial load level. The expression is as follows,

$$L_p = \left(1 + \frac{0.1L}{h}\right)\left(1 - 1.2\frac{P}{f_c A_g}\right)h \qquad (2\text{-}90)$$

where L_p is plastic hinge length, L is the height of reinforced concrete column, P is axial force, h is depth of reinforced concrete column, f_c is unconfined concrete strength and A_g is gross sectional area of reinforced concrete column.

2.6.4.2.2 Bond slip deflection

When the end section is in the plastic stage, bond strength between concrete and main reinforcements deteriorates. Bond strength of main reinforcements was dropped by half of its elastic bond strength, see Figures 2-19-2-22. (Lehman and Moehle 2000)

$$l_{by} = \frac{f_y \phi_{main}}{4 f_{b,e}} \qquad (2\text{-}91)$$

$$l_{bp} = \frac{\left(f_s - f_y\right)\phi_{main}}{4 f_{b,p}} \qquad (2\text{-}92)$$

$$f_{b,p} = 0.5\sqrt{f_c} \qquad (2\text{-}93)$$

$$u_t = \int \varepsilon_s dx = \frac{\varepsilon_y l_{by}}{2} + \frac{\left(\varepsilon_s + \varepsilon_y\right)}{2} l_{bp} \qquad (2\text{-}94)$$

where l_{bp} is anchorage length in plastic stage, l_{by} is anchorage length in yield condition, u_t is bond slip, f_s is steel stress, f_y is yield strength of reinforcements, ϕ_{main} is diameter of main reinforcements, $f_{b,p}$ is bond strength of reinforcements in plastic stage, f_c is concrete strength, ε_y is yield strain of reinforcements, ε_s is the current strain of main reinforcements and $f_{b,e}$ is bond strength of reinforcements in elastic stage.

In general, bond slip of reinforced concrete column in plastic stage is similar to the one in elastic stage.

Alsiwat and Saatcioglu (1992) examined bond slip of reinforced concrete column when subjected to lateral load. They divide the bond slip condition into four stages such as, elastic stage, yield plateau, strain hardening and pull out zone. Pullout zone is a stage when concrete cover spalls and the main reinforcements are in constant stress and strain within a certain length. Pullout of reinforcements is prevented by increasing the lap length, see Figure 2-23.

In Elastic Stage,

$$f_{by} = \frac{f_y \phi_{main}}{4 l_d} \tag{2-95}$$

$$l_d = \frac{440 f_y A_s}{K_d \sqrt{f_c}\, 400} \geq 300 \tag{2-96}$$

$$l_e = \frac{f_s \phi_{main}}{4 f_{b,e}} \tag{2-97}$$

where ϕ_{main} is diameter of main reinforcements, f_y is yield strength of main reinforcements, f_{by} is bond strength in yield stage, f_c is concrete strength of unconfined concrete, l_d is development length, A_s is area of main reinforcements, K_d is three times diameter of main reinforcements and l_e is bond slip of tensile main reinforcements in elastic stage.

For yield plateau and strain hardening,

Bond strength beyond yield strength of main reinforcements is related to the frictional force resisted by rib of main reinforcements. The expression is shown as follows,

$$f_{b,p} = \left(5.5 - 0.07\frac{s_{lu}}{h_{lu}}\right)\sqrt{\frac{f_c}{27.6}} \tag{2-98}$$

$$L_{bp} = \frac{\left(f_s - f_y\right)\phi_{main}}{4 f_{b,p}} \tag{2-99}$$

where s_{lu} is the spacing of lugs of main reinforcements, h_{lu} is height of lugs of main reinforcements, ϕ_{main}, is diameter of main reinforcements, f_c is concrete strength, and $f_{b,p}$ is bond strength of main reinforcements.

$$u_t = \int \varepsilon_s dx = \frac{\varepsilon_y l_{by}}{2} + \frac{\left(\varepsilon_s + \varepsilon_y\right)}{2} l_{bp} + \varepsilon_s l_{bc} \tag{2-100}$$

where l_{bc} is the length of pull out zone, ε_s is steel strain, ε_y is yield strain of steel reinforcements, l_{by} is an elastic lapped length and l_{bp} is an elastic lapped length.

Bond slip rotation is defined similar to Lehman and Moehle's expression.

2.6.4.2.3 Shear deflection

When concrete cracks during lateral load, shear deformation is increased because the cracks reduce the shear rigidity. Therefore, shear deflection is not related to shear modulus of uncracked concrete. Paulay and Priestley (1992) proposed using truss mechanism to estimate the shear deflection by the following equations,

$$K_{v,45} = \frac{\rho_s}{1+4n\rho_s} E_s bd \tag{2-101}$$

$$\Delta_{shear} = V\frac{L}{K_{v,45}} E_s bd \tag{2-102}$$

where $K_{v,45}$ is shear stiffness, ρ_s is volumetric transverse reinforcement ratio, n is axial load capacity ratio, E_s is Young's modulus of main reinforcements, b is width of section, d is depth of section, V is shear force and Δ_{shear} is shear deflection.

It is difficult and complicated to calculate shear deflection by non-linear analysis. Therefore, shear deflection was formulated by semi-empirical method by relating to axial load capacity, flexural and shear conditions (Xiao and Zhang 2008). The formulation is given as follows,

$$\Delta_{shear} = \left(\frac{0.3}{1+\dfrac{\rho_s f_{yt}}{\rho_{main} f_y}} + \frac{1}{\sqrt{\lambda}} + 0.5n \right) \frac{VL}{G_{eq} A_g} \tag{2-103}$$

where Δ_{shear} is shear deflection, ρ_s is volumetric transverse reinforcement ratio, and ρ_{main} is main reinforcement ratio, λ is shear span depth ratio, n is axial compressive stress ratio (n=0.5 when n>0.5), L is height of reinforced concrete column, f_y is yield strength of main reinforcements, f_{yt} is yield strength of transverse reinforcements, V is shear force, G_{eq} is shear modulus of concrete being equal to $0.4E_{con,}$ and A_g is gross area of reinforced concrete column section.

Priestley et al (1994) have demonstrated that shear deflection at any stage is directly proportional to shear deflection corresponding to yield of main reinforcements. Shear deflection when first yield of main reinforcements is given in the following equations.

$$\Delta_{shear,y} = \frac{V_y L}{0.4E_{con} 0.9A_g} \frac{E_{con} I_g}{M_y / \varphi_y} \tag{2-104}$$

$$\Delta_{shear} = \frac{V}{V_y} \Delta_{shear,y} \tag{2-105}$$

where $\Delta_{shear,\ y}$ is shear deflection when main reinforcements is yielded, Δ_{shear} is shear deflection in post-peak stage, V_y is yield shear strength, L is height of reinforced concrete column, A_g is area of reinforced concrete column section, E_{con} is modulus of elasticity of concrete, I_g is second moment area of inertia of reinforced concrete column, M_y is yield moment, φ_y is yield curvature and V is shear force added on the reinforced concrete column.

2.7 Stirrup Detailing for Lateral Load

Saatcioglu and Ozcebe (1989) conducted experiments to investigate structural behaviour of reinforced concrete column with intermediate crossties having 90º end hooks in one end. The intermediate crosstie is extended to 10 times diameter of transverse reinforcements. Their study has indicated that structural behaviour of the column having intermediate crossties using 90º end hook is similar to the one with 135º end hook.

Vintzileou and Stathatos (2007) assessed configuration of transverse reinforcements detailed according to Eurocode 8. Configuration is a crucial factor in providing ductility of reinforced concrete column. If no intermediate crosstie is provided to reinforcement hoops, lateral strength and ductility of reinforced concrete column is limited. They concluded that reinforcement hoops are used in low to moderate seismic zone. When intermediate transverse reinforcements are added, lateral strength and ductility of reinforced concrete columns is then increase.

2.8 Transverse Reinforcement in Hong Kong

Transverse reinforcements in Hong Kong are mainly designed to prevent buckling of main reinforcements. Spacing and configuration of transverse reinforcements become less restricted as compared to the one designed in severe seismic zone. In Hong Kong, main reinforcements of reinforced concrete column are normally designed as 40mm diameter bars. So the minimum diameter of transverse reinforcements is about 10mm which is one fourth of main reinforcement diameter. Maximum spacing of transverse reinforcements in reinforced concrete column is 300mm. End hook of reinforcement hoops is 90º. BS8110 (1985) states that restrained bar should be provided in each alternative main reinforcements. There is no definition on restrained bars in BS 8110 (1985). Local engineers designed configuration of transverse reinforcements of reinforced concrete columns which maximize concreting area in core concrete by providing short crossties to restrain main reinforcements.

2.9 Hysteresis Behaviour of Reinforced Concrete Column

Two methods in analyzing reinforced concrete column subjected to cyclic loading are based on stress-strain behaviour of materials and hysteresis model. In this study, only the hysteresis model will be discussed. Hysteresis model consists of elastic stiffness, strain hardening of reinforced concrete member, unloading stiffness and reloading stiffness.

Takeda et al (1970) proposed a hysteresis model to predict cyclic behaviour of reinforced concrete column and there are 7 rules with reference to Figure 2-24. Behaviour of reinforced concrete column is divided into three segments under monotonic load, see Figure 2-24a. The segments consists of several parameters such as stiffness of uncracked concrete, stiffness of yield member and cracked concrete and yield strength and ultimate stiffness. When the reinforced concrete column is uncracked, it is considered as elastic.

If a reinforced concrete column is subjected to a force greater than the negative cracking force, it deflects according to the negative cracked stiffness, see segment 4 in Figure 2-24b. If deflection in unloading stage is smaller than the maximum excursion point, it is unloaded according to segment 5 of Figure 2-24b. This means the unloading force is pointing towards the positive cracking moment in the unloading stage. When reinforced concrete column is reloaded in the positive direction, deformation is towards previous maximum excursion point in the positive direction. When reloading displacement is smaller than the maximum excursion in the whole loading stage, the loading deformation would be similar to segment 4 and 5 in Figure 2-24b. Unloading stiffness of reinforced concrete column is given in Eq. 2-98 and is shown in segment 4 in Figure 2-24c.

The unloading stiffness is given as follows,

$$K_{un} = K_y \left(\frac{\Delta_y}{\Delta_m} \right)^{0.4} \qquad (2\text{-}106)$$

where K_{un} is unloading stiffness, K_y is yield stiffness, Δ_y is yield displacement and Δ_m is the maximum excursion point in the unloading stage.

When unloaded at a deflection larger than the yield deflection, a new unloading stiffness is introduced as shown in segment 11 of Figure 2-24c. When reloaded again in the positive direction, lateral force in load deflection relationship is pointing towards maximum excursion point in the positive direction. When unloaded again in the negative direction, the unloading stiffness is then towards maximum excursion point in the negative direction.

When unloaded in the negative direction being smaller than maximum excursion point in previous loading cycles in both directions, the unloading stiffness in the negative direction is equal to 70% of the previous unloading stiffness.

Takeda's model provides accurate approximation to hysteresis behaviour of reinforced concrete column but the rules are complicated and difficult to use.

Saiidi (1982) proposed a Q-Hyst model to simulate hysteresis model subjected to lateral load. There are four rules in this model such as initial stiffness, strain-hardening, unloading and reloading stiffness. The initial stiffness is considered in the elastic stage.

Plastic stiffness is related to confined concrete and main reinforcements. The unloading stiffness deteriorates in the unloading stage due to the cracking of confined concrete and crushing of unconfined concrete, see Figure 2-25. The unloading stiffness is represented by the following equation,

$$K_{un} = K_y \left(\frac{\Delta_y}{\Delta_m} \right)^{0.5} \tag{2-107}$$

where K_{un} is unloading stiffness of reinforced concrete column, K_y is yield stiffness of reinforced concrete column, Δ_y is yield displacement and Δ_m is deflection at maximum excursion point of the whole cycle in both directions.

Umemura et al (1998) modified Takeda's model (1970) by considering the deteriorations of force in hysteresis model in reinforced concrete column. When a reinforced concrete column is loaded cyclically, strength deteriorates in each cycle. Deterioration of strength in each cycle is related to axial load capacity and volumetric transverse reinforcement ratio and given by the following equations. The expression of deterioration was shown as follows,

$$\Delta_{r2} = \Delta_{r1} \left(1 + \chi_r \frac{|\Delta_m|}{|\Delta_y|} \right)^{0.5} \tag{2-108}$$

$$\chi_r = 0.12n - 0.11\rho_s + 0.068 \tag{2-109}$$

where Δ_{r2} is increased deformation of pointed peak, Δ_{r1} is deformation of previous pointed peak, Δ_m is deflection of previous peak on opposite side, χ_r is stiffness degradation index, n is axial loading capacity and ρ_s is volumetric transverse reinforcement ratio. The notations on deformation are shown with reference to Figure 2-26.

Phan et al (2007) modified Q-hyst model proposed by Saiidi (1982) as O-hyst model. Unloading stiffness of reinforced concrete column is assumed to continue to one third of the yield load in the other direction rather than zero as shown in Figure 2-27.

2.10 Damage of Reinforced Concrete Column

Behaviour of reinforced concrete column under monotonic lateral load is different from the one subjected to cyclic loading. For instance, reinforced concrete column fails in flexural manner under monotonic loading but the column may fail in shear or bond slip under cyclic loading. In order to assess the structural behaviour subjected to cyclic load, damage model is applied to quantify damage of reinforced concrete column when subjected to cyclic loading.

Park and Ang (1985) quantified damage level by relationship lateral deflection and dissipated energy under cyclic loading. Damage level is related to crack width of reinforced concrete column and define in Table 2-1. Damage is influenced by maximum excursion and energy dissipation during cyclic loading. Expression related to damage is given as follows,

$$D = \frac{\Delta_m}{\Delta_u} + \frac{\beta_{Park}}{F_y \Delta_u} \int dE \qquad \text{(2-110)}$$

$$\beta_{Park} = \left(-0.447 + 0.073 \frac{L}{d_s} + 0.24 nos + 0.314 \rho_{main} \right) 0.7^{\rho_s} \tag{2-111}$$

where Δ_m is maximum inelastic deformation in the whole cycle, Δ_u is ultimate deformation which defined as the deformation with 20 % reduction in strength of reinforced concrete column, β_{Park} is degradation parameter, F_y is lateral force in yield condition, E is hysteresis energy dissipated during the loading cycle, L is height of column, d_s is depth of column, nos is number of cycle and ρ_{main} is main reinforcement ratio. Threshold value on reinforced concrete column to be repaired was defined as 0.4.

Chung et al (1987) proposed a damage model based on strength degradation. The model is similar to Miner's model. Miner (1945) related strength degradation with displacement. Chung's model is related to maximum excursion of displacement or curvature and dissipation of energy during cyclic loading.

$$n_{f.i} = \left(M_i - M_{f,i} \right) / \Delta M_i \tag{2-112}$$

$$D = \sum_i \left(w_i^+ \frac{n_i^+}{n_{f,i}^+} + w_i^- \frac{n_i^-}{n_{f,i}^-} \right) \tag{2-113}$$

$$w_i^+ = \frac{\sum_{j=1}^{n_i^+} k_{ij}^+}{n_i^+ k_{i,ave}^+} \frac{\varphi_i^+ + \varphi_{i-1}^+}{2\varphi_i^+} \tag{2-114}$$

where D is damage index, $n_{f,i}$ is the number of cycle to failure, w_i^+ is weighting coefficient on damage at curvature i in positive direction, w_i^- is weighting coefficient on damage at curvature i in negative direction, n_i^+ is number of cycle reaching curvature in positive loading direction, n_i^- is number of cycle reaching curvature in negative loading direction, n_{fi}^{+} is number of cycle reaching curvature under failure in positive loading direction, n_{fi}^{-} is number of cycle reaching curvature under failure in negative loading direction, n_{fi} is number of cycle reaching curvature under failure, $k_{i,j}^{+}$ is the stiffness of a specimen cycled to failure to curvature i, φ_i^{+} is curvature of column at the i^{th} in positive direction, φ_{i-1}^{+} is curvature of column at the $i\text{-}1^{th}$ in positive direction, M_j is moment at curvature j, M_{fi} is moment subjected to monotonic loading, ΔM_i is deviated moment between moment subjected to projected moment based on the strain hardening and $k_{i,ave}^{+}$ is moment subjected to monotonic loading and and subscript j was the j^{th} cycle at curvature i and average stiffness of a specimen cycled to failure at curvature i.

The damage of reinforced concrete column is threshold on repairable when D<0.01

Kunnath et al (1997) proposed a model to assess fatigue failure of reinforced concrete column. Fatigue failure is defined as a structure to deform after n number of cycle at a particular displacement. It modifies the fatigue plastic strain model proposed by Mander (1994) to form a fatigue deflection model. The expression of fatigue model is shown as follows,

$$N_{f.i} = 2\left(\frac{\theta_i}{10.6}\right)^{3.51} \tag{2-115}$$

$$D = \sum \frac{n_{hfi}}{N_{fi}} \tag{2-116}$$

where θ_i is the drift ratio of reinforced concrete member, N_{fi} is number of complete cycle causing failure at a particular drift ratio i, n_{hfi} is the number of half completed cycle at a particular drift ratio in the cyclic loading and D is damage index.

Hindi and Sexsmith (2001) proposed a damage model based on sophisticated nonlinear analysis. The expression in describing the model is as follows,

$$D_n = \frac{\left(A_o - A_n\right)}{A_o} \tag{2-117}$$

where D_n is damage at the n^{th}-times cycle of reinforced concrete column in cyclic loading test, A_o is strain energy in the reinforced concrete member subjected to monotonic loading and A_n is strain energy of reinforced concrete column reminding after n^{th} cycle of lateral loading. Definitions of A_o and A_n are referred to Figures 2-28 and 2-29.

Khashee (2005) proposed a damage index for reinforced concrete columns. It is related to energy dissipation and is modified from Kunnath and Jenne's model (1994). Khasee's model is expressed by the following equation,

$$D_{KJ} = 1 - \frac{K_{\sec}}{K_e} = 1 - \frac{\left(F_y + pK_e\left(u_m - u_y\right)\right)}{F_y}\frac{1}{\mu_m} = \left(1-\chi\right)\left(1-\mu_m^{-1}\right) \tag{2-118}$$

$$D_p = \frac{D_{KJ}}{D_{KJ,u}} = \frac{\left(1-\mu_m^{-1}\right)}{\left(1-\mu_u^{-1}\right)} \tag{2-119}$$

where D_{KJ} is damage index proposed by Kunnath and Jenne (1994), K_{sec} is secant stiffness at maximum excursion in cyclic loading, K_e is elastic stiffness, F_y is yield load, χ is strain hardening index, u_m is displacement at maximum excursion point, u_y is yield displacement,

μ_m is displacement ductility at maximum excursion point, μ_u is ultimate displacement ductility and D_p is are and the damage index proposed by Khashee (2005).

Kim et al (2005) conducted non-linear finite element analysis on reinforced concrete column subjected to lateral load. Their damage index model is related to fatigue of reinforced concrete structure. There are two damage models in quantifying the damage on concrete and reinforcements respectively. This model gives reasonable quantification of reinforced concrete column. Fatigue model of reinforcements and concrete are based on Coffin-Manson equation (Mander et al 1994) and Kakuta's model (Kakuta et al 1982).

For reinforcement model

$$\varepsilon_{ap} = 0.0777\left(\frac{N_{2fr}}{1.5s_k}\right)^{-0.486} \tag{2-120}$$

For concrete model

$$\log\frac{N_{2fc}}{2s_k} = \begin{cases} \dfrac{1}{\beta_{Kim}}\left[1-\dfrac{\left(\varepsilon_{uc}-\varepsilon_{\min}\right)^2-\left(\varepsilon_{uc}-\varepsilon_{\max}\right)^2}{\left(\varepsilon_{uc}-\varepsilon_{\min}\right)^2}\right]; \varepsilon_{\max} < 0.7\varepsilon_{uc} \\ \dfrac{0.09\varepsilon_{cu}\left(\varepsilon_{\max}-\varepsilon_{\min}\right)}{\left(\varepsilon_{cu}-\varepsilon_{uc}\right)\beta_{Kim}\left(\varepsilon_{cu}-\varepsilon_{\min}\right)}; \varepsilon_{\max} \geq 0.7\varepsilon_{uc} \end{cases} \tag{2-121}$$

where ε_{ap} is the average plastic strain on minimum strain by number of cycle, ε_{min} is maximum strain by number of cycle, ε_{max} is maximum strain by number of cycle, ε_{uc} is peak strain of unconfined concrete, ε_{cu} is ultimate strain of confined concrete, N_{2fr} is number of complete cycles to failure for reinforcing bars, s_k is strength incremental factor between confined concrete (f_{cc}) and unconfined concrete (f_{co}), β_{Kim} is material constant equal to 0.0588and N_{2fc} is number of complete cycles to failure for concrete.

Tensile damage index is related to stress in main reinforcements. When tensile strain in main reinforcements reached ultimate strain of reinforcements, damage index is 0.75. Damage index becomes 0.4 when reinforcement strain is at the yield plateau. Tensile damage index is defined as follows,

$$DI_{tensile} = 1.2\left[\frac{\varepsilon_{ts}}{2\left(1-0.3\sum\frac{1}{N_{2fr}}\right)\varepsilon_{tu}}\right]^{0.67} \tag{2-122}$$

where ε_{ts} is tensile strain at the analysis, ε_{tu} is ultimate tensile strain of reinforcements, N_{2fr} is the number of half cycle in tensile stage and $DI_{tensile}$ is the damage index in tensile stage.

Compressive damage index is defined as 0.75 when compressive strain reaches ultimate strain of concrete. While the compressive strain is at the peak strain of concrete, the index is 0.4 and concrete at this stage is considered as irrepairable. Compressive damage index is defined as follows,

$$DI_{compressive} = 1-\left(1-0.3\sum\frac{1}{N_{2fc}}\right)\left(\frac{2\varepsilon_{cu}-\varepsilon_{cs}}{2\varepsilon_{cu}}\right)^{2} \tag{2-123}$$

where $DI_{compressive}$ is damage index in compressive state, ε_{cu} is ultimate compressive strain, ε_{cs} is compressive strain in the analysis, N_{2fc} is the number of half cycle in compression.

Ranf et al (2006) conducted an experiment study with six specimens. The main difference in the tests is cyclic loading pattern. There are eight damage stages, such as significance of flexural cracking, significant spalling, residual cracking, bar buckling, hoop fracture, 20% loss of lateral load, 50% loss of lateral load and loss of axial load. Cumulative damage model is related to maximum excursion drift ratio and cumulative drift ratio of reinforced concrete column subjected to lateral load. Test data are obtained from specimens failed in flexural shear mode. Parameters in the damage model are calculated by least square analysis. The damage model is related to drift ratio and cumulative drift ratio in the form of,

$$D = \alpha_p \frac{\Delta_m}{L} + \beta_p \frac{\sum \Delta_p}{L} \tag{2-124}$$

where Δ_m is the maximum excursion point in the whole cyclic loading stage, Δ_p is the plastic deflection in each cycle, L is height of reinforced concrete column, D is the damage index, α_p is parameter of drift ratio at maximum excursion point and β_p is parameter of sum of plastic drift ratio.

The parameters α_p and β_p in eight stages are shown in Table 2-2

Erduran and Yakut (2007) proposed damage model in relation to deflection of reinforced concrete column. The damage model is related to three classes of configuration of transverse reinforcements. They are low, moderate and high ductility. Damage model is also influenced by slenderness of reinforced concrete column and yield strength of main reinforcements.

$$D = \begin{cases} \left(1 - e^{-\left(\frac{\Delta}{a_{EY}}\right)^{b_{EY}}}\right) 0.5\left(1 - \cos\frac{\pi\Delta}{c_{EY}}\right) / C_s / C_{fy} if\, \Delta \le c_{EY} \\ \left(1 - e^{-\left(\frac{\Delta}{a_{EY}}\right)^{b_{EY}}}\right) / C_s / C_{fy} if\, \Delta > c_{EY} \end{cases} \tag{2-125}$$

$$C_s = \frac{0.95}{21.12}\frac{L}{r_y} \tag{2-126}$$

$$C_{fy} = 0.4\frac{f_y}{439} + 0.6 \quad for \quad f_y \geq 220MPa \tag{2-127}$$

where D is damage index, Δ is deflection of reinforced concrete column, a_{EY}, b_{EY} and c_{EY} are shown in Table 2-3, L is height of column, r_y is radius of gyration in weak axis, f_y is yield reinforcement strength, C_s is correction factor on slenderness ratio, C_{fy} is correction factor on yield strength of main reinforcements.

There are two critical points in the damage model, such as yield displacement and ultimate displacement. Ultimate displacement is defined as displacement corresponding to 15% reduction of peak strength in the post peak range. There are four stages in damage model that are negligible, light, moderate and heavy damage. When crack width of reinforced concrete column is increased to 0.2, 1 and 2mm, reinforced concrete column is classified as negligible, light and moderate damage respectively. Erduran and Yakut (2007) assumed that the deflections under $0.2\delta_y$, $0.6\delta_y$ and $1\delta_y$ are related to 0.2, 1 and 2mm crack width. The corresponding damage index is 0.5%, 7.5% and 30% respectively. When deflection reaches yield deflection, the damage index is equal to 0.3. If the deflection is greater than the ultimate the deflection, the corresponding damage index will be 0.9.

The above model is only used for reinforced concrete column that is failed in flexural mode. Erduran and Yakut (2007) proposed a formula to assess the damage of reinforced concrete column which is failed under shear mode. Shear force capacity ratio is defined as shear force to shear capacity in flexural mode and it ranges from 0.55 to 1. Ultimate deflection of shear critical element is as follows,

$$\frac{\Delta_u}{\Delta_y} = -1.07\left(\frac{V_s}{V_f}\right)^2 + 2.4\left(\frac{V_s}{V_f}\right) - 0.3 \;\; \leq 1.00 \tag{2-128}$$

where Δ_u is ultimate deflection of shear critical failure of reinforced concrete column, Δ_y is yield deflection, V_s is shear strength capacity and V_f is flexural strength capacity.

If the shear capacity ratio is equal to 1, the corresponding damage index will be increased from 30% to 90%. This is attributed to brittle failure on shear critical reinforced concrete column. Expression for shear critical reinforced concrete column is adjusted by the following expression.

$$D = \begin{cases} \left(1 - e^{-\left(\frac{\Delta}{0.0065 C_s C_{fy} C_{sc}}\right)^4}\right) 0.5\left(1 - \cos\frac{\pi\Delta}{0.005}\right) & for\ \Delta \leq 0.005 \\ \left(1 - e^{-\left(\frac{\Delta}{0.0065 C_s C_{fy} C_{sc}}\right)^4}\right) & for\ \Delta > 0.005 \end{cases} \tag{2-129}$$

where D is damage index, Δ is deflection of reinforced concrete column, C_s is correction factor on slenderness ratio, C_{fy} is correction factor on yield strength of main reinforcements and C_{SC} is correction factor on shear capacity.

2.11 Summary

Stress-strain relationship of confined concrete has been studied by many scholars. It is, however, only applicable for specific type of reinforcement configurations. The main difference between confined and unconfined concrete is that confined concrete can provide higher strength and ductility through proper detailing of the transverse reinforcements. In particular, the reinforced concrete column with less amount of transverse reinforcements may be classified as unconfined.

For reinforced concrete column subjected to seismic loading, cyclic behaviour becomes critical. Hysteretic behaviour is related to ductility of reinforced concrete column and ductility is affected by the amount and configuration of transverse reinforcements.

Damage model is used to assess damage of reinforced concrete column after seismic action. Damage of a reinforced concrete column is related to crack width or shear strength reduction. There are two types of damage mode. One is related to fatigue of reinforced concrete column and the other is related to energy dissipation.

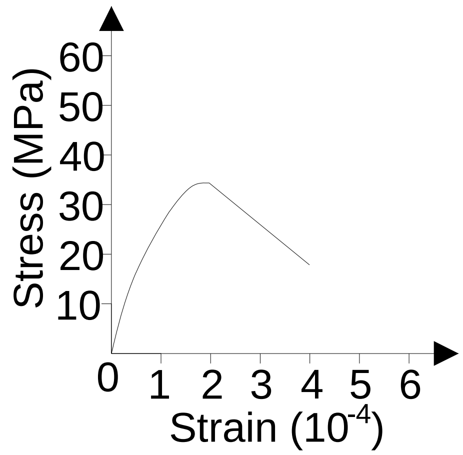

Figure 2-1: Typical Stress-strain Relationship of Unconfined Concrete

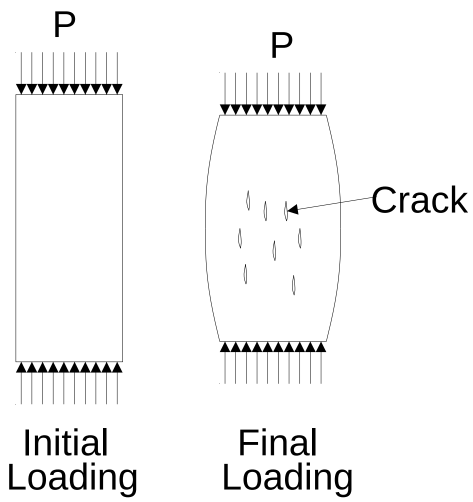

Figure 2-2 Bulging of Concrete Column

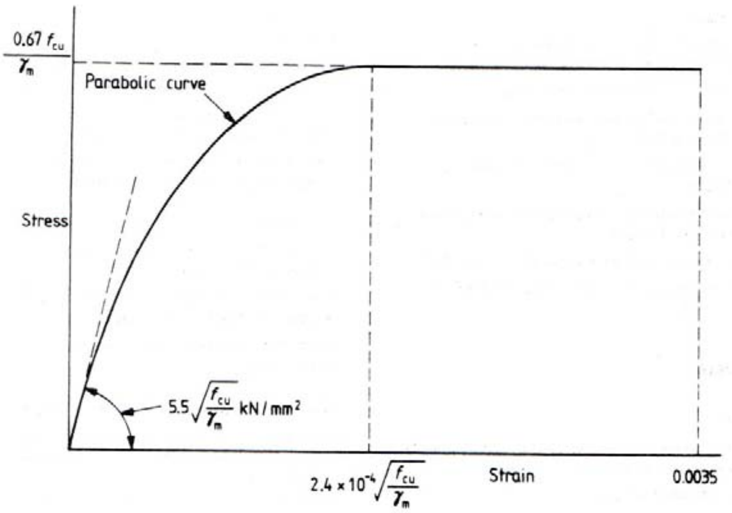

Figure 2-3 Typical Stress Strain Relationship in Design Code (Extracted from Code of Practice for the Structural Use of Concrete-1987)

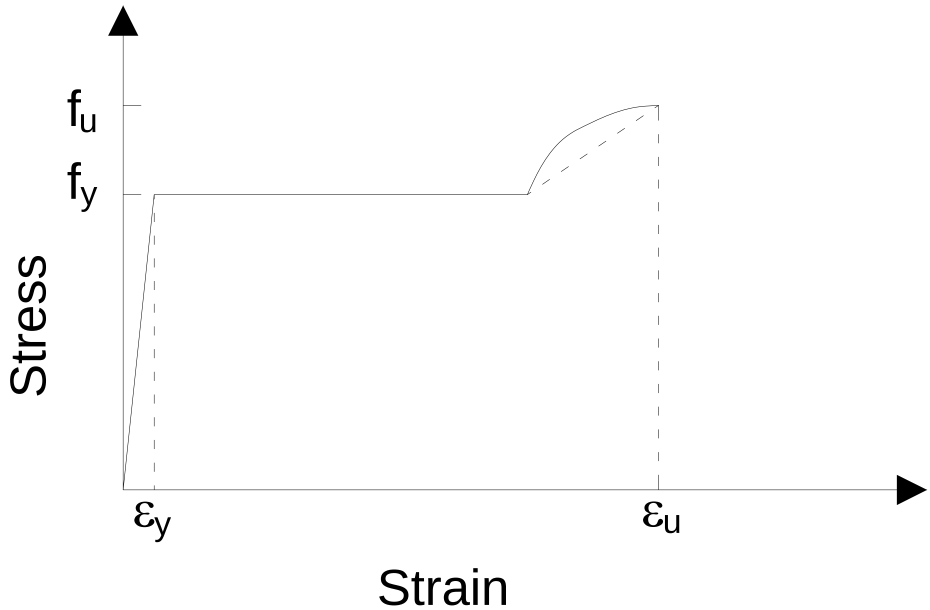

Figure 2-4 Typical Stress-Strain Relationship of Reinforcing Steel

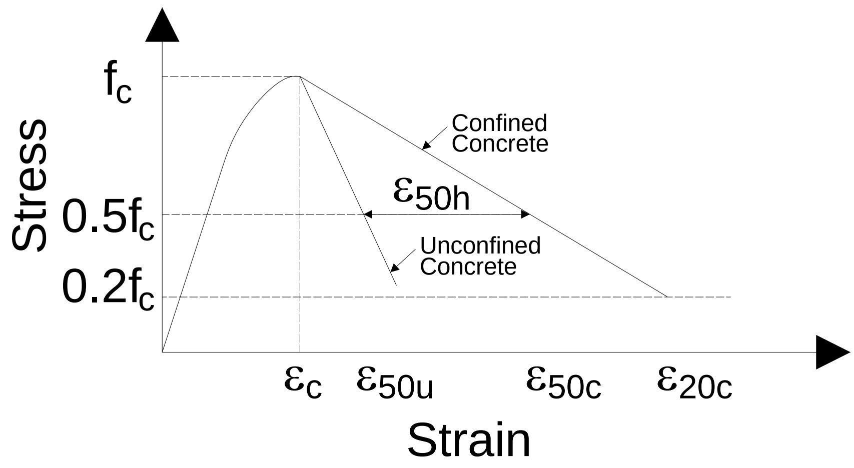

Figure 2-5 Stress-Strain Relationship of Confined Concrete in Kent and Park Model

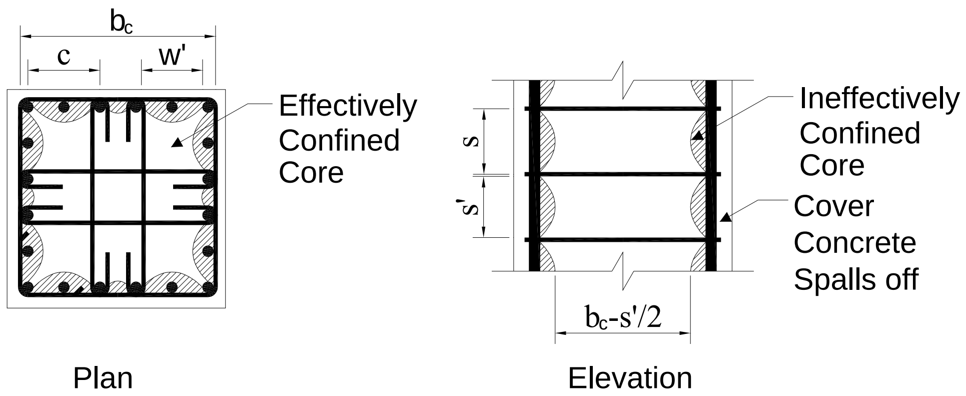

Figure 2-6 Effectively Confined Concrete Area

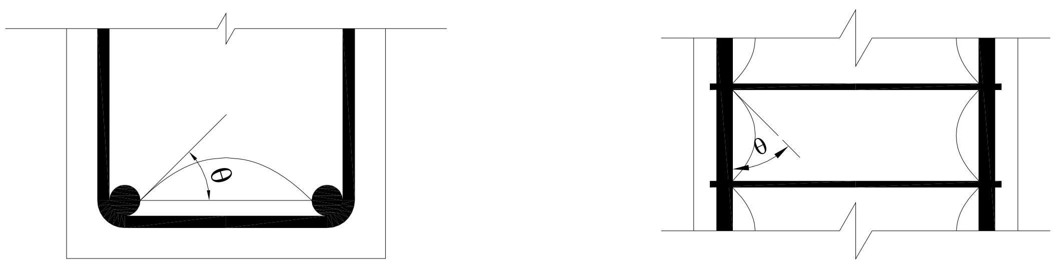

(a) Plan View (b) Elevation

Figure 2-7 Angle of Arch Action in Confined Concrete

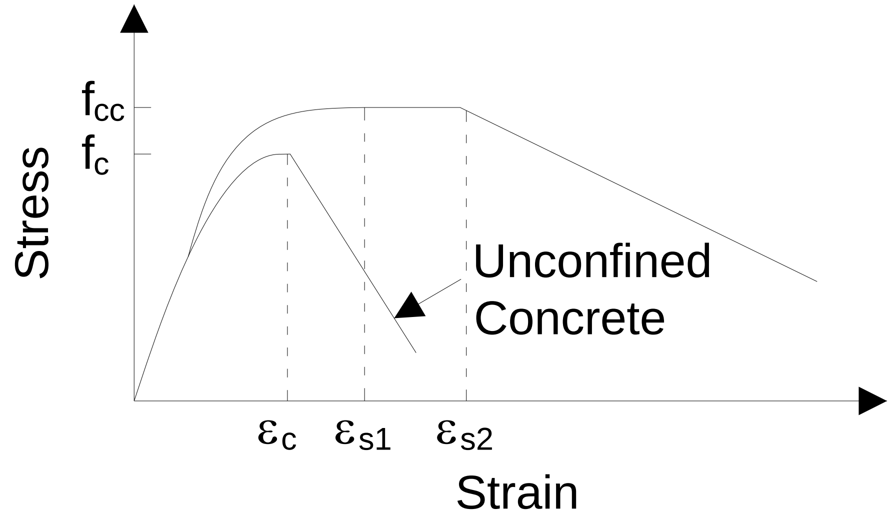

Figure 2-8 Stress-Strain Relationship of Confined Concrete in Skeikh's Model (1982)

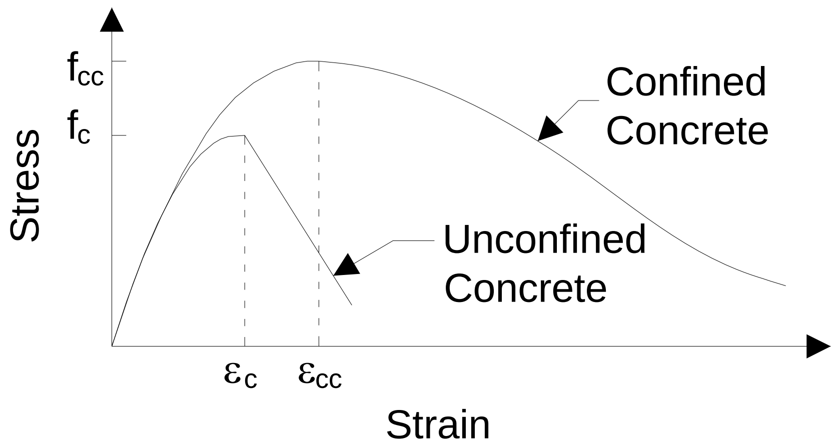

Figure 2-9 Stress-strain Relationship of Confined Concrete in Shah's Model (1985)

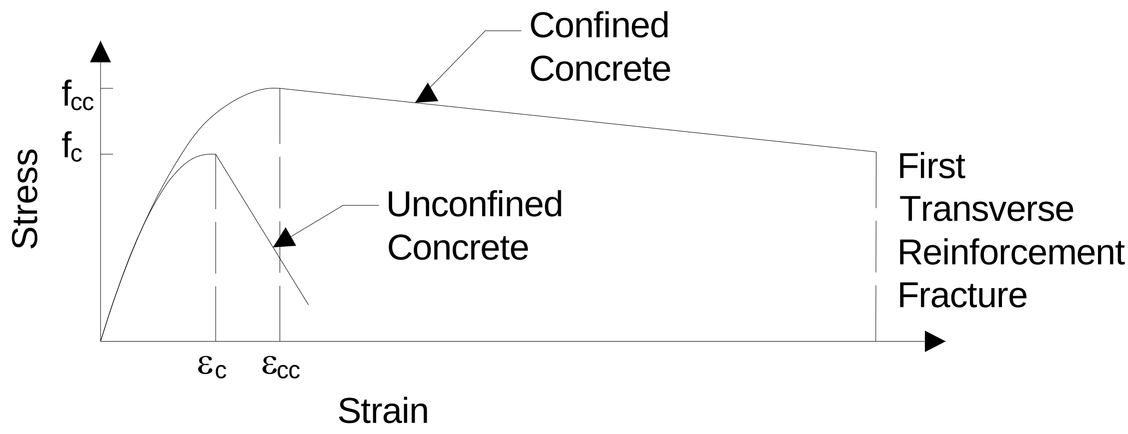

Figure 2-10 Stress-Strain Relationship of Confined Concrete in Mander's model

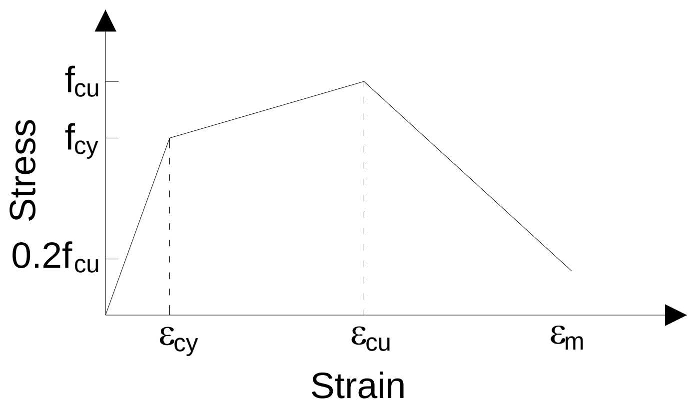

Figure 2-11 Stress-Strain Relationship of Confined Concrete in Meyer's model

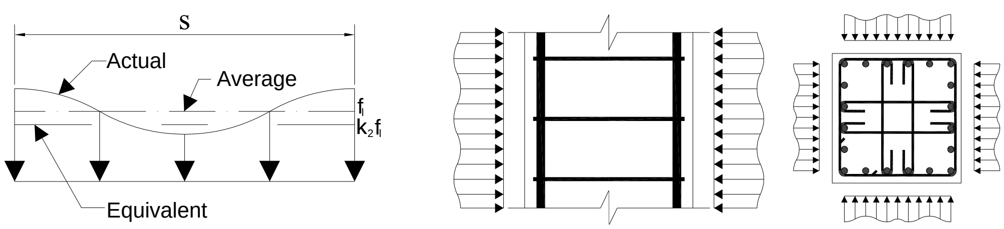

Figure 2-12 Equivalent Stress Distribution (Saatcioglu's Model)

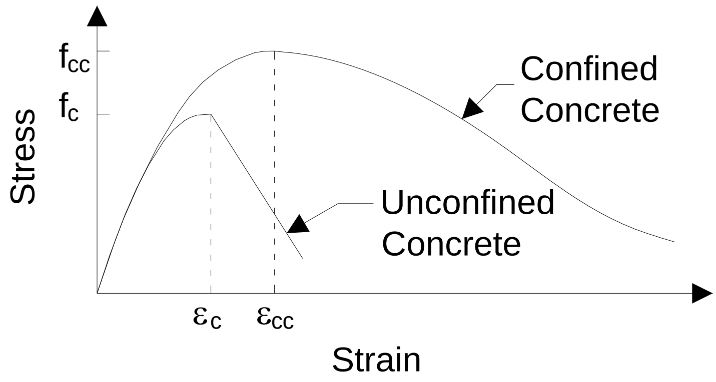

Figure 2-13 Stress-Strain Relationship in Paultre Model

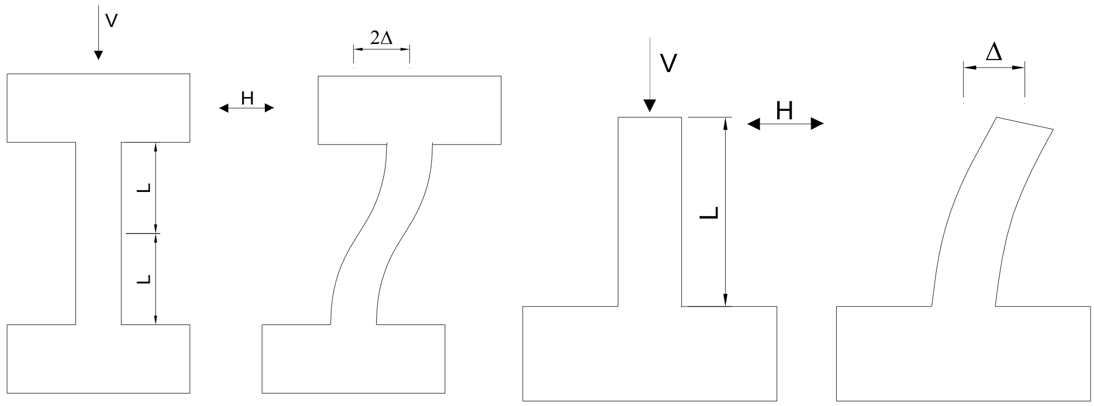

(a) Double Curvature (b) Single Cantilever

(similar to column with two floors) (similar to a half column with one floor)

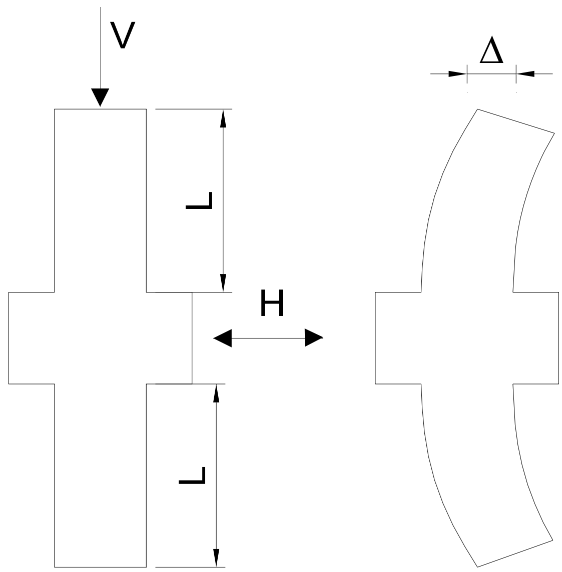

(c) Specimen with Single Stub similar to Two Half Column with a Floor between Them

Figure 2-14 Experimental Tests in Reinforced Concrete Column

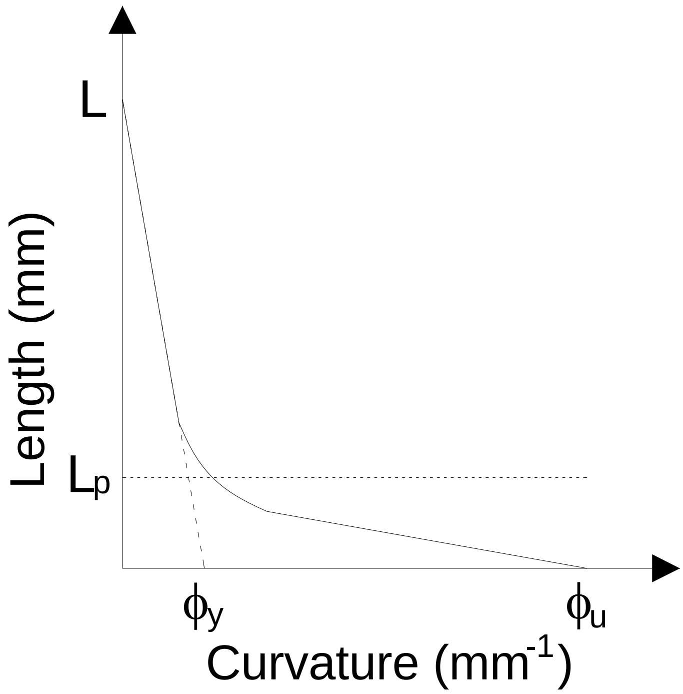

Figure 2-15 Curvature Distribution

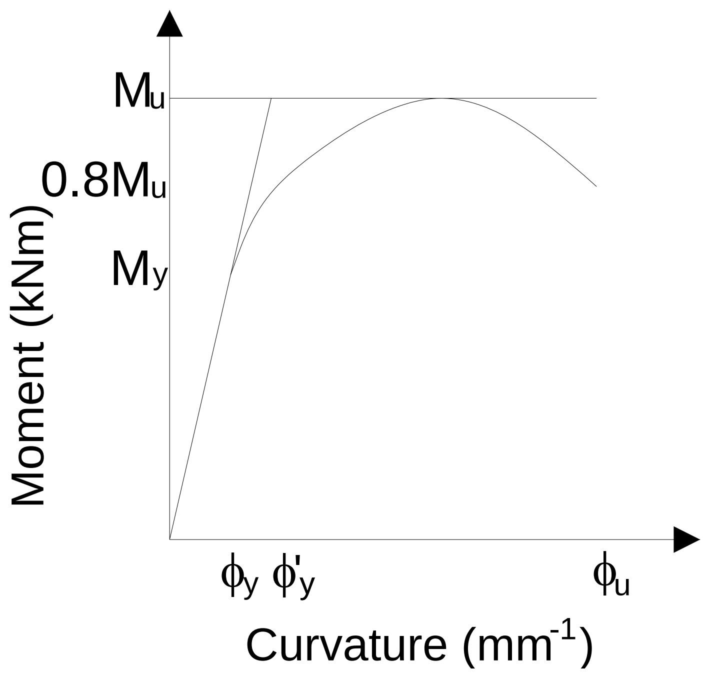

Figure 2-16 Moment Curvature

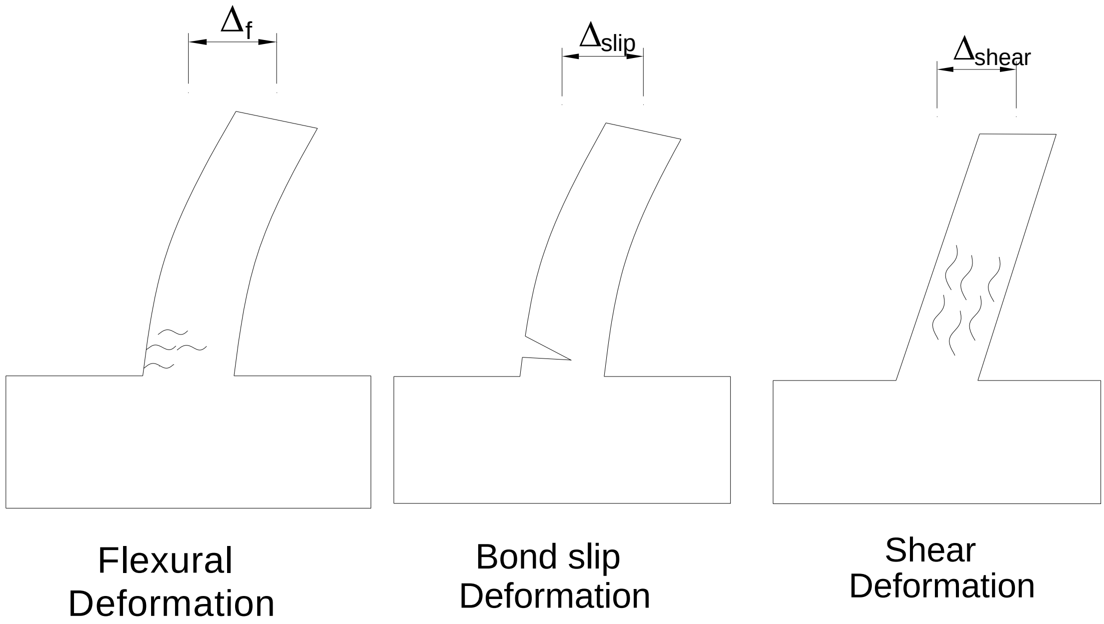

Figure 2-17 Modes of Deformation

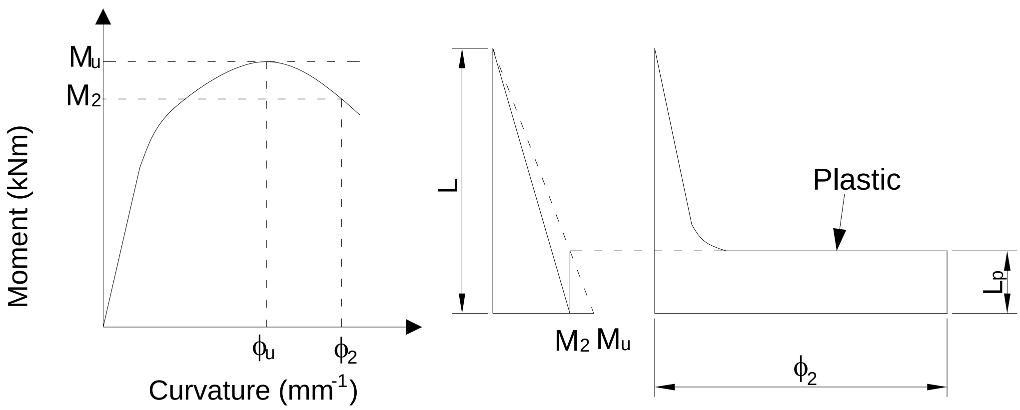

(a) Moment Curvature

(b) Plastic Hinge Length

Figure 2-18 Formation of Plastic Hinge

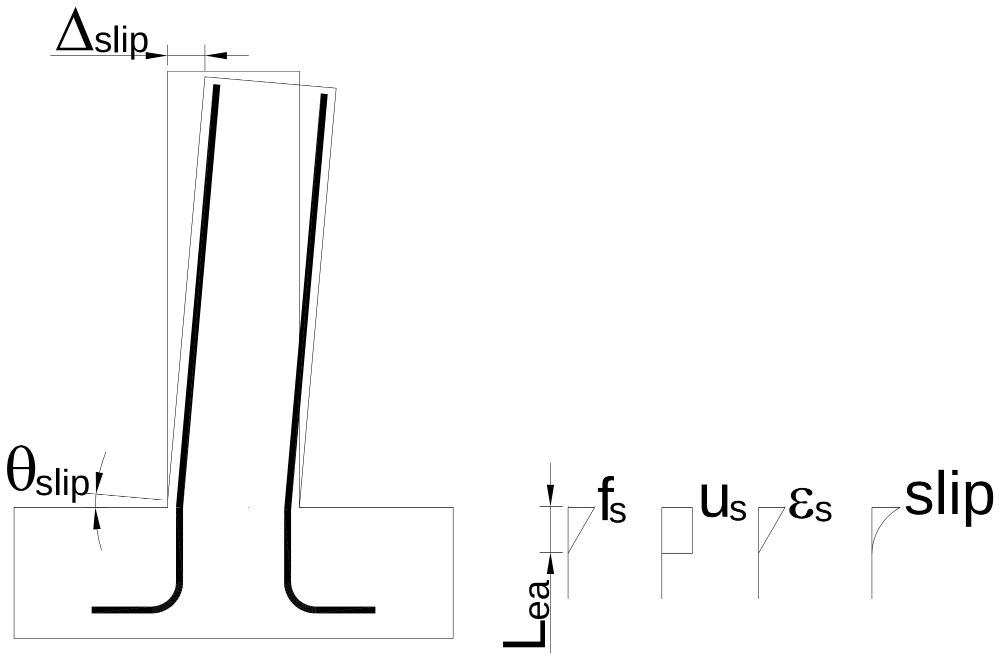

Figure 2-19 Bond Slip Deflection in Elastic Stage

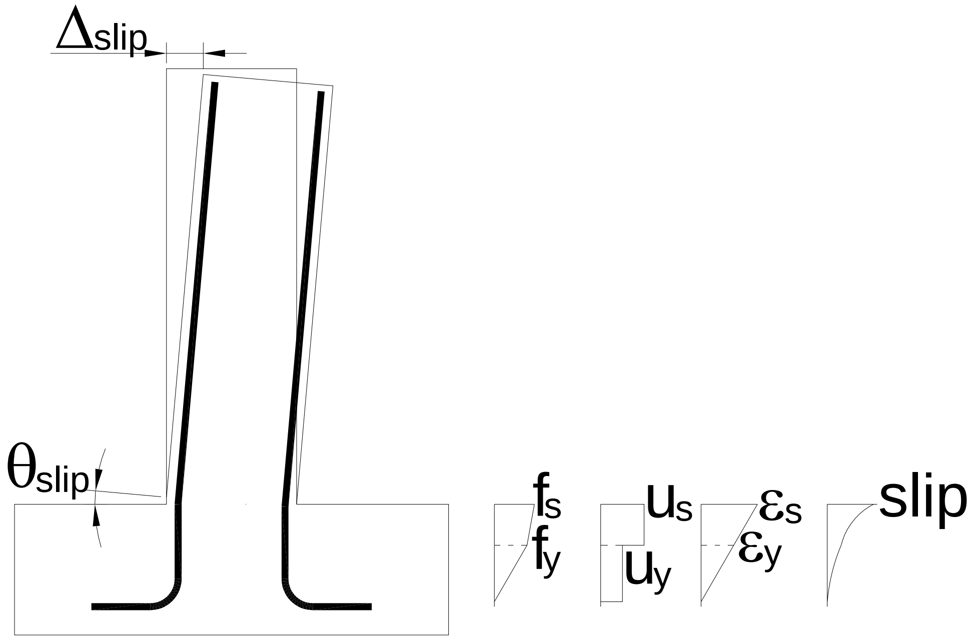

Figure 2-20 Bond Slip Deflection in Plastic Stage

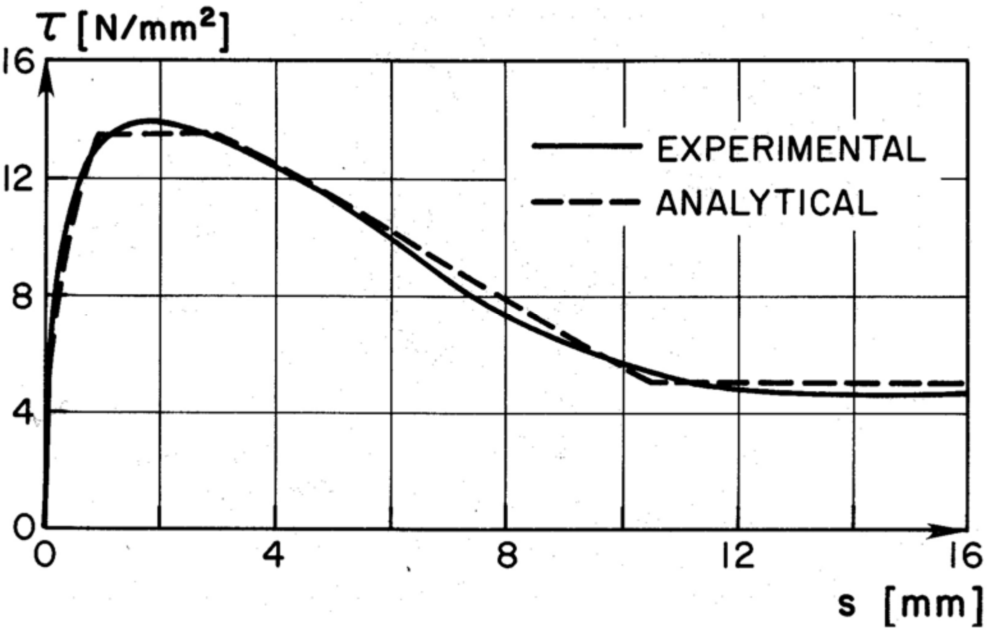

Figure 2-21 Bond Stress against Slippage, Proposed by Eligenhausen et al (1983)

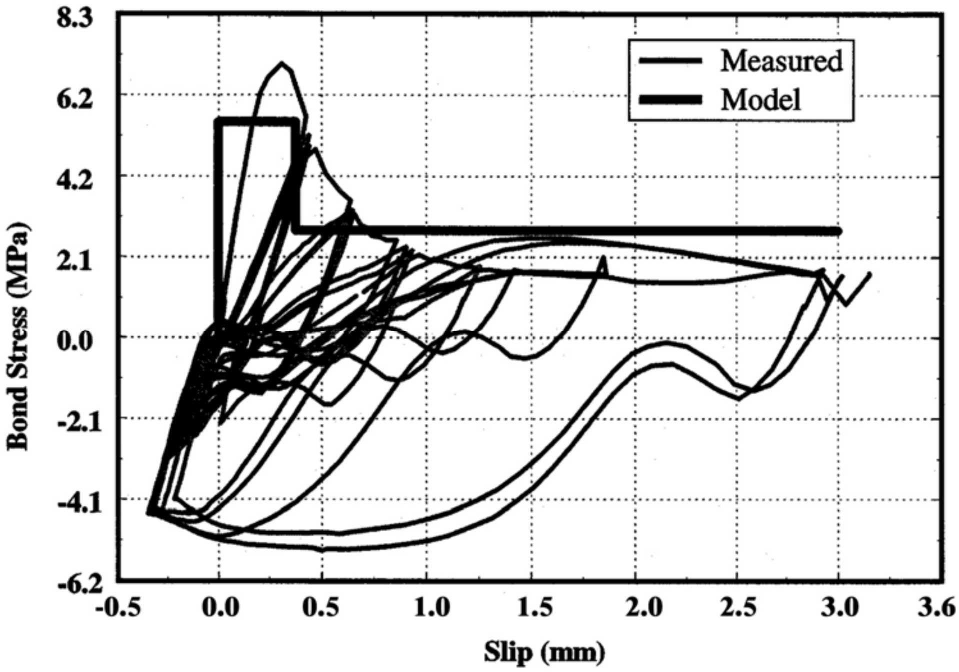

Figure 2-22 Bond Strength against Slippage, Proposed by Lehman and Moehle (2000)

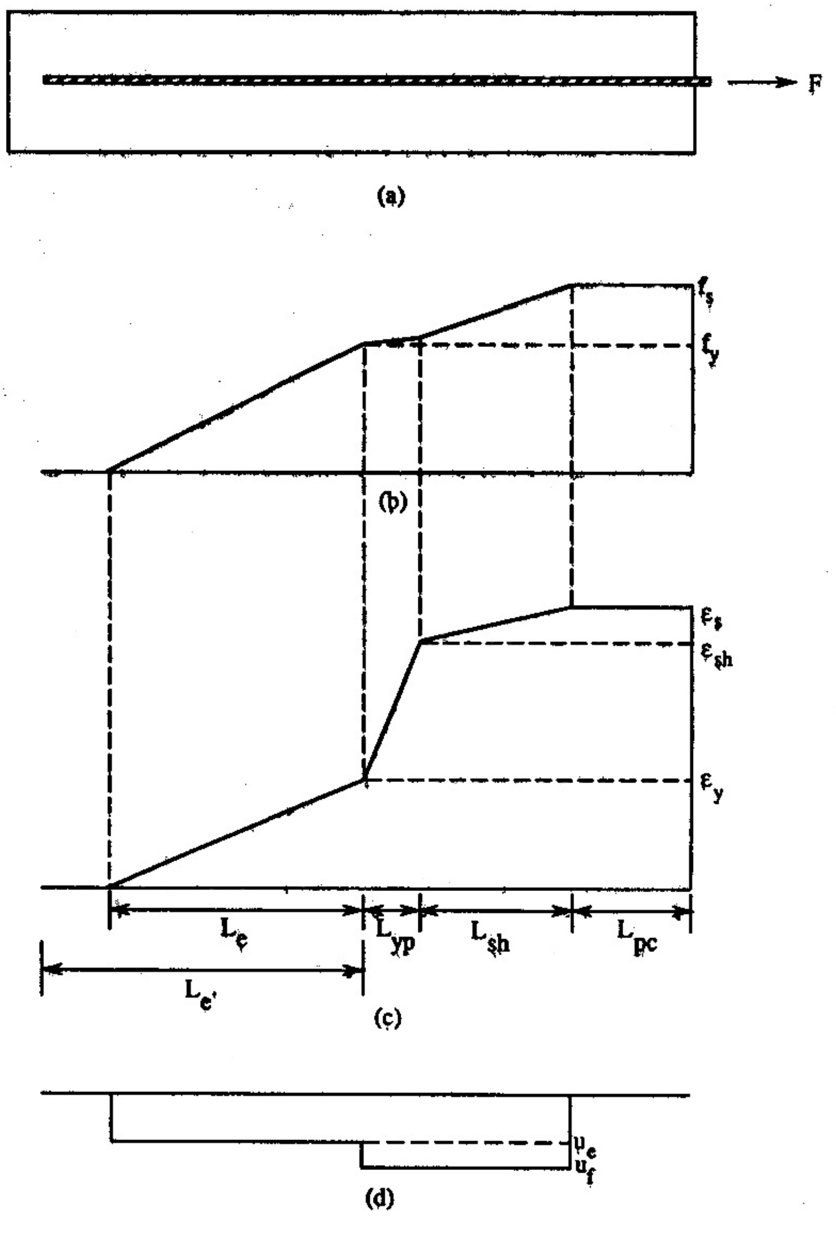

Figure 2-23 Bond Strength Model between Main Reinforcements and Concrete, Proposed by Alwisat and Saatcioglu (1992) (a) Pull-out of Reinforcement from Concrete Block; (b) Stress-strain Relationship of Reinforcement; (c) Anchorage Length of Reinforcement; (d) Bond Strength of Reinforcement

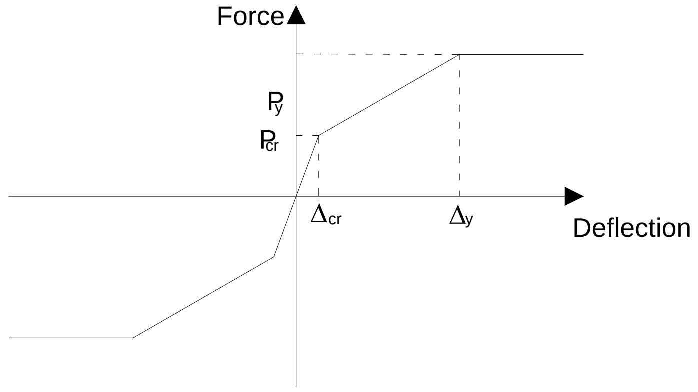

(a) Monotonic Curve

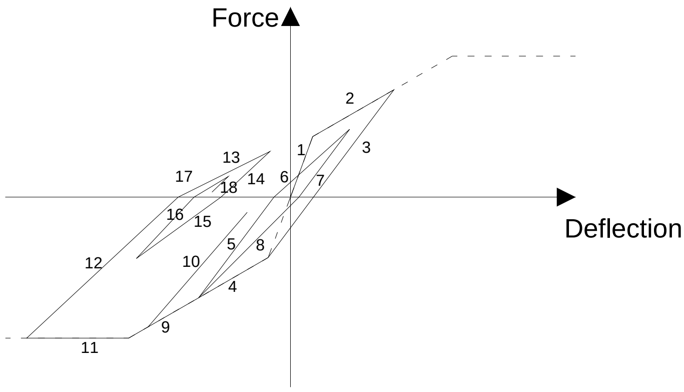

(b) Cyclic Load beyond Cracking Load

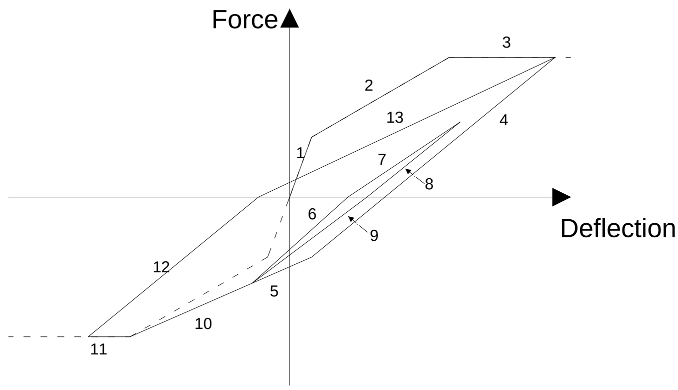

(c) Cyclic Load beyond Yield Load

Figure 2-24 Hysteresis Model, Proposed by Takeda et al (1970)

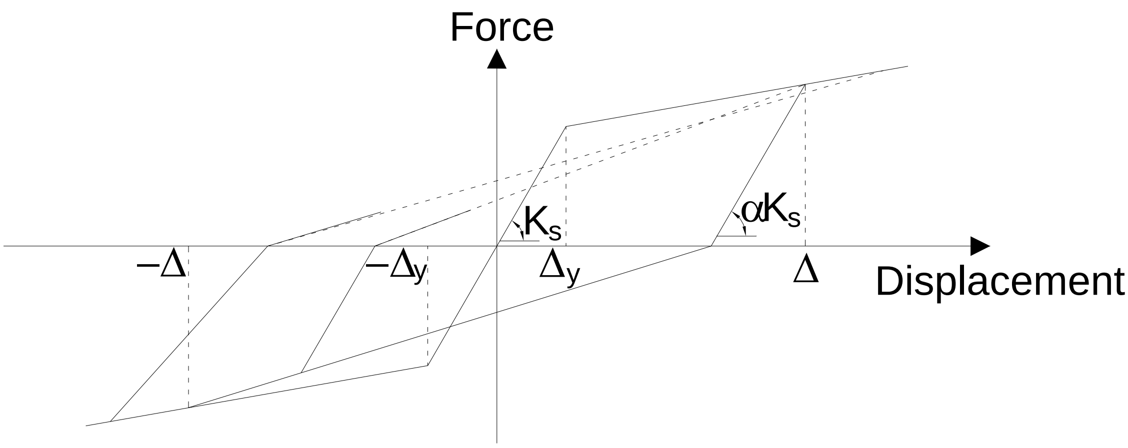

Figure 2-25 Hysteresis Model Proposed by Saiidi (1982)

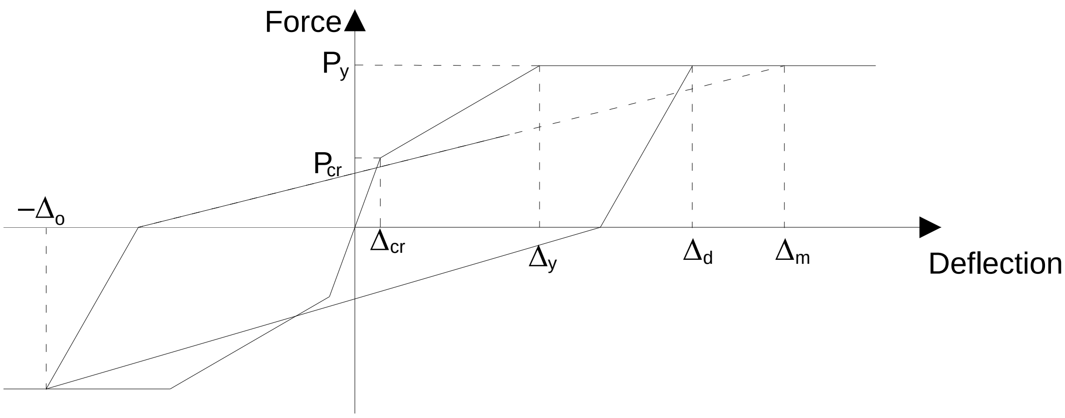

Figure 2-26 Hysteresis Model, Proposed by Umemura et al (1998)

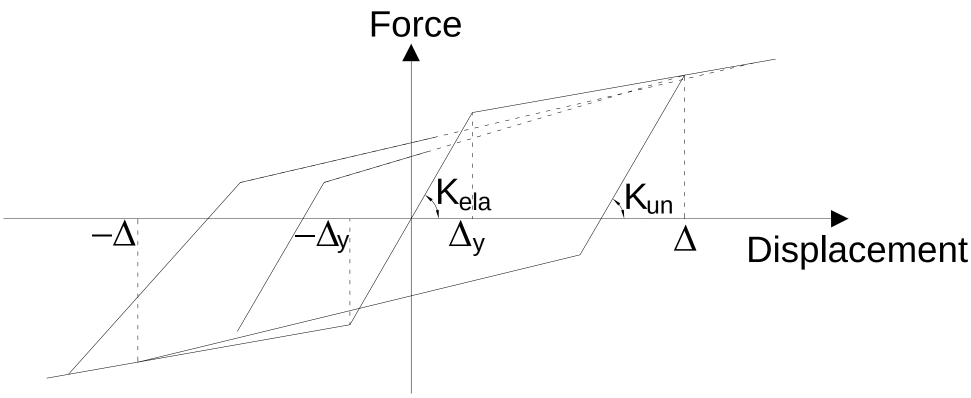

Figure 2-27 Hysteresis Model, Proposed by Phan et al (2008)

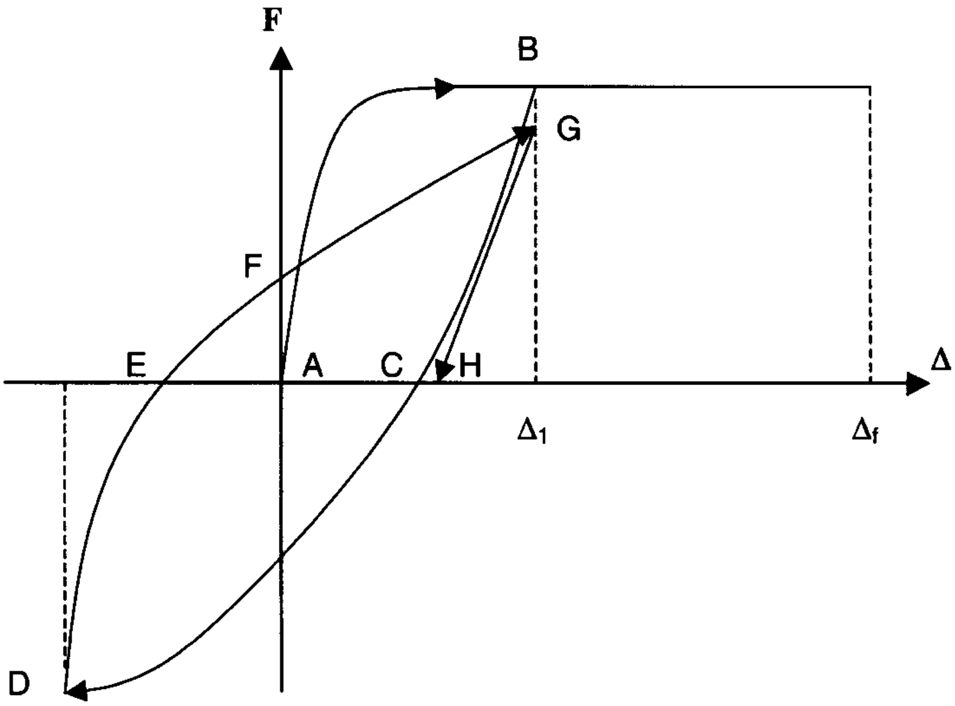

Figure 2-28 Hysteresis Behaviour of Reinforced Concrete Column, Proposed by Hindi and Sexsmith (2001)

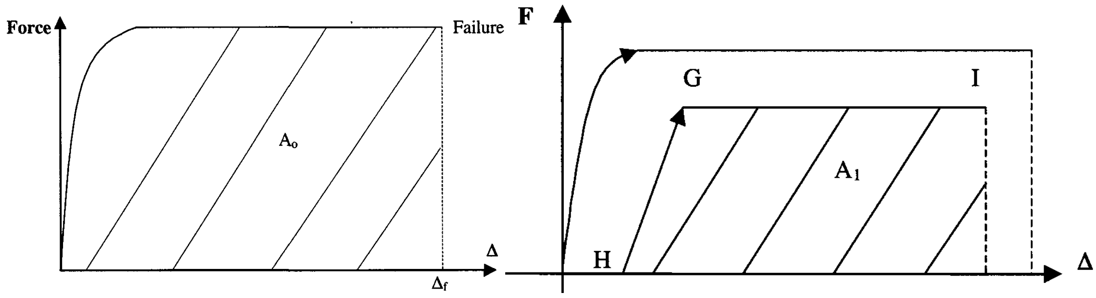

(a) (b)

Figure 2-29 Force Deflection Curve (a) in Monotonic Loading, (b) Remaining Strain Energy Stored after One Cyclic Loading

Table 2-1 Degree of Damage Proposed by Park and Ang (1985)

Degree of Damage	Physical Appearance	Simulated Damage Index
Slight	Localized minor cracking	<0.1
Minor	Light cracking in Concrete	$0.1<D<0.25$
Moderate	Localized spalling of Concrete	$0.25<D<0.4$
Severe	Extensive Crashing of Concrete	$0.4<D<0.8$
	Disclosure of Buckled Reinforcements	
Collapse	Collapsed of Column	$D>0.8$

Table 2-2 Parameters in Different Stages Proposed by Ranf et al (2006)

Damage Stages	$1/\alpha_p$	$1/\beta_p$
Significance of flexural cracking	0.56	-42.7
Residual cracking	1.97	237
Significant spalling	1.92	12400
Onset of bar buckling	2.96	410
Hoop fracture	3.35	781
20% loss of lateral load	3.75	775
50% loss of lateral load	4.00	670
loss of axial load	5.09	612

Table 2-3 Parameters on Damage Model Proposed by Erduran and Yakut (2007)

	Low ductility	Moderate Ductility	High ductility
a	0.0119	0.017	0.0205
b	1.4206	1.1021	0.9859
c	0.0093	0.0123	0.0144

3. Axial Loading Tests

3.1 Introduction

One of the major elements in the seismic resistant design is ductility. Concrete is strong in compression but brittle in nature. Reinforced concrete columns are normally detail with closely spaced transverse reinforcements in confining the lateral expansion when subjected to compressive loading. In this study, the confinement action of reinforced concrete column with non-seismic detailing is investigated in assessing the seismic resistance. In the previous chapter, stress-strain relationship of confined concrete was studied. Configuration of transverse reinforcement of reinforced concrete column considered in previous models (Mander et al 1988, Saatcioglu and Razvi 1992) is different from that normally specified in Hong Kong. In order to ascertaining the degree of confinement action in reinforced concrete columns with non-seismic detailing, uni-axial compressive tests were conducted on 12 specimens.

All specimens have the same dimensions, main reinforcement ratio and varying volumetric transverse reinforcement ratio. Details of the test program are depicted in this chapter. These include specimen design, construction process of reinforced concrete column specimen, material used, instrumentation and test setup.

3.2 Experimental Test

3.2.1 Design of Reinforced Concrete Column Specimens

Reinforced concrete column specimens considered in this study were designed according to BS8110 (1985). Strength of the specimens was between 20 and 40MPa, as normal strength concrete with characteristics strength in this range is commonly used in the existing buildings. Size of prototype column is 800mmx800mm to represent columns in typical buildings in Hong Kong. Prototype column has high main reinforcement ratio and typically 4% of gross sectional area. Both main and transverse reinforcements are high yield steel bars with characteristics yield strength at 460MPa. Quarter scaled specimens were prepared and full discussion on the scale factor is given in the next section.

Degree of confinement action provided by local transverse reinforcement detailing is examined in this study. Spacing of transverse reinforcement is an important parameter in providing sufficient confinement action to reinforced concrete column. Typical spacing of transverse reinforcement to resist severe seismic action in plastic hinge zone of prototype column is 100mm, being the minimum spacing according to ACI 318 (2002). Hence, transverse reinforcement ratio with seismic detailing is T4-25. Volumetric transverse reinforcement ratios of T4-25 and T2.5-75 detailing are 2.3% and 0.18% respectively. Transverse reinforcements of the other specimens also include T2.5-25 and T2.5-50. Another parameter affecting the confinement action is volumetric transverse reinforcement ratio. Specimens with average volumetric transverse reinforcement ratios between non-seismic requirement (T2.5-75) and the one required in seismic zone (T4-75) are also tested. The average value is 1.24% and the corresponding transverse reinforcement detailing is T4-43.75.

Three different configurations of transverse reinforcement are considered. Configuration of transverse reinforcement of reinforced concrete column specimens is shown in Figure 3-1.

Type M detailing represents local detailing when short crossties are used instead of long crosstie. This configuration of transverse reinforcement detailing can promote compaction of concrete. Type L detailing consists of transverse reinforcement hoops and long crossties anchored to main reinforcements in both directions. Type L detailing is similar to seismic detailing. Type S detailing consists of long crossties being fixed to main reinforcements in one direction only. Hooks of all three types of transverse reinforcements detailing, however, are in 90 degree. The hooks are also evenly distributed along height of specimens.

3.2.2 Scaled Reinforced Concrete Column Specimens

Tests were carried out by a Forney machine. Size of reinforced concrete column specimens is limited by characteristics of the loading machine such as loading capacity and availabilities of testing space. Loading capacity of the loading machine is 2000kN and the available testing space is sufficient for a specimen of

200x200x500mm. Loading capacity and dimensions of the prototype are 22000kN and 800x800x2000mm respectively. As height of specimens must be less than clear height of the testing space, quarter scaled specimens are designed. Size of specimens is 200x200x500mm. Aspect ratio of specimens is 0.4. Loading capacity of specimens is estimated to be 1850kN.

Constructions of specimens were divided into three batches of concrete. The first batch of concrete consists of specimens having transverse reinforcements in form of T4L25, T4M25 and T4S25, where T4L25 implies that diameter and spacing of transverse reinforcement are 4 and 25 respectively and with type L detailing. The second batch of concrete consists of T2L75, T2M75 and T2S75. The third batch of concrete consists of T4L43.75, T4M43.75, T2L25, T2M25, T2L50 and T2M50. As there is deficiency on preparing concrete mix for specimens T4L43.75, T2L25, T2M25 and T2L50, there are two concrete strengths in the third batch. Details of reinforced concrete column specimens are shown in Table 3-1.

3.3 Material Properties

3.3.1 Concrete

Concrete mix consists of sand (fine aggregate), cement, 5mm aggregate (coarse aggregate) and water. Maximum aggregate size was scaled down from 20mm to 5mm. Coarse aggregates were made of river sand and sieved by 1mm sieve. Mix proportion of concrete is shown in Table 3-2. There were 3 batches of concrete.

For each batch of concrete, six cubes of size 150x150x150mm, and 4 cylinders of 100mm diameter and 200mm height were prepared. 3 cubes and 1 cylinder were tested after 28 days of casting. One of the cylinders in every batch was installed with strain gauges of gauge length 60mm of type TML PML-60-2L to determine stress-strain relationship and Young's Modulus of unconfined concrete. Peak strain of cylinder is about 0.002. In total, 18 cubes and 12 cylinders were tested in a compressive test machine and the loading rates added on the cubes and the cylinders were 450kN and 200kN per minute respectively.

3.3.2 Steel Reinforcement

10mm diameter deformed bars and 4mm or 6mm high strength steel wires were used as main and transverse reinforcements respectively. Yield strengths of the reinforcements were determined by carried out tensile tests on the reinforcements. Three samples were tested for each type of reinforcements. Gauge length of the samples was about 200mm and installed with 2mm strain gauge (TML strain gauge: FLA-2-11-3LT) on both sides of the samples (see Figures 3-2 and 3-3). Yield strength is determined by taking the average of the yield strength obtained from the three samples. Yield strain of main reinforcements is 0.0027. Size of transverse reinforcements used in the specimens is smaller than the smallest size plain steel bars available in the industry. High strength steel wires were used. Yield strength of the steel wires was specified as 0.002 proof strength. Mechanical characteristics of steel reinforcements are shown in Table 3-3.

3.4 Specimens Construction

Main reinforcements of the specimens are at 4% of gross cross-sectional area, which is equivalent to 20T10. This is the main reinforcement ratio commonly used in Hong Kong. Strain gauges (FLA-2-11-3LT) were installed on the observed section. Details of strain gauge arrangement are reported in the next section. Reinforcement cage is shown in Figure 3-4. Figure 3-5 shows the arrangement of transverse reinforcements along the length of the specimens. The observed zone of the specimens is at the middle section. Spacing of transverse reinforcement in the end sections is half of that in the observed zone to prevent failure at the end sections due to stress concentration. Cover to all reinforcements is 10mm. Spacers were installed on the reinforcement cage. The spacers were made of cement paste. Concrete was prepared by a concrete mixer in the laboratory. 300ml of super-plasticizer (per m^3 of concrete) was added into the concrete mix to increase workability of concrete as the specimens were heavily reinforced. The concrete mix achieved a 180mm slump. Specimens were cast vertically and concrete was compacted by a poker vibrator. Formwork of the specimens and cube were removed one week after casting. Specimens were air cured under ambient temperature in the laboratory. Capping compound (Forney's product HiCap) was cast at the ends of the specimens to provide uniform loading. The process of capping is shown in Figure 3-6.

3.5 Instrumentation and Test Setup

3.5.1 Instrumentation

Strain gauges with 2mm gauge length (Kyowa FLA-2-11-3LT) were installed on main and transverse reinforcements and detailed locations of the strain gauges are shown in Figures 3-7 to 3-9. Strain gauges were installed on all the main reinforcements at mid-height to record the response of the main reinforcements. For transverse reinforcements, strain gauges were installed in two layers. First layer was located at mid-height of specimens while second layer was located at quarter height of specimen. Strain gauges in these two layers were installed on the surface of reinforcement hoops and crossties. Pairs of strain gauges were installed on reinforcement hoop. One strain gauge was installed on legs with hoop opening while another strain gauge was installed on legs without opening. For long and short crossties, strain gauges were installed in the middle of the crossties. Four long crossties were installed with strain gauges in type L detailing, and they were in perpendicular directions. One long crosstie and two short crossties were installed with strain gauges in type M detailing. The two crossties are in the same direction in these layers. Four 8mm plain bars were cast at center on each side in every specimen at the observed zone with 200mm gauge length as shown in Figure 3-10. Longitudinal displacements were measured by four linear variable displacement transducers (Kyowa DTJ-A-200 LVDT) with 200mm strokes, see Figure 3-10. Strain gauges installed in transverse reinforcement measured expansion and confinement action and strain gauges installed in the longitudinal reinforcement gave reference to confined concrete strain measured from LVDT. Locations of strain gauges installed in transverse reinforcements are shown in Figure 3-10. Strains on concrete surface were measured by a pair of strain gauges (vertical, PML-120-2L, and horizontal, PML-60-2L) in each faces, see Figure 3-10. Load cell, LVDT and strain gauges were connected to a data acquisition system and the data was recorded by a computer. Load against displacement was plotted interactively to monitor the compressive test.

3.5.2 Test Procedure

The compression tests were divided into two groups. In the first group, specimens T4L25, T4M25 and T4S25 were tested by a Forney universal testing machine, which is a manually controlled testing machine of 2000kN loading capacity. All the other specimens were tested by a MTS 815 Rock Mechanics test system, a servo-controlled hydraulic compressive machine. The loading machine allows displacement control with a loading capacity of 4500kN. The axial compressive strain rate specified in the tests was 0.0004/s.

In all the loading tests, 50mm steel plates were installed on top and bottom of each specimen to facilities even distribution of the loading. Each specimen was pre-loaded to 1/5 of its loading capacity to ensure that it was centrally loaded. Strains on the concrete surfaces were compared. If the difference in strains between two surfaces was greater than 20%, the specimen was adjusted by moving it sideway and wooden slices were inserted to balance the loading plate. The specimen was then preloaded again until it was loaded concentrically. Test was terminated when strength of a specimen dropped to 50% of its peak strength, or whenever obvious sign of collapse was observed.

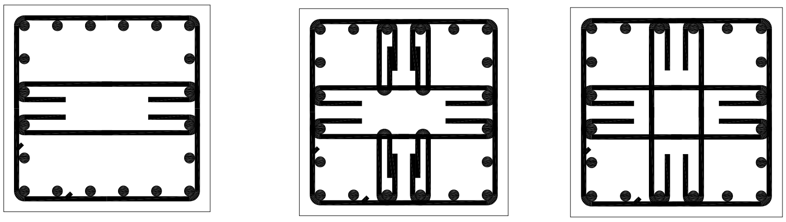

Type S Detailing Type M Detailing Type L Detailing

Figure 3-1 Configuration of Transverse Reinforcement

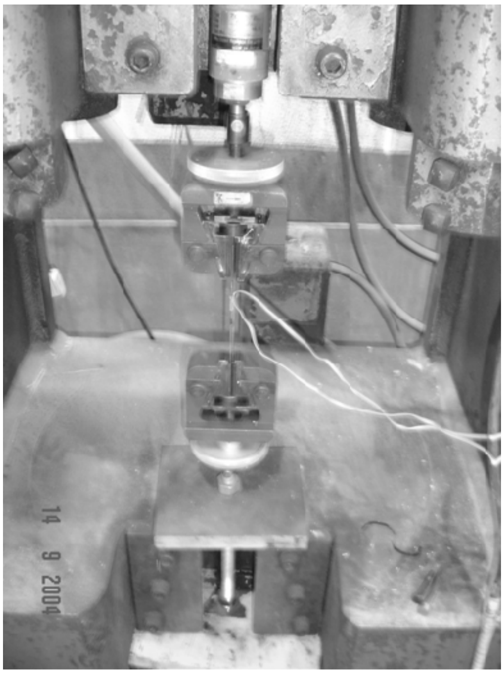

Figure 3-2 Tensile Test of Transverse Reinforcement

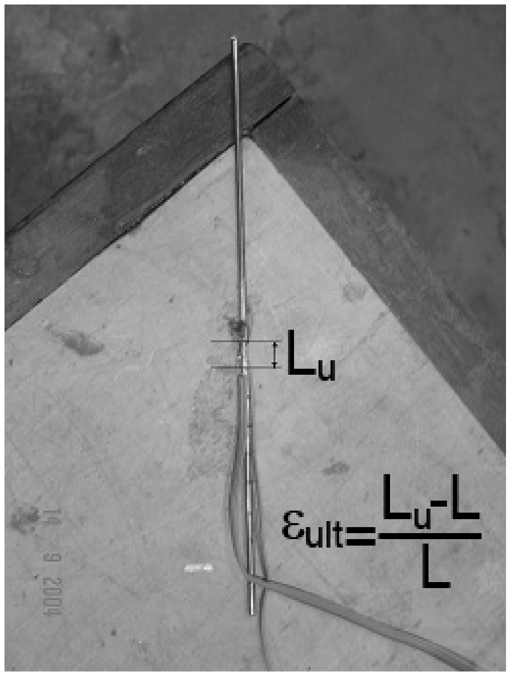

Figure 3-3 Measurement of Ultimate Strain of Transverse Reinforcement

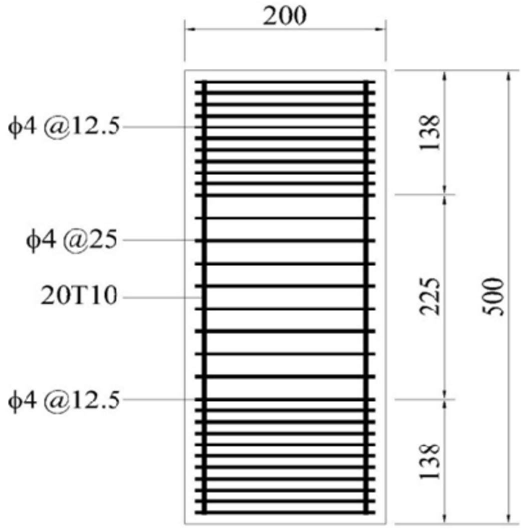

Figure 3-4 Typical Detailing

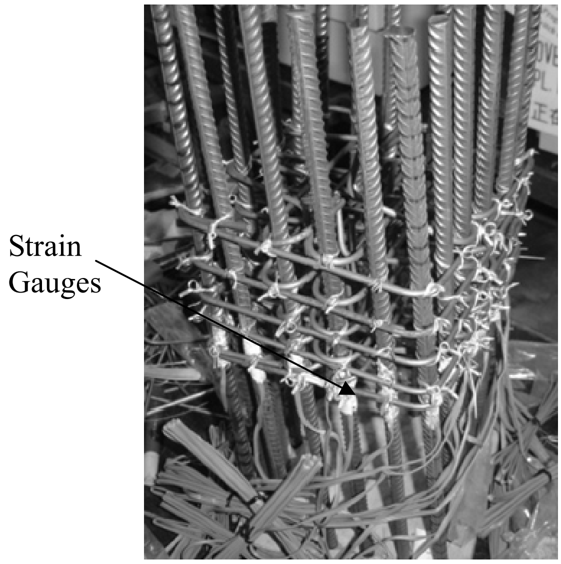

Figure 3-5 Reinforcements and Strain Gauges

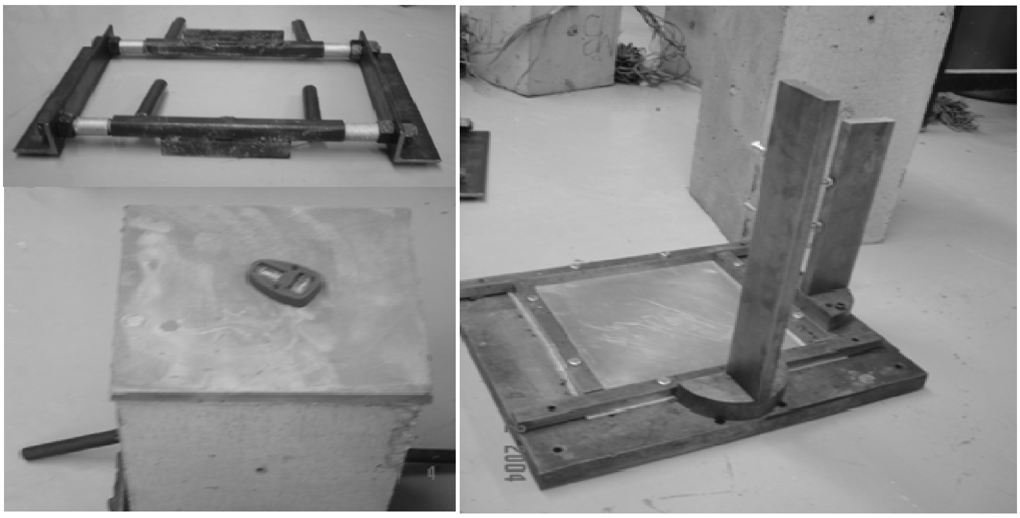

Figure 3-6 Capping Process of Reinforced Concrete Specimens (Upper Left: Frame to hold up the specimen; Lower Left: Preparing the Capping Compound and Right: Steel Frame to Align the Verticality of Specimen

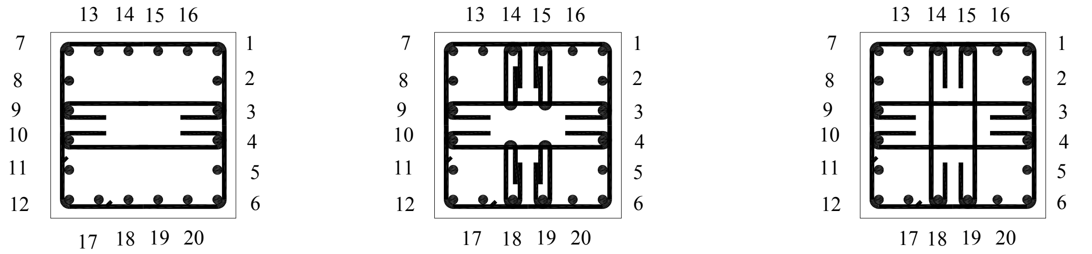

(a) Type L Detailing (b) Type M Detailing (c) Type S Detailing

Figure 3-7 Main Reinforcement Strain Gauge Location

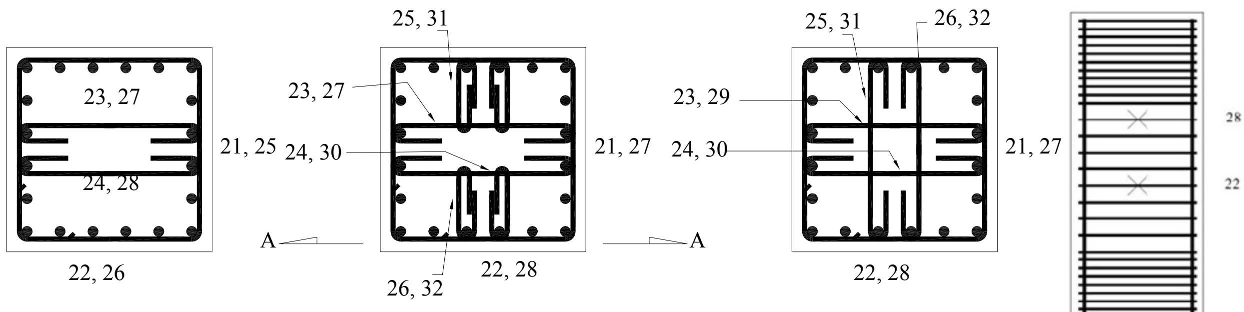

Type L Detailing Type M Detailing Type S Detailing

Section A-A
Elevation

Figure 3-8 Transverse Reinforcement Strain Gauge Location

Figure 3-9 Reinforcement Detailing

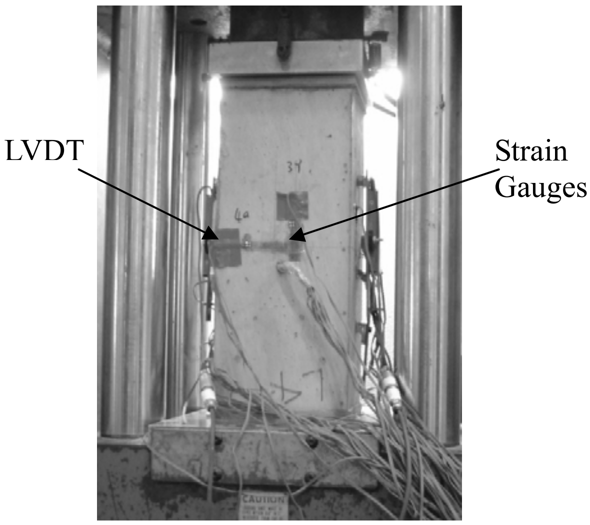

Figure 3-10 Strain Gauges and LVDT

Table 3-1 Characteristics of Specimens

Label	Transverse Reinforcement (mm)	f_{cu} (N/mm^2)	ρ_s
T4L25	ϕ4@25	33.5	2.28%
T4M25	ϕ4@25	33.5	2.28%
T4S25	ϕ4@25	33.5	1.71%
T4L43.75	ϕ4@43.75	16.5	1.31%
T4M43.75	ϕ4@43.75	27.5	1.31%
T2L25	ϕ2.5@25	16.5	0.56%
T2M25	ϕ2.5@25	16.5	0.56%
T2L50	ϕ2.5@50	16.5	0.28%
T2M50	ϕ2.5@50	27.5	0.28%
T2L75	ϕ2.5@75	23.75	0.19%
T2M75	ϕ2.5@75	23.75	0.19%
T2S75	ϕ2.5@75	23.75	0.14%

Table 3-2 Mix Proportion of Concrete

Water	Cement	Fine aggregate	5mm aggregate
1	1.6	3.16	5.97

Table 3-3 Mechanical Properties of Steel Reinforcement

Diameter (mm)	Mechanical properties of reinforcement			
	Yield Strength (MPa)	Yield Strain	Ultimate Strength (MPa)	Ultimate Strain
2.5 (T2@25,T2@50)	950	N/A*	1050	0.11
2.5 (T2@75)	560	N/A*	600	0.11
4	612.25	N/A*	641.62	0.12
10	531.2	0.027	662.49	0.164

*No obvious yield point

4. Results of Axial Loading Tests

4.1 Introduction

This chapter presents observations obtained from testing of reinforced concrete column specimens. Stress-strain relationship of confined concrete in reinforced concrete column and effectiveness of transverse reinforcement configuration on confinement action were examined.

Stress-strain relationship of confined concrete in reinforced concrete column with non-seismic detailing is formulated by conducting non-linear regression analysis. Parameters of the stress-strain relationship include peak strength, peak strain and ultimate strain of confined concrete. Ultimate strain is defined as the strain of which post peak strength of confined concrete is dropped to 80% of its peak strength. Stress-strain relationship of reinforced concrete column with non-seismic detailing are compared with that observed in other studies.

4.2 Observations

4.2.1 Unconfined Concrete Specimen

Plain concrete specimens were tested. A hairline crack was observed when the specimen was subjected to 0.8 peak loads at the loading stage. Cracks propagated quickly after peak load and the strength dropped quickly. The specimen eventually failed with fully developed diagonal cracks. Stages of plain concrete test are shown in Figure 4-1.

Stress-strain behavior of plain concrete is shown in Figure 4-2. Stress of plain concrete is defined as load over area of plain concrete and strain is defined as averaged displacement measured from four LVDTs divided by the gauge length of LVDT. The ultimate strain of plain concrete is 0.0069 while strain at peak strength is 0.002.

4.2.2 Confined Concrete

All reinforced concrete column specimens were tested with the same loading rate at 0.2mm per minute. Figures 4-3 to 4-9 show condition of the specimens at failure. The first vertical crack due to lateral expansion appeared in specimens with closely spaced transverse reinforcement. Meanwhile, sign of distress was shown on load-deformation relationship plotted instantaneously by computer. Cracks on concrete surface propagated dramatically until spalling off of concrete cover. Loading on the specimens increased after spalling. Transverse reinforcements started to resist concrete expansion due to vertical compression and to restrain main reinforcements from buckling. Loading was reduced gently in post peak loading stage. The specimens failed when main reinforcements buckled and transverse reinforcements opened up. Vertical cracks were observed inside the core concrete. After the transverse reinforcements fractured in specimens with high volumetric transverse reinforcement ratio (T4-25), compressive strength of specimens reduced drastically.

Specimens with low volumetric transverse reinforcement ratio (T2-75) behaved differently from that with high volumetric transverse reinforcement ratio (T4-25). They were able to increase to peak strength at a level similar to plain concrete specimen. Buckling of main reinforcements occurred with long buckling length because transverse reinforcements had large spacing and provided less amount of lateral restraint as compared to those with high volumetric transverse reinforcement ratio. However, compressive strength in post peak region dropped gradually.

Ultimate strain in specimens with low volumetric transverse reinforcement ratio (Specimen T2L75) was less ductile than that with high volumetric transverse reinforcement ratio (Specimen T4L25). Buckling strain of main reinforcement in specimen T2L75 was smaller than that in specimen T4L25. Buckling length of main reinforcement in specimen T2L75 was roughly equal to height of specimen. Buckling of main reinforcements was easily observed in specimen T4L25. The effective length of buckling was about twice the spacing of transverse reinforcements. Crushing of confined concrete was found at intervals between the transverse reinforcements.

4.2.3 Transverse Reinforcements

Strains in the transverse reinforcements were monitored by strain gauges installed at mid-height. When specimens were loaded initially, lateral strain acting on transverse reinforcements due to compression was not significant. When the axial strain was larger than peak strain of plain concrete, strains of transverse reinforcements increased rapidly to confine lateral expansion of core concrete in resisting the expansion due to Poisson's effect induced by compressive loading. In the meantime, micro-cracks expanded drastically. Most of the confining action was attributed to reinforcement hoops in transverse reinforcements. Strains in reinforcement hoops were larger than those in the long crossties and short crossties, see Figures 4-10 to 4-15. Long crossties remained elastic prior to reaching peak strength of confined concrete. As a result, they were able to provide confinement to the specimens by resisting lateral expansion induced from axial load. The confinement action increased the ductility of the specimens. Short crossties provided some confining action in the specimens. All short crossties except those in specimen T4M25 remained elastic throughout the loading stage as shown in Figures 4-14 and 4-15. Long crossties were anchored thoroughly to main reinforcements. Short crossties provided relatively lesser anchorage to main reinforcements. This is due to bond strength along anchorage length between transverse reinforcements and concrete.

Reinforcement hoop resists most of the lateral expansion from core concrete. Strain in reinforcement hoops near the opening is smaller than the one far away from opening. Opening of reinforcement hoop reduces the efficiency in restraining lateral expansion. In addition, there are fractures of transverse reinforcements in case of closely spaced transverse reinforcements. All transverse reinforcements except short crossties yielded prior to crushing of confined concrete. Long crossties provide lateral restrain to main reinforcements to resist main reinforcements from buckling. This enhances efficiency of the specimens. Transverse reinforcement hoops in type S detailing fractured because most of the confinement action is provided from the reinforcement hoops. Specimens with type M detailing were effective in resisting main reinforcements from buckling as compared to those with type S detailing. Peak strength of specimens with type L detailing was larger than that in specimens with type M detailing and also much larger than that in specimens with type S detailing. Strains in long crossties at type L detailing were larger than that in short crossties at type M detailing in the same location.

Effectiveness of the specimens is related to spacing of transverse reinforcements. Fracture of transverse reinforcements occurred when transverse reinforcements were closely spaced as shown in Figures 4-6 and 4-7. Both of them were in specimens with type S detailing. When the specimens are closely spaced, 90º hooks of transverse reinforcements also provide anchorage to main reinforcements.

Configurations of transverse reinforcements influence the contribution of transverse reinforcements to ultimate strain, see Tables 4-4 and 4-5. The tables show strains in reinforcement hoops, long crossties and short crossties at peak strength and ultimate strain respectively. The specimens with type L detailing resisted lateral expansion more evenly than the one with type M detailing. Strains in reinforcement hoops of specimens with type M detailing were greater than those obtained from long crossties and short crossties.

Long crossties in type M detailing have more contribution in resisting lateral expansion than that in short crossties. When compressive stress reached peak strength of specimens, strain in short crossties was equal to 40% strain in transverse reinforcement hoops. However, when the compressive stress dropped to 80% peak strength in post-peak region, strain in short crossties was equal to 20% of strain measured in reinforcement hoops see Figures 4-10 to 4-15.

Short crossties in type M detailing contribute to increase strength and ductility as compared with the stress-strain relationship of specimen T4M25 and T4S25 as shown in Figure 4-16. Although strains in short crossties did not yield at peak strength of specimens, the strains were further increased to confine lateral expansion until the ultimate strain of confined concrete was reached, see Figures 4-14 to 4-15. Strain in reinforcement hoop of type M detailing increased much more than the strain corresponding to type L detailing, see Figures 4-10 to 4-11. Reinforcement hoop provides most of the resistant in lateral expansion. The increase in transverse reinforcement strains are similar to all specimens and are not affected by the difference in volumetric transverse reinforcement ratio.

Transverse reinforcement strains in reinforced concrete specimen are also affected by spacing of transverse reinforcement. The volumetric transverse reinforcement ratio in specimen T4-43.75 was larger than that in specimen T2-25. Transverse reinforcement strain in both specimens T4L43.75 and T4M43.75 were, however, smaller than that in both specimens T2L25 and T2M25. Spacing of transverse reinforcement is more important than volumetric transverse reinforcement ratio in providing confinement action.

4.2.4 Concrete Strength

Concrete strength of specimens is another factor affecting the effectiveness of reinforced concrete column. When the concrete strength is reduced, the peak strain of unconfined concrete is then increased. The corresponding lateral strain acted on transverse reinforcements would be increased. This can increase the resisting stress acting to core concrete.

4.2.5 Yield Strength of Transverse Reinforcement

Yield strength of transverse reinforcement is an important factor. When the yield strength is increased, the lateral resistance provided by transverse reinforcement would be increased. In particular, transverse reinforcement provides confinement to the concrete core by resisting the expansion of concrete mainly when it is under elastic manner.

4.3 Axial Behavior

4.3.1 Confined Concrete Stress

Confined concrete stress is defined as the loading of confined concrete divided by the prescribed area inside transverse reinforcement hoop. Loading resisted by confined concrete is calculated by subtracting the contribution due to concrete covers and main reinforcements from total loading. This is expressed by the following equation,

$$f_c = \frac{P - f_{uc}A_{uc} - f_s A_{st}}{A_{cc}} \quad (4\text{-}1)$$

where P is compressive force of reinforced concrete column, f_{uc} is unconfined concrete stress, A_{uc} is area of concrete cover, f_s is steel stress, A_{st} is area of reinforcements, f_c is confined concrete stress and A_{cc} is area of confined concrete.

4.3.2 Confined Concrete Strain

Confined concrete strain is estimated from main reinforcement strains, strains on concrete surface and displacement of LVDT. Strain in the specimens is calculated as the average of four measurements obtained from LVDT divided by the gauge length of LVDT. Due to uneven spalling of concrete cover, a small amount of eccentricity was induced. Averaged values of two transducer readings were used in calculating confined concrete strain during post-peak stage. The stress-strain relationship of the specimens is shown in Figure 4-16. Loading against strain are also shown in Figure 4-17. Transverse reinforcement strain against axial strain is also shown in Figures 4-10 to 4-15.

4.4 Analysis of Test Results

4.4.1 Spacing of Transverse Reinforcements

Based on Figure 4-16, specimen with seismic detailing (Specimen T4M25) had larger increase in peak strength and was more ductile than that with non-seismic detailing (Specimen T2M75). For instance, increase in strength with reference to unconfined concrete strength on Specimen T4M25 was about 1.6 while Specimen T2M75 was about 1.02. As spacing of the transverse reinforcement increases, restraint in concrete expansion reduces and concrete fails by orthogonal tensile failure with limited confinement action. Short crosstie is more effective in confining core concrete when transverse reinforcement is closely spaced. Strains in short crossties of Specimen T2M25 were greater than that of Specimen T4M43.75. The overall confining action depends on the amount of volumetric transverse reinforcement ratio such that confinement action in Specimen T4M43.75 was much more effective than Specimen T2M25. From Table 4-2, when the spacing of transverse reinforcements was 25mm, behavior of Specimen T4M25 was similar to Specimen T4L25. Vice versa, for large spacing of transverse reinforcement, Specimen T2M75 performs similar to Specimen T2S75. Therefore, when transverse reinforcements are closely spaced, short crossties perpendicular to long crossties are still effectively in providing the confinement. Strain at peak strength and ultimate strain increase when spacing of transverse reinforcements is reduced.

4.4.2 Configuration of Transverse Reinforcement

Crossties are restrained by main reinforcements in both directions in type L detailing, see Figure 4-18. For type M detailing, one side of the crossties in x-direction is restrained by main reinforcements while y-direction crossties are restrained by other ties in x-direction. As indicated in Table 4-2, confined concrete strength of specimens with type L detailing is higher than those with type M detailing. So confinement provided by type L detailing is more effective than type M detailing. Since for type M detailing, confinement in zone 5 depicts in Figure 4-18, long crossties were only provided in x-direction. On the contrary, for type L detailing, crossties provided confinement in zone 5 in both directions. Confinement provided in type M detailing becomes more effective when spacing of transverse reinforcement reduces. Strains at peak strength and ultimate strain of specimens with type L detailing were higher than those with type M detailing. When volumetric transverse reinforcement ratio of specimen increases and spacing of transverse reinforcements reduces, the difference in peak strength, peak strain and ultimate strain between type L and M detailing reduces. As volumetric transverse reinforcement ratio of Specimen T4M43.75 was larger than that of Specimen T2M25, peak strain and ultimate strain in Specimen T4M43.75 was smaller than that in Specimen T2M25. So spacing of transverse reinforcement is a crucial factor to influence the confined concrete strength.

4.5 Stress-strain Relationship Model

Stress-strain relationship of confined concrete in specimens with non-seismic detailing was different from those developed in previous studies in predicting the stress-strain relationship of reinforced concrete column with seismic detailing. In this study, mathematical model of reinforced concrete column with non-seismic detailing is formulated by conducting non-linear regression analysis based on the experimental data.

Three parameters are considered including peak confined concrete strength, peak strain and ultimate strain in confined concrete. The model consisted of an ascending and a descending branch. The ascending branch was based on the model proposed by Propovics (1973) and also used by Mander et al (1988) and Saatcioglu and Razvi (1999). It is in the form of,

$$f_{cco} = \frac{f_{cc} x r}{r - 1 + x^r} \tag{4-2}$$

$$x = \frac{\varepsilon_c}{\varepsilon_{cc}} \tag{4-3}$$

$$r = \frac{E_{con}}{E_{con} - E_{sec}} \tag{4-4}$$

where f_{cc} is peak strength, f_{cco} is confined concrete stress, ε_c is confined concrete strain, ε_{cc} is peak strain, E_{con} is initial modulus of unconfined concrete and E_{sec} is secant modulus of confined concrete corresponding to peak strength.

In considering the set of data obtained from this study, the descending branch is proposed to be in the form of a linear relationship between peak strength and 80% peak strength in the post peak region. Descending branch of confined concrete is expressed by the following equations,

$$f_{cco} = f_{cc} - E_{des}\left(\varepsilon_c - \varepsilon_{cc}\right) \tag{4-5}$$

$$E_{des} = \frac{0.2 f_{cc}}{\varepsilon_{80cc} - \varepsilon_{cc}} \tag{4-6}$$

where f_{cc} is peak strength, f_{cco} is confined concrete stress, ε_c is confined concrete strain, ε_{cc} is peak strain, ε_{80cc} is ultimate strain and E_{des} is modulus of descending branch in confined concrete.

The ultimate strain of confined concrete is determined as the strain at 80% post peak strength. Further increase in compressive strain leads to loss of concrete strength, buckling of main reinforcements and open up of reinforcement hoops.

The test data has shown that volumetric transverse reinforcement ratio and configuration of transverse reinforcements are important factors in affecting the stress-strain relationship of confined concrete with non-seismic detailing. Confinement action is more effective with increasing volumetric transverse reinforcement ratio. Spacing of transverse reinforcements also affects the effectiveness of transverse reinforcement in providing confinement to concrete. Therefore, the parameters considered in stress-strain model include the volumetric transverse reinforcement ratio, configuration of transverse reinforcements, yield strength of transverse reinforcements and unconfined concrete strength.

4.5.1 Peak Strength

Peak strength is linearly related to a confinement increment ratio (f_{cc}/f_c) proposed by Skeikh et al (1982), modified by Mander et al (1984) and used by Saatcioglo and Razvi (1999). The index is directly proportional to confinement effective index (K_e), volumetric transverse reinforcement ratio (ρ_s) and yield strength of transverse reinforcement (f_{yt}) but inversely proportional to unconfined concrete strength (f_c), being the compressive strength. This is related to efficiency of rectangular transverse reinforcement configuration in resisting lateral expansion and is assumed to be unity when the expansion is resisted by circular reinforced concrete column. Confinement increment ratio (f_{cc}/f_c) is determined from non-linear regression analysis and related to parameters of reinforced concrete column. The confinement increment ratio (f_{cc}/f_c) and confinement effective index (K_e) are shown in the following equations.

$$\frac{f_{cc}}{f_c} = 1 + \alpha_{stress} \frac{K_e \rho_s f_{yt}}{f_c} \tag{4-7}$$

$$K_e = \frac{\left(1 - \sum_{i=1}^{n} \frac{c_i}{b_c h_c}\right)\left(1 - 0.5\frac{s'}{b_c}\right)\left(1 - 0.5\frac{s'}{h_c}\right)}{1 - \rho_{main}} \tag{4-8}$$

where α_{stress} is index for different configuration, f_{cc} is confined concrete strength, f_c is unconfined concrete strength, f_{yt} is yield strength of transverse reinforcement, K_e is effectively confinement ratio, c_i is horizontal clear spacing of crossties, b_c is width of transverse reinforcement measured from centerline, h_c is length of transverse reinforcement measured from centerline, s' is clear spacing of transverse reinforcement, ρ_{main} is main reinforcement ratio and ρ_s is volumetric transverse reinforcement ratio. Table 4-5 gives the numerical values of α_{stress} and correlation among different detailing. Eq.(4-7) provides very close agreement with the experimental results. Figure 4-19 compares the peak strength estimated by Eq.(4-7) and experimental results.

4.5.2 Strain at Peak Strength

Strain at peak strength in confined concrete with non-seismic detailing is linearly related to confinement strength index. The relationship is similar to the model proposed by Mander et al (1988). The parameter of the strain increment ratio is determined by non-linear regression analysis. Peak strain is represented by the following equations,

$$\varepsilon_{cc} = \varepsilon_{uc}\left(1+\beta_{strain}\left(K_{conf}-1\right)\right) \qquad (4\text{-}9)$$

$$K_{conf} = \frac{f_{cc}}{f_c} \qquad (4\text{-}10)$$

where ε_{cc} is strain at peak strength, ε_{uc} is unconfined concrete peak strain, β_{strain} is index ratio for configuration of transverse reinforcement, K_{conf} is confinement strength increment ratio, f_{cc} is confined concrete strength and f_c is unconfined concrete strength. Table 4-5 gives numerical values of β_{strain} and correlation among different detailing. Figure 4-20 compares the strain at peak strength between the predicted value and experimental results.

4.5.3 Ultimate Strain

The ultimate strain of confined concrete is defined as strain at 80% peak strength in descending branch. It is related to volumetric transverse reinforcement ratio, yielding of transverse reinforcements and confined concrete strength. Similar to Paulay's expression (Paulay and Priestley 1992), the ultimate strain is expressed by the following equations.

$$\varepsilon_{cu} = 0.004 + \gamma_{ult} \frac{\rho_s K_{conf} f_{yt}}{f_{uc}} \varepsilon_{sm} \qquad (4\text{-}11)$$

where ε_{sm} is ultimate strain of transverse reinforcement, ε_{cu} is ultimate strain of confined concrete, ρ_s is volumetric transverse reinforcement ratio, K_{conf} is strength increment ratio, f_{yt} is yield strength of transverse reinforcement ratio, f_{uc} is unconfined concrete strength and γ_{ult} is index ratio. Table 4-5 gives numerical values of γ_{ult} and correlation among different detailing. Figure 4-21 compares the ultimate strain between the predicted value and experimental results.

4.6 Comparison between Test Result and Previous Models

Eq.(4-7) to Eq.(4-11) predict the stress-strain relationship of confined concrete. Comparison of confined concrete relationship between experimental results and predicted value is shown in Figure 4-22.

Previous models (Mander et al 1988, Saatcioglu and Razvi 1992 and Legeron and Paultre 2003) provide the stress-strain relationships of confined concrete in specimens with seismic detailing. As a result, previous models overestimate the performance of non-seismic detailing. For example, 90º end hooks cannot provide full anchorage in resisting buckling of main reinforcement and loss of confined concrete stress. Table 4-7 shows that the difference between confined concrete stress-strain model obtained from present study and previous studies.

4.6.1 Peak Strength and Peak Strain

Stress-strain relationship of reinforced concrete column with non-seismic detailing is compared with previous models using statistical measurement, such as, mean difference and correlation analysis. Mean difference ratio is defined as the average ratio of the difference between predicted value and experimental data. Mean difference ratio determines dispersion of data from the predicted values. Correlation analysis is also conducted to measure relationship between experimental data and analytical model. The t-distribution values of each model in comparing with experimental data against 95% confidence interval are shown in Table 4-6. In general, higher mean differences are obtained by model proposed by previous studies except the model proposed by Hoshikuma (1997) because Hoshikuma's regression model considers the data with a wider range of volumetric transverse reinforcement ratio.

There is large difference between previous model and the experimental results because configuration of transverse reinforcement differs. Therefore, previous models cannot accurately reflect peak strength and corresponding strain for the detailing considered in this study.

4.6.2 Stress-strain Curves

The experimental data are compared with analytical values obtained from the model proposed in previous studies, see Figure 4-23. Initial modulus of unconfined concrete is the same among all models except Hoshikuma's and Tassio's model. For those two models, initial slope of unconfined concrete are derived differently. In the initial stage, lateral expansion induced by Poisson's effect from compression is very small. There is little confinement action at this stage leading to close agreement between previous studies.

When axial load is increased to a certain level, transverse reinforcement resists lateral expansion and induces confining stress to core concrete. Strength of core concrete and peak strain are increased. Lateral restraints provided by the transverse reinforcement affect the stress-strain relationship in the pre-peak stage. Reinforcement hoop with 90º end hooks have less resistance to lateral expansion and the short crossties are less effective in resisting the lateral expansion. This leads to the experimental results being different from previous studies.

Post peak behavior and ductility of reinforced concrete columns relate to effectiveness of transverse reinforcement in resisting lateral expansion of core concrete. There are large differences between predicted value obtained from Mander's model and experimental data in the post-peak range for any volumetric transverse reinforcement ratio. As expected, slope in descending branch of the stress-strain relationship in the experimental data is steeper than the one in Mander's model.

Saatcioglu's model considers the post-peak behavior of reinforced concrete column with high volumetric transverse reinforcement. Hence, the post-peak behavior of reinforced concrete column with low volumetric transverse reinforcement cannot be accurately predicted.

Paultre's model is similar to Saatcioglu's model. Skeikh's model overestimates the ductility of specimens with high volumetric transverse reinforcement ratio but underestimates the ductility when volumetric transverse reinforcement is small. This is because slope of descending branch defined by Skeikh and Uzumeri (1982) is inversely related to volumetric transverse reinforcement ratio. From the experiments, when the volumetric transverse reinforcement ratio reduces, slope of the descending branch increases sharply.

Hoshikuma's model gives a relative good prediction in post-peak behavior for this type of specimens. Tassio's model shows good prediction of post-peak behavior when spacing of transverse reinforcement is small while the behavior is overestimated when spacing of transverse reinforcement increases.

The proposed model in describing the stress-strain relationship of confined concrete in reinforced concrete columns with non-seismic detailing provides a good relationship in both ascending and descending region of the stress-strain relationship.

4.7 Summary

Confinement action of columns with non-seismic detailing is assessed by conducting axial loading tests on twelve specimens with different transverse reinforcement details. From the tests results, the following are observed:-

(1) Type L detailing provides better confinement action.

(2) Short crossties are less effective in providing confinement action as compared with long crossties.

(3) Detailing using short crossties in lieu of long crossties is not recommended especially at large transverse reinforcement spacing.

Stress-strain relationship of confined concrete with non-seismic detailing is different from previous models. The proposed relationship agrees well with the experimental results and uses subsequently in predicting the hysteretic behavior of reinforced concrete column with non-seismic detailing.

(a) Initial Stage of Testing (b) Specimen at Peak Strength (c) Specimen after Failure

Figure 4-1 Testing of Plain Concrete

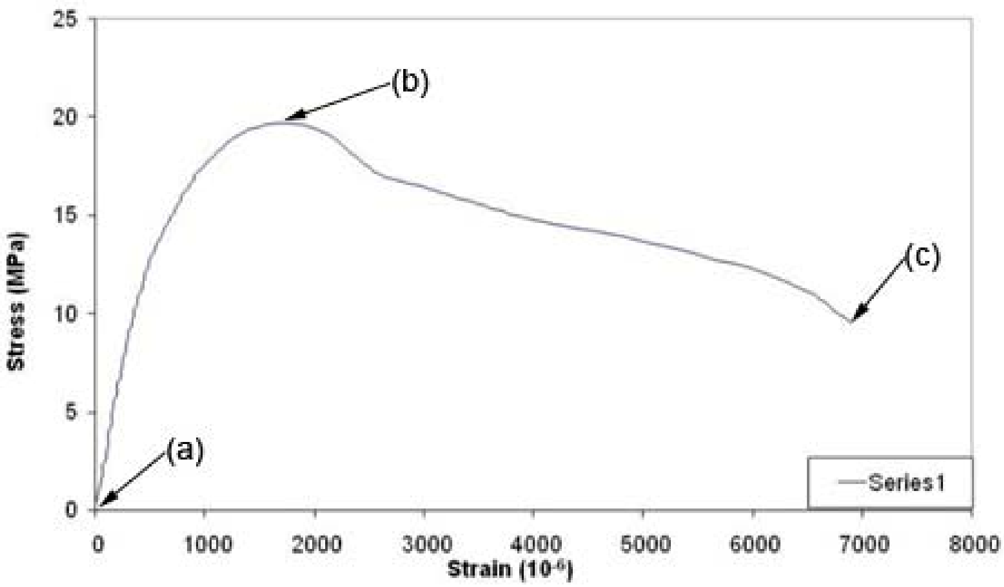

Figure 4-2 Stress-strain Relationship of Plain Concrete

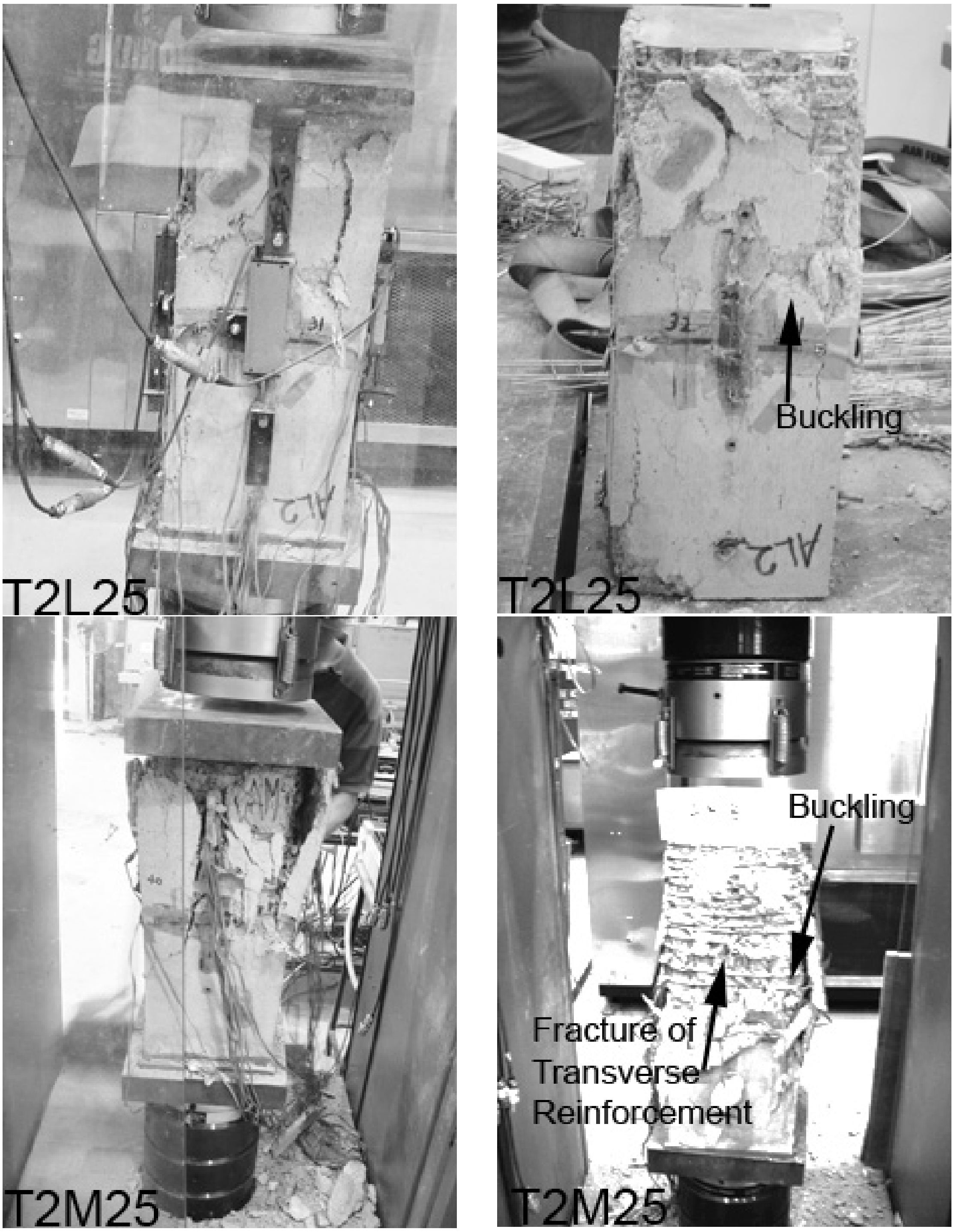

Figure 4-3 Failure of Reinforced Concrete Specimens (Left: Failure of Specimens, Right: Concrete Cover Peeled off after Failure, Top: Specimen T2L25 and Bottom: Specimen T2M25)

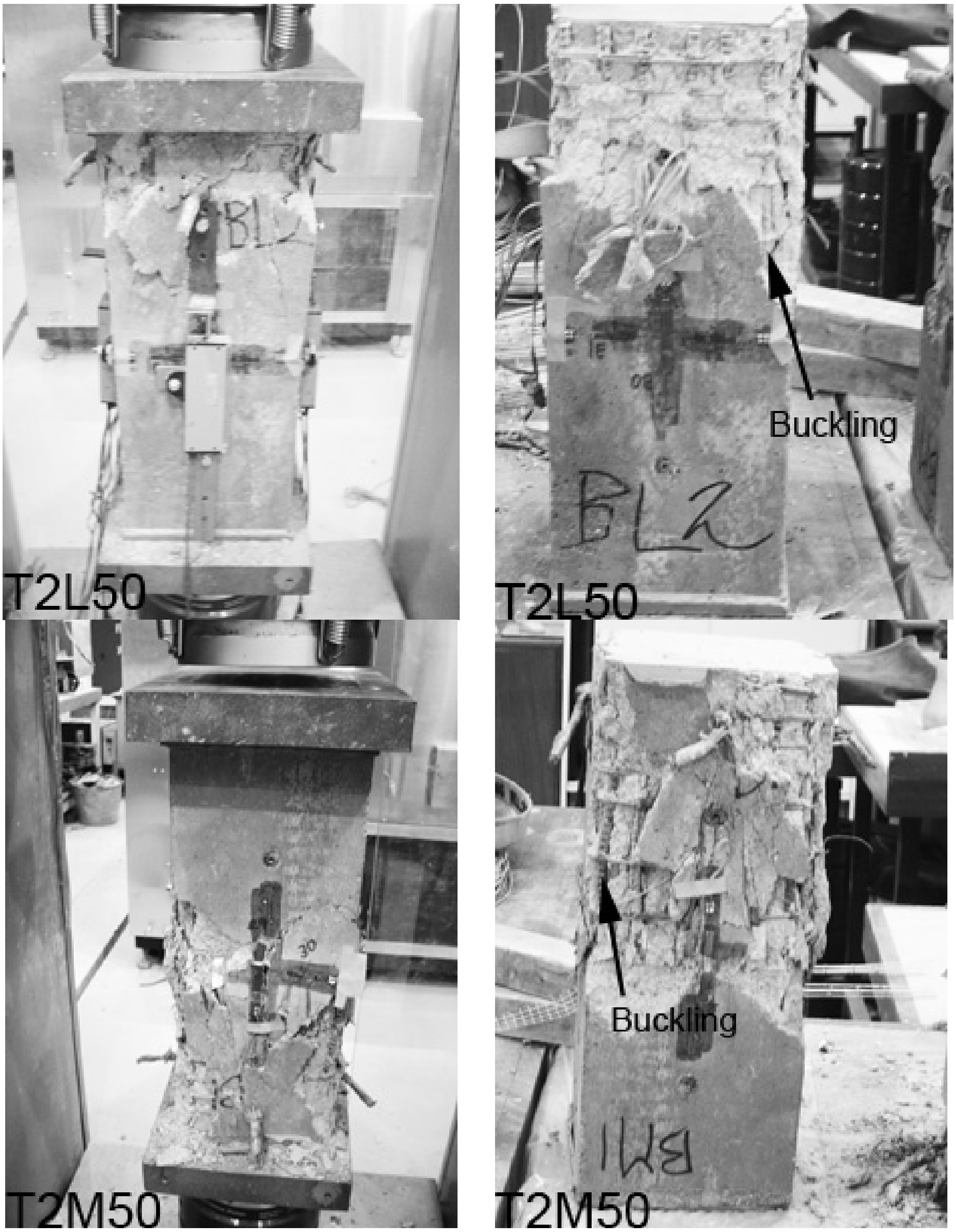

Figure 4-4 Failure of Reinforced Concrete Specimens (Left: Failure of Specimens, Right: Concrete Cover Peeled off after Failure, Top: Specimen T2L50 and Bottom: Specimen T2M50)

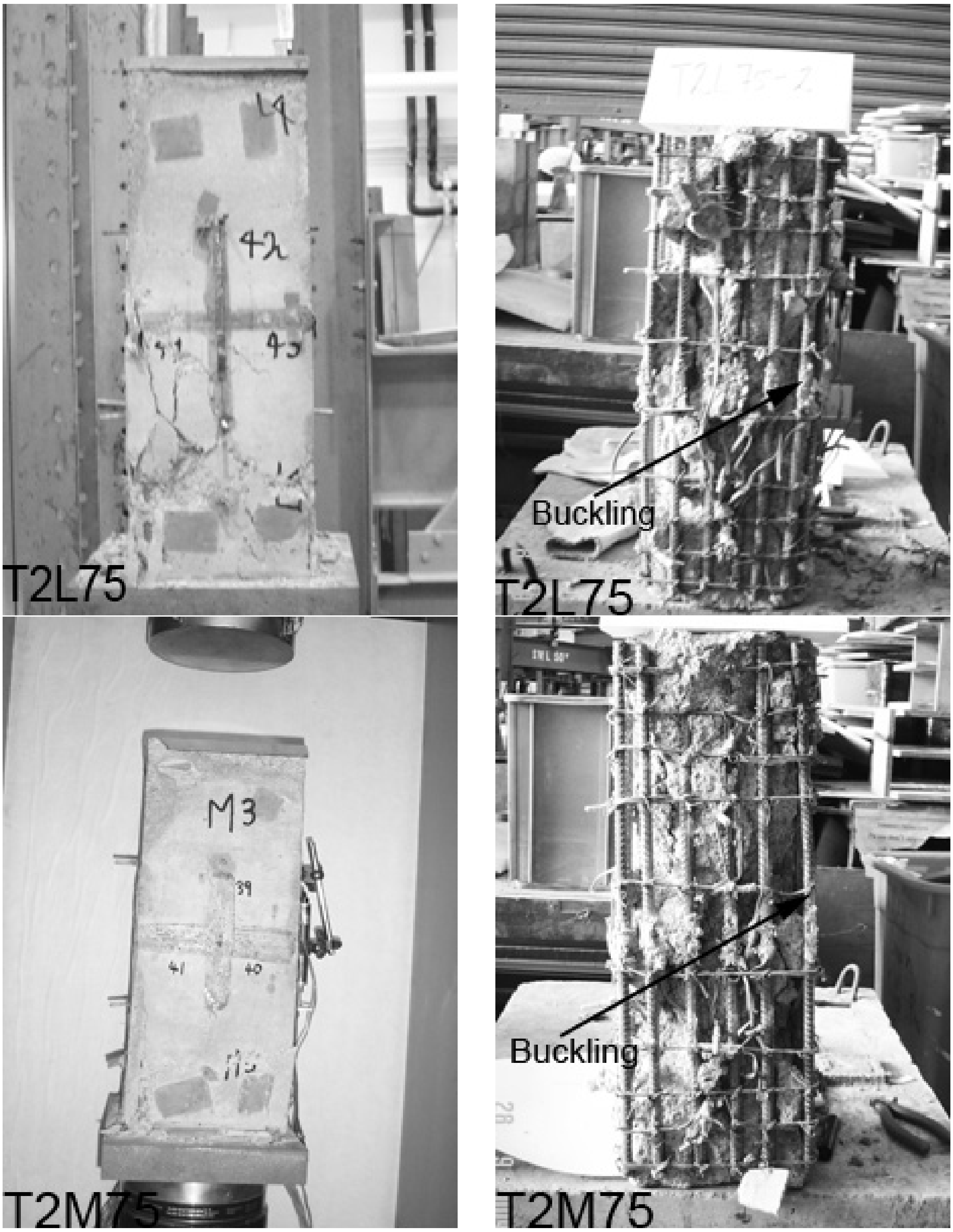

Figure 4-5 Failure of Reinforced Concrete Specimens (Left: Failure of Specimens, Right: Concrete Cover Peeled off after Failure, Top: Specimen T2L75 and Bottom: Specimen T2M75)

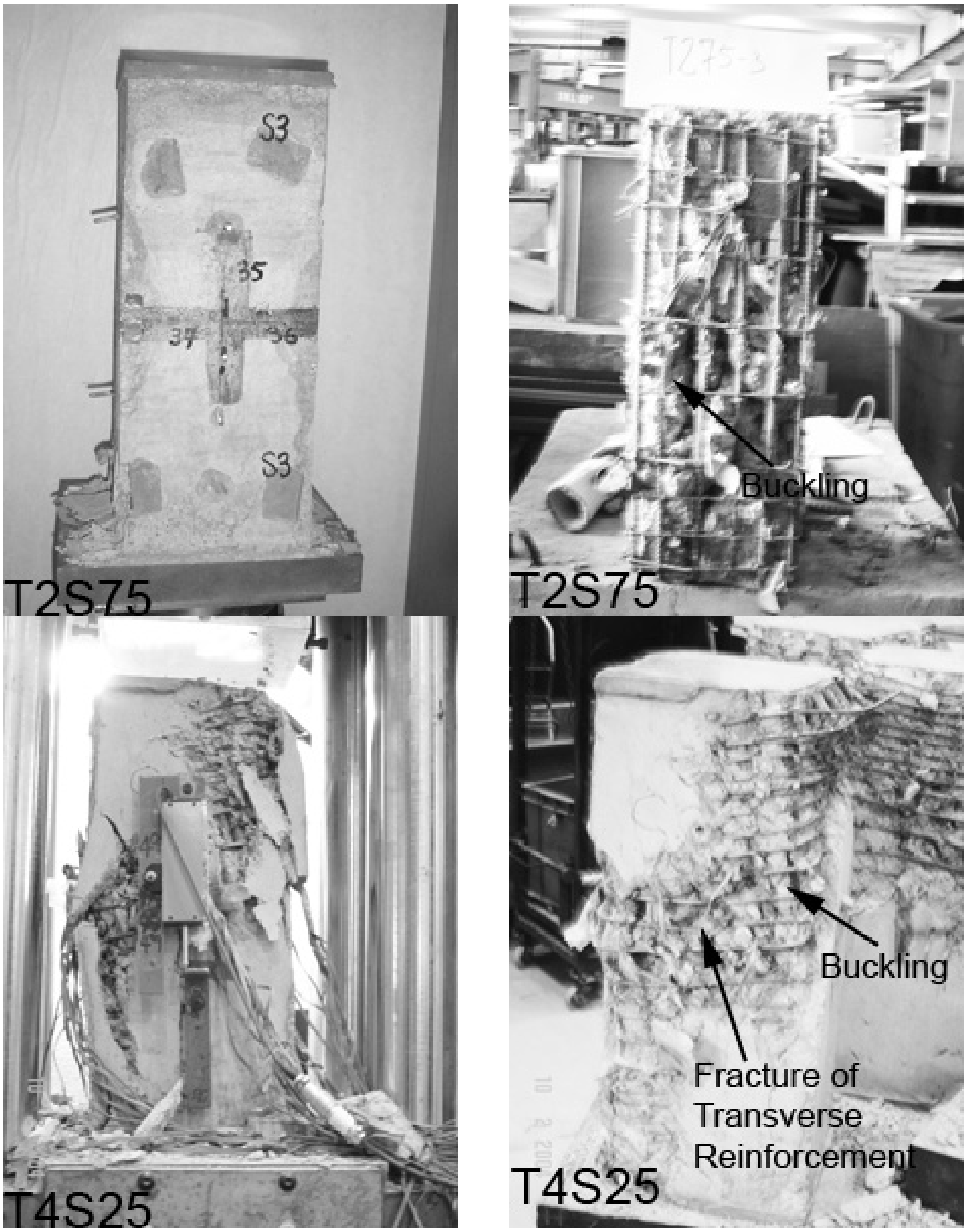

Figure 4-6 Failure of Reinforced Concrete Specimens (Left: Failure of Specimens, Right: Concrete Cover Peeled off after Failure, Top: Specimen T2S75 and Bottom: Specimen T4S25)

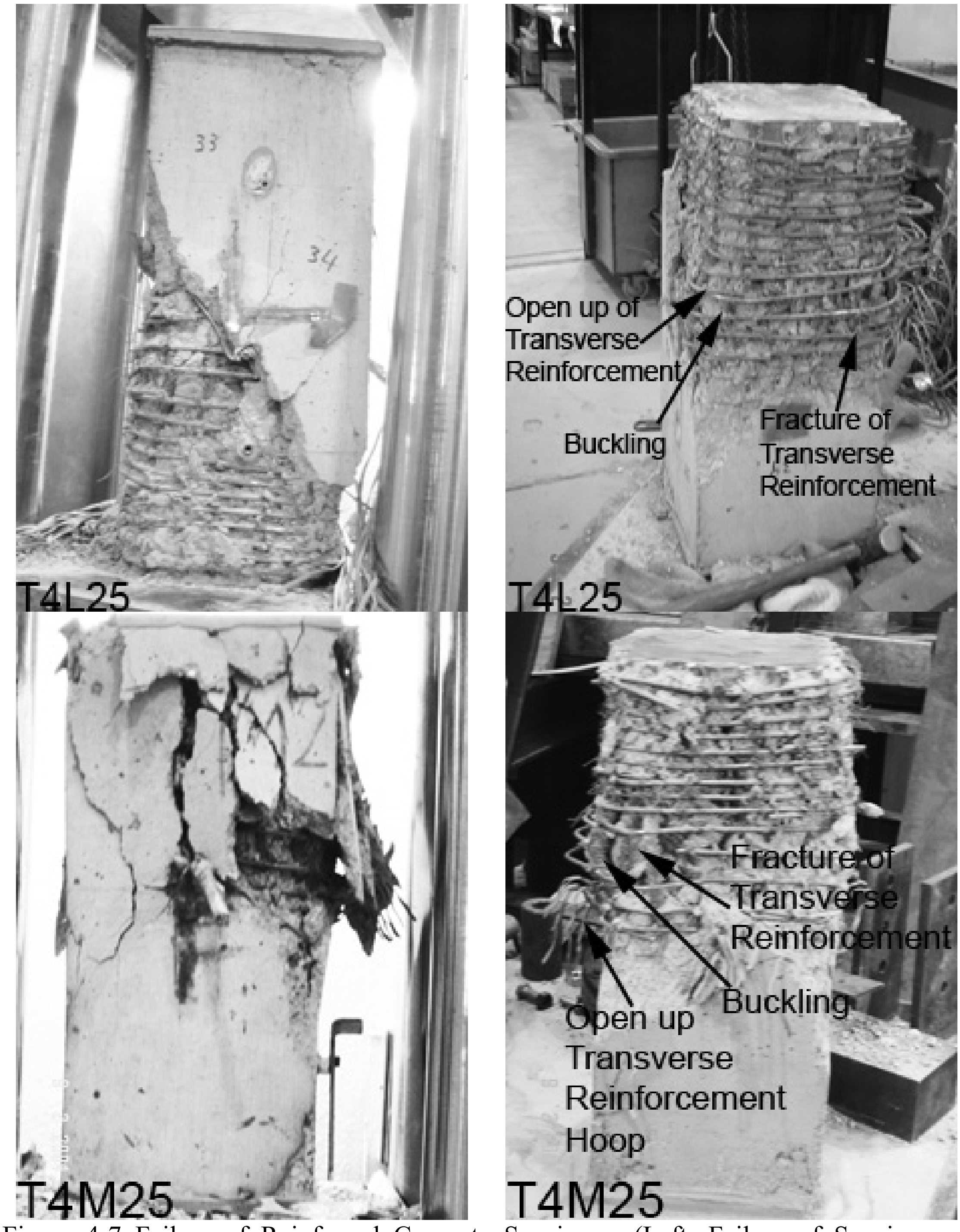

Figure 4-7 Failure of Reinforced Concrete Specimens (Left: Failure of Specimens, Right: Concrete Cover Peeled off after Failure, Top: Specimen T4L25 and Bottom: Specimen T4M25)

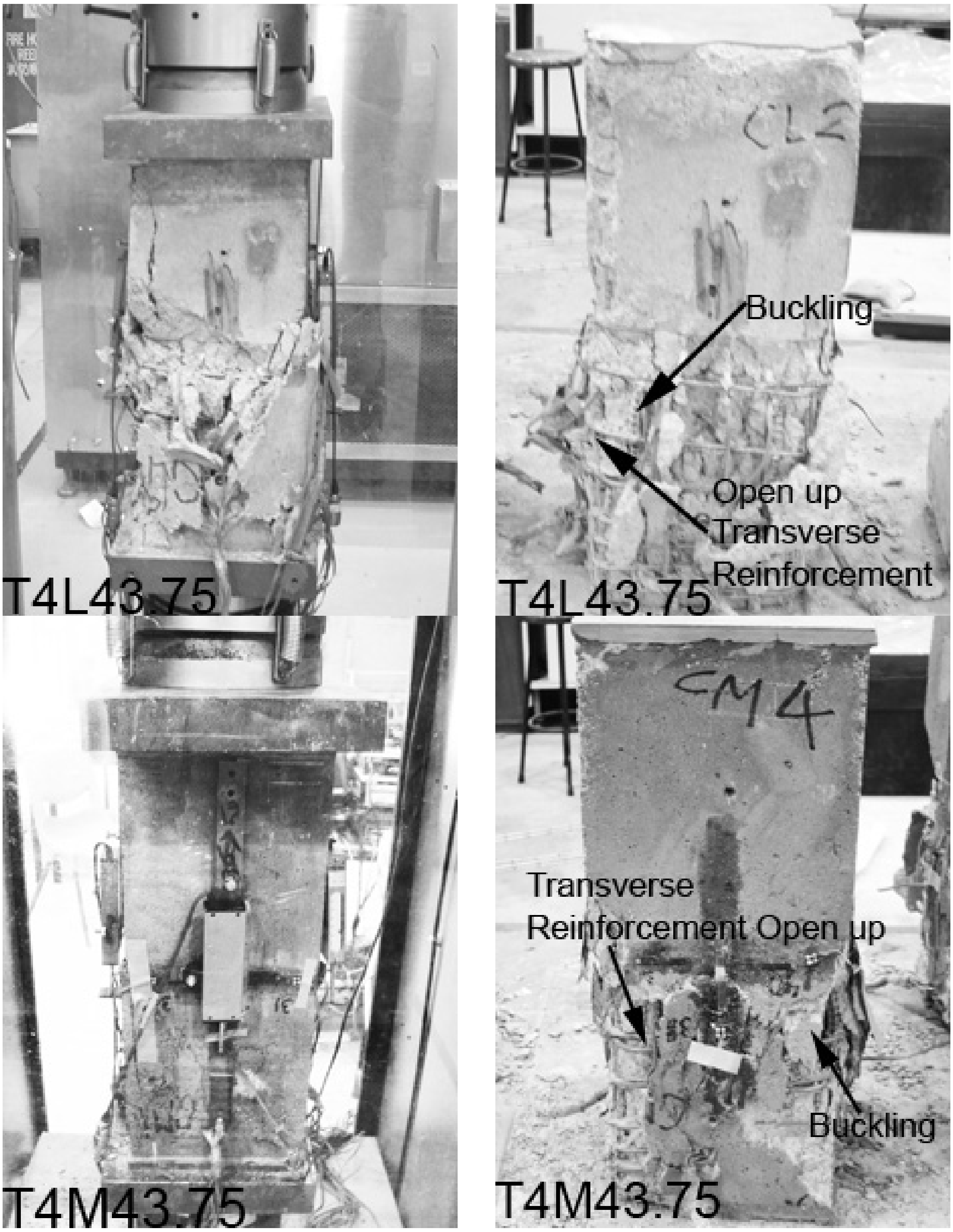

Figure 4-8 Failure of Reinforced Concrete Specimens (Left: Failure of Specimens, Right: Concrete Cover Peeled off after Failure, Top: Specimen T4L43.75 and Bottom: Specimen T4M43.75)

a) Specimen before testing $\varepsilon=0$

b) Specimen at Post Peak Load $\varepsilon=0.007361$

c) Specimen at Ultimate Strain $\varepsilon=0.010693$

Figure 4-9 Compressive Test of Specimen T2M50

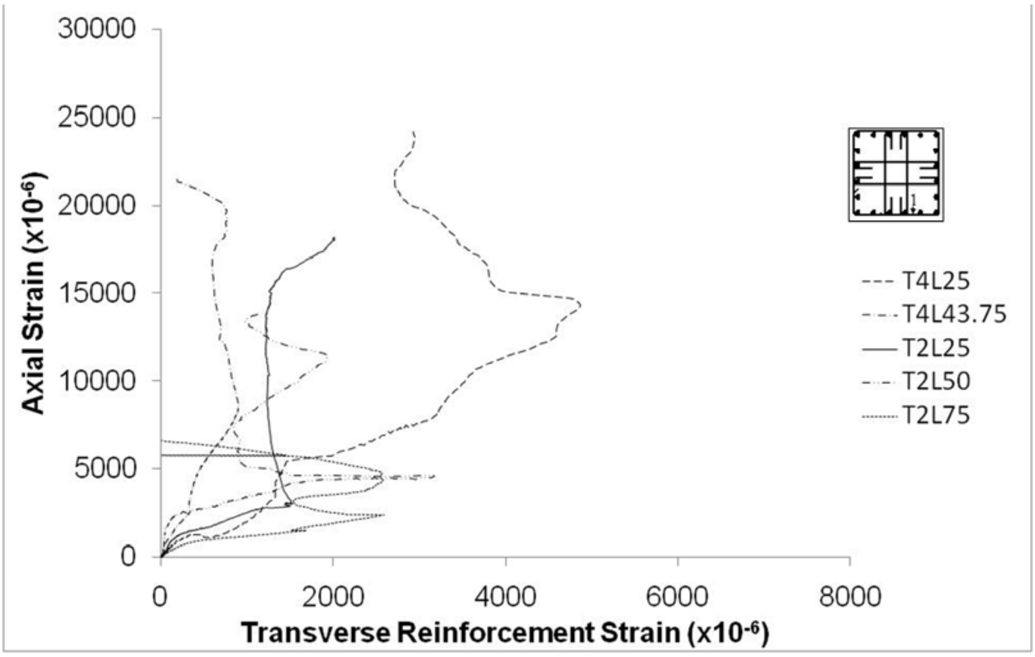

(a) Type L Detailing

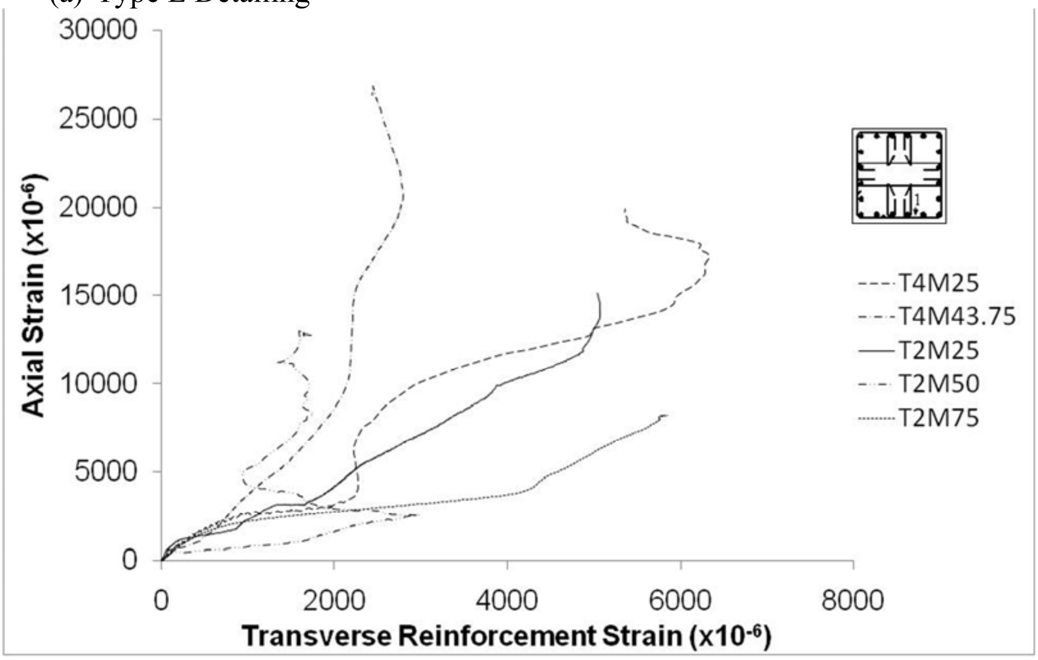

(b) Type M Detailing

Figure 4-10 Strain on Reinforcement Hoop at Location 1 against Axial Strain (Cont'd)

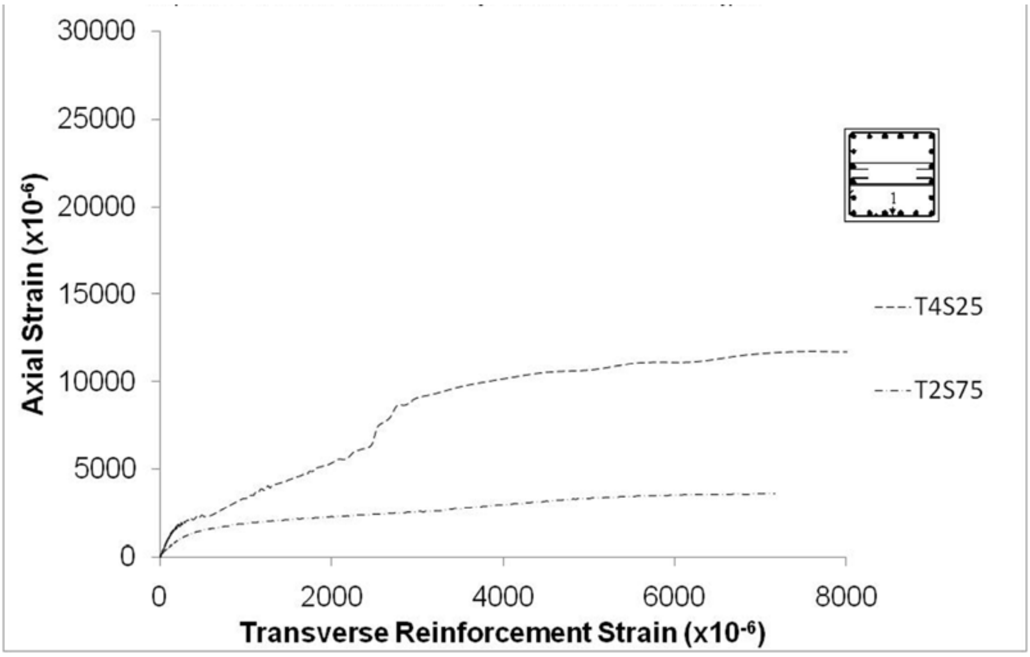

(c) Type S Detailing
Figure 4-10 Strain on Reinforcement Hoop at Location 1 against Axial Strain

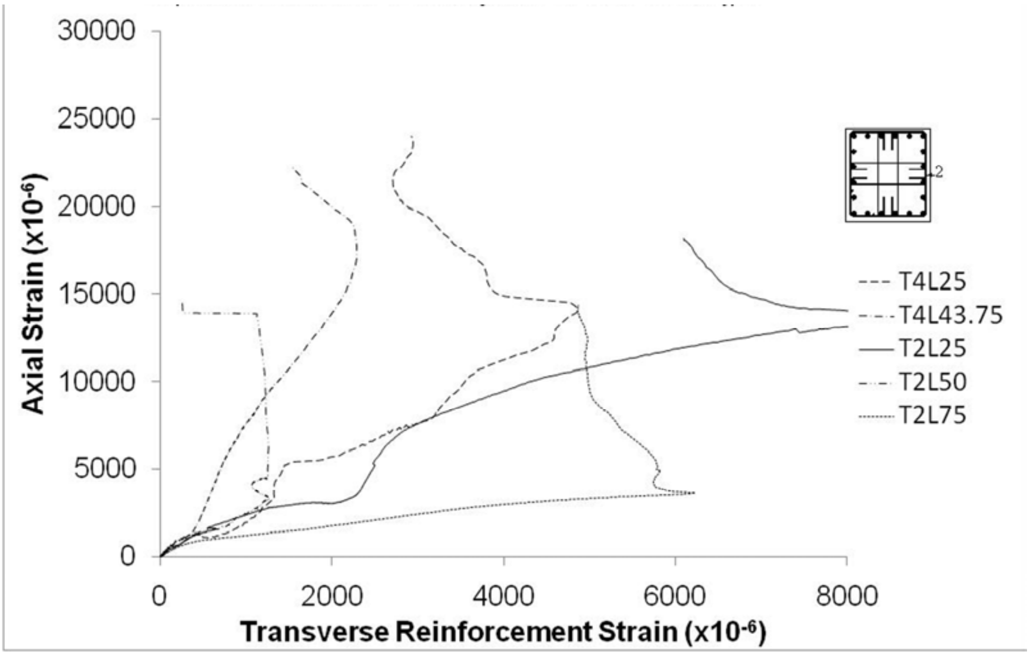

(a) Type L Detailing

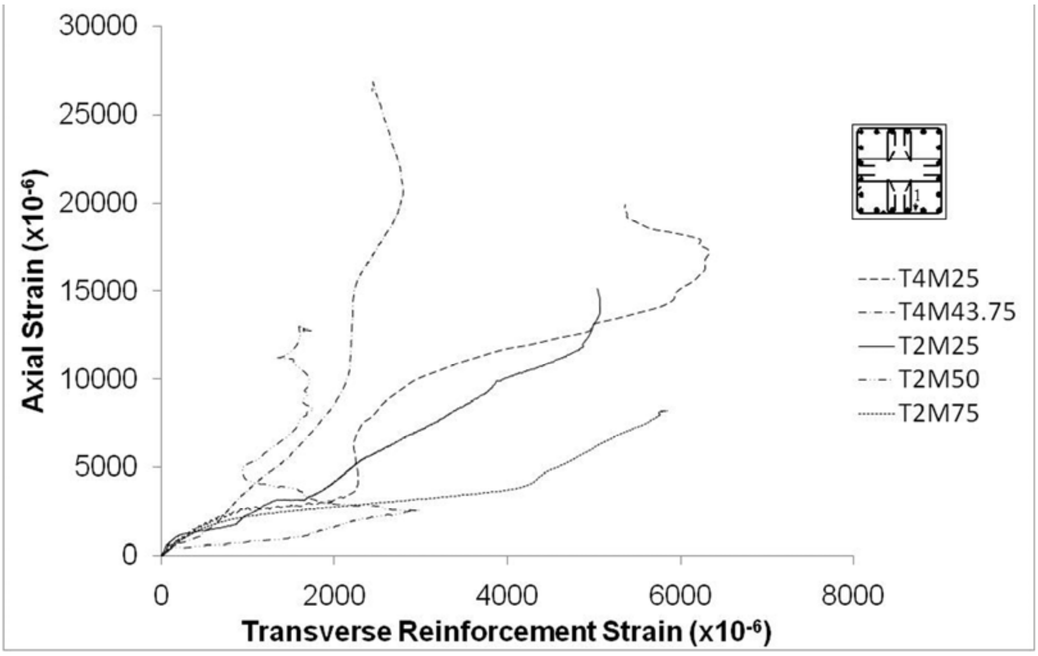

(b) Type M Detailing

Figure 4-11 Strain on Reinforcement Hoop at Location 2 against Axial Strain (Cont'd)

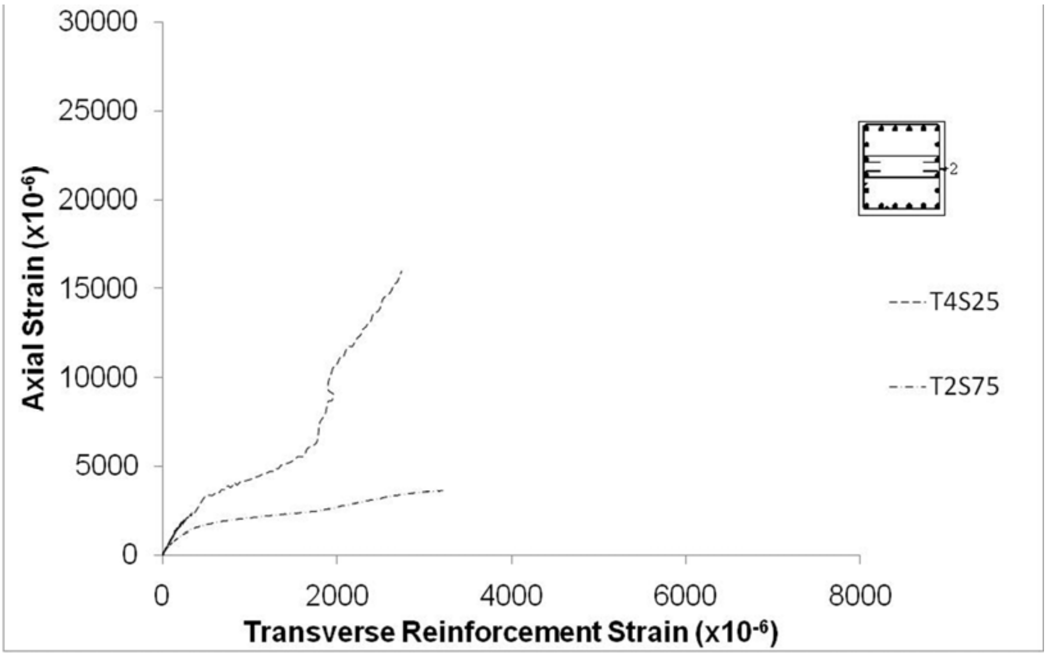

(c) Type S Detailing
Figure 4-11 Strain on Reinforcement Hoop at Location 2 against Axial Strain

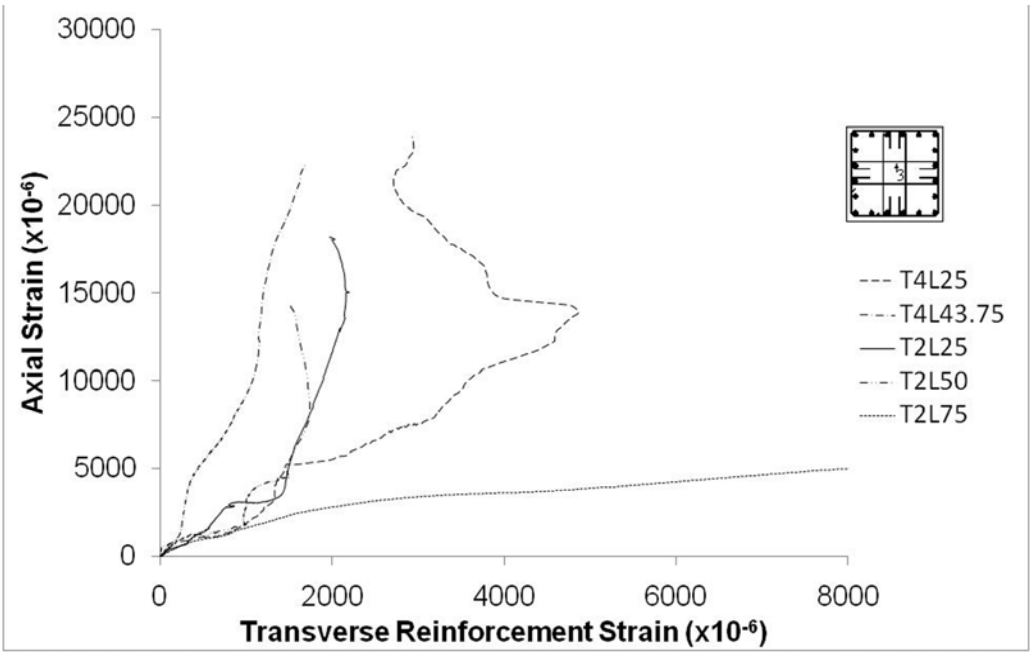

(a) Type L Detailing

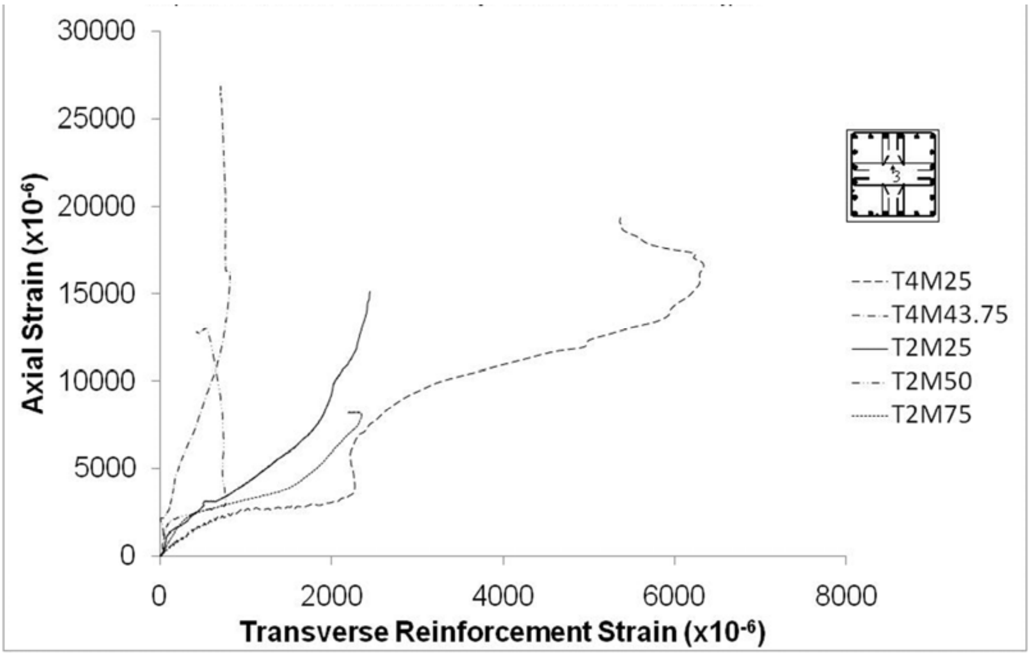

(b) Type M Detailing

Figure 4-12Strain on Long Crossties at Location 3 against Axial Strain (Cont'd)

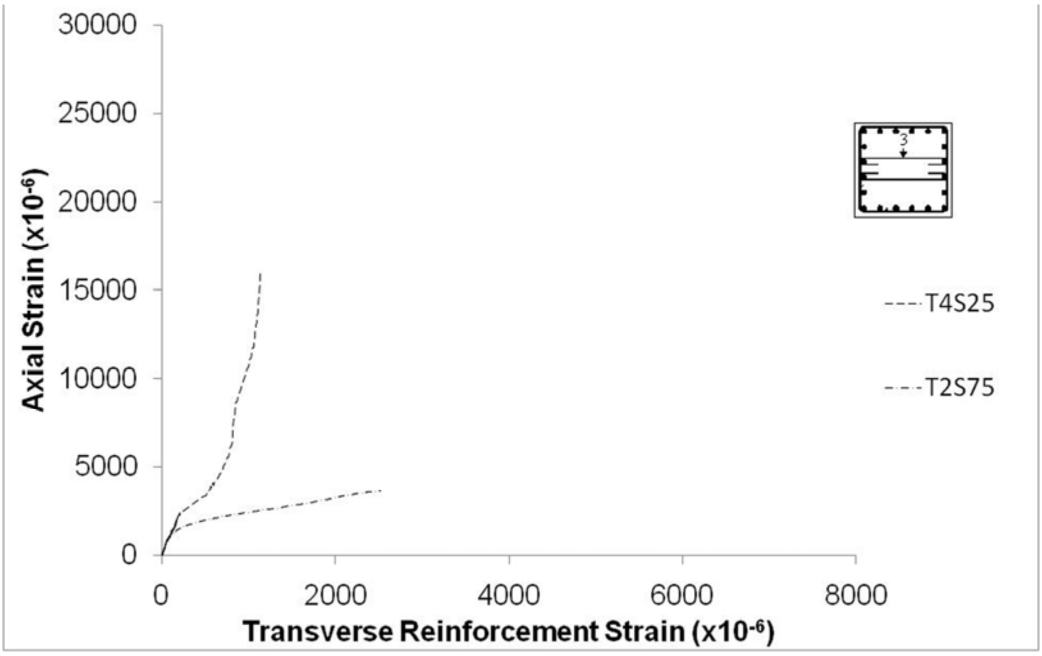

(c) Type S Detailing

Figure 4-12 Strain on Long Crossties at Location 3 against Axial Strain

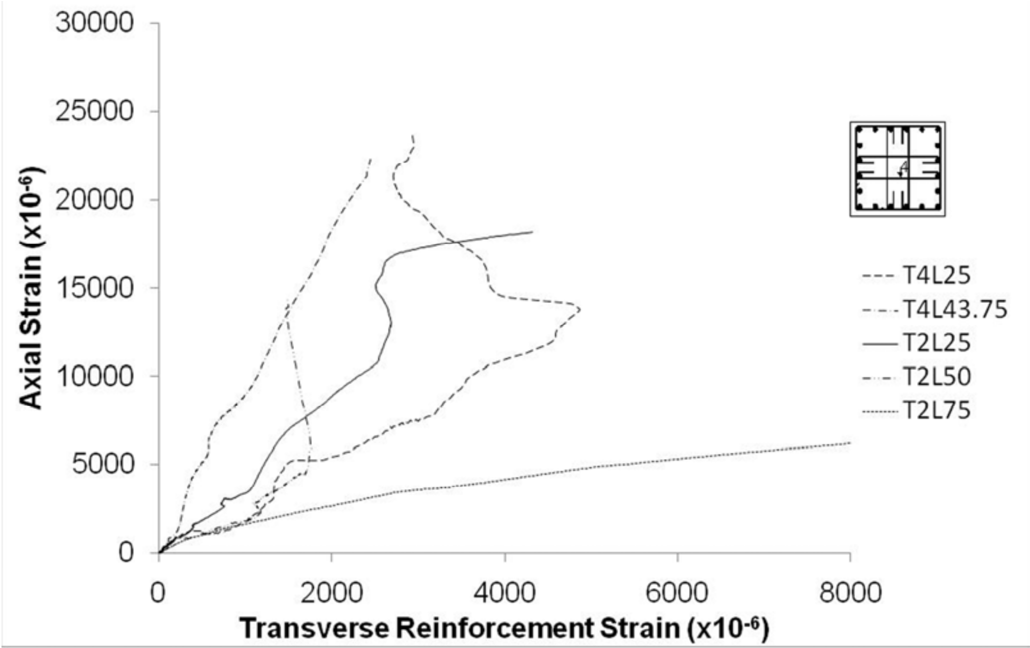

(a) Type L Detailing

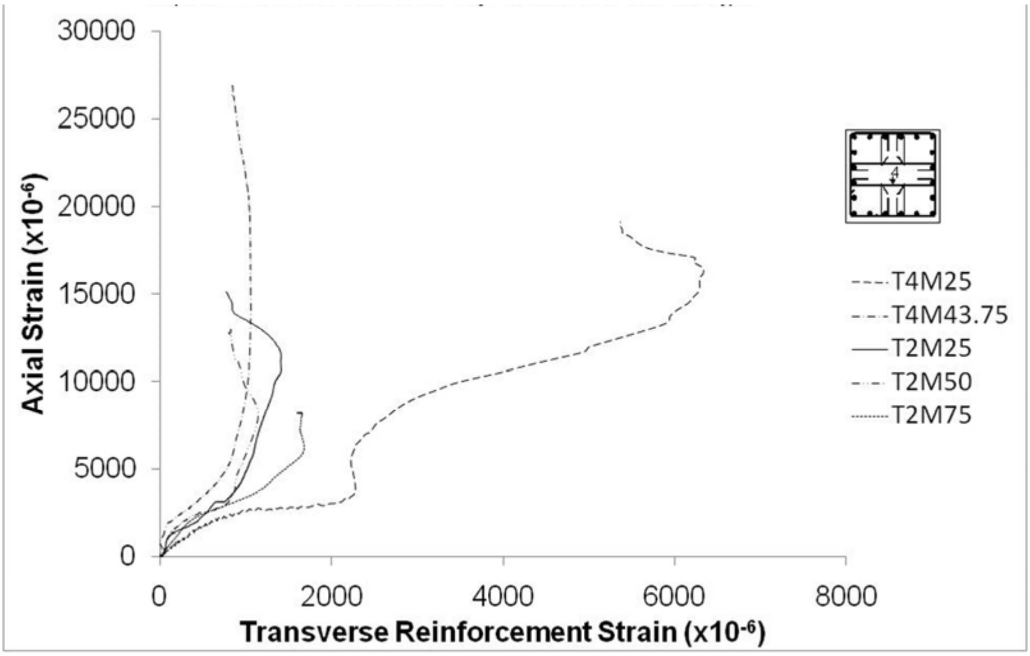

(b) Type M Detailing

Figure 4-13 Strain on Long Crossties at Location 4 against Axial Strain (Cont'd)

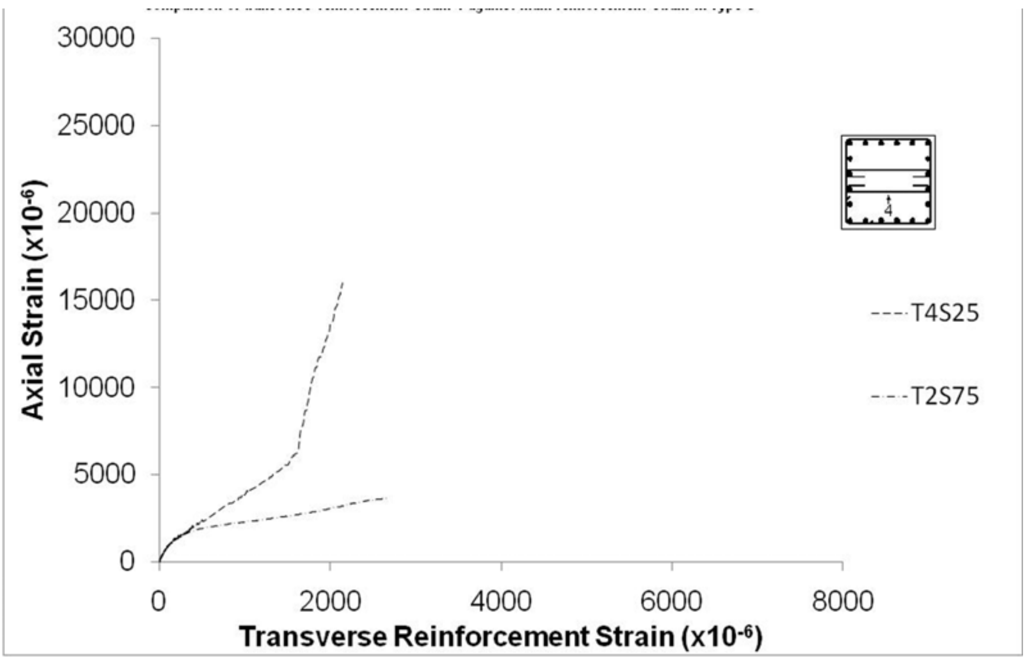

(c) Type S Detailing

Figure 4-13 Strain on Long Crossties at Location 4 against Axial Strain

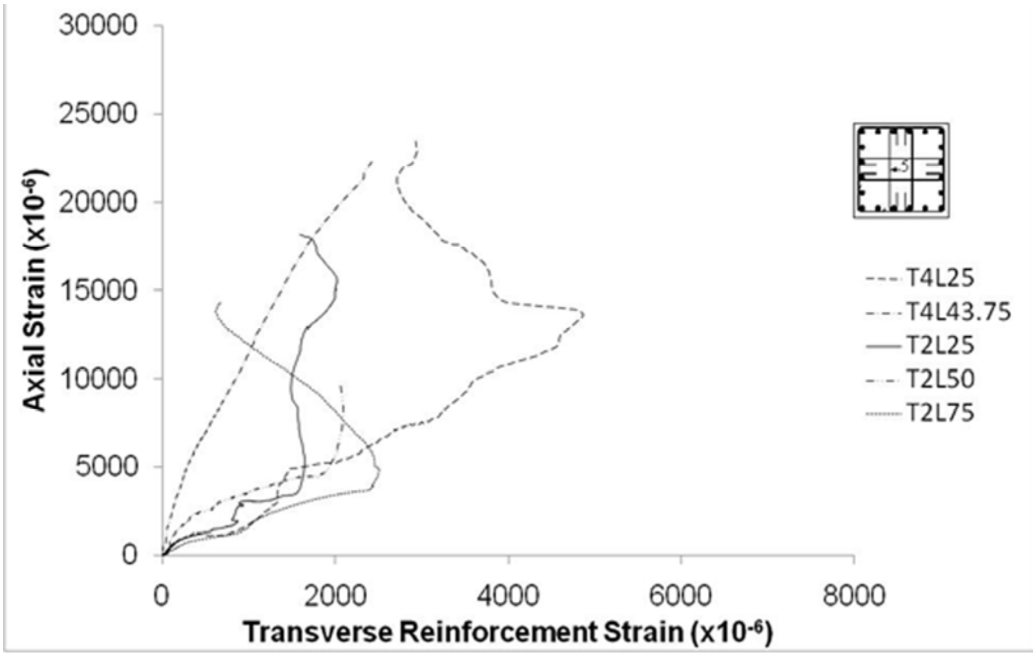

(a) Type L

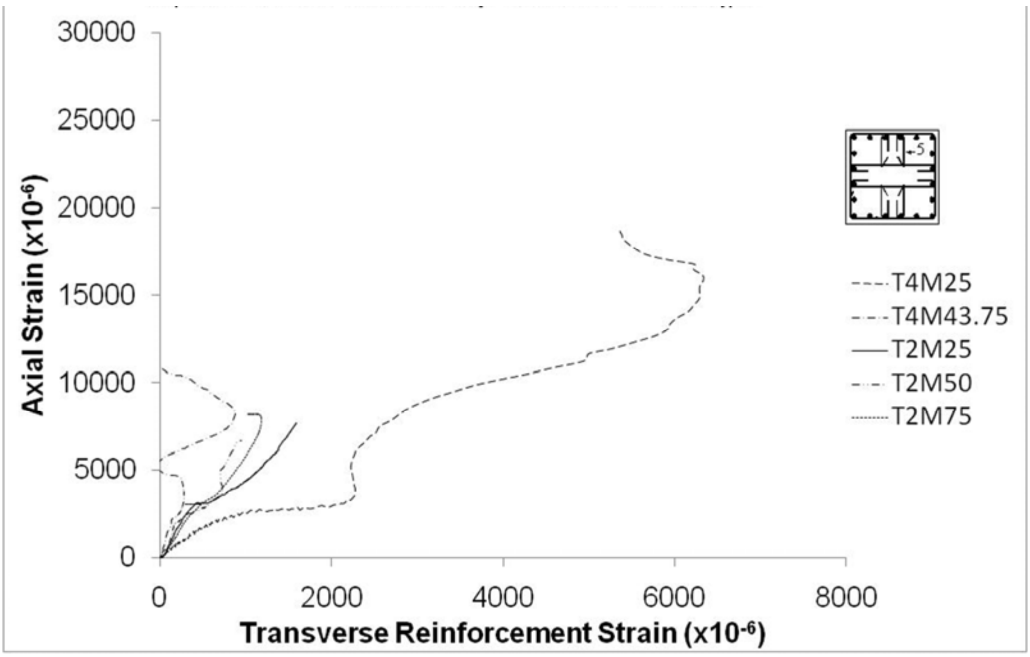

(b) Type M Detailing

Figure 4-14 Strain on Long and Short Crossties at Location 5 against Axial Strain

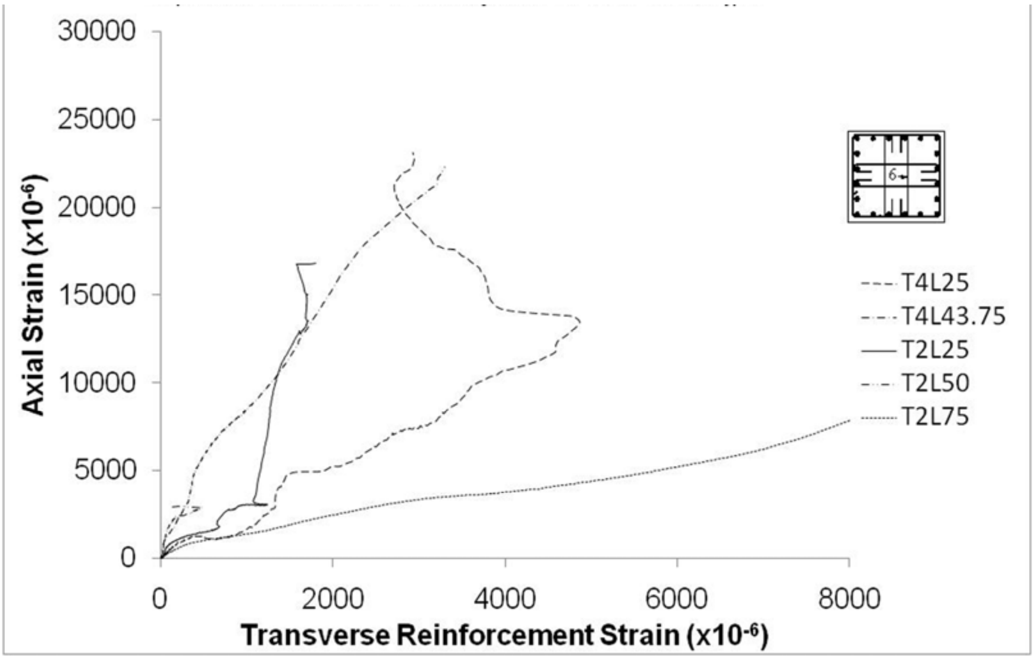

(a) Type L Detailing

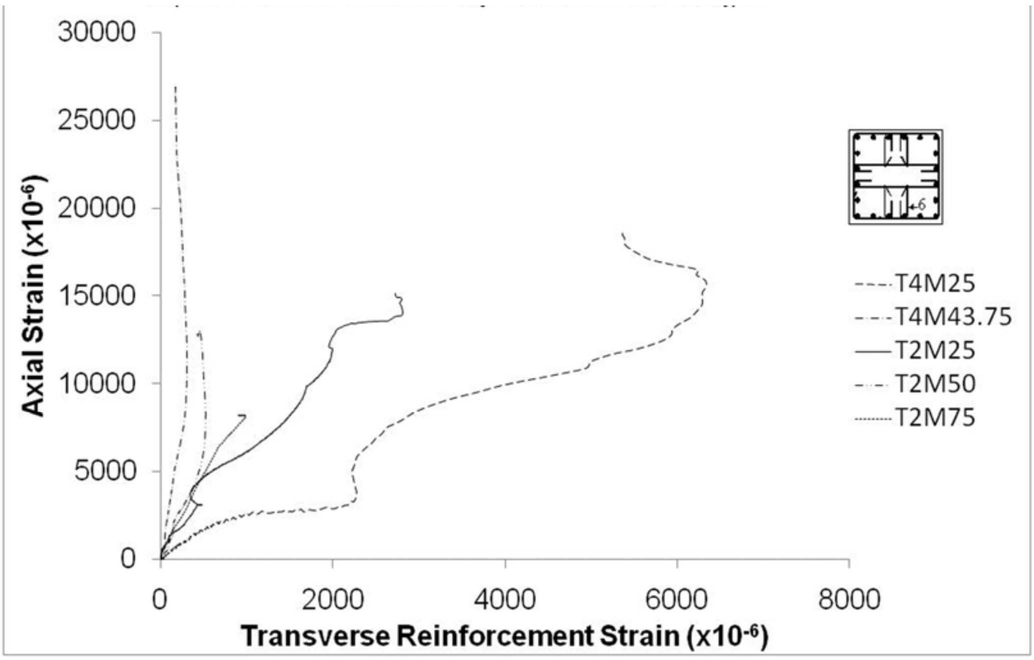

(b) Type M Detailing

Figure 4-15 Strain on Long and Short Crossties at Location 6 against Axial Strain

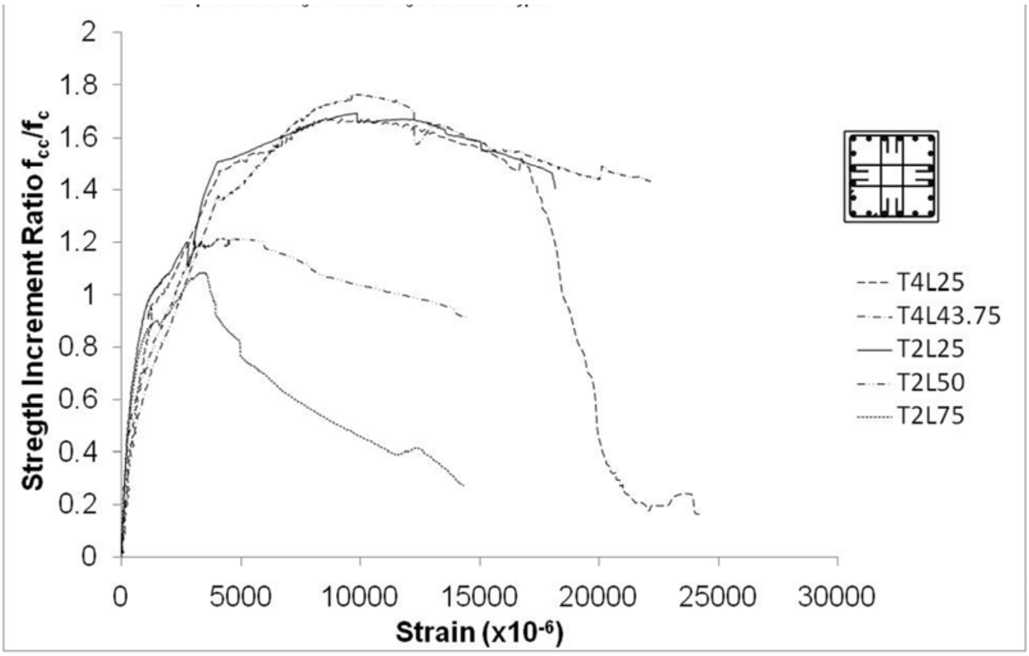

(a) Type L Detailing

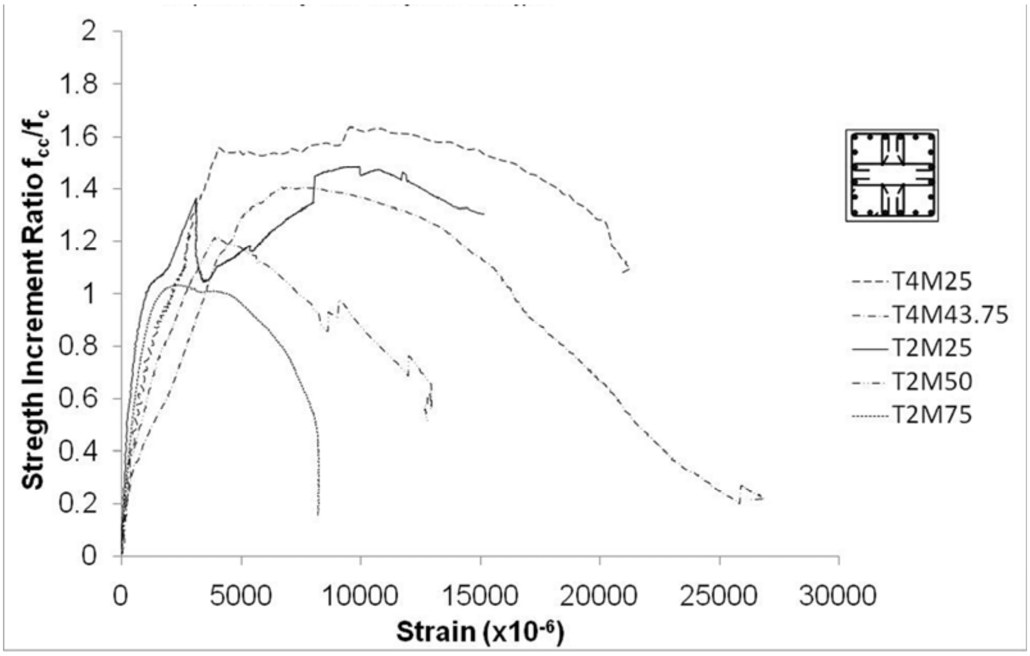

(b) Type M Detailing

Figure 4-16 Confined Concrete Stress against Strain for Different Types of Detailing (Cont'd)

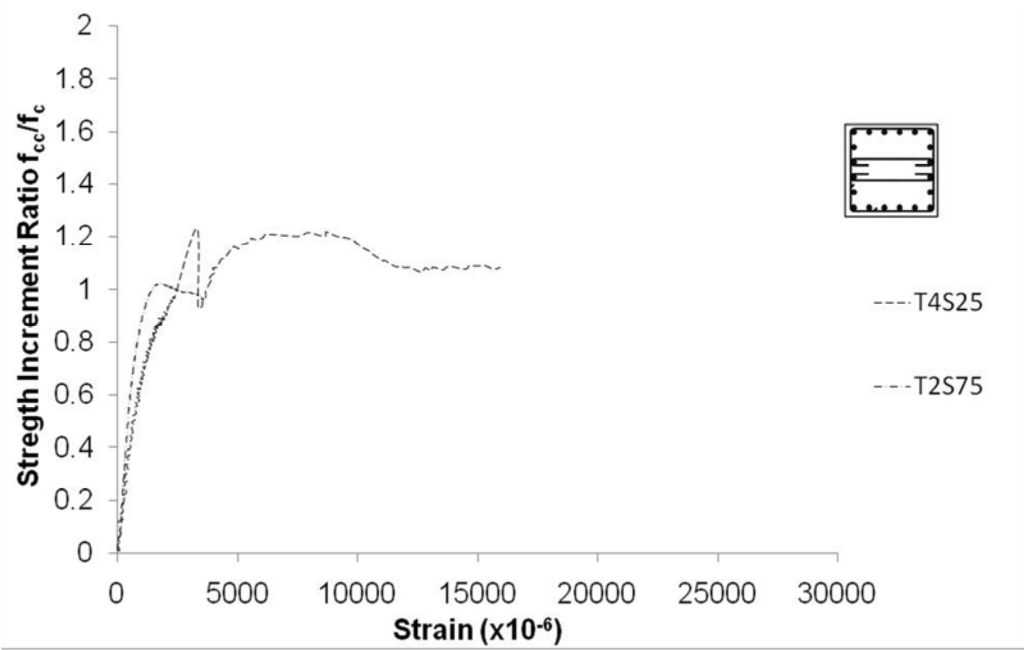

(c) Type S Detailing
Figure 4-16 Confined Concrete Stress against Strain for Different Types of Detailing

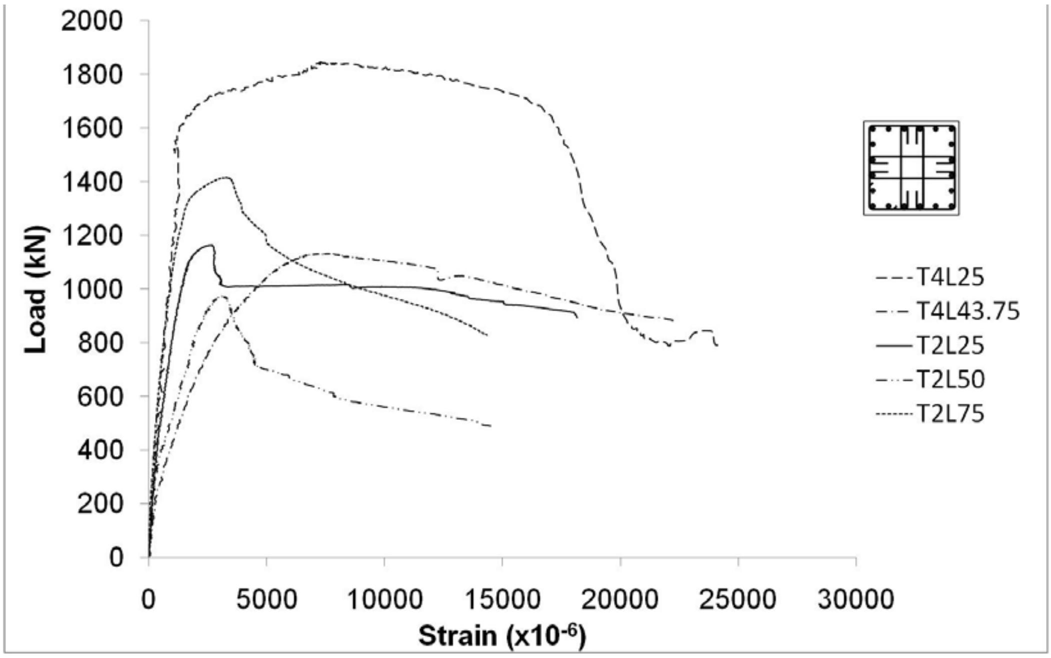

(a) Type L Detailing

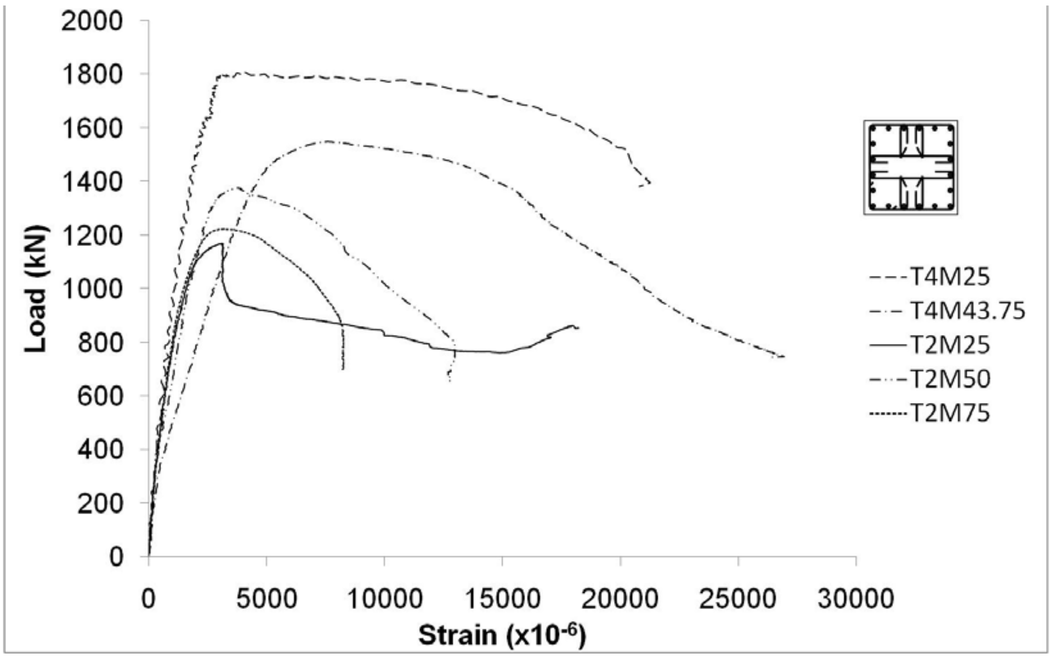

(b) Type M Detailing

Figure 4-17 Loads against Strain (Cont'd)

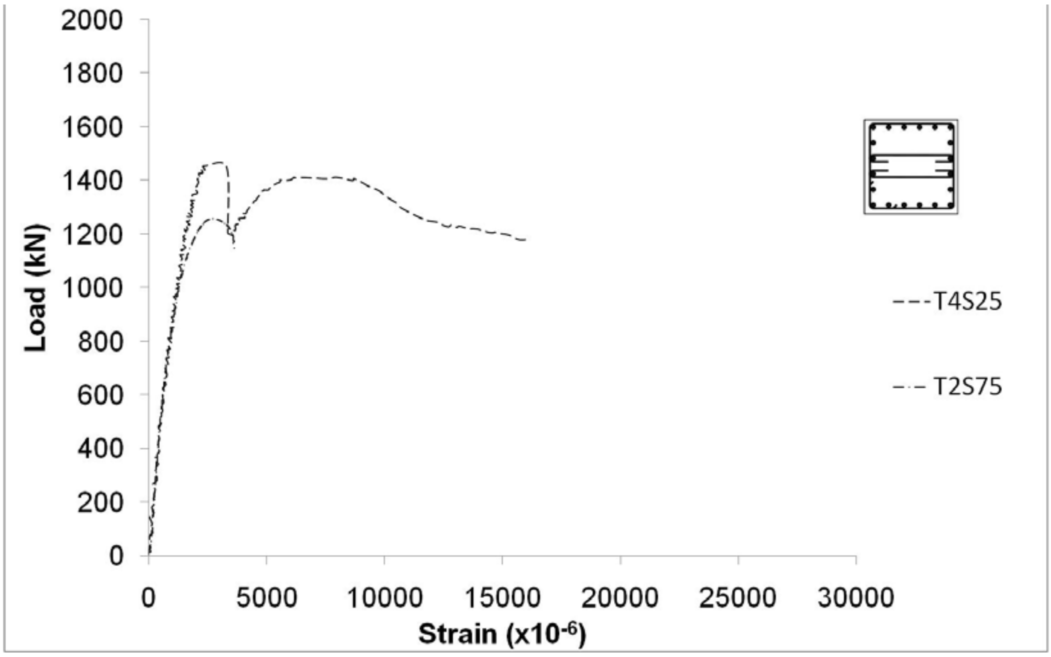

(c) Type S Detailing

Figure 4-17 Loads against Strain

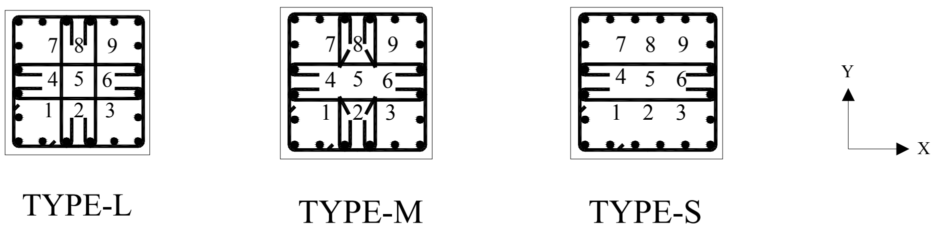

Figure 4-18 Confining Zone in Transverse Reinforcement

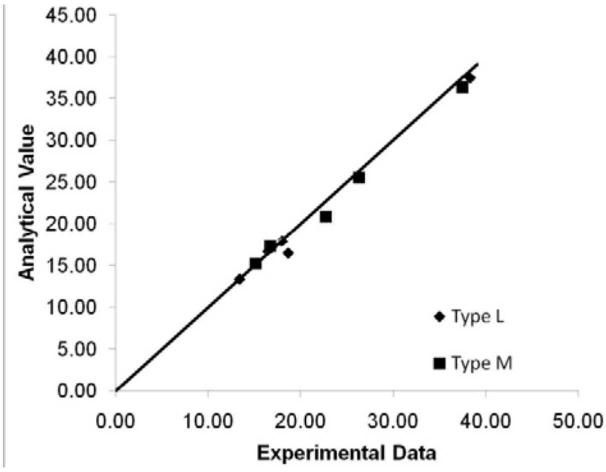

Figure 4-19 Comparison of the Predicted Value against Experimental Results of Confined Concrete Strength

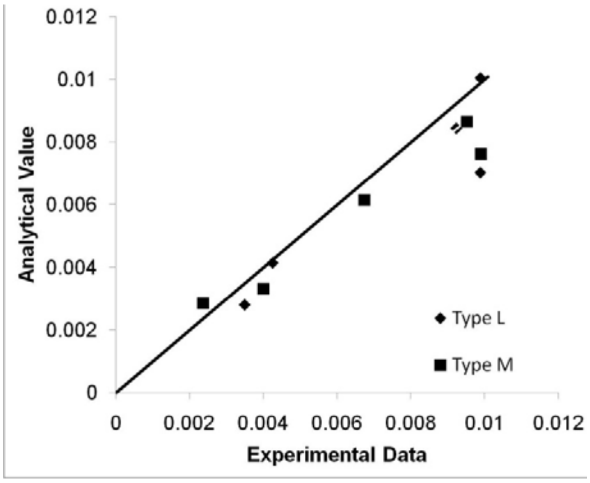

Figure 4-20 Comparison of the Predicted Value against Experimental Results of Strain at Peak Strength

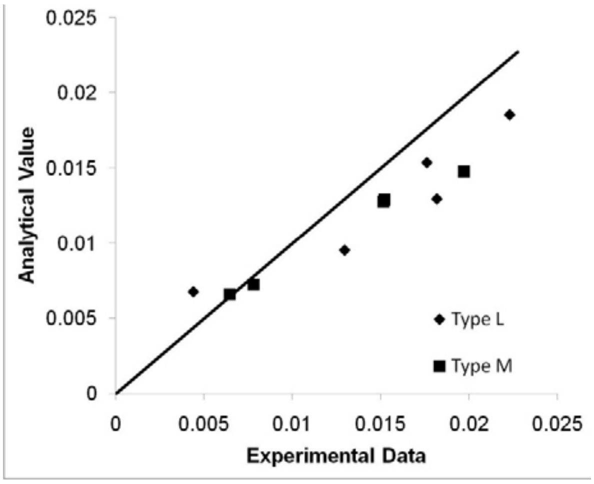

Figure 4-21 Comparison of the Predicted Value against Experimental Results of Ultimate Strain

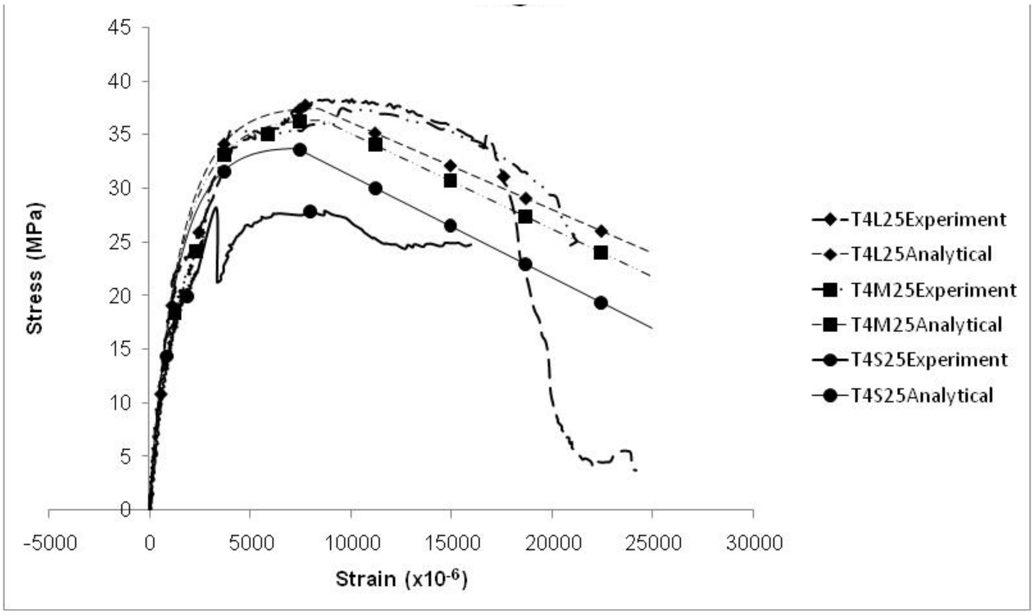

(a) Specimens with T4@25

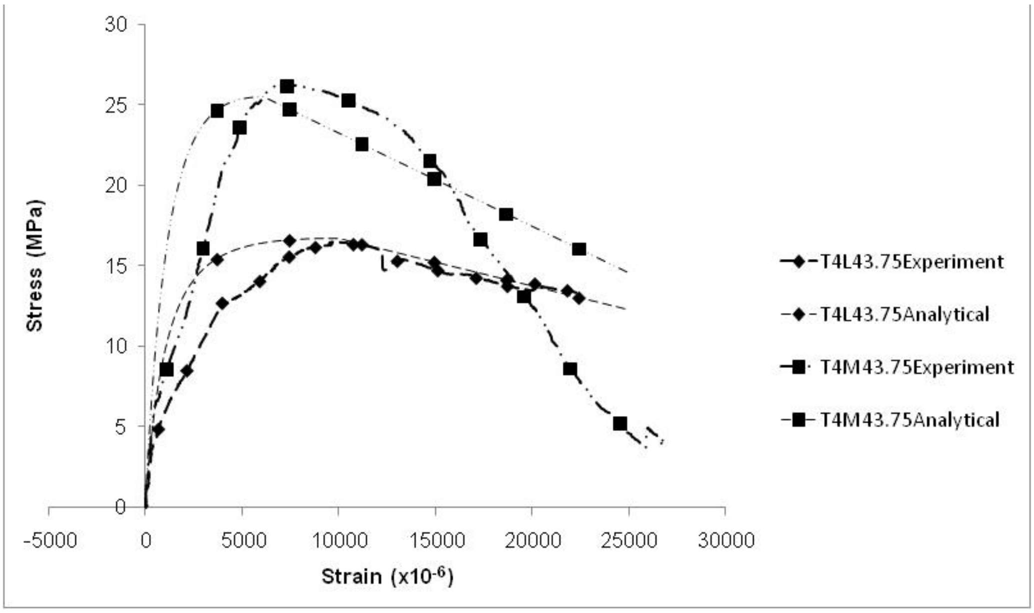

(b) Specimens with T4@43.75

Figure 4-22 Comparison of Stress-strain Relationship of Confined Concrete between Experimental Result and Predicted Value (cont'd)

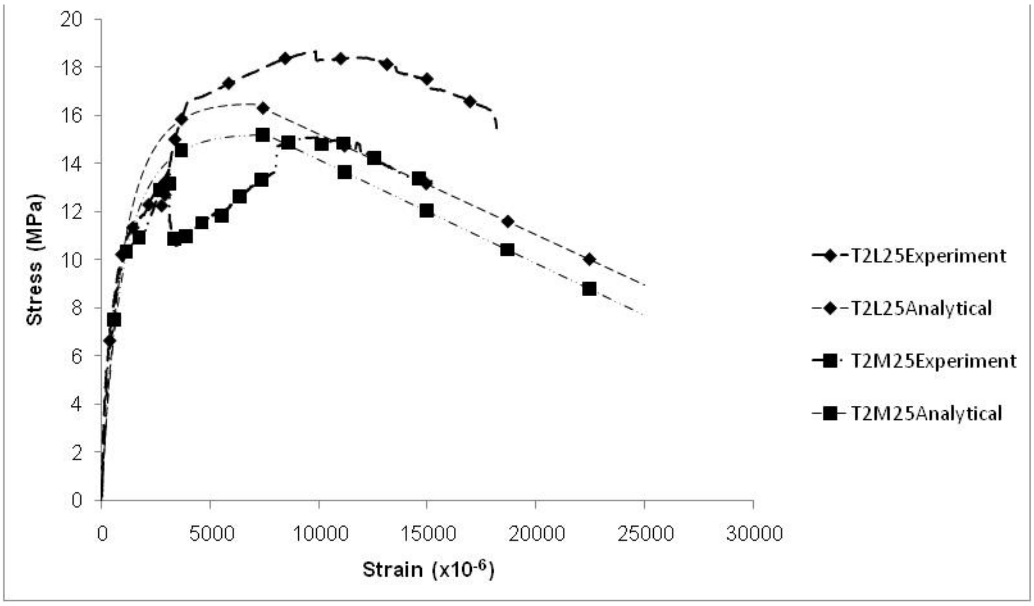

(c) Specimens with T2@25

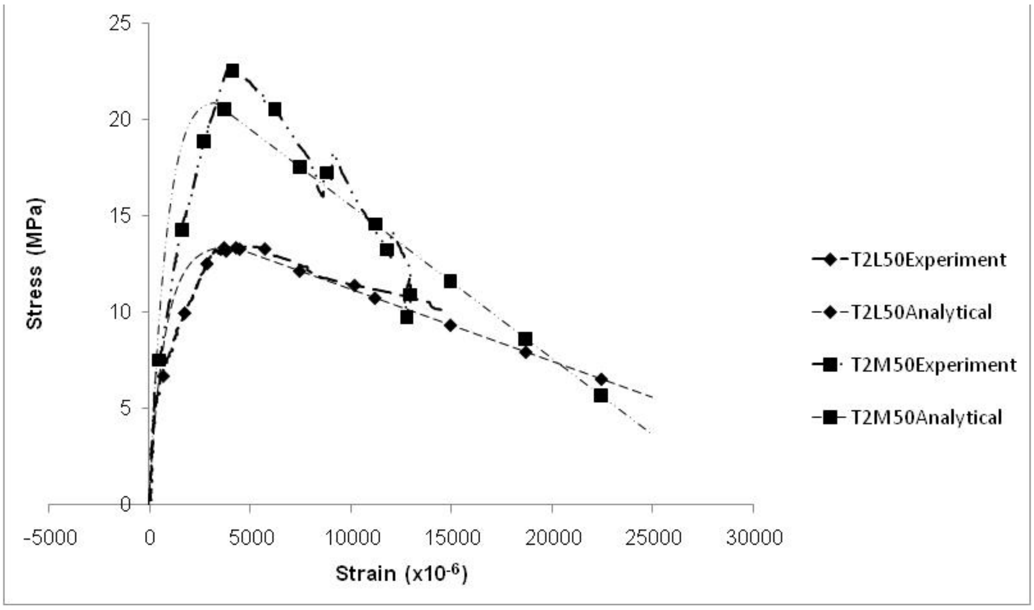

(d) Specimens with T2@50

Figure 4-22 Comparison of Stress-strain Relationship of Confined Concrete between Experimental Result and Predicted Value (cont'd)

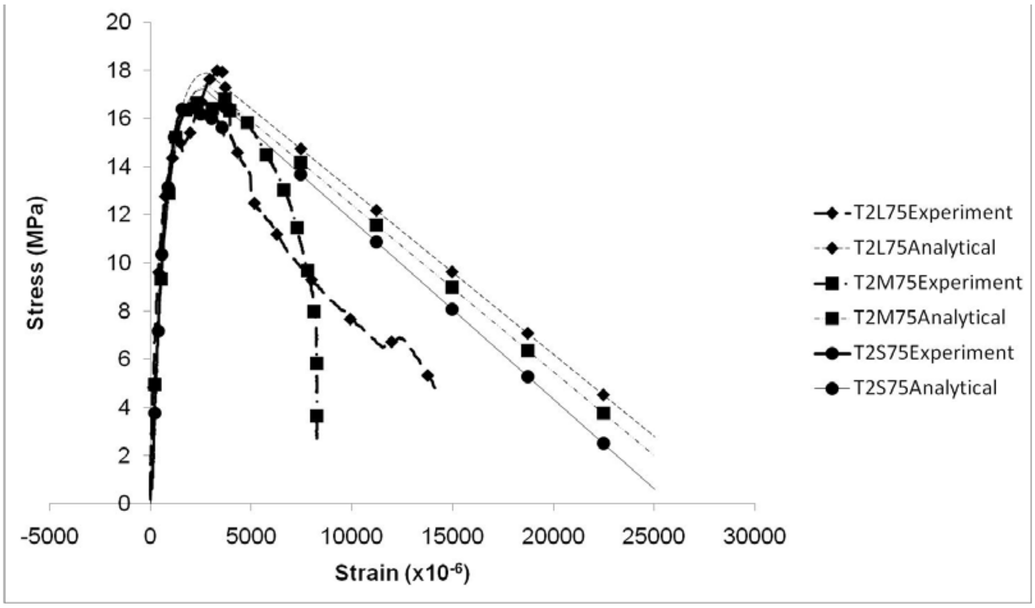

(e) Specimens with T2@75

Figure 4-22 Comparison of Stress-strain Relationship of Confined Concrete between Experimental Result and Predicted Value (cont'd)

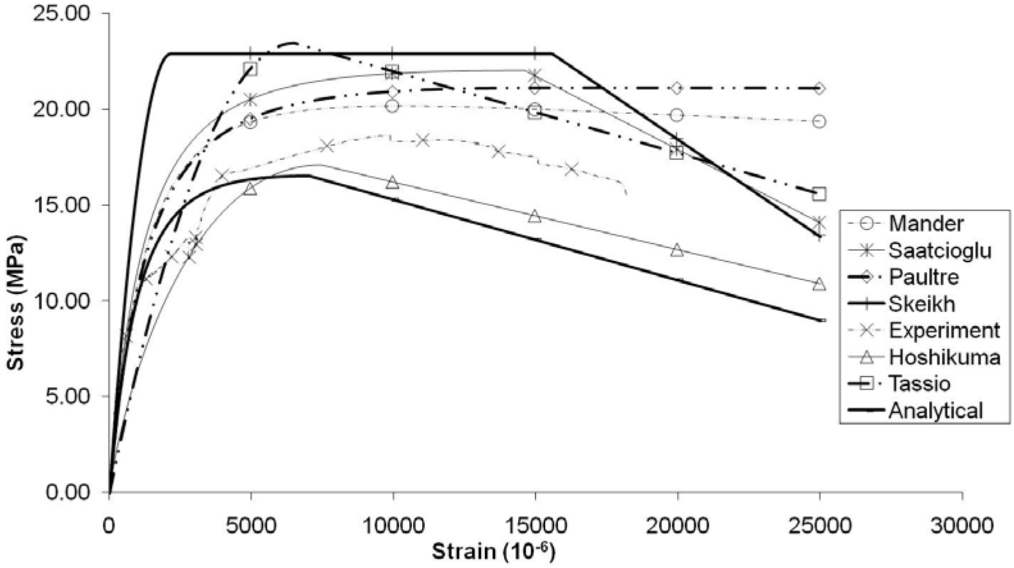

(a) Specimen T2L25

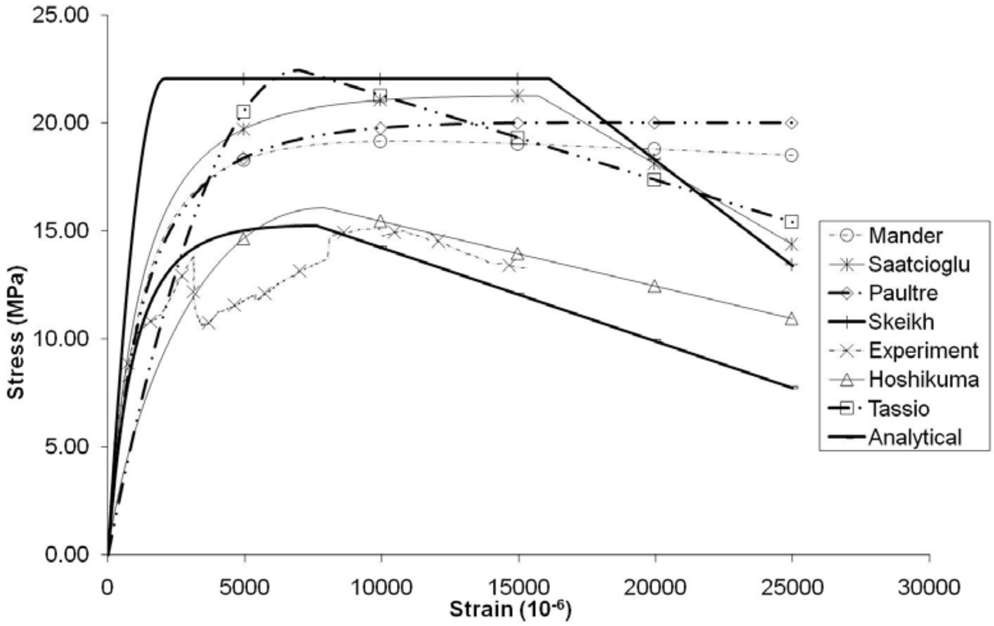

(b) Specimen T2M25

Figure 4-23 Comparison of Confined Concrete Stress-strain Relationship among Previous Models, Proposed Model and Experimental Data (Cont'd)

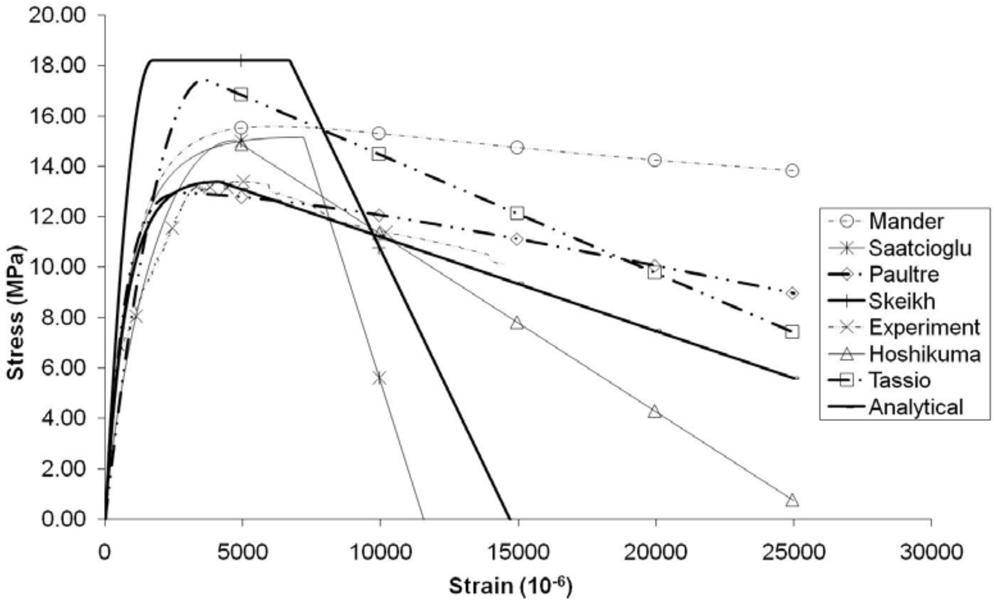

(c) Specimen T2L50

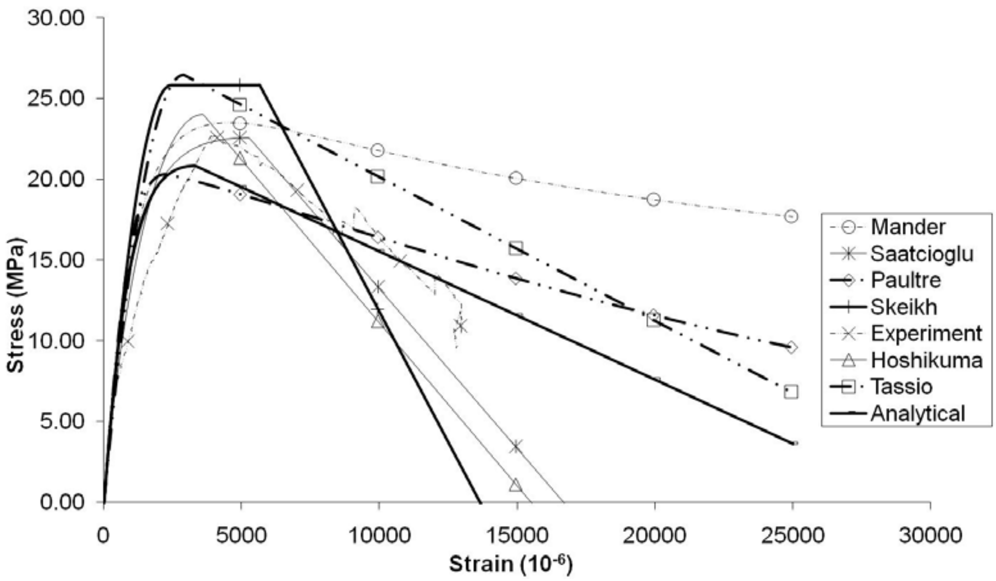

(d) Specimen T2M50

Figure 4-23 Comparison of Confined Concrete Stress-strain Relationship among Previous Models, Proposed Model and Experimental Data (Cont'd)

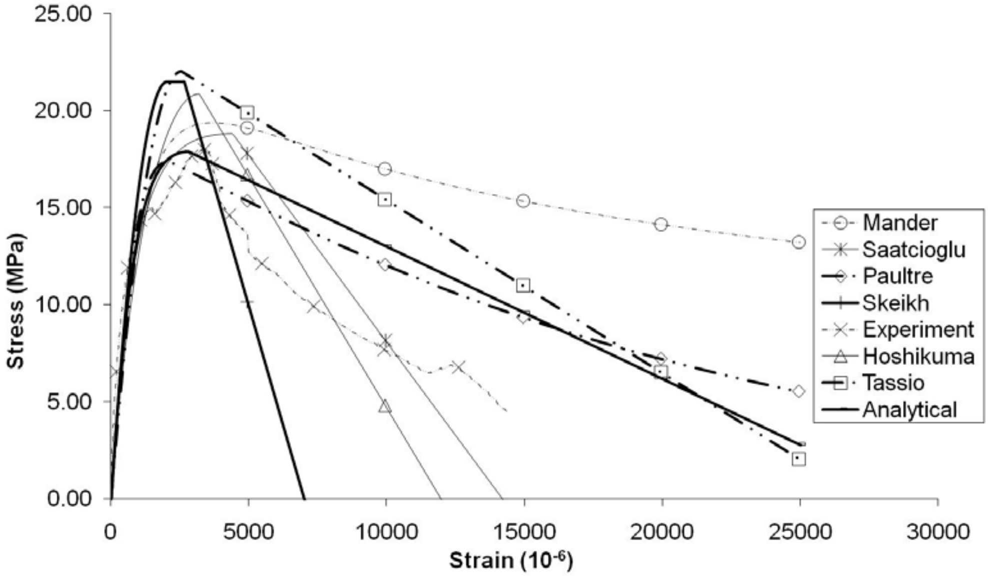

(e) Specimen T2L75

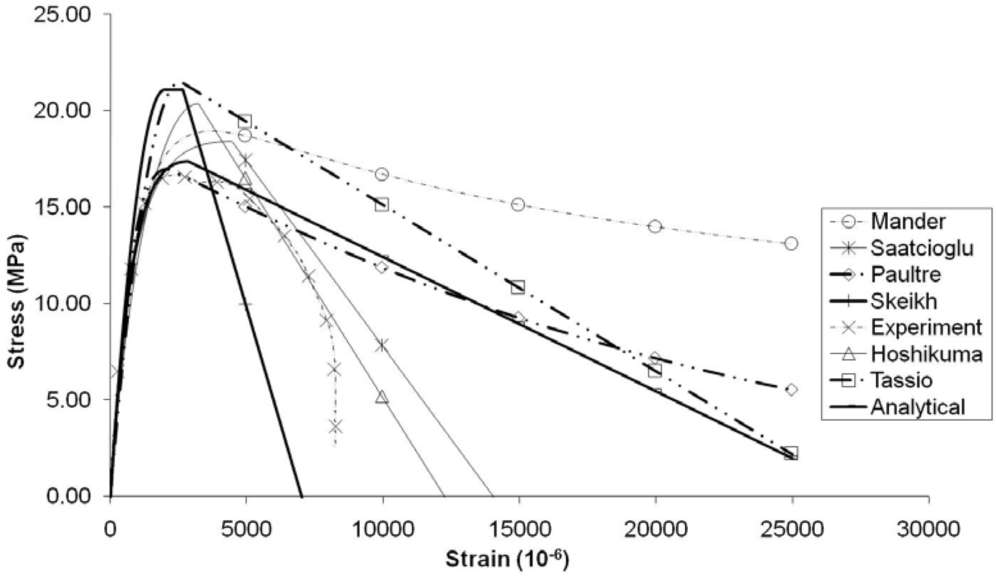

(f) Specimen T2M75

Figure 4-23 Comparison of Confined Concrete Stress-strain Relationship among Previous Models, Proposed Model and Experimental Data (Cont'd)

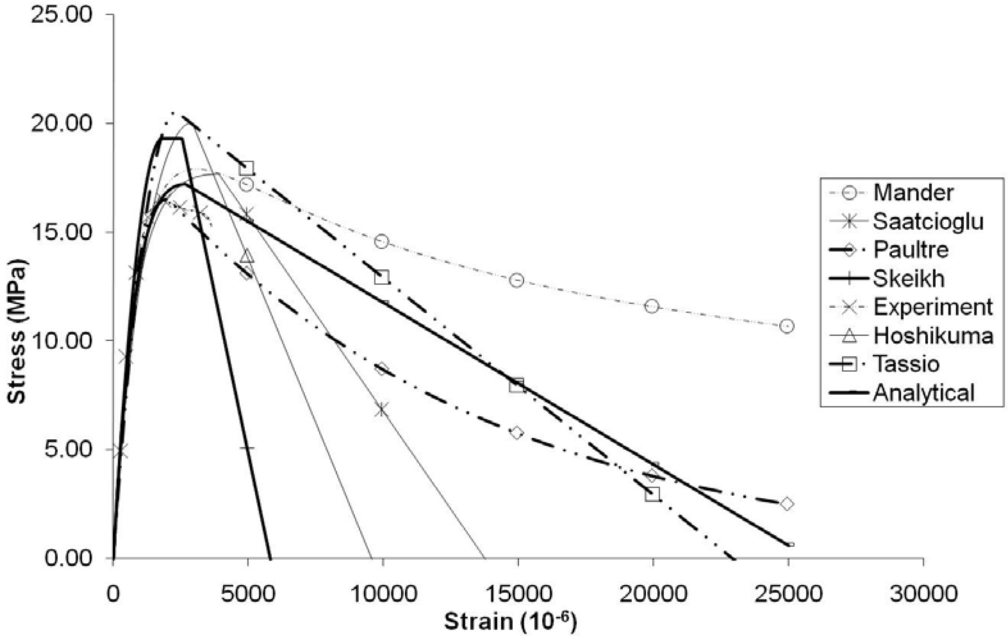

(g) Specimen T2S75

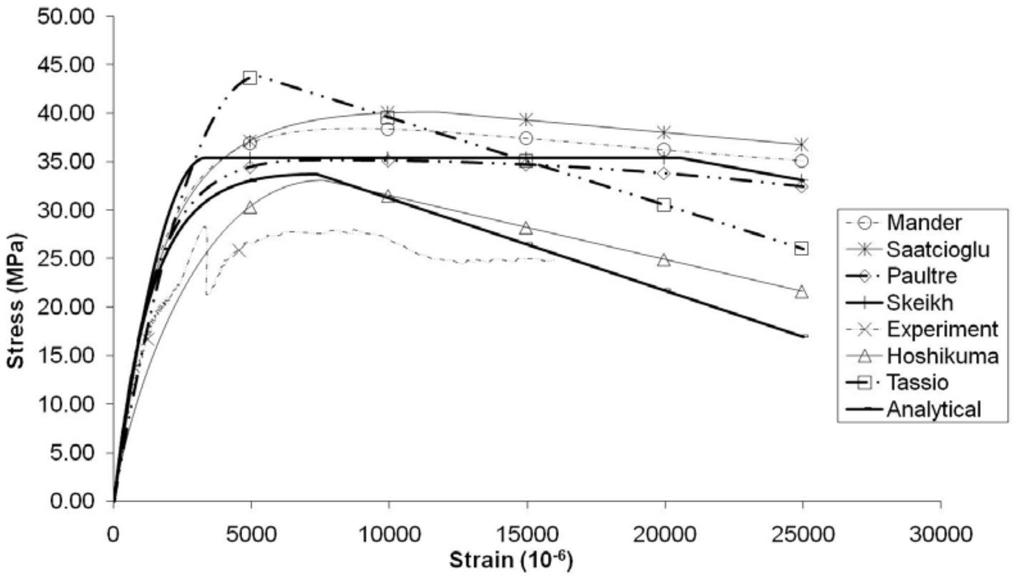

(h) Specimen T4S25

Figure 4-23 Comparison of Confined Concrete Stress-strain Relationship among Previous Models, Proposed Model and Experimental Data (Cont'd)

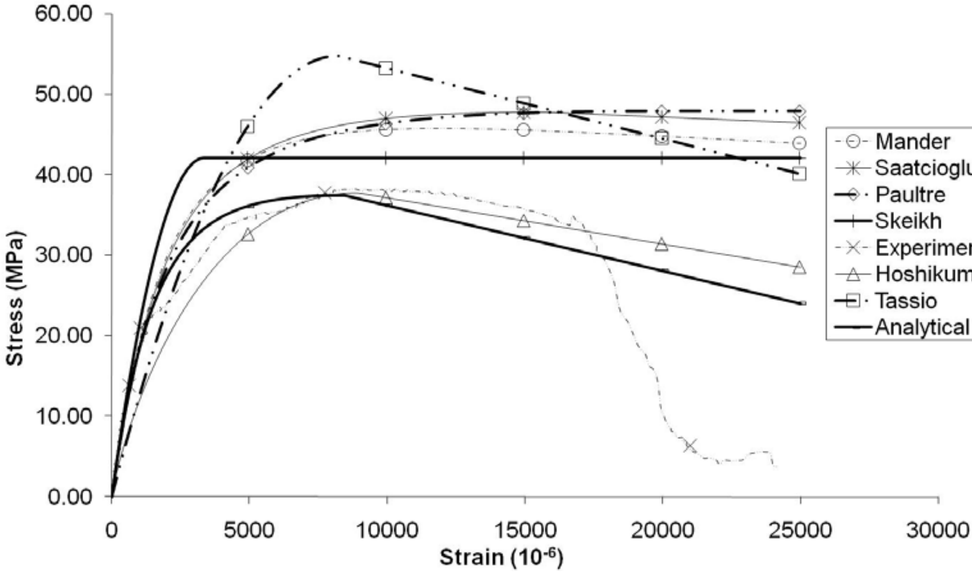

(i) Specimen T4L25

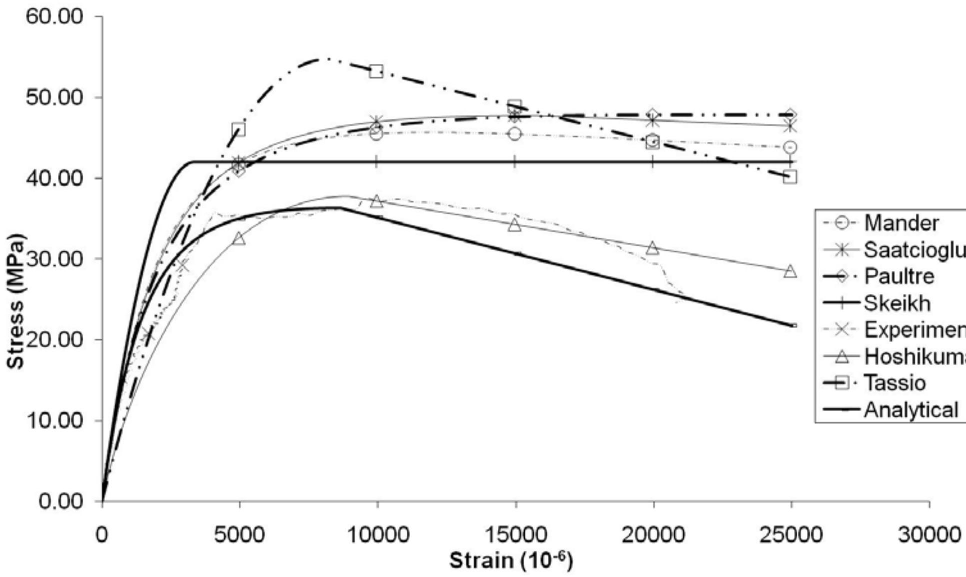

(j) Specimen T4M25

Figure 4-23 Comparison of Confined Concrete Stress-strain Relationship among Previous Models, Proposed Model and Experimental Data (Cont'd)

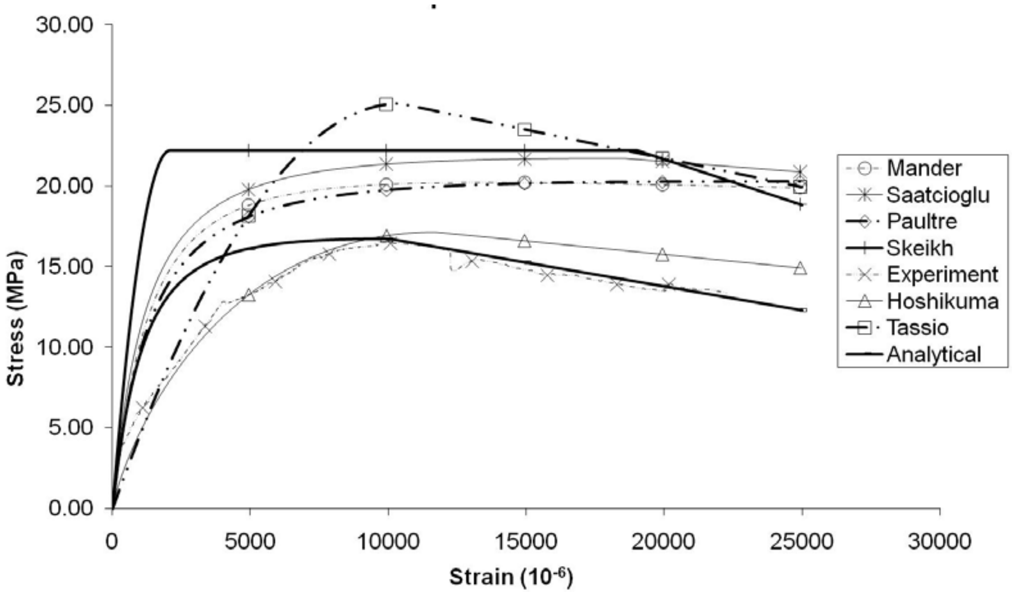

(k) Specimen T4L43.75

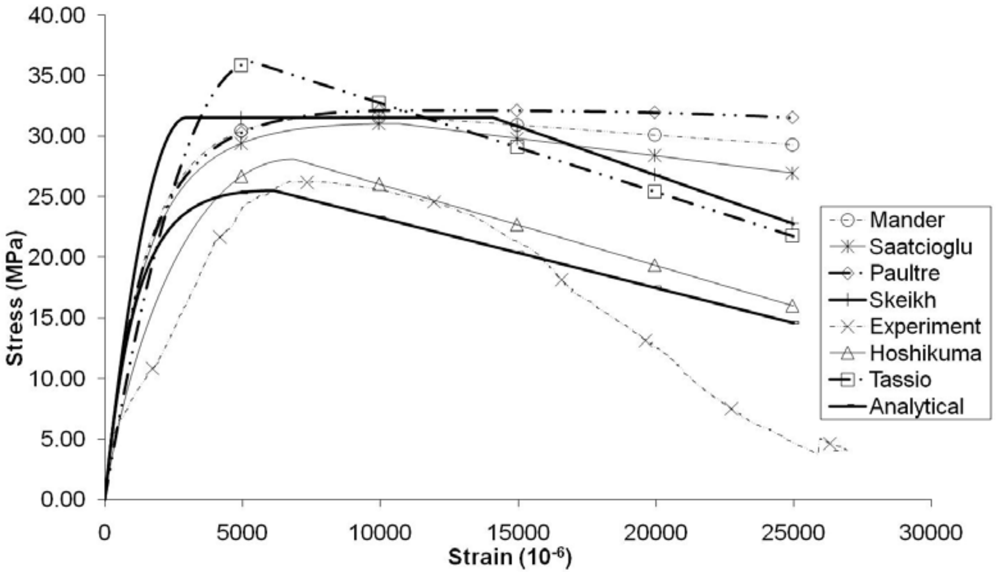

(l) Specimen T4M43.75

Figure 4-23 Comparison of Confined Concrete Stress-strain Relationship among Previous Models, Proposed Model and Experimental Data

Table 4-1 Stress Comparison

Specimen	σ_{exp} (N/mm^2)	σ_m (N/mm^2)	σ_s (N/mm^2)	σ_p (N/mm^2)	σ_{pred} (N/mm^2)	σ_{ave}/σ_m	σ_{ave}/σ_s	σ_{ave}/σ_p	$\sigma_{ave}/\sigma_{pred}$
T4L25	38.31	45.72	47.78	47.89	37.44	119%	125%	125%	98%
T4M25	37.48	45.72	47.78	47.89	36.33	122%	127%	128%	97%
T4S25	28.30	30.48	40.18	35.17	33.75	108%	142%	124%	119%
T4L43.75	16.50	20.21	21.72	20.29	16.72	122%	132%	123%	101%
T4M43.75	26.32	31.64	31.07	32.16	25.50	120%	118%	122%	97%
T2L25	18.67	20.16	22.01	21.10	16.50	108%	118%	113%	88%
T2M25	15.12	19.14	21.27	20.01	15.23	127%	141%	132%	101%
T2L50	13.43	15.59	15.15	12.93	13.38	116%	113%	96%	100%
T2M50	22.72	23.50	22.59	20.31	20.85	103%	99%	89%	92%
T2L75	18.01	19.37	18.83	17.39	17.89	108%	105%	97%	99%
T2M75	16.68	18.94	18.41	16.97	17.36	114%	110%	102%	104%
T2S75	16.50	17.89	17.67	16.52	17.22	108%	107%	100%	104%

σ_{exp} The average stress of concrete specimen
σ_m The maximum confined concrete stress calculated according to Mander et al (1988)
σ_s The maximum confined concrete stress calculated according to Saatcioglu and Razvi (1999)
σ_p The maximum confined concrete stress calculated according to Legeron and Paultre (2003)

Table 4-2 Strength Increment, Strain at Peak Strength and Ultimate Strain

Specimen	f_{cu} (N/mm^2)	$f_{cc,exp}$ (N/mm^2)	$f_{cc,exp}/0.76f_{cu}$	$\varepsilon_{cc,\ exp}$	$\varepsilon_{cu,\ exp}$	μ_{exp}
T4L25	33.5	38.31	1.50	0.009222	0.01761	1.91
T4M25	33.5	37.48	1.47	0.009502	0.019691	2.07
T4S25	33.5	28.30	1.11	0.003312	0.015962	4.82
T4L43.75	16.25	16.50	1.34	0.009875	0.022293	2.26
T4M43.75	27.5	26.32	1.26	0.006729	0.015151	2.25
T2L25	16.25	18.67	1.51	0.009873	0.018175	1.84
T2M25	16.25	15.12	1.22	0.009888	0.015189	1.54
T2L50	16.25	13.43	1.09	0.004245	0.012958	3.05
T2M50	27.5	22.72	1.09	0.004000	0.007789	1.95
T2L75	23.75	18.01	1.00	0.003488	0.004401	1.26
T2M75	23.75	16.68	0.92	0.002367	0.006449	2.72
T2S75	23.75	16.50	0.91	0.001791	0.003622	2.02
A	33.5	16.70		0.002558	0.004166	
B	23.75	19.67		0.001733	0.003416	
C	27.5	16.84		0.002523	0.004218	
D	16.25	12.93		0.002158	0.003152	

Table 4-3 Transverse Reinforcement Strain at Peak Strain of Confined Concrete

Specimen	Transverse Reinforcement Strain at ε_{cc} (Location)							
	21	22	23	24	25	26	$\varepsilon_{l\ cro}/\varepsilon_{ho}$	$\varepsilon_{s\ cro}/\varepsilon_{ho}$
T4L25	3360		3577	3053	3513	3953	106%	118%
T4M25	2804	2049	1904	1858	853	1128	68%	40%
T4S25	951	488	469	801			84%	
T4L43.75	839	1338	1063	1121	828	1257	94%	
T4M43.75	1685	1356	359	887	500	230	53%	30%
T2L25	1235	4231	1877	2267	1496	1325	54%	
T2M25	3911		2034	1337		1706	52%	44%
T2L50	1546	1084	1277	1558	1380		101%	
T2M50	1242	2295	745	872	732	369	38%	32%
T2L75	1787	5711	3342	2821	2087	3228	59%	
T2M75	1174	638	373	464	336	230	40%	29%
T2S75	832	583	365	427			51%	

Table 4-4 Transverse Reinforcement Strain at Ultimate Strain of Confined Concrete

Specimen	Transverse Reinforcement Strain at ε_{cu} (Location)							
	21	22	23	24	25	26	$\varepsilon_{l\ cro}/\varepsilon_{ho}$	$\varepsilon_{s\ cro}/\varepsilon_{ho}$
T4L25	3415		4976	4203	6022	6902	146%	
T4M25	5362	1366	2252	2118	1044		42%	19%
T4S25	10517	2739	1127	2148			20%	
T4L43.75		1535	1682		2415	3299	159%	
T4M43.75	2240	1794	810	1053		276	47%	12%
T2L25	2005	6098	1965	4325	1591		71%	
T2M25	5036		2453	759		2731	49%	54%
T2L50	1071	1150	1599	1491			139%	
T2M50	1617	2679	728	1135		518	42%	19%
T2L75	2575	5752	6372	4363	2477	5014	111%	
T2M75	5110	2738	2091	1671	1078	675	41%	21%
T2S75	6701	3144	2441	2612			39%	

Table 4-5 Parameters of Proposed Stress-strain Model

Type of Detailing	α		β		γ	
	Value	Correlation	Value	Correlation	Value	Correlation
Type L	2.61	99.2%	5.19	96.5%	0.25	95.7%
Type M	2.41	96.4%	5.70	95.1%	0.23	90.6%

Table 4-6 Mean Difference of Peak Stress and Peak Strain against Analytical Model

Analytical model	Peak Stress		Peak Strain	
	Mean Difference %	Correlation %	Mean Difference %	Correlation %
Mander (1984)	16	99	26	96
Saatcioglu and Razvi (1999)	19	98	61	98
Paulture et al (2003)	13	98	41	96
Skeikh and Uzumeri (1980)	24	99	-58	41
Hoshikuma (1997)	6	99	0	91
Tassio (1991)	35	99	-16	92
Proposed	-2	100	-9	95

Table 4-7 T-Distribution of Peak Stress and Peak Strain against Analytical Model

Analytical model	Peak Stress		Peak Strain	
	t-distribution	% of likelihood	t-distribution	% of likelihood
Mander (1984)	4.3	0.21	4.2	0.22
Saatcioglu and Razvi (1999)	3.7	0.52	5.1	0.06
Paulture et al (2003)	2.3	4.57	2.4	3.77
Skeikh and Uzumeri (1980)	12.4	0	2.9	1.64
Hoshikuma (1997)	2.2	5.99	0.6	54.50
Tassio (1991)	4.8	0.1	2.9	1.65
Proposed	-1.9	8.44	2.4	4.14

5 Cyclic Loading Test

5.1 Introduction

Cyclic behavior of reinforced concrete columns is affected by configuration of transverse reinforcement and volumetric transverse reinforcement ratio (Vintzileou and Stathatos 2007). Review on cyclic loading tests of reinforced concrete columns with different transverse reinforcement details is given in Chapter 2. In order to ascertain the seismic resistance of reinforced concrete columns with non-seismic detailing, cyclic loading tests were conducted on twelve specimens. The tests were used to compare the cyclic behavior of reinforced concrete column with different axial load, volumetric transverse reinforcement ratio and detailing (Type L and M detailing).

All specimens have the same dimensions and main reinforcement ratio but with varying volumetric transverse reinforcement ratio and different axial load ratio. Details of the test program are depicted in this chapter. These include specimen design, loading pattern, construction process of reinforced concrete column specimen, material, instrumentation and test procedure.

5.2 Description of Specimens

Traditionally, reinforced concrete columns in Hong Kong were mainly designed according to Code of Practice for the Structural Use of Concrete in Hong

Kong 1987. Characteristics of prototype reinforced concrete columns, for example size and material properties, are given in Chapter 3. Dimension of reinforced concrete column section is 800x800mm. Clear height of column in Hong Kong is normally around 2.5-3.0m. Contra-flexure point of reinforced concrete column is assumed at the mid-height of column, i.e. mid-height is the effective height. Failure mode of column is similar to two cantilevers moving in different directions. So, the specimens are designed as cantilever.

Tests were conducted in Structural Laboratory of South China University of Technology. There are constraints in the laboratory such as loading frame, loading capacity of actuator and reaction wall. Height of loading frame is about 3650mm and loading capacity of actuator is 1500kN. As there is a height limit on laboratory setup, height of specimens was designed as 895mm. Hence, the available height for testing specimen was about 1700mm because hydraulic jack and roller support used up some of the space. Scale of specimens is designed as 0.4 which gives us a total height of 1620mm measured from the base of strong ground. Column stub was designed to provide column reaction and was fixed to strong ground by rods. The column stub size is 1300 (L) x 2200 (W) x 500 (H) mm, see Figure 5-1 and 5-2.

Concrete cover of column and column stubs are 15mm and 20mm respectively. Main reinforcements are 20T16 at approximately 4% of gross area of specimen. This represents a high main reinforcement ratio, being typically used in Hong Kong. Yield strength of the main reinforcements is 460MPa. Main reinforcements and transverse reinforcements were ordered locally and transported from Hong Kong to South China University of Technology.

Column stubs is 500mm. There are two aisles of 75mm width on the strong ground, at 1500mm center-to-center, see Figure 5-3. Width of the column stubs, being perpendicular to direction of loading, is 2200mm. Length of column stub, being parallel to direction of loading, is 1300mm. Column stubs were designed to resist overturning moment caused by actuator. 20T20 Grade 2 steel to Chinese standard were used. Shear capacity of column stub is provided by transverse reinforcement.

In the experimental study, transverse reinforcement detailing was divided into two types. Type L detailing has long crossties fixed to main reinforcement in both sides while type M detailing allows short crossties to fix to main reinforcement on one side while another side fixed to the long crossties being perpendicular to short crossties (See Figure 5-2). Another parameter to be considered is volumetric transverse reinforcement ratio, while is defined according to Park (1992). The range of volumetric transverse reinforcement ratio considered in this study is between 0.0014 and 0.0115. Low volumetric transverse reinforcement ratio represents reinforced concrete columns designed according to the Code of Practice in Structural Concrete 1987 (using T10-300). For high volumetric transverse reinforcement ratio, the transverse reinforcement are designed to resist severe seismic attack (using T16-100) according to ACI-318 (2002). Specimens with average volumetric transverse reinforcement ratio between high and low volumetric transverse reinforcement ratio were also tested (using T16-175). Detailed arrangement of specimens is shown in Table 5-1 and Figures 5-1 to 5-2.

Loading capacity is also another aspect to be considered in this investigation in the range between $0.3f_cA_g$ and $0.6f_cA_g$, because structural columns in Hong Kong have high axial load ratio especially for columns underneath a transfer plate in a high rise building while 0.3 f_cA_g is the limit of loading capacity used in severe seismic zone.

5.3 Material

5.3.1 Concrete

Maximum aggregate size of prototype column is 20mm. Maximum aggregate size of specimens is designed as 8mm due to 0.4 scaled models. It is preferably to use concrete with maximum aggregate size being 10mm because ready mix concrete with 10mm maximum aggregate are available locally in China. Therefore, maximum aggregate size is 10mm.

Concrete was mixed in two batches. For the first batch, compressive strength of concrete is about 46MPa while it is about 44MPa in the second batch. Compressive strength is obtained by carrying out compressive tests on 150x150x150mm cubes. Cylinder strength is assumed to be equal to 0.78 of the cube strength (Bangash 1998). Three concrete cubes were tested after 28 days of concrete casting, and three more concrete cubes were tested shortly prior to testing of the specimens. Cube tests were conducted in a compressive machine of the laboratory in South China University of Technology. Material properties of concrete are summarized in Table 5-2.

5.3.2 Steel

Main reinforcements of the specimens are 16mm diameter high yield deformed type 2 bars while transverse reinforcement are 4mm and 6 mm high yield steel bars because smaller diameter steel bars were not available in the market. Pairs of strain gauges (TML FLA-2-11-3LT) are installed at mid-span on the steel bars, see Figure 3-2. Three main reinforcements and transverse reinforcements were tested in the laboratory of the Hong Kong Polytechnic University. 16mm high yield deformed bars were tested by a Forney's Universal Testing Machine while small diameters bars were tested by MTS Insight 30. Loading rate of reinforcements is about 30MPa per minute according to BS EN 10002-1 2001. Properties of steel reinforcements are summarized in Table 5-3.

For column stub, longitudinal and transverse reinforcements are 20mm and 12mm Grade 2 steel bars respectively. Characteristics strength of Grade 2 steel bars is 335MPa. Three main and transverse reinforcements were tested in the structural laboratory of South China University of Technology. Details of the reinforcements were summarized in Table 5-3.

5.4 Specimens Construction

The specimens are constructed in the Heavy Structural Laboratory at South China University of Technology. Strain gauges (TML FLA-2-11-3LT) were installed on main reinforcements and transverse reinforcements. Spacers made of cement paste are placed on bottom layers of the reinforcement in the column stubs.

An actuator is attached to the column head by steel plates. Spacing of transverse reinforcements at the column head is reduced by half. This increases confinement and prevents fracture of column head from stress induced by the actuator.

With the exception, spacing of transverse reinforcements for specimens with transverse reinforcement at T6@35 is not reduced because the transverse reinforcements are sufficiently stiff to resist the stress concentration effect at the column head.

In addition, five 8mm-steel rods were threaded to specimens to measure the rotation. Ready mixed concrete was ordered from batching plant and the column stub was first cast. Concrete was then vertically poured to complete the specimens. Poker vibrators were used to compact the concrete. Slump of concrete mix was 150mm (See Figures 5-4 to 5-7). Prior to the commencement of the loading test, cement paste was placed on top of the column as capping to smoothen the surface between the column head and the steel frame.

5.5 Instrumentation

Fourteen electrical dial gauges were installed. One electrical dial gauge was fixed to the supporting frame to measure the deflection at top of specimen. Five pairs of electrical dial gauges measured the vertical movement of steel bars to estimate rotation along the height of specimen. Curvature is calculated as the ratio of difference in rotation to the gauge length. Gauge length of steel bars for each interval is 80mm. Total gauge length of the measuring zone is 400mm (1.5 times the specimen width), which is about the plastic hinge length. A pair of electrical dial gauges are installed on top of column stub to measure possible rotation of the column stub. Displacement on column stub was measured by electric dial gauge to ensure that the specimens were properly mounted on strong ground. Ten strain gauges were installed on two main reinforcements at 400mm above the column stub to locate possible bond slip and to counter-check with the curvature estimated from the electrical dial gauges. Strain gauges installed on main reinforcements also determine yield strain of main reinforcements. Strain gauges are also installed on transverse reinforcements in three layers to assess the confinement and shear strain along height of specimen, see Figure 5-8. Four strain gauges are installed in type L detailing. Two strain gauges are installed on reinforcement hoops. The rest are installed on long crossties in different directions. Five strain gauges are installed in type M detailing at each layers. Two strain gauges are fixed to reinforcement hoops. One of them is fixed to long crossties, being perpendicular to lateral load direction while other strain gauges are fixed to short crossties. Data was obtained from the data acquisition system connected to a computer. The data was only recorded when it reaches the excursion point to prevent overheating the data acquisition system. Details on strain arrangement and electrical dial gauges are shown in Figures 5-8 to 5-11.

5.6 Test Setup

There are two loading systems in the test as shown in Figure 5-11. Constant vertical load is initially added to specimen by hydraulic jack to the predetermined loading value through a roller joint installed between specimen and hydraulic jack. This allows specimen to slide freely when subjected to horizontal load provided by actuator. Loading capacity of hydraulic jack is 5000kN. Roller joint consists of a roller and steel beams. Steel beams provide platform for roller movement. Ends of steel beam have bars to prevent roller from moving away from the steel beams, see Figure 5-12.

The actuator was mounted on the reaction wall by a steel frame (see Figure 5-12). Loading capacity of MTS 243 actuator is 1500kN with standard stoke of 500mm. Actuator was connected to specimen by fixing 40mm steel plates on the column head with anchorage rods. Actuator was loaded hydraulically under force controlled prior to yielding of the specimen. The actuator was then loaded under displacement controlled until the horizontal force is reduced to 80% peak load. Yield load is determined when the main reinforcement yields as defined by Park (1992), see Figure 5-13. Test setup is shown in Figures 5-11 to 5-12.

5.7 Loading Consideration

In this study, reinforced concrete columns were subjected to cyclic loading and under different loading rates, reinforcement configuration and volumetric transverse reinforcement ratio. The axial load ratio ranges from $0.3f'_cA_g$ to $0.6f'_cA_g$.

Yield displacement is calculated as discussed in Chapter 2. This gives a reference in determining the yield displacement. Horizontal load is initially applied by force control to the pre-determined 75% yield load. The load is applied in two cycles to 75% yield load. Loading is then increased to yield load after two cycles of loading. Yield strain of main reinforcement is counterchecked and lateral load added to column specimens is increased at 20kN intervals until yielding of main reinforcement. Afterwards, the actuator was in displacement controlled.

The displacement history is increased with multiples of yield displacement until specimens cannot sustain 80% of its peak load. The displacement history is shown in Figure 5-14. Loading rate of specimens is at 0.05mm/s for smaller displacement and the load rate increases to 0.7mm/s for large displacement.

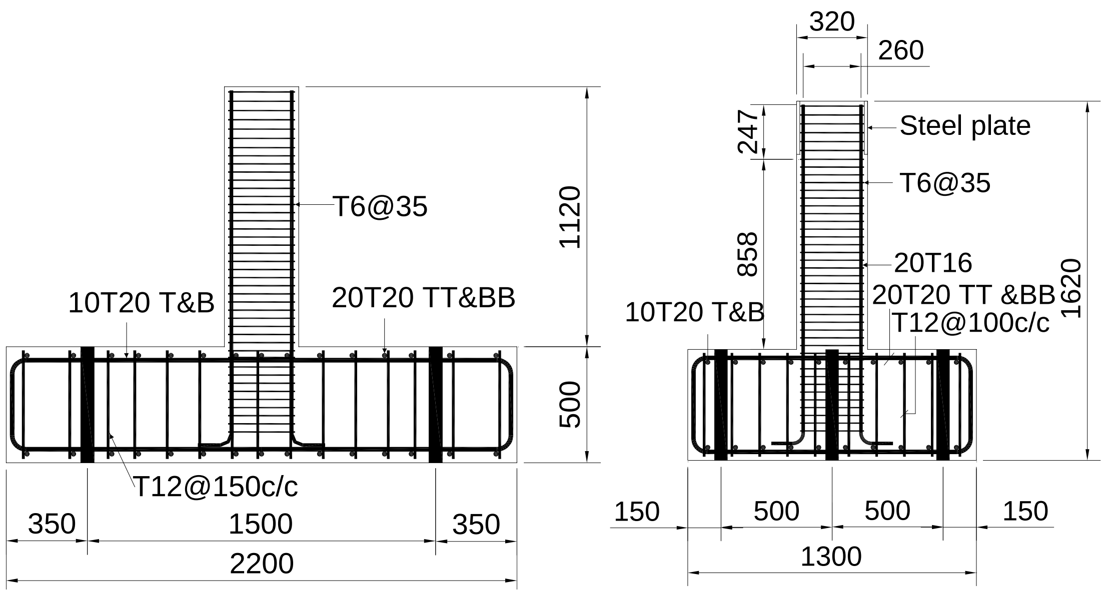

i. Elevation ii. Section

(a) Specimens T6L35

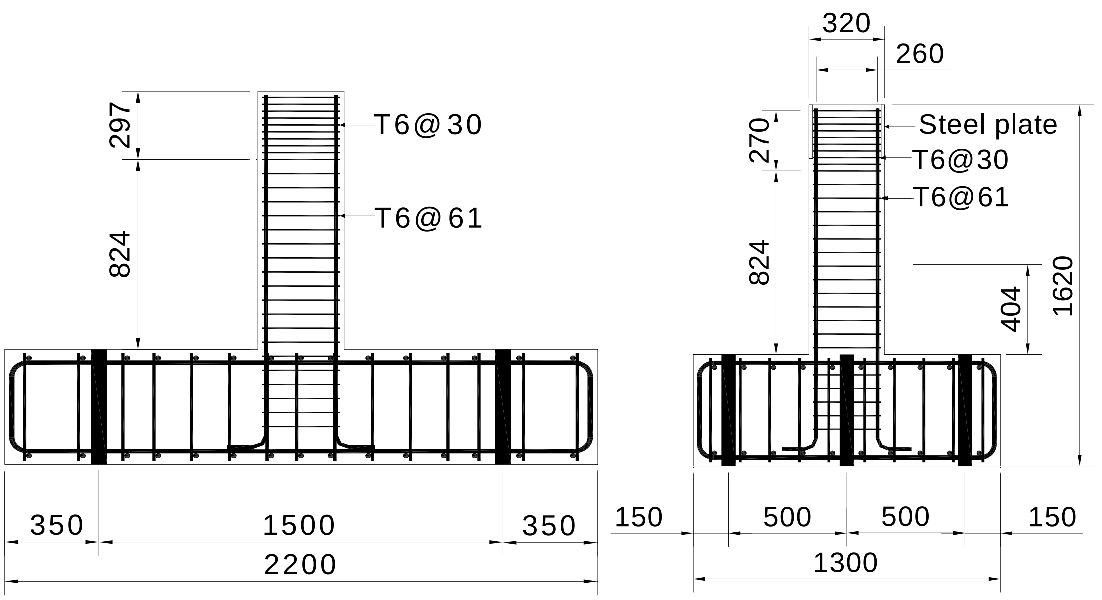

i. Elevation ii. Section

(b) Specimens T6@61

Figure 5-1 Details of Transverse Reinforcement in the Experiment (cont'd)

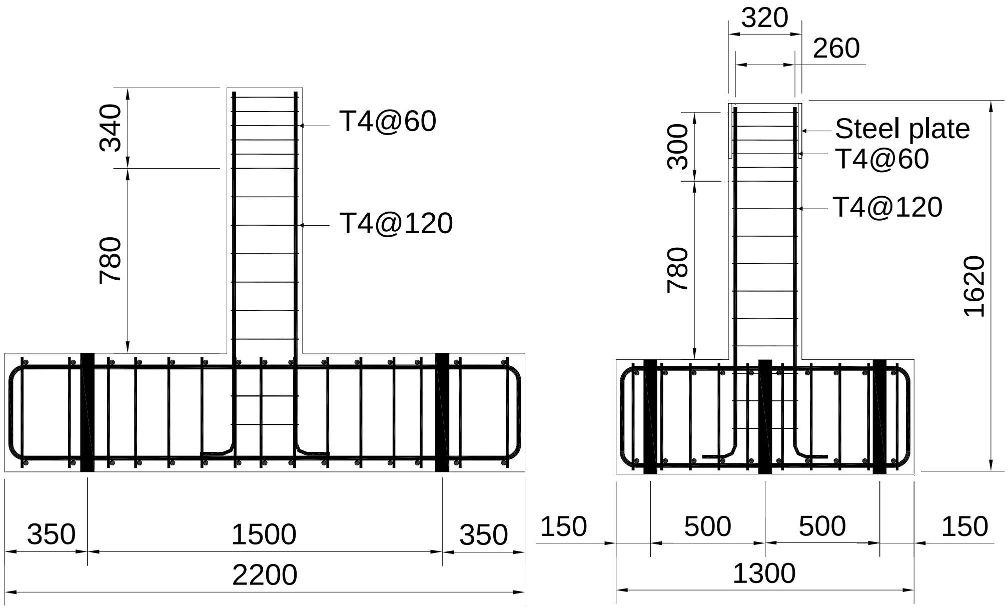

i. Elevation ii. Section

(c) Specimens T4@120

Figure 5-1 Details of Transverse Reinforcement in the Experiment

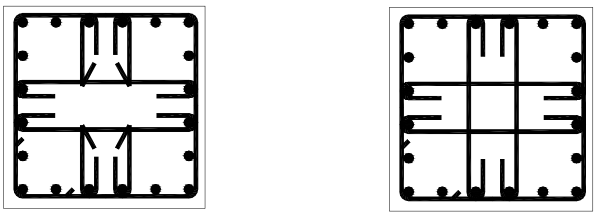

(a) Type M Detailing (b) Type L Detailing

Figure 5-2 Reinforcement Details

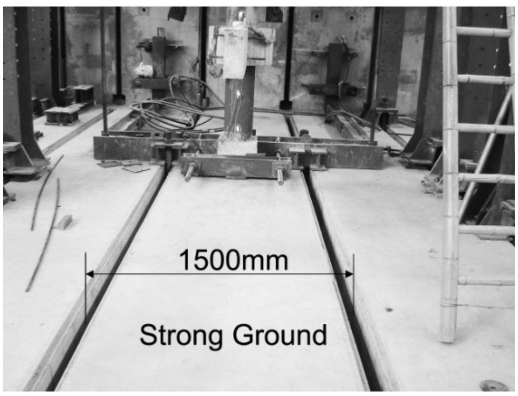

Figure 5-3 Strong Ground

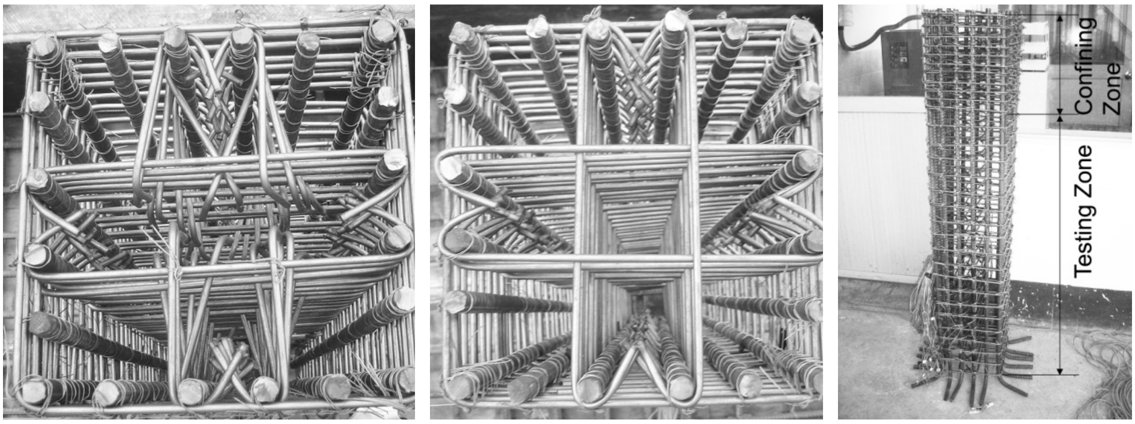

(a) Type M Detailing (b) Type L Detailing (c) Elevation

Figure 5-4 Reinforcement Cage (Section and Elevation)

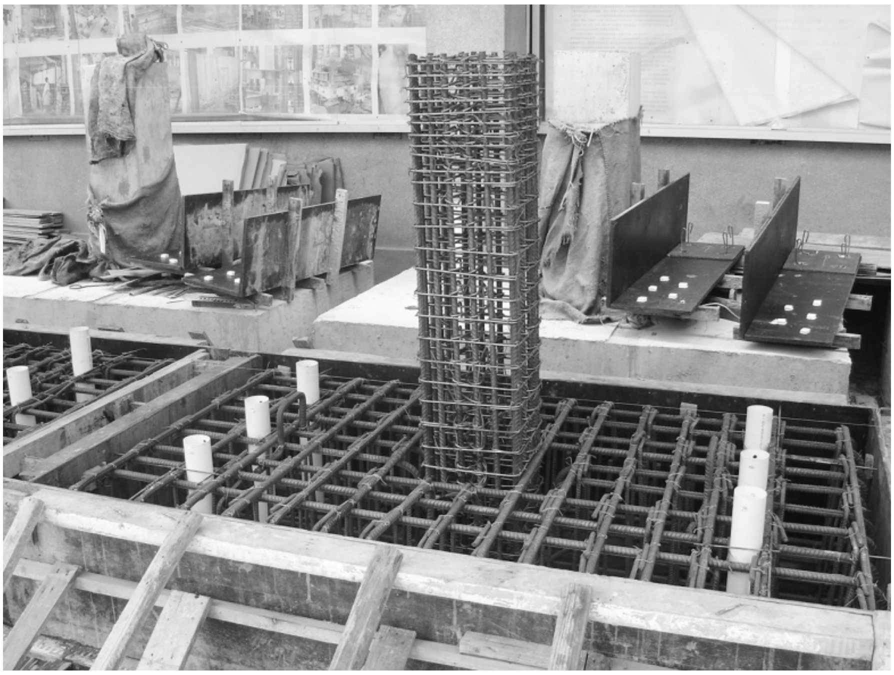

Figure 5-5 Construction of Specimens

(a) Concreting of a Column Stub

(b) Vibration of Concrete

Figure 5-6 Concrete Placing

Figure 5-7 Reinforced Concrete Specimens

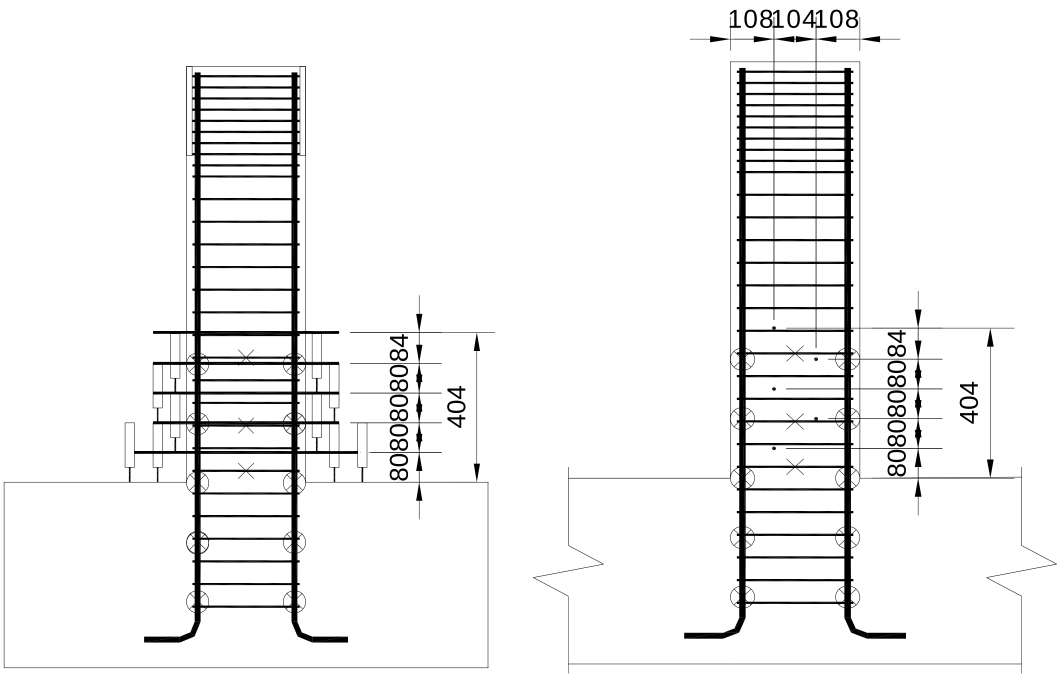

(a) Elevation (b) Section

Figure 5-8 Instrumentation (Main Reinforcement and Transverse Reinforcement)

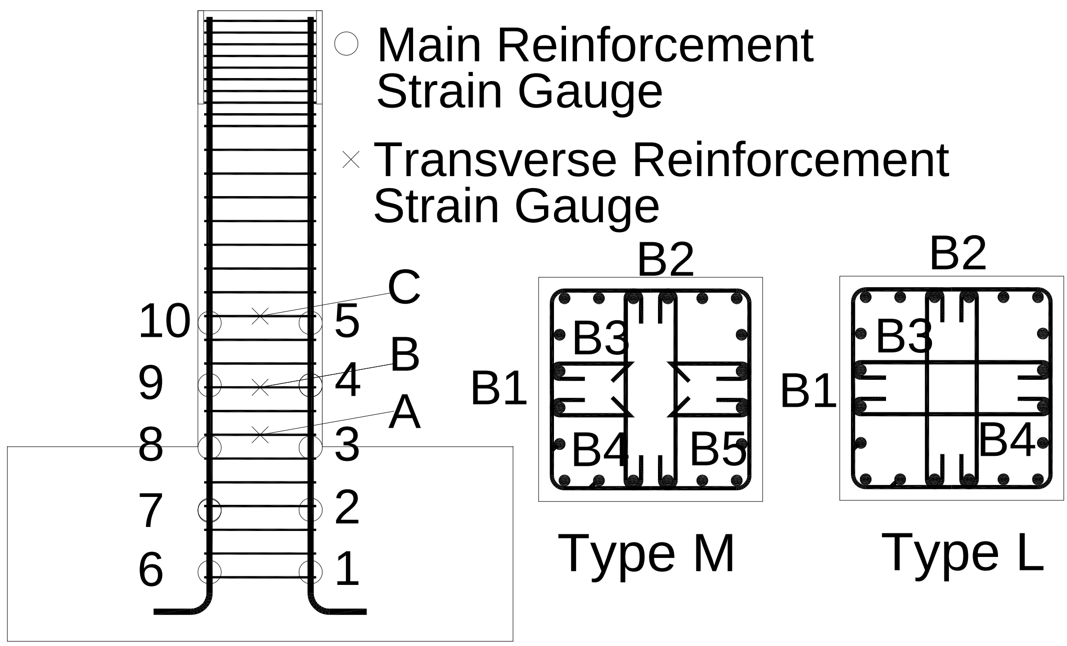

Figure 5-9 Strain Gauge Location of Specimens

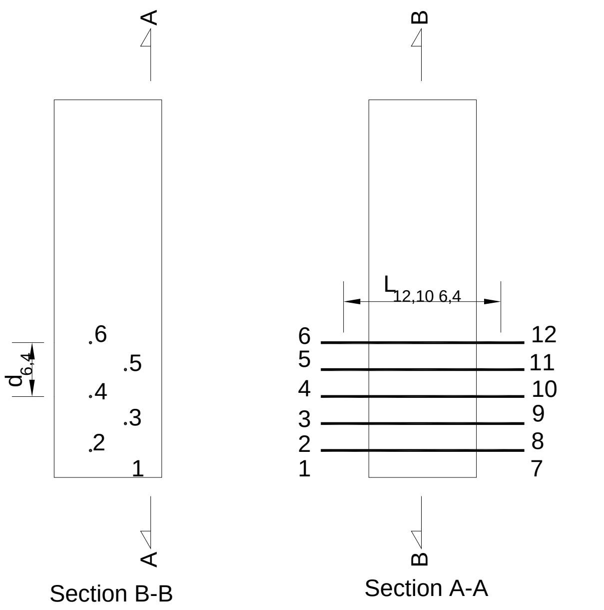

Figure 5-10 Transducer Location of Specimens

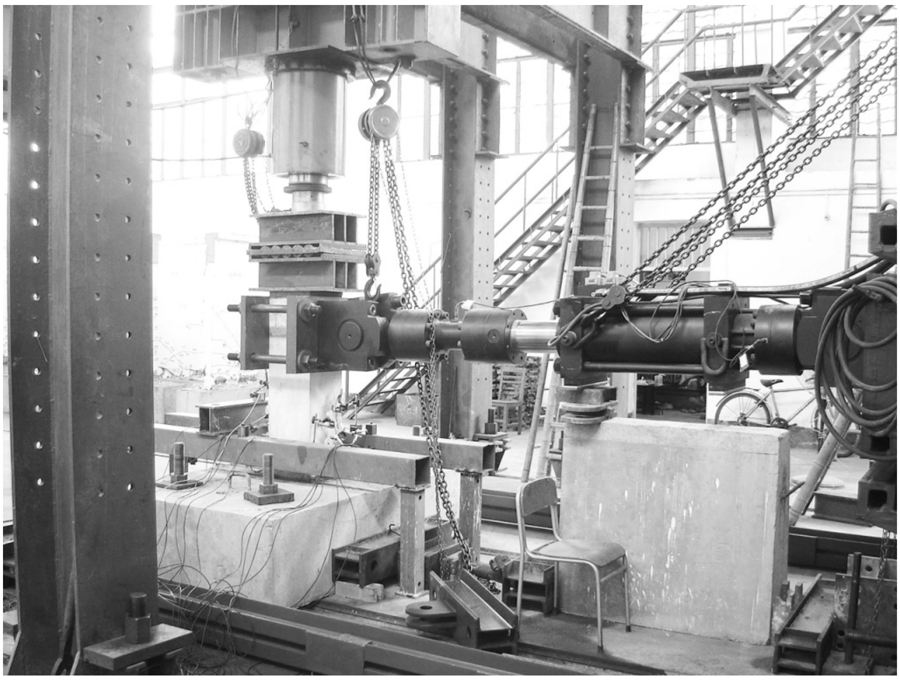

Figure 5-11 Testing Frame

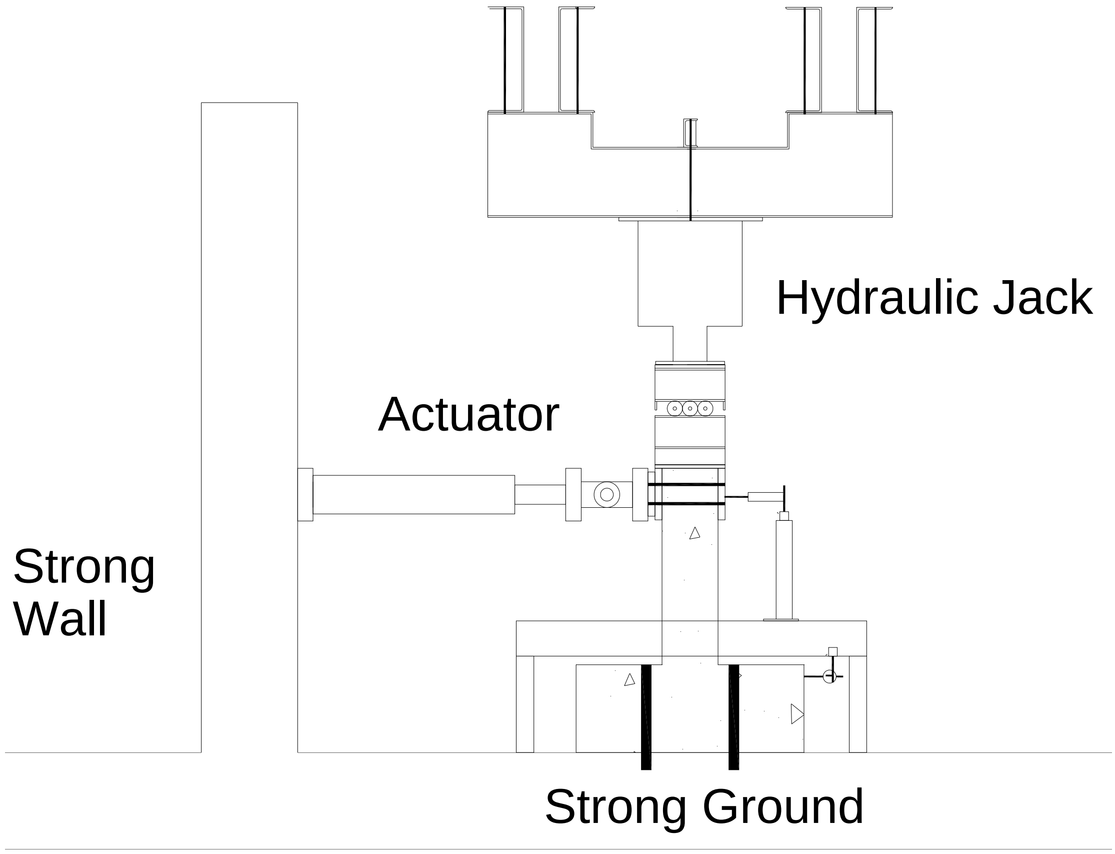

Figure 5-12 Setup of the Loading Frame (Elevation)

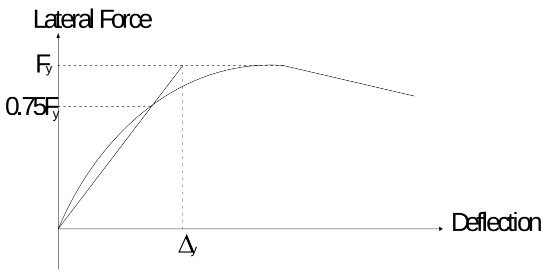

Figure 5-13 Lateral Force Deflection Curve

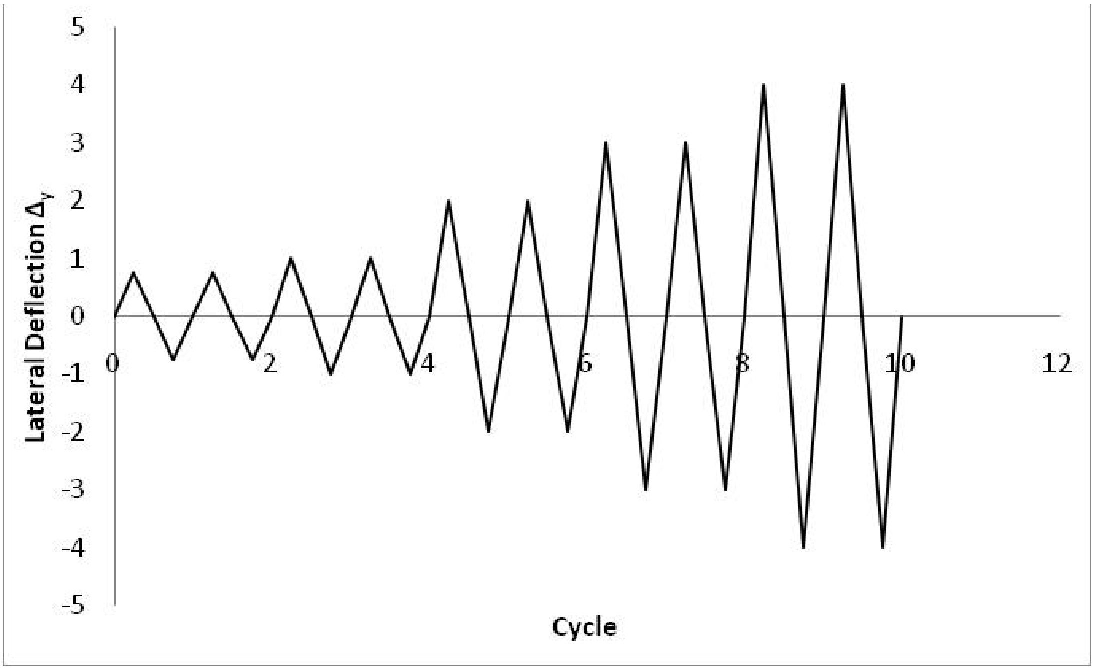

Figure 5-14 Loading History

Table 5-1 Details of Specimens

Name	n	ρ_s
T6L35A	0.6	0.022756
T6L35C	0.3	0.022756
T6M35A	0.6	0.022756
T6M35C	0.3	0.022756
T6L61B	0.45	0.013057
T6L61C	0.3	0.013057
T6M61A	0.6	0.013057
T6M61B	0.45	0.013057
T4L120A	0.6	0.00295
T4L120C	0.3	0.00295
T4M120A	0.6	0.00295
T4M120C	0.3	0.00295

n is Force per area per unconfined concrete strength

ρ_s is volumetric transverse reinforcement ratio

Table 5-2 Concrete Cube Strength

	28 days Strength (MPa)	Testing Strength (MPa)
1st Batch	37	44
2nd Batch	35	42

Table 5-3 Steel Reinforcement

Diameter of Reinforcement	Properties of Main Reinforcement			
	Yield Strain	Yield Strength (Nmm^{-2})	Ultimate Strain	Ultimate Strength (Nmm^{-2})
4mm		745	0.08	752
6mm		529	0.07	553
12mm		362		523
16mm	0.0027	509	0.20	635
20mm		394		602

6. Results of Cyclic Loading Tests

6.1. Introduction

This chapter presents results obtained from cyclic loading tests carried out on reinforced concrete column specimens. Physical observations on specimens were performed. Effectiveness of transverse reinforcement configurations was examined.

Test data were analysed to investigate moment-curvature relationship of specimens. Curvature profile against height of column is used to estimate the plastic hinge length. Additionally, force against deflection; main reinforcement strains and transverse reinforcement strains against height were plotted to observe main reinforcement and transverse reinforcement behavior when specimens were subjected to cyclic loading.

Axial load were initially added to specimens at 0.3, 0.45 or $0.6f_cA_g$ to investigate hysteresis behavior of specimens under different axial loads. Lateral load was applied on right hand side to produce a clockwise moment, see Figure 6-1. The specimens were subjected to compressive stress at the left hand side while tensile stress was acting on the right hand side. When carrying out the experiment, lateral load was reversed when reaching $0.75F_y$ where F_y is the pre-determined yield strength of specimen. Yield strength of specimen is determined by equivalent energy approach similar to Eurocode 8 (BS EN

1998-1). Cyclic lateral load was continually applied to the specimen until the lateral load dropped to 80% of maximum value attended by the specimen.

6.2 Observation

Characteristics of specimens were described in Chapter 5 and summarized in Table 6-1. Based on the observation, there were possible shrinkage strains on the surfaces of specimens.

Specimen T6L35A was initially loaded to $0.6f_cA_g$. The specimen was first loaded to 0.75 of pre-determined yield load in the push-pull cycle. There was no visible crack when main reinforcement yielded. Lateral load was then loaded under displacement increment. Drift ratio of specimen was increased to 0.93% or (8.48mm, being lateral deflection) in the second cycle. No crack was observed on the surface of the specimen. When drift ratio increased to 1.67% (10.06mm), visible crack appeared at 240mm above footing on sides B and D (with reference to Figure 6-2). Cracks were observed at the tensile zone and inclined at approximately 60º to the horizontal. Cracks width, crack length and numbers of cracks increased when the drift ratio was increased to 1.58% (19mm), see Figure 6-3. Cracks propagated to 480mm above footing. Cracks spread over the surface of specimen when the drift ratio was increased to 2.63% (23.6mm). After several loading cycles, the lateral drift ratio reached 3.21% (28.7mm). Concrete cover spalled off and crack widths increased significantly, see Figure 6-4. Flexural cracks were observed on the sides B & D and at 600mm above the surface of footing. When lateral drift was increased to 3.82% in the push cycle, a flexural crack was observed to develop to 670mm, being clear height of specimen. Main reinforcement buckled. Transverse reinforcement hoops opened up and fractured. Concrete cover in a zone within 175mm from the footing spalled off. The specimen finally failed in flexural shear mode.

Specimen T6L35C was initially loaded to $0.3f_cA_g$, see Figure 6-5. No crack was observed when main reinforcement yielded. When drift ratio was increased to 2.25% (20.15mm), visible cracks were found. The inclined cracks were located on lateral faces of the specimen and between 200mm and 340mm above footing. Crack width and number of cracks increased when the drift ratio was increased to 3.51% (31.45mm). The cracks then dispersed to 690mm above footing. At the same time, the specimen reached its peak lateral load. Crack widths were widened in the following reverse cycle in which the maximum drift ratio reached 3.51%. Concrete cover spalled off at this stage and at about 400mm above footing. When drift ratio was further increased to 4.45% (39.87mm), spalling of concrete cover was extended to 240mm above footing. Main reinforcement buckled and transverse reinforcement hoops opened up and fractured. The specimen was failed in a flexural-shear mode.

Specimen T6M35A was initially loaded to $0.6f_cA_g$, see Figure 6-6. No crack was induced prior to yielding of main reinforcement. When the drift ratio was increased to 1.37% (12.25mm), visible cracks were observed. Cracks were located between 200mm and 480mm above footing. Inclined angle of cracks was approximately 60º measured from the horizontal axis. When drift ratio was further increased to 2.17% (19.46mm), crack width and number of cracks increased. Cracking zone was between 100mm and

670mm above footing. When drift ratio was increased to 3% (26.87mm), the lateral load reached its peak value. Concrete cover spalled at a zone between 160 and 200mm above footing. Buckling of main reinforcement and fracture of transverse reinforcement were not observed and the test was terminated when lateral force dropped to 80% from its maximum value. The specimen was failed in a flexural-shear mode.

Specimen T6M35C was initially loaded to $0.3f_cA_g$, see Figure 6-7. No crack was observed after yielding of main reinforcement. Yielding displacement was 0.78% (6.99mm). Cracks were observed between 120mm and 690mm above footing when drift ratio was increased to 1.89% (16.88mm). When drift ratio was at 2.93% (26.23mm), cracks elongated and crack width increased. Cracking zone was between 100mm and 690mm above footing. At the same time, lateral load reached its peak value. When the drift ratio was further increased to 4.12% (36.88mm), crack width further increased. There was spalling of concrete cover at this stage. New visible cracks were observed. Cracks propagated and concrete cover spalled at a zone 360mm above footing. Transverse reinforcement hoops fractured and main reinforcement buckled. The specimen was failed in a flexural-shear mode.

Specimen T6L61B was initially loaded to $0.45f_cA_g$, see Figure 6-8. No crack was observed after main reinforcement yielded. When drift ratio was increased to 1.26% (11.28mm), cracking zone was between 160mm and 690mm above footing. When the drift ratio was further increased to 1.99% (17.77mm), specimen reached its peak strength. Cracks were dispersed between 160mm and 720mm above footing. Crack length elongated and crack width increased. Number of cracks also increased. When the drift ratio was increased to 2.72% (24.32mm), crack widths of flexural shear cracks widened. Number of cracks also increased. Concrete cover spalled. Spalling zone of concrete cover was between 100mm and 280mm above footing. Buckling of main reinforcement and fracture of transverse reinforcement hoop was not observed because the test terminated when lateral load was reduced to 80% of its maximum value in the post-peak stage. The specimen was failed in a flexural-shear mode.

Specimen T6L61C was initially loaded at $0.3f_cA_g$, see Figure 6-9. No crack was found on the lateral sides when main reinforcement yielded. Drift ratio at yield was 0.66% (5.91mm). Cracks were located between 160mm and 690mm above footing. When the drift ratio was increased to 1.68% (15.01mm), more cracks were observed. Cracking zone was between 160mm and 690mm above footing. The crack angle was approximately 60º to the horizontal. When drift ratio was increased to 2.77% (24.82mm), lateral load reached its peak value. Cracks were dispersed on a zone between 80mm and 690mm above footing. Number of cracks and crack width increased. When the drift ratio finally reached 3.80% (33.98mm), large flexural shear cracks were induced. Concrete cover peeled off. Spalling zone of concrete cover was between 0 and 480mm above footing. Transverse reinforcement hoops fracture and main reinforcement buckled. The test terminated when the strength of specimen was below 80% of its strength in the post-peak region. The specimen was failed in a flexural-shear mode.

Specimen T6M61A was initially loaded to 0.6_cA_g, see Figure 6-10. No crack was observed after yielding of main reinforcement. When drift ratio was increased to 1.07% (9.52mm) in the push cycle, cracks were dispersed between 160mm and 690mm above footing. When drift ratio was increased to 0.81% (7.28mm) in the pull cycle, a small crack was found between 200mm and 240mm above footing. When the drift ratio was further increased to 1.67% (14.96mm), both crack width and number of cracks increased. Cracks were dispersed between 160mm and 920mm above footing. A new flexural shear crack was formed when the drift ratio was further increased to 2.32% (20.77mm). Concrete cover spalled off between 200mm and 240mm above footing. Buckling of main reinforcement and fracture of transverse reinforcement were not observed because the test stopped when lateral load was reduced to 80% of its maximum value in the post peak stage. The specimen was failed in a flexural-shear mode.

Specimen T6M61B was initially loaded to $0.45f_cA_g$, see Figure 6-11. No crack was observed after yielding of main reinforcement. When drift ratio was increased to 1.69% (15.15mm), cracks spread between 160mm and 690mm above footing. Subsequently, lateral load reached its maximum value. When drift ratio was further increased to 2.13% (19.06mm), width, length and number of cracks increased. The cracks were at 60º to the horizontal. When the drift ratio was further increased to 2.97% (26.56mm), crack width of flexural shear cracks increased significantly. Concrete cover spalled off at the zone between 160mm and 280mm above footing. Buckling of main reinforcement and fracture of transverse reinforcement hoop were not observed throughout the test. The specimen was failed in a flexural-shear mode.

Specimen T4L120A was initially loaded to $0.6f_cA_g$, see Figure 6-12. Crack was generated when the drift ratio was increased to 0.53% (4.74mm) prior to yielding of main reinforcement. The cracking zone was between 160mm and 690mm above footing. When the drift ratio was increased to 0.95% (8.55mm), crack width was increased to 1mm and the number of cracks also increased. When the drift ratio was increased to 1.41% (12.65mm), concrete cover spalled at a zone between 200mm and 690mm above footing. Main reinforcement remained elastic throughout the test and buckled in the direction of loading. Buckling length of main reinforcement was about three times the transverse reinforcement spacing. Finally, transverse reinforcement fractured. The specimen was failed in a shear mode.

Specimen T4L120C was initially loaded to $0.3f_cA_g$, see Figure 6-13. When the drift ratio was increased to 0.68% (6.08mm) prior to yielding of main reinforcement, cracks were observed in a zone between 160mm and 600mm above footing. When drift ratio was increased to 1.01% (9mm), width and number of cracks increased. When the drift ratio was increased to 2.01% (18mm), one failure crack was formed at footing and extended to 690mm above footing. Buckling of main reinforcement and fracture of transverse reinforcement were not observed because the test terminated when the strength was dropped to 80% of its maximum value. The specimen was failed in a shear mode.

Specimen T4M120A was initially loaded to $0.6f_cA_g$, see Figure 6-14. When the drift ratio was increased to 0.89% (7.92mm), there were visible cracks on the surface. The cracking zone was between 300 and 450mm above footing. When the drift ratio was increased to 1.67% (14.94mm), the crack width increased and the number of cracks also increased. Spalling of concrete cover was observed and the spalling zone was between 200mm and 600mm above footing. Buckling of main reinforcement was observed in the direction of movement. Buckling length of main reinforcement was equal to three times the transverse reinforcement spacing. Transverse reinforcement also fractured. The specimen was failed in a shear mode.

Specimen T4M120C was initially loaded to $0.3f_cA_g$, see Figure 6-15. When drift ratio was increased to 0.99% (8.84mm) prior to yielding of main reinforcement, cracks were observed. The cracks were located between 160mm and 690mm above footing. When drift ratio was further increased to 1.97% (17.60mm), concrete cover spalled off in the zone between 200mm and 300mm above footing. The specimen was failed in a shear mode.

Based on the observations, specimens with high volumetric transverse reinforcement ratio failed in flexural mode while those with small volumetric transverse reinforcement ratio failed in shear mode. Similar conclusions are drawn when shear capacity compared with flexural capacity of specimens calculated according to ACI-318 (2002), BS 8110 (1997) and GB 50011 (2002), see Table 6-2

6.3 Force-deflection Relationship

Three parameters are considered in this study, including (a) volumetric transverse reinforcement ratio, (b) configuration of transverse reinforcement and (c) axial load capacity ratio. Firstly, force-deflection relationship serves as a very important indicator in the design. It predicts the structural behavior of reinforced concrete column when subjected to cyclic load. Force-deformation curve consists of several parameters, namely (1) yield deflection, (2) yield force, (3) initial stiffness, (4) strain hardening, (5) maximum force, (6) descending branch, (7) unloading stiffness and (8) reloading stiffness. These parameters are related to the extent of confinement. Confinement action is related to volumetric transverse reinforcement ratio and axial load capacity ratio. Unloading and reloading stiffness are characteristics of cyclic loading. When a specimen is subjected to cyclic loading, the compressive side of a section would change to tension when loading direction is reversed. So, the characteristics of load deformation are related to volumetric transverse reinforcement ratio; axial load ratio and configuration of transverse reinforcement.

6.3.1 Volumetric Transverse Reinforcement Ratio

Based on the findings in Chapter 4, strength and ductility of reinforced concrete columns increase with volumetric transverse reinforcement ratio. Behavior of specimens when subjected to cyclic loading is similar to the one subjected to uni-axial loading. Strain energy of transverse reinforcement provides resistance to lateral expansion of core concrete. This increases lateral strength and ductility of reinforced concrete columns.

Unloading and reloading stiffness also increase with volumetric transverse reinforcement ratio. This is because the transverse reinforcement enhances both stiffness and ductility. The transverse reinforcement resists formation of cracks and prevents deteriorating of the confined concrete.

6.3.2 Axial Load Ratio

Effect of axial load capacity ratio to the behavior of columns is substantially different from the influence due to volumetric transverse reinforcement ratio, see Table 6-3. Yield strength and maximum strength increase with increasing axial load capacity ratio. However, yield deflection, deflection corresponding to maximum strength, ultimate deflection, unloading and reloading stiffness increase with reducing axial load ratio, see Figures 6-16 and 6-17. For example: yield deflection, deflection at maximum strength and ultimate deflection of specimen T6L61B were 9.98mm, 16.38mm and 26.5mm respectively while for specimen T6L61C were 13.58mm, 23.99mm and 33.12mm respectively. So deflection increases with reducing axial load capacity ratio. On the other hand, yield force and maximum strength in specimen T6L61B was 330kN and 535kN respectively while for specimen T6L61C were 329kN and 516kN respectively. So yield force and maximum strength increase with increasing axial load capacity ratio. Also, the ultimate deflection and ductility of specimen when subjected to high axial load were smaller than that subjected to low axial load.

Unloading and reloading stiffness ratios reduce with increasing axial load capacity ratio. When axial load increases, compressive strength on external side of the section is increased to balance the increase in axial load and more lateral cracks are then induced in the section. Unloading stiffness ratio reduces with formation of induced cracks. The unloading stiffness of specimens with high axial load ratio was less stiff than specimens with low axial load ratio. This is similar to the case of reloading stiffness. Propagation of cracks has adversely affected the confinement and led to the deterioration of unloading and reloading stiffness.

6.3.3 Configuration of Transverse Reinforcement

Configuration of transverse reinforcement is an important parameter affecting the hysteresis behavior. Based on the test results, specimens with type L detailing performed better on hysteresis behavior as compared with specimens with type M detailing. Long crossties were more effective in providing confinement action. When subjected to lateral load, all long crossties are stretched to provide the necessary confinement action.

On the contrary, for specimens with type M detailing, stress in short crossties in the tension zone was released at this stage. This reduces the strain energy provided by transverse reinforcement in resisting lateral expansion. This reduces the lateral strength and ductility of specimens with type M detailing, see Figures 6-18 to 6-22.

For unloading and reloading stiffness, the unloading stiffness of specimens with type M detailing was smaller than those with type L detailing because type M detailing provided lesser confinement action on specimens. Stiffness of core concrete was deteriorated. So the unloading and reloading stiffness reduced.

6.4. Moment-curvature Relationship

Moment-curvature relationship can be used to estimate the plastic hinge length. Moment is calculated as lateral force multiplied by moment arm, being the distance measured from the base of column to centerline of actuator. Curvature of a section is calculated from the difference in transducer displacements over the depth of section and the distance between transducers. It is calculated by Eq. (6-1) and Eq. (6-2), see Figure 6-23.

$\varepsilon_{31}=(\delta_3-\delta_1)/d_{31}$ (6-1)

$\varphi_{9,7,3,1}=(\varepsilon_{97}-\varepsilon_{31})/L_{9,7,3,1}$ (6-2)

where ε_{31} is strain located at the mid-point of transducers 3 and 1, δ_3 is the vertical displacement measured from transducer, d_{31} is the distance between point 1 and point 3, $\varphi_{9,7,3,1}$ is the curvature of transducers between point 9 and point 3 as shown in Figure 6-23 respectively and $L_{9,7,3,1}$ is the width between point 9 and point 3. Curvature could not be measured towards the end of loading cycles because of spalling of concrete cover. Moment-curvature relationships of all specimens are plotted in Figures 6-24 and 6-25.

6.4.1 Axial Load Ratio

As shown in Figure 6-24, maximum moment of specimen T6L35B was smaller than that of specimen T6L35A whereas ultimate curvature of T6L35B was larger than that of T6L35A, see Table 6-4. Curvature ductility of specimens increases with reducing axial load ratio. The increase in maximum moment in specimens under high axial load ratio is larger than specimens with low axial load ratio. This is similar to that observed in force-deflection relationship.

6.4.2 Volumetric Transverse Reinforcement Ratio

Maximum moment of specimen T4L120A was smaller than that of specimen T6L35A. Ultimate curvature of specimen T4L120A was smaller than that of specimen

T6L35A. Specimens with high volumetric transverse reinforcement ratio have larger moment capacity and larger ductility. It follows that strength and ductility increase with high volumetric transverse reinforcement ratio.

6.4.3 Configuration of Transverse Reinforcement

Maximum moment of specimen T6M61C was smaller than that of specimen T6L61C. Ultimate curvature of specimen T6M61C was smaller than that of specimen T6L61C. Specimens with type L detailing performed better than that in specimens with type M detailing. Since, strength and ductility depend on degree of confinement which depends on the effectiveness of transverse reinforcement.

6.5 Curvature Distribution along the Height of Column

Specimens were loaded under displacement control after yielding. Curvature profile and corresponding flexural strength along height of specimens were developed. The reaction force was then obtained. Curvature profile illustrated the yield section of specimen. This can be used to estimate the plastic hinge length, see Figures 6-26 and 6-27. Yield curvature of specimens was calculated by the following method. When main reinforcement yielded under tension or compression, the neutral axis of the section was found by trial and error method. The yield curvature is defined as the ratio of yield strain of main reinforcement to neutral depth. The calculation programme is shown in Appendix A.

6.5.1 Axial Load Ratio

In general, specimens with high axial load ratio have larger plastic hinge length than specimens with low axial load ratio. The plastic hinge length of specimen T6L35A is larger than that of specimen T6L35B. Plastic hinge length is related to confinement action in specimens. From Figures 6-26 and 6-27, ultimate curvature increases with reducing axial load ratio. The difference between ultimate curvature and yield curvature reduces with increasing axial load ratio because strain energy in transverse reinforcements is partially dissipated by the increase in the axial load. Hence, the plastic hinge length increases with axial load ratio. Derivation of plastic hinge length will be discussed in Chapter 7.

6.5.2 Volumetric Transverse Reinforcement Ratio

Specimens with high volumetric transverse reinforcement ratio have higher curvature ductility ratio because transverse reinforcement provides effective confinement to core concrete, see Figures 6-26 and 6-27. There was a substantial change in the curvature from yield to ultimate along the height of specimen. Plastic hinge length was reduced by increasing volumetric transverse reinforcement ratio. Yield curvature also increases with increasing volumetric transverse reinforcement ratio.

6.5.3 Configuration of Transverse Reinforcement Ratio

Specimens with type M detailing provide smaller curvature ductility than specimens with type L detailing, see Table 6-4 and Figures 6-26 and 6-27. Lateral strength of type M detailing was smaller than that in type L detailing. Yield curvature and ultimate curvature of specimens with type L detailing were larger than that in type M detailing. There is, however, no difference on plastic hinge length between type L and type M detailing under the same axial load and volumetric transverse reinforcement ratio. Curvature profile against height in specimens with type L detailing is similar to that of type M detailing.

6.6 Main Reinforcement Strain Distribution along Height of Column

Strain gauges were installed on a pair of main reinforcement, see Figures 5-9 and 5-10. The main reinforcement were located along the side perpendicular to loading conditions as shown in Figure 6-2. Five strain gauges were installed, see Figure 5-9. Strains in a main reinforcement below the footing were recorded to estimate the anchorage length and possible bond slippage. From Figures 6-27 and 6-28, stub column effect was observed as the main reinforcement strains at the base of footing were smaller than that at 150mm above the footing.

6.6.1 Axial Load Ratio

Main reinforcement in all specimens initially yielded under compression because the axial load ratio was relatively high ($0.3\text{-}0.6f_cA_g$). For specimens with high axial load

($0.6f_cA_g$), main reinforcement did not yield under tension throughout the test because high confined concrete stress in the compressive side balanced the high axial load. On the contrary, compressive strains in specimens with high axial load were larger than that with low axial load, see Figures 6-27 and 6-28.

6.6.2 Volumetric Transverse Reinforcement Ratio

Main reinforcement strains in specimens with high volumetric transverse reinforcement ratio are higher than that in specimens with low volumetric transverse reinforcement ratio. This is related to the confinement action of specimens. Confined concrete strength and ductility increases with increasing volumetric transverse reinforcement ratio. Obviously, main reinforcement strains increase due to an increase in confined concrete strain.

6.6.3 Configuration of Transverse Reinforcement

Main reinforcement strains in specimens with type L detailing are higher than that in specimens with type M detailing because type L detailing provides more effective confinement than that in type M detailing. Specimens with type L detailing have higher ductility than that with type M detailing.

6.7. Transverse Reinforcement

Strain gauges were installed on three layers of transverse reinforcement, see Figure 5-9. In each layer, 4 and 5 strain gauges were installed on type L and type M detailing respectively. Strain gauges were fixed to reinforcement hoop with 90º end hook, long crossties and short crossties. Based on the strain gauge readings, contribution of the transverse reinforcement to restrain the core concrete was assessed.

Lateral tensile cracks developed inside core concrete when axial load was applied. Tensile cracks then react with the transverse reinforcement. Transverse reinforcement strain increases and reacts with the core concrete. In short, confined concrete stress increases with volumetric transverse reinforcement ratio.

Configuration of transverse reinforcement is an important parameter in providing confinement action to core concrete. Type M detailing provides less effective confinement action than type L detailing. The ultimate transverse reinforcement strain increases with improving configuration of transverse reinforcement, see Figure 4-22.

6.7.1 Reinforcement Hoop near the Hook

Middle layer of the transverse reinforcement, 150mm above footing, has a higher strain than the other layers, located at 0mm and 400mm from the top of footing. The middle layer is located in the critical zone of specimens subjected to higher loading, see Figures 6-30 and 6-31.

6.7.2 Reinforcement Hoops far from Hook

Middle layer of transverse reinforcement has higher strain and similar to transverse reinforcement on the hoop far from opening, see Figures 6-32 and 6-33. Transverse reinforcement strains on the hoops far from the hook were larger than that near the hook because the lateral restraint of transverse reinforcement hoop far from the opening was more rigid than that near the hook. The transverse reinforcement strain increases with increasing compression.

6.7.3 Long Crossties Perpendicular to Loading

Strains in long crossties were similar to the strains in reinforcement hoops under cyclic load. Tensile strains at the middle layer of transverse reinforcement had the highest strain when the transverse reinforcement was in the compressive zone of the column section. When the transverse reinforcement was in the tensile zone in the next half cycle, transverse reinforcement strains reduced. Strains on long crossties perpendicular to loading increases with drift ratio. From Figures 6-34 and 6-35, when the axial load increases, transverse reinforcement strains increase with increasing confined concrete stress in core concrete under the same drift ratio. Confinement action becomes more effective by increasing the volumetric transverse reinforcement ratio of specimens.

6.7.4. Transverse Reinforcement Parallel to Lateral Load Direction

In Figures 6-36 to 6-38, strains in long crossties are higher than that in short crossties because short crossties provide less effective confinement to core concrete during the ultimate displacement. When both specimens were subjected to the same amount of lateral load and having same volumetric transverse reinforcement ratio, short crossties achieved higher strains than that in the long crossties. The lateral strength and ultimate deflection of specimens with type M detailing are smaller than that in specimens with type L detailing. So, specimen with type M detailing is less ductile than those with type L detailing.

6.8 Summary

Specimens with non-seismic detailing were tested. Hysteresis behavior of specimens subjected to cyclic load was estimated. Specimens failed in flexural shear mode due to small shear span-depth ratio. Lateral force-deflection and moment-curvature relationship were examined. Maximum lateral force increases with increasing volumetric transverse reinforcement ratio and increasing axial load capacity ratio. This is attributed to effectiveness of transverse reinforcement in providing confinement action to core concrete. Transverse reinforcement strains increases with axial load due to propagation of lateral cracks under expansion. Ductility of specimens increases with increasing volumetric transverse reinforcement ratio but reduces with increasing axial load capacity ratio. Strain energy of transverse reinforcement increases with increasing volumetric transverse reinforcement ratio. More strain energy is dissipated from the transverse reinforcement when axial load capacity ratio increases.

Lastly, main reinforcement and transverse reinforcement strains are investigated. Main reinforcement strains could be used to estimate the plastic hinge length of specimens. Based on the observation, type L detailing provides more effective confinement action as compared with type M detailing because the long crossties provide better anchorage to the main reinforcement. Short crossties could only provide confinement action when they are within the compressive zone. Hence, lateral strength and ductility of specimen with type M detailing are smaller than that with type L detailing.

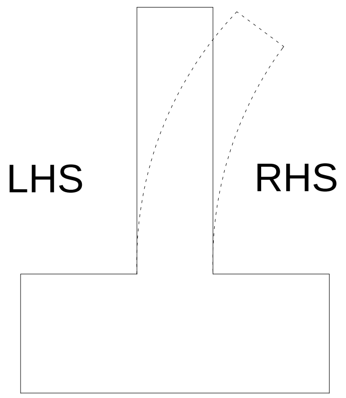

Figure 6-1 Deformed Shape of Specimen

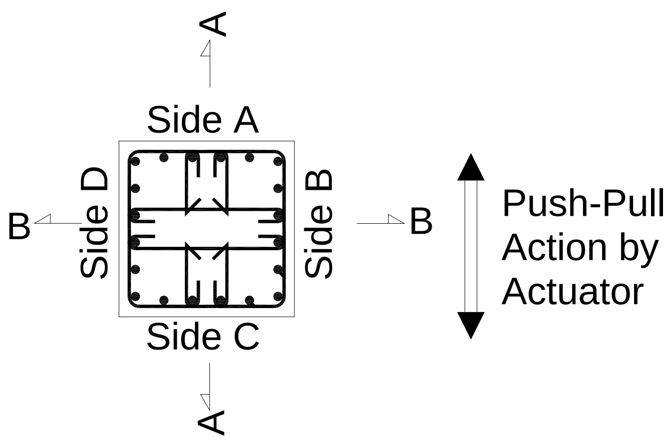

Figure 6-2 Faces of Reinforced Concrete Specimens

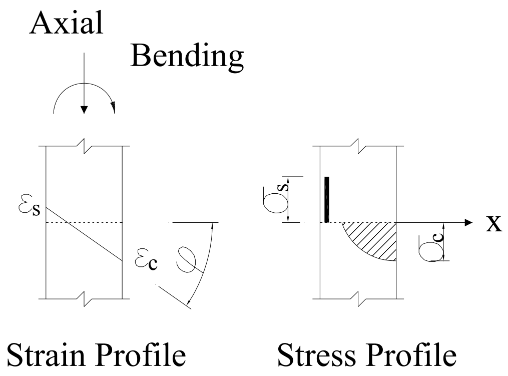

Figure 6-3 Stress-strain Profile of Confined Concrete

Figure 6-4 Specimen T6L35A (Top Left: 14.13mm, Top Right: 18.99mm, Bottom Left: 28.69mm , Bottom Right: at Failure)

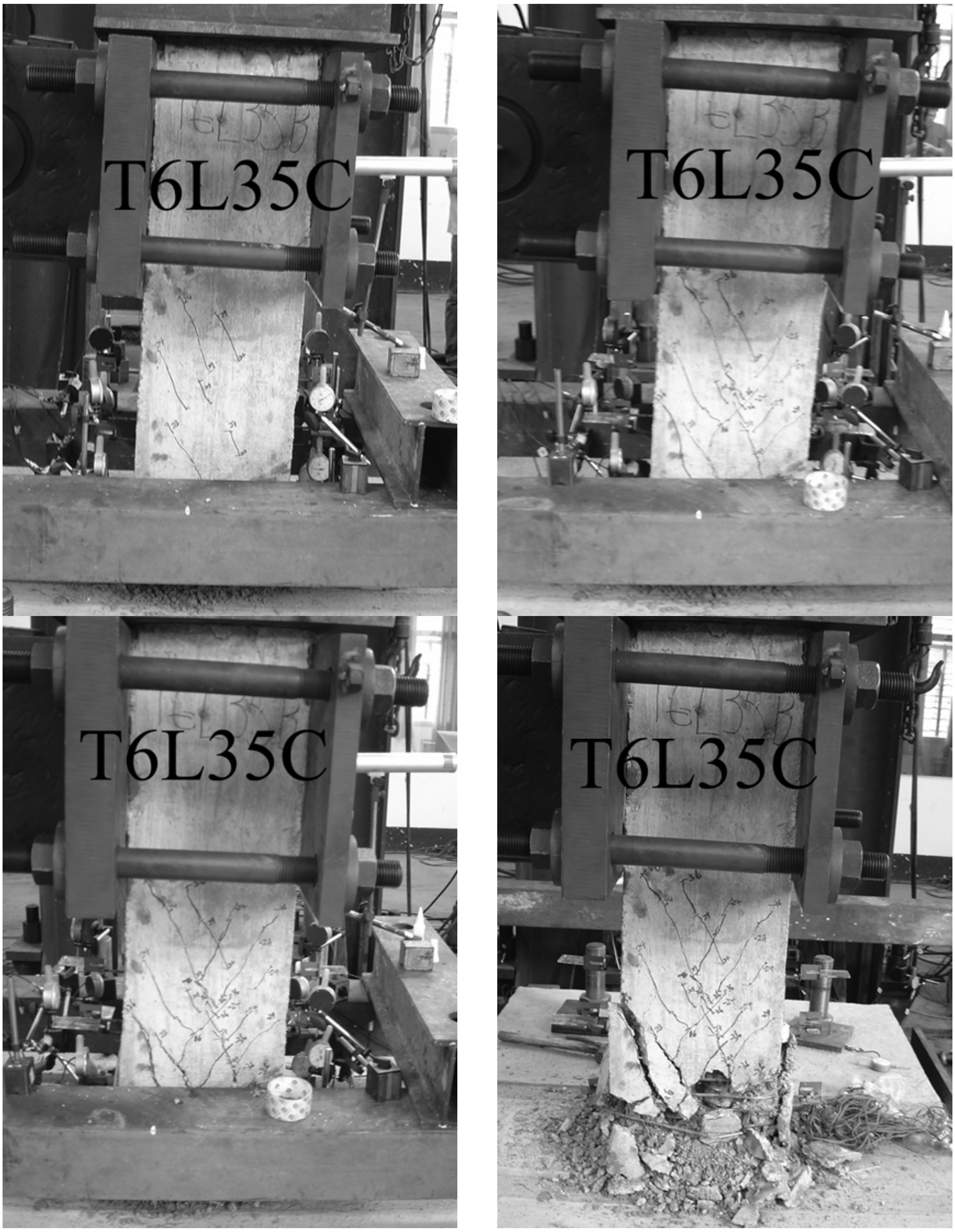

Figure 6-5 Specimen T6L35C (Top Left: at 20.15mm, Top Right: at 31.49mm, Bottom Left: at 39.58mm, Bottom Right: at Failure)

Figure 6-6 Specimen T6M35A (Top Left: at 12.54mm, Top Right: at 19.45mm, Bottom Left: at 26.87mm, Bottom Right: at Failure)

Figure 6-7 Specimen T6M35C (Top Left: at 16.88mm, Top Right: at 26.96mm, Bottom Left: at 36.87mm, Bottom Right: at Failure)

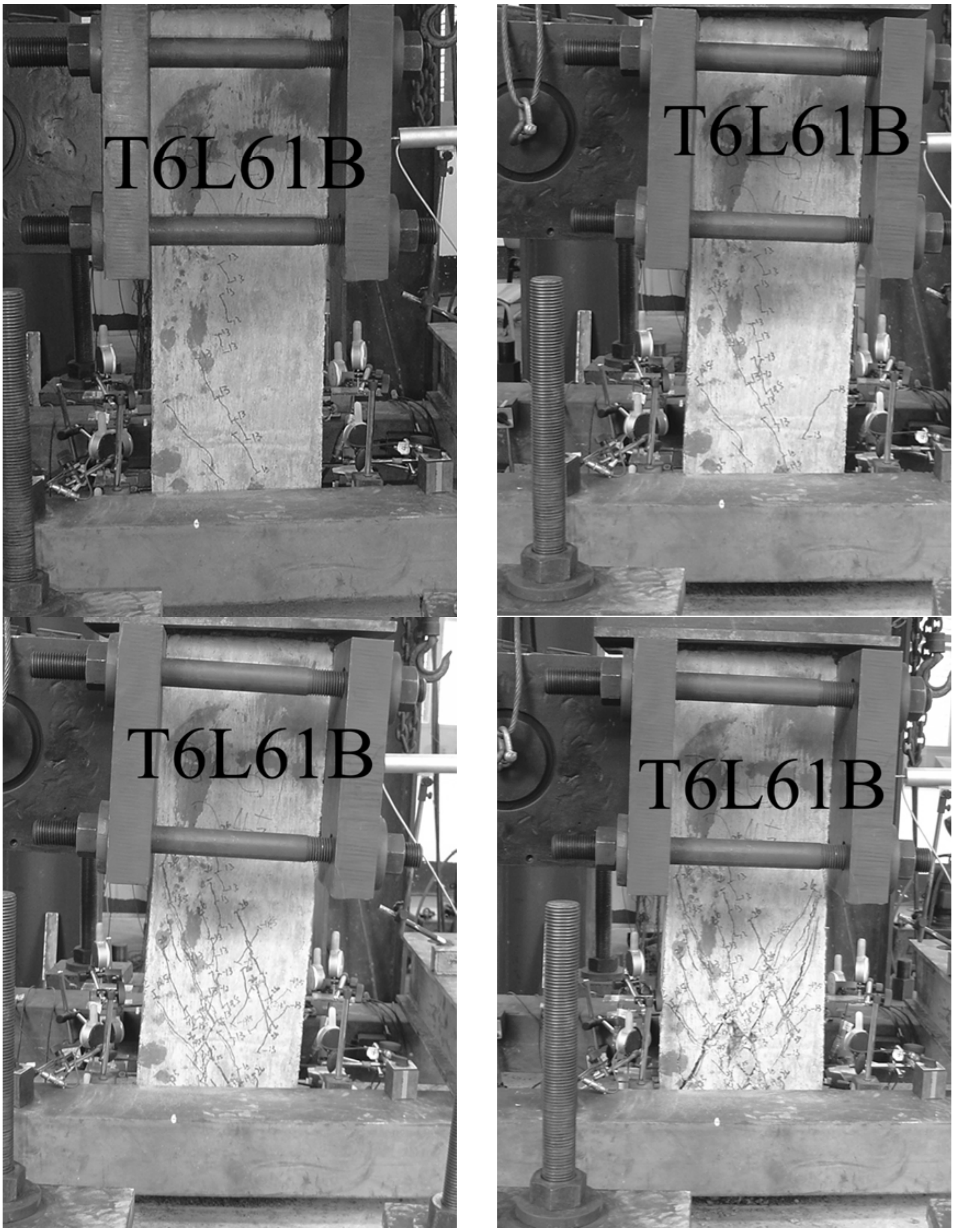

Figure 6-8 Specimen T6L61B (Top Left: at 11.27mm, Top Right: at 17.81mm, Bottom Left: at 24.31mm, Bottom Right: at Failure)

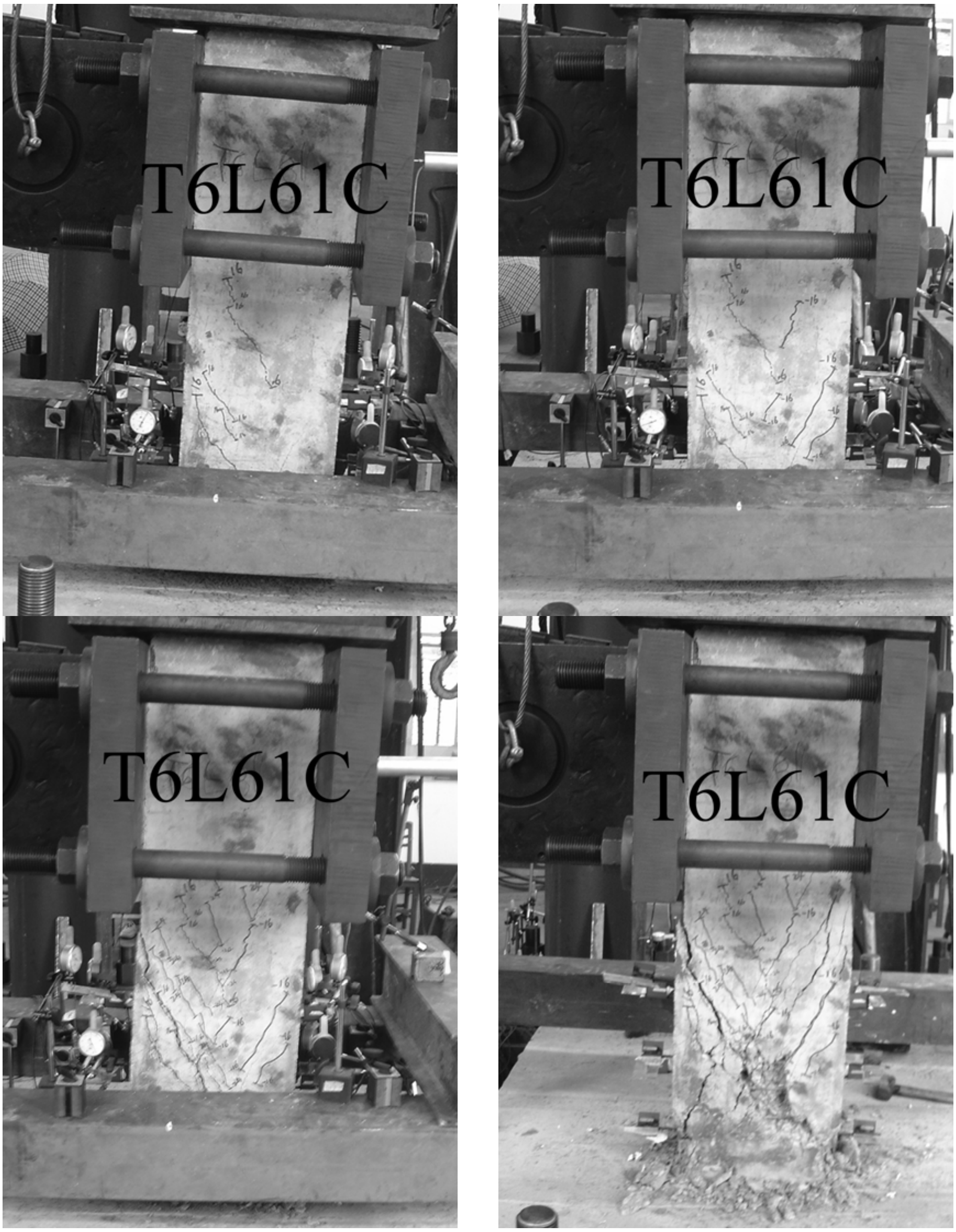

Figure 6-9 Specimen T6L61C (Top Left: at 15.08mm, Top Right: at -10.55mm, Bottom Left: at 24.38mm, Bottom Right: at Failure)

Figure 6-10 Specimen T6M61A (Top Left: at 9.61mm, Top Right: 14.95mm, Bottom Left: at 20.76mm, Bottom Right: at Failure)

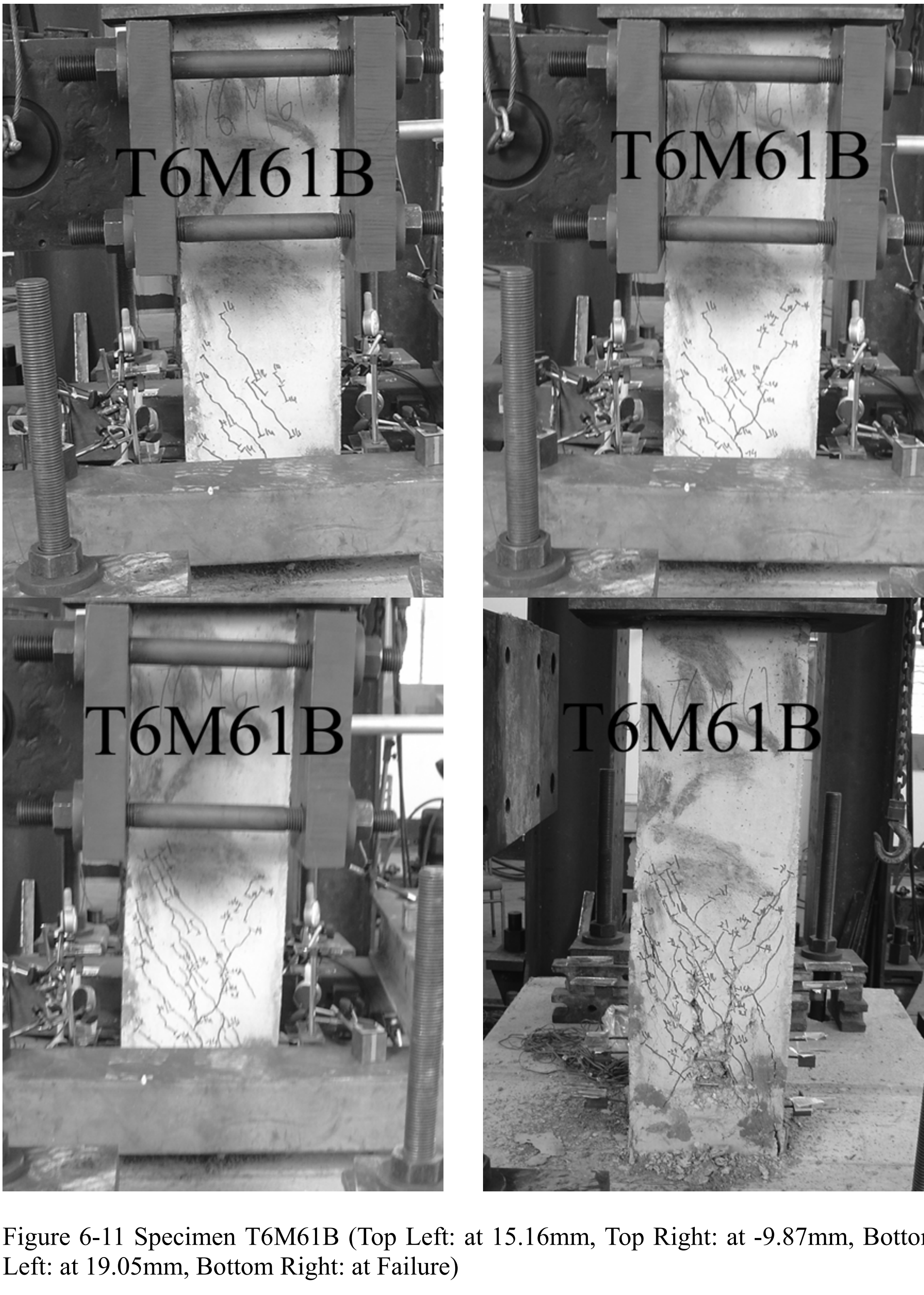

Figure 6-11 Specimen T6M61B (Top Left: at 15.16mm, Top Right: at -9.87mm, Bottom Left: at 19.05mm, Bottom Right: at Failure)

Figure 6-12 Specimen T4L120A (Top Left: at 3.76mm, Top Right: at 4.74mm, Bottom Left: at 12.61mm, Bottom Right: at Failure)

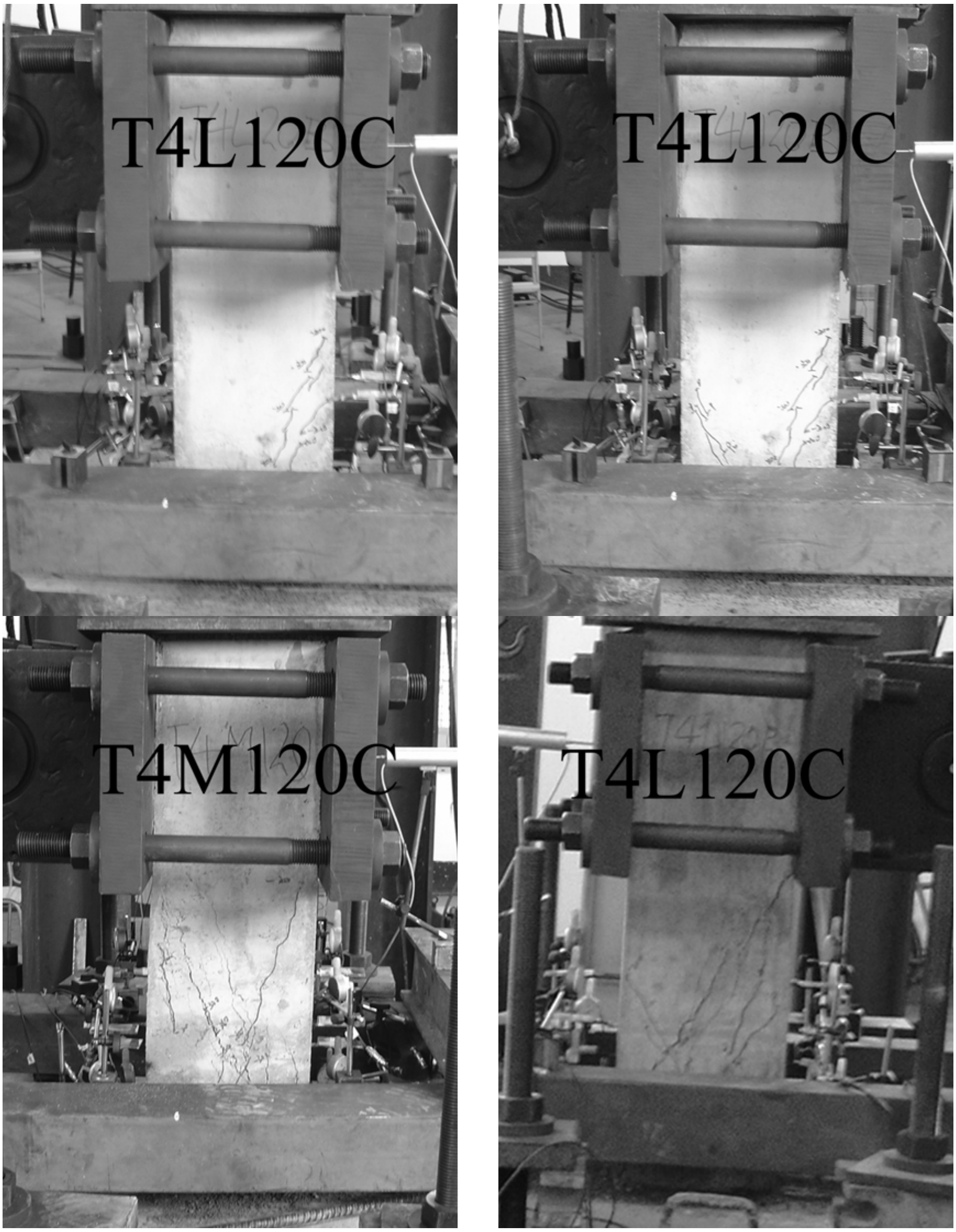

Figure 6-13 Specimen T4L120C (Top Left: at 3.51mm, Top Right: at 5.78mm, Bottom Left: at 12.57mm, Bottom Right: at Failure)

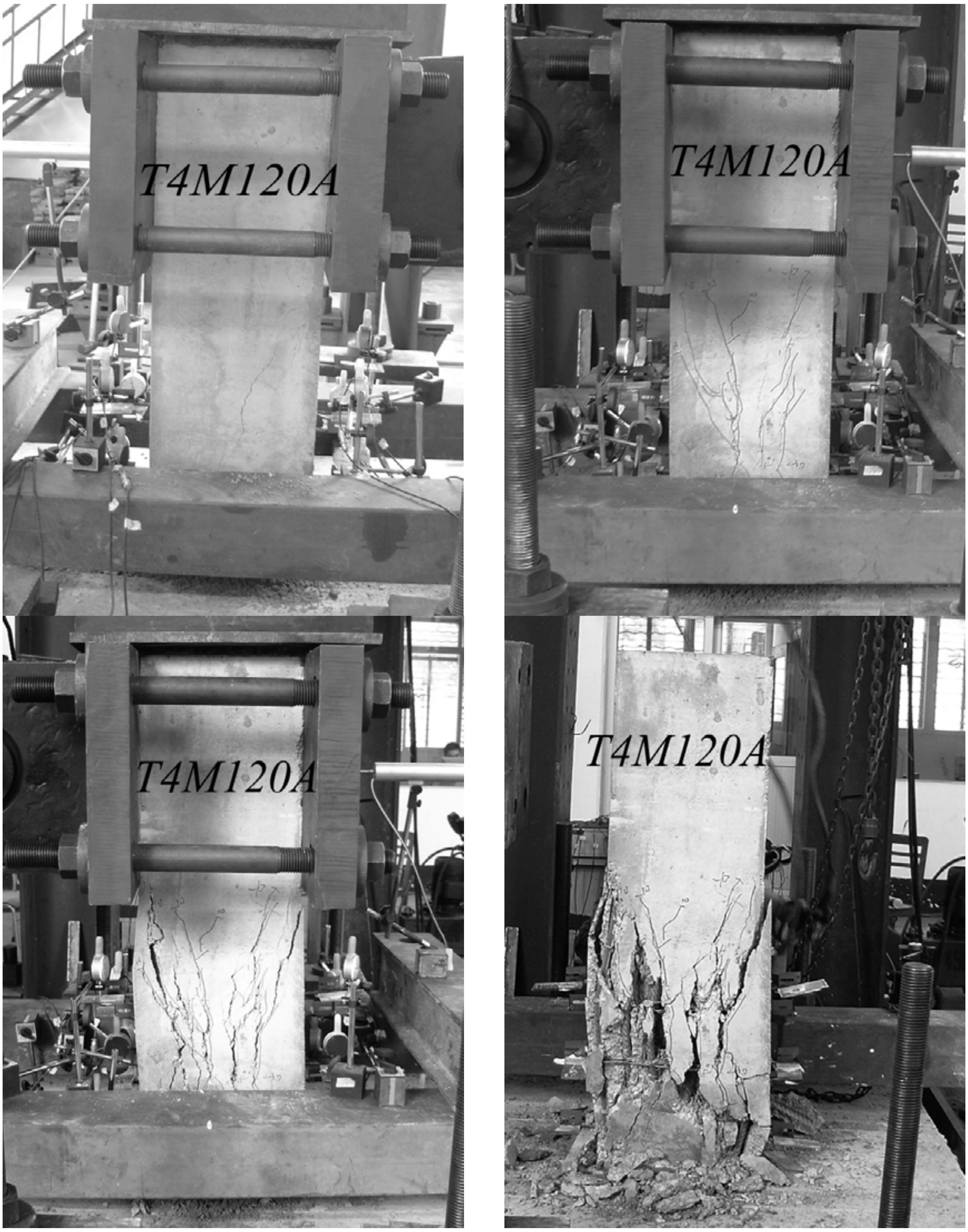

Figure 6-14 Specimen T4M120A (Top Left: at 3.74mm, Top Right: at 9.07mm, Bottom Left: at 14.93mm, Bottom Right: at Failure)

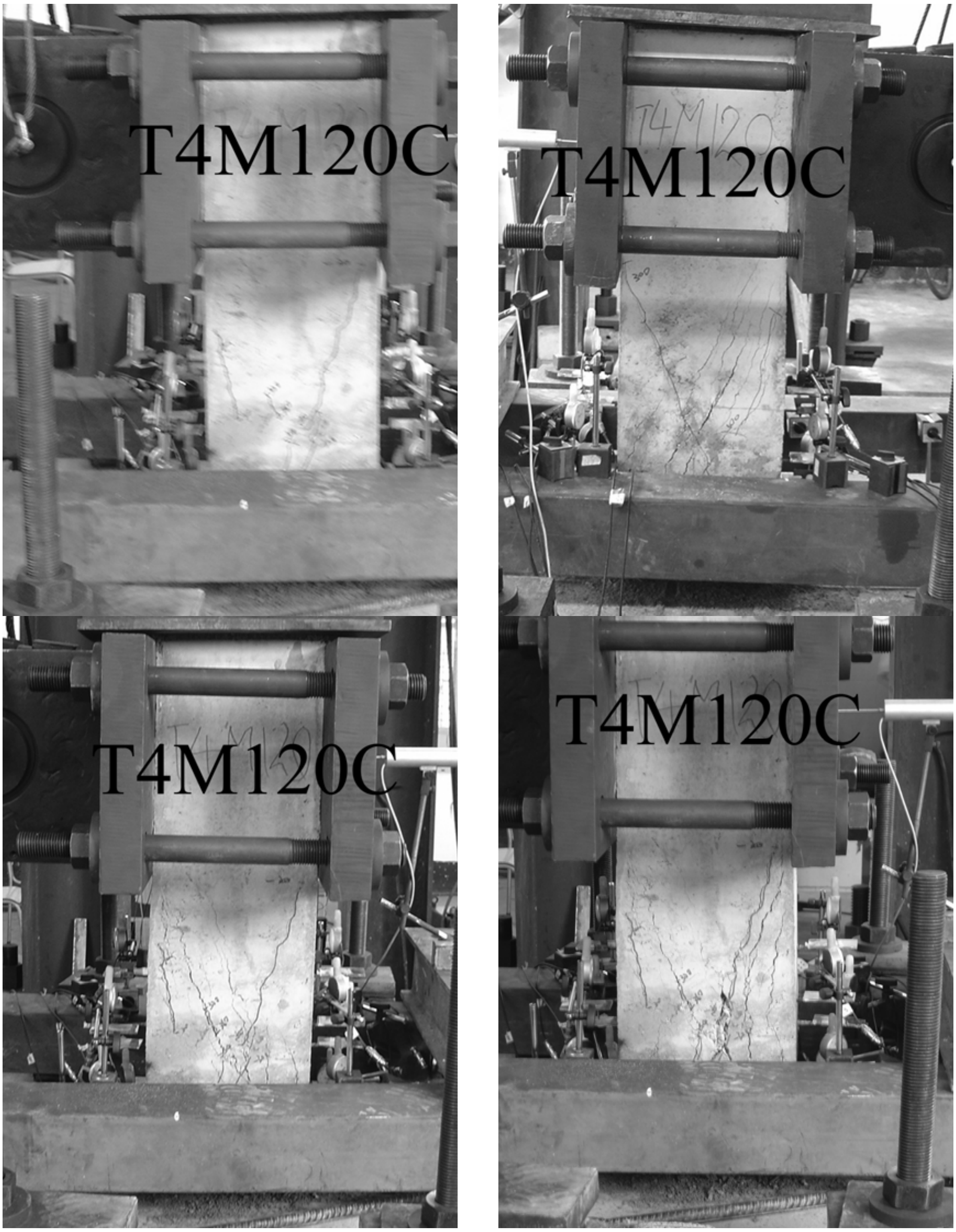

Figure 6-15 Specimen T4M120C (Top Left: at 8.16mm, Top Right: at -5.47mm, Bottom Left: at17.60mm, Bottom Right: at Failure)

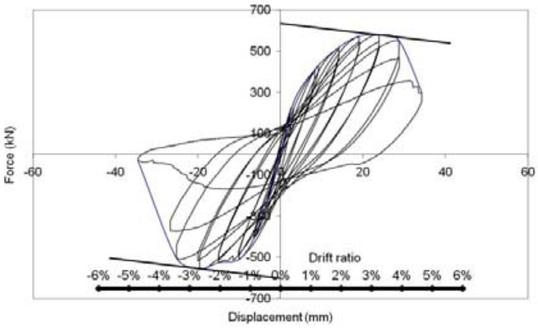

(a) Specimen T6L35A

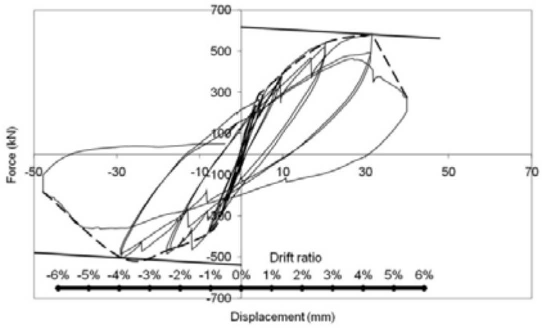

(b) Specimen T6L35C

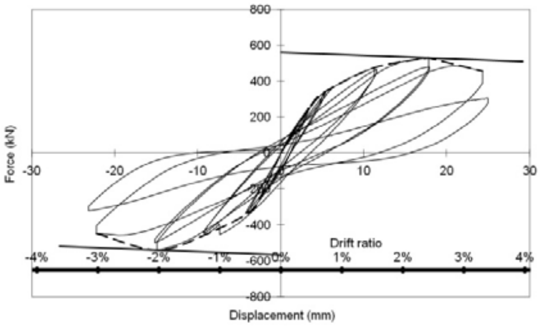

(c) Specimen T6L61B

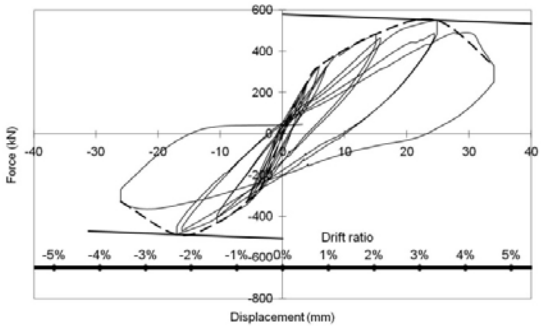

(d) Specimen T6L61C

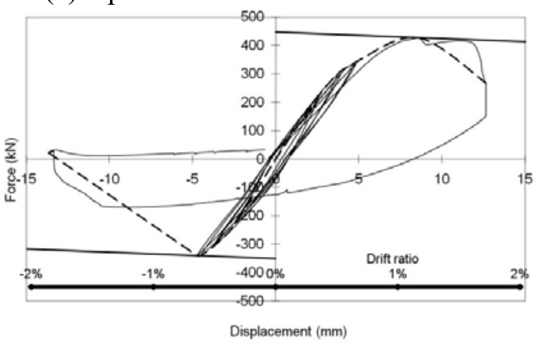

(e) Specimen T4L120A

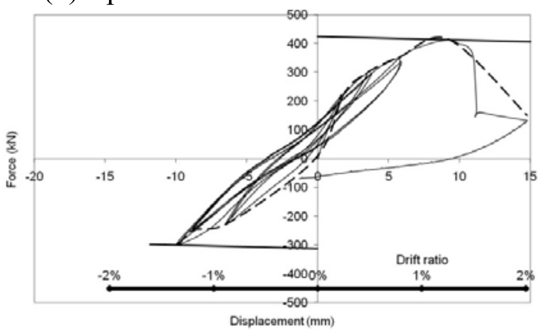

(f) Specimen T4L120C

Figure 6-16 Force-deflection Curves of Specimens with Type L Detailing

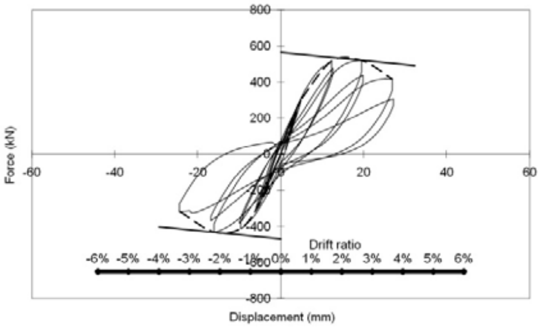

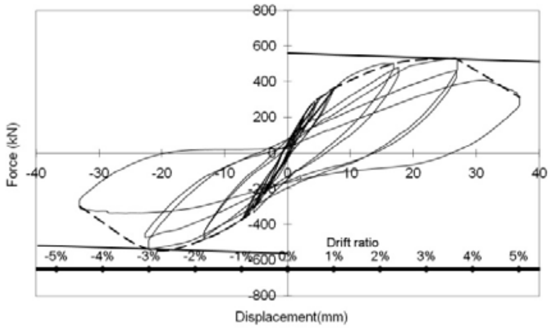

(a) Specimen T6M35A (b) Specimen T6M35C

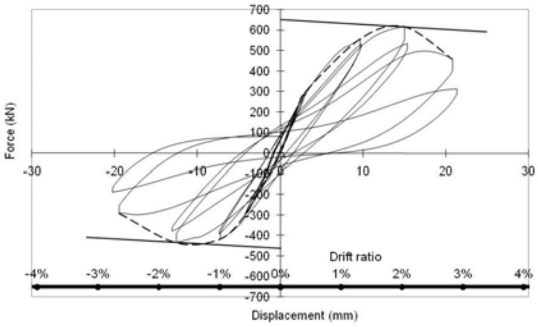

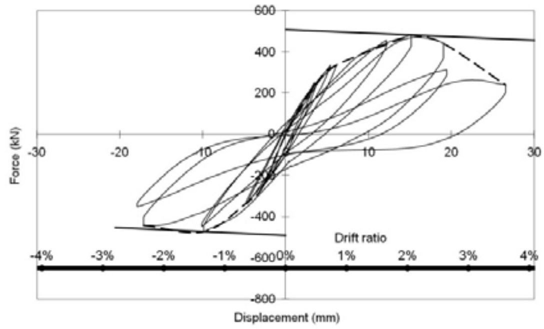

(c) Specimen T6M61A (d) Specimen T6M61B

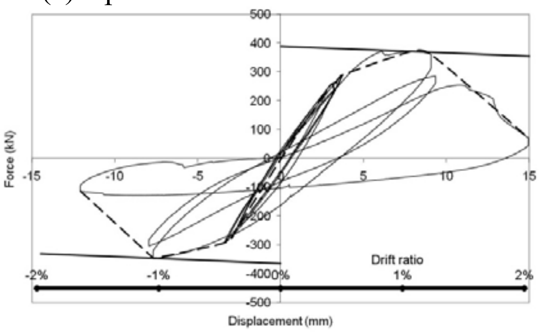

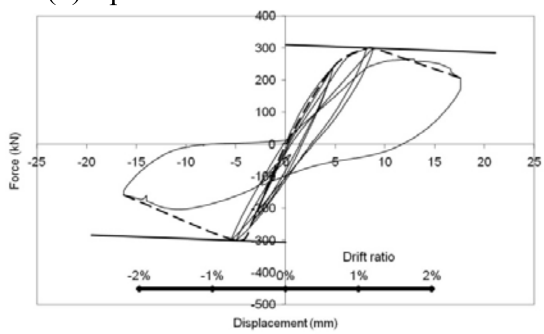

(e) Specimen T4M120A (f) Specimen T4M120C

Figure 6-17 Force-deflection Curves of Specimens with Type M Detailing

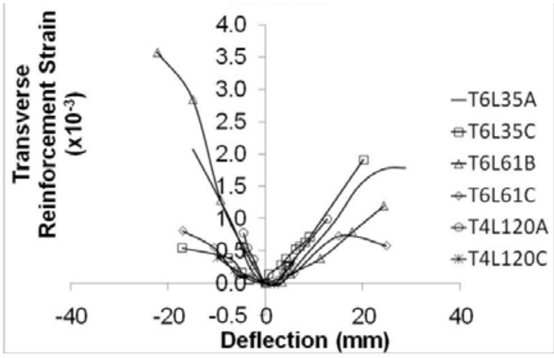

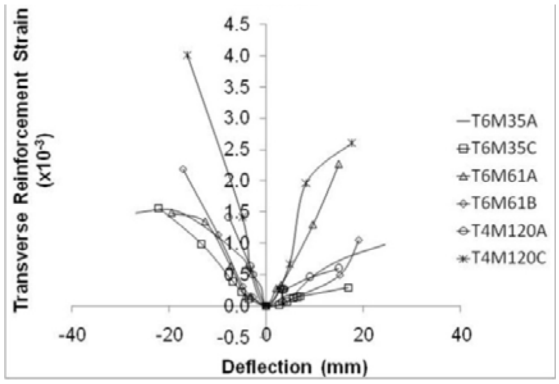

(a) Type L Detailing (b) Type M Detailing

Figure 6-18 Transverse Reinforcement Strain (on Hoops near Hook) against Deflection

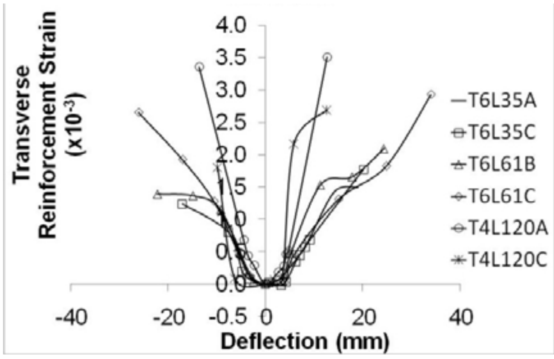

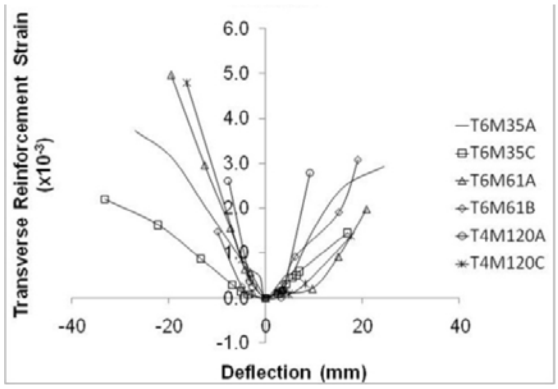

(a) Type L Detailing (b) Type M Detailing

Figure 6-19 Transverse Reinforcement Strain (on Hoops far away from Hook) against Deflection

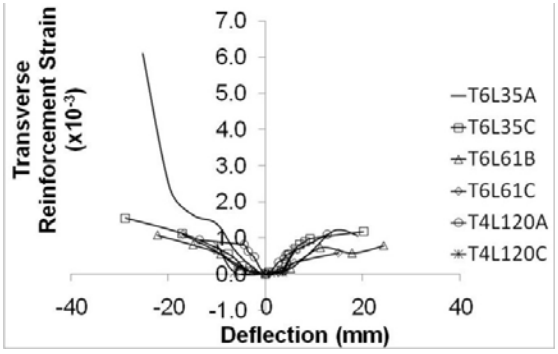

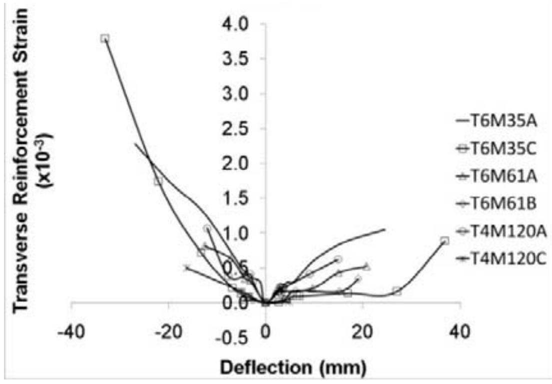

(a) Type L Detailing

(b) Type M Detailing

Figure 6-20 Transverse Reinforcement Strain (on Long Crossties Perpendicular to the Loading Direction) against Deflection

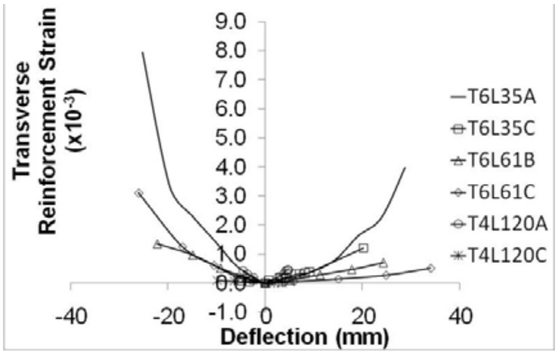

Figure 6-21 Transverse Reinforcement Strain (on Long Crossties Parallel to the Loading Direction) against Deflection (Type L Detailing)

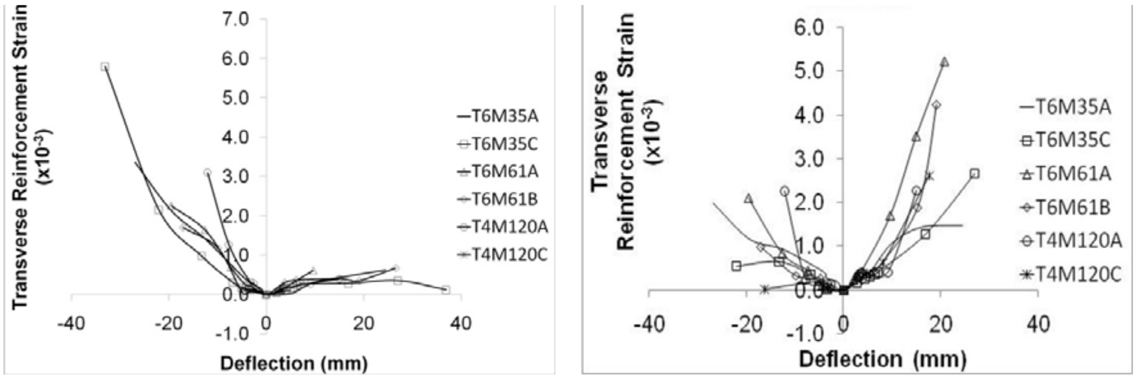

(a) Left Hand Side of Figure 6-1 (b) Right Hand Side of Figure 6-1

Figure 6-22 Transverse Reinforcement Strain (on Short Crossties Parallel to the Loading Direction) against Deflection

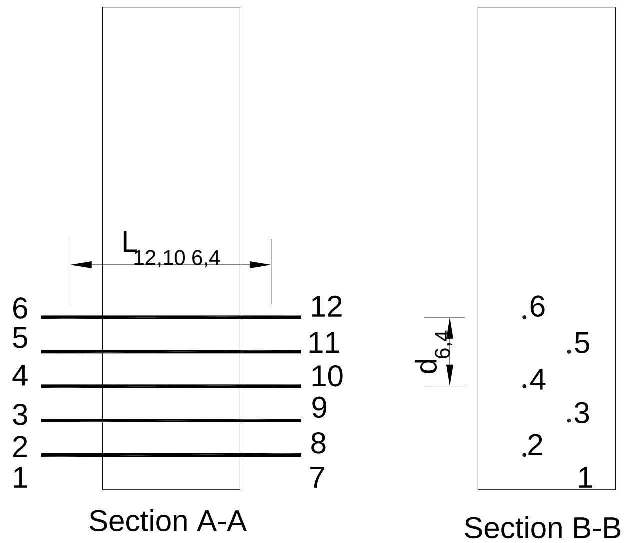

Figure 6-23 Instrumentation of Transducers for Curvature Measurement

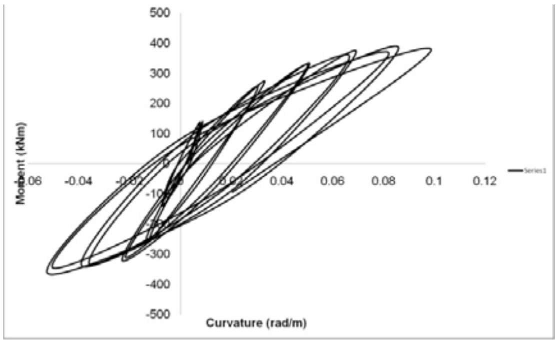

(a) Specimen T6L35A

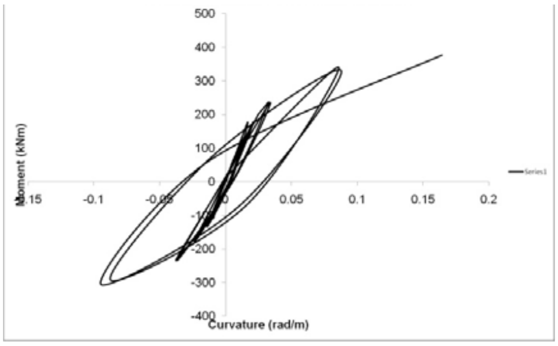

(b) Specimen T6L35C

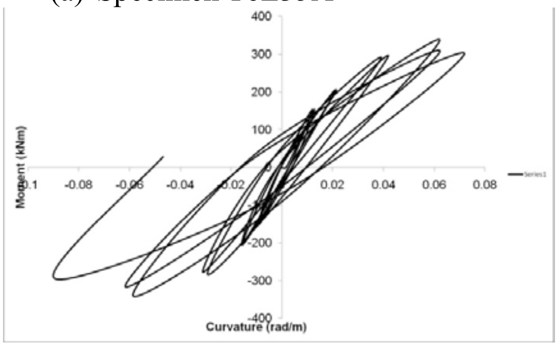

(c) Specimen T6L61B

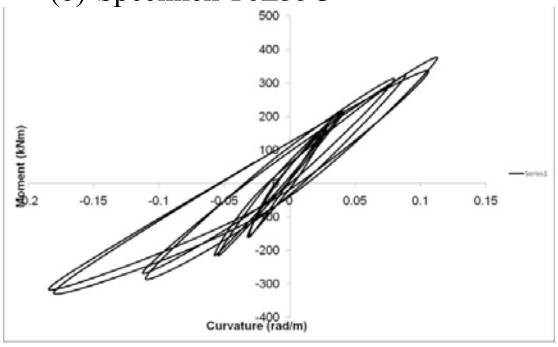

(d) Specimen T6L61C

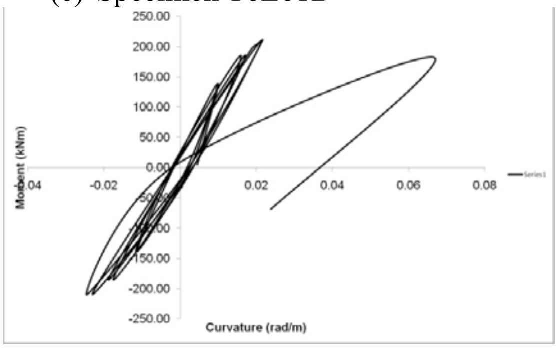

(e) Specimen T4L120A

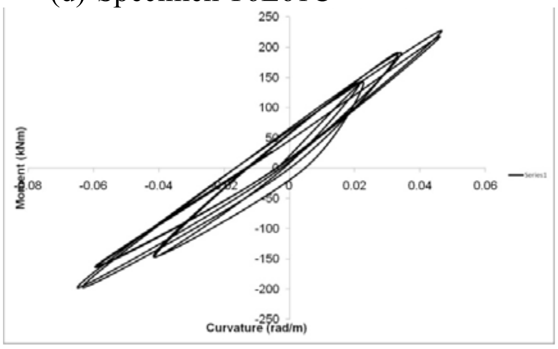

(f) Specimen T4L120C

Figure 6-24Moment-curvature Curve of Specimens with Type L Detailing

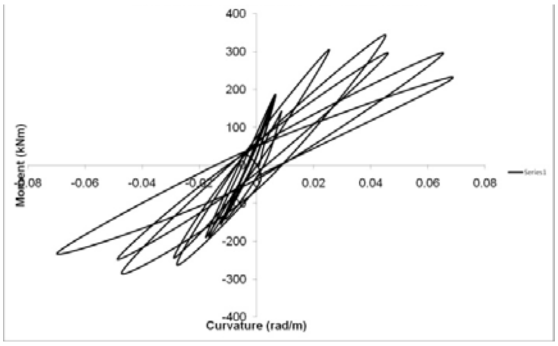

(a) Specimen T6M35A

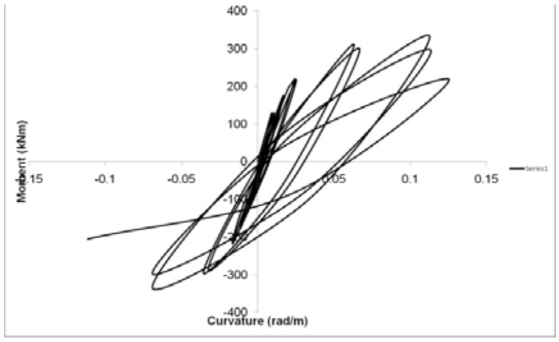

(b) Specimen T6M35C

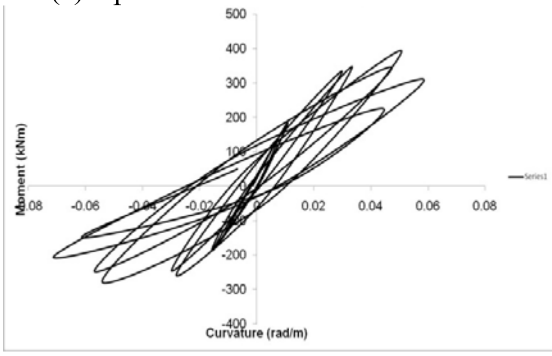

(c) Specimen T6M61A

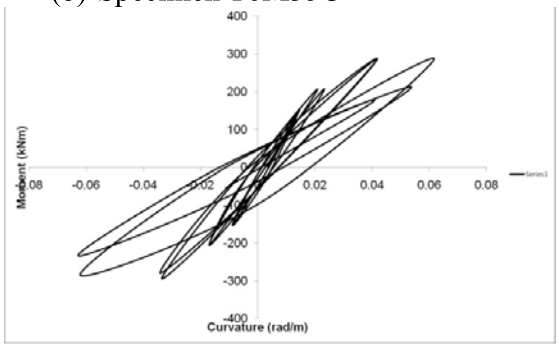

(d) Specimen T6M61B

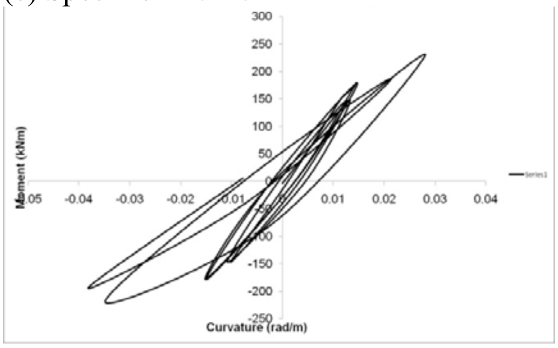

(e) Specimen T4M120A

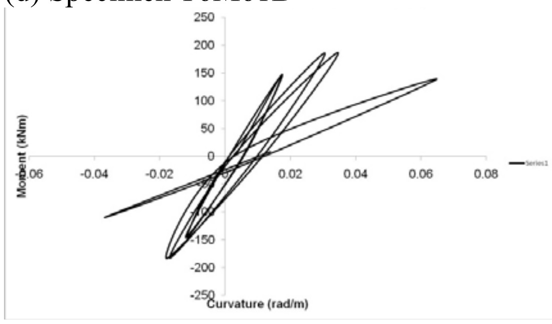

(f) Specimen T4M120C

Figure 6-25 Moment-curvature Curve of Specimens with Type M Detailing

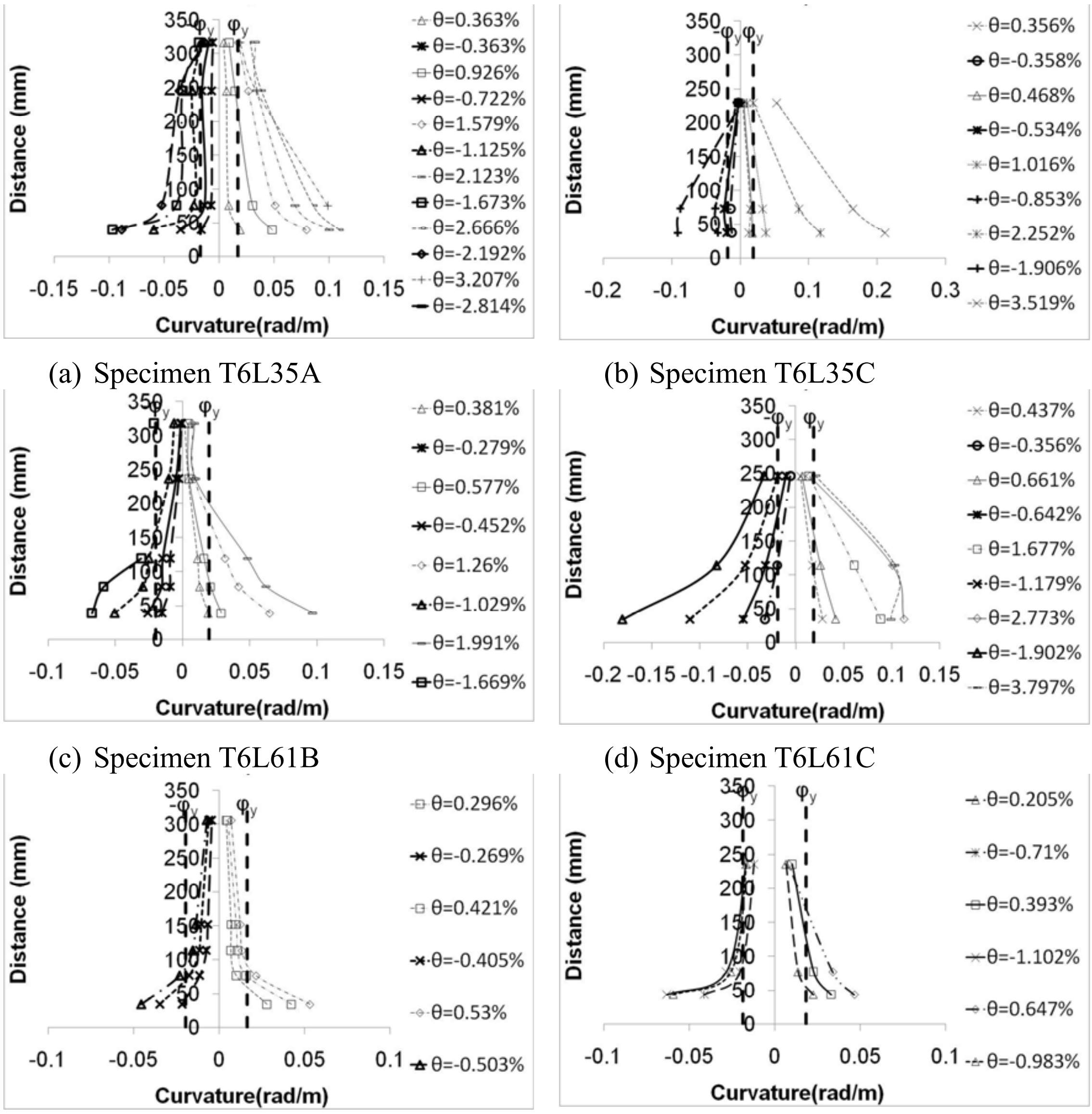

(a) Specimen T6L35A

(b) Specimen T6L35C

(c) Specimen T6L61B

(d) Specimen T6L61C

(e) Specimen T4L120A

(f) Specimen T4L120C

Figure 6-26 Variation of Curvature from Distances above Footing (Type L Detailing)

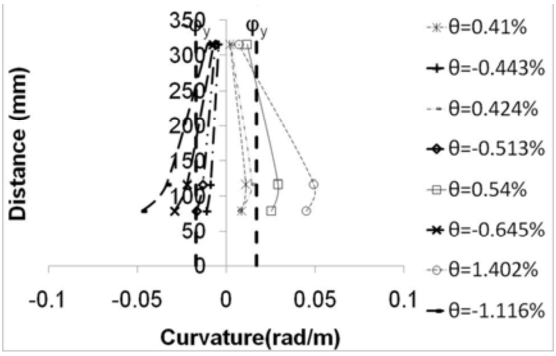

(a) Specimen T6M35A

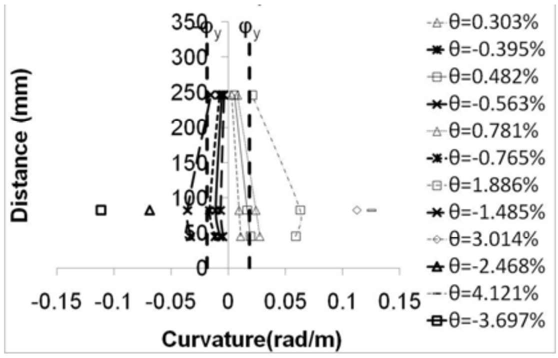

(b) Specimen T6M35C

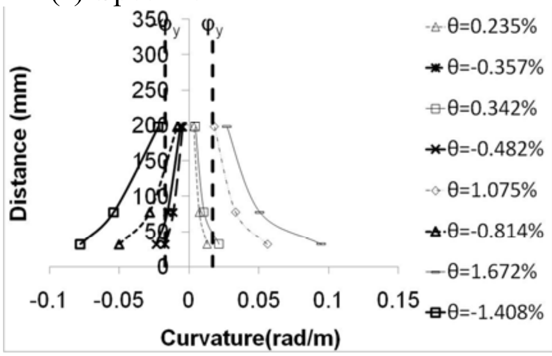

(c) Specimen T6M61A

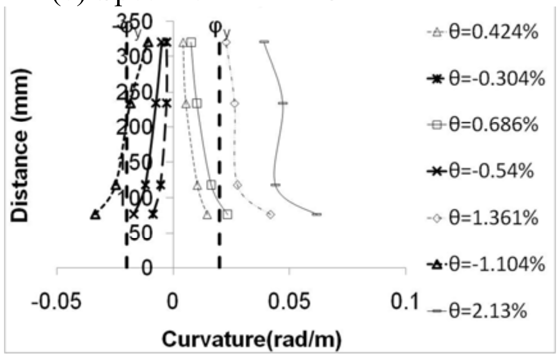

(d) Specimen T6M61B

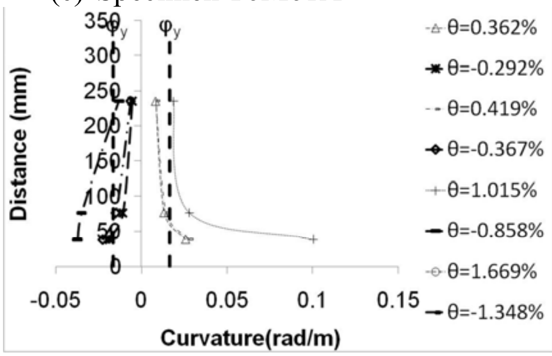

(e) Specimen T4M120A

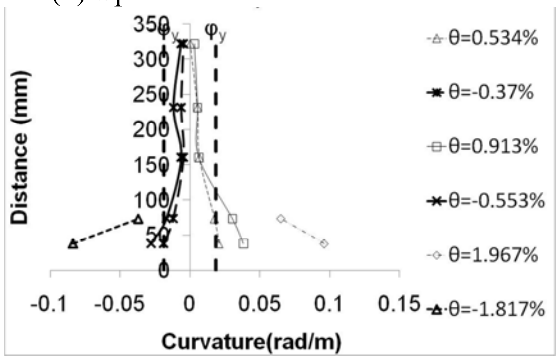

(f) Specimen T4M120C

Figure 6-27 Variation of Curvature from Distances above Footing (Type M Detailing)

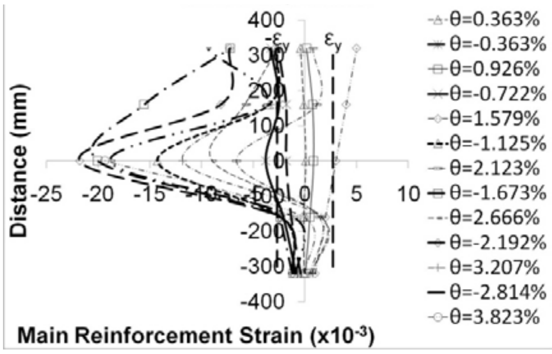

(a) Specimen T6L35A

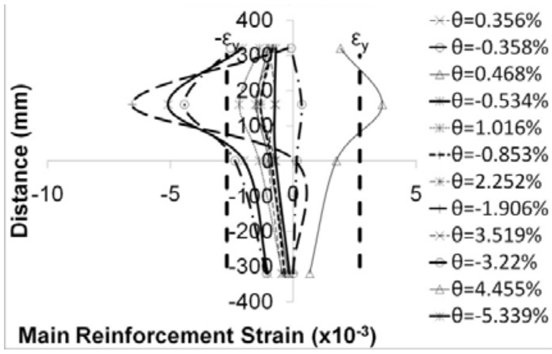

(b) Specimen T6L35C

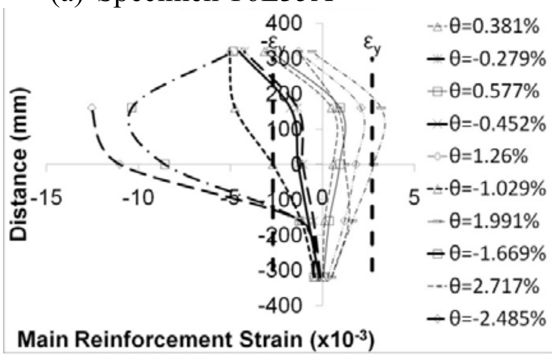

(c) Specimen T6L61B

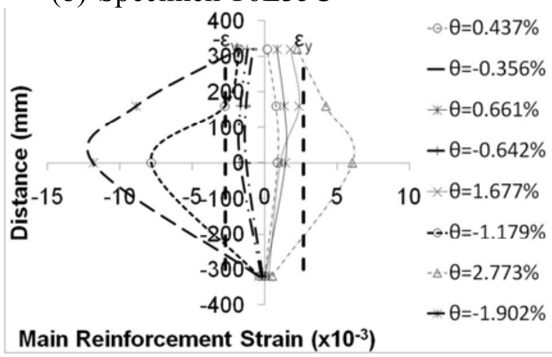

(d) Specimen T6L61C

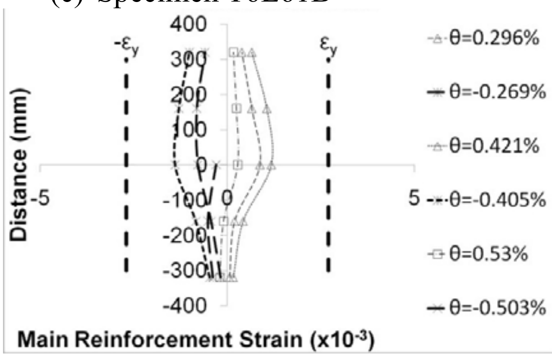

(e) Specimen T4L120A

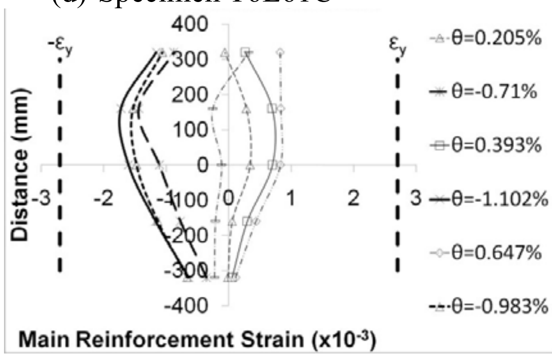

(f) Specimen T4L120C

Figure 6-28 Variation of Main Reinforcement Strain from Distances above Footing (Type L Detailing)

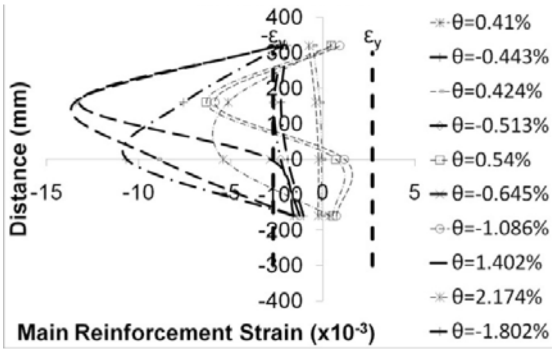

(a) Specimen T6M35A

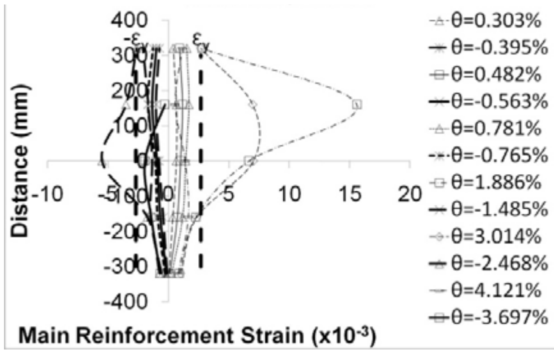

(b) Specimen T6M35C

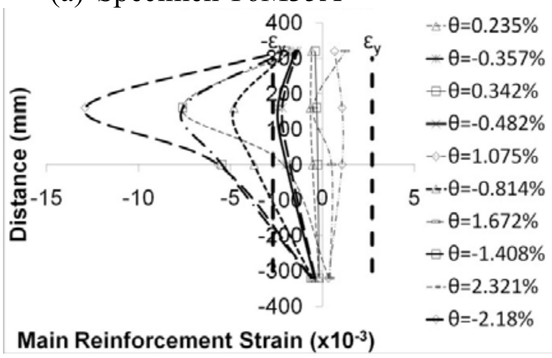

(c) Specimen T6M61A

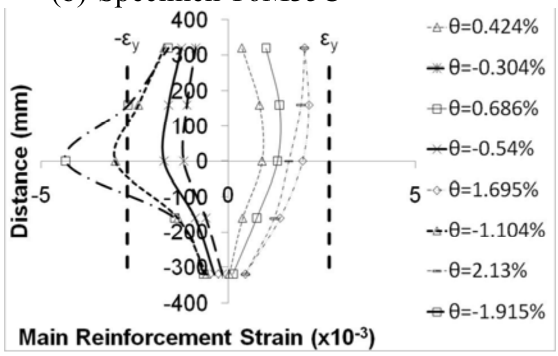

(d) Specimen T6M61B

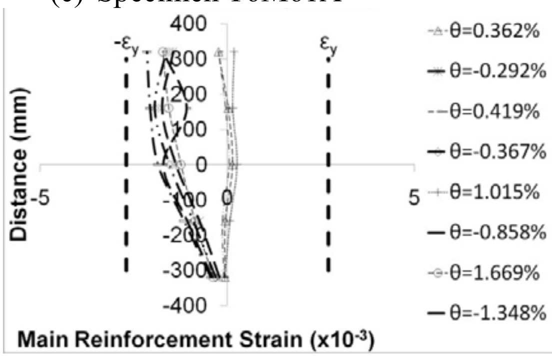

(e) Specimen T4M120A

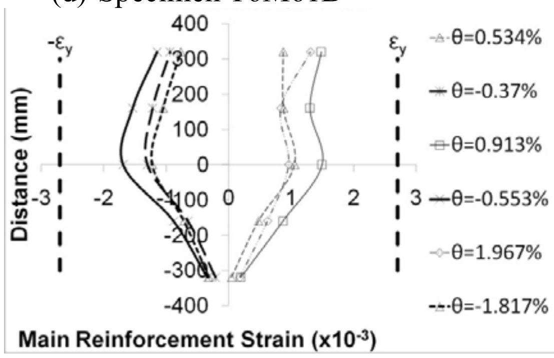

(f) Specimen T4M120C

Figure 6-29 Variation of Main Reinforcement Strain from Distances above Footing (Type M Detailing)

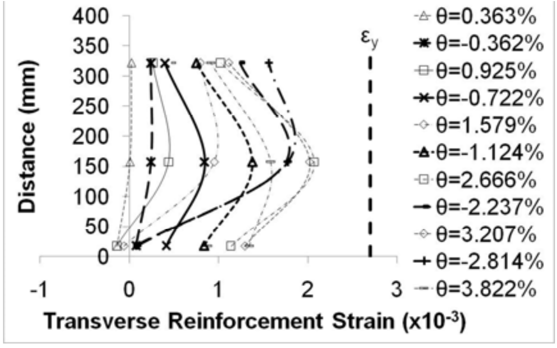

(a) Specimen T6L35A

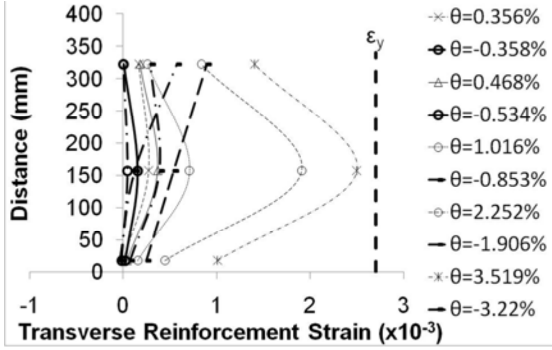

(b) Specimen T6L35C

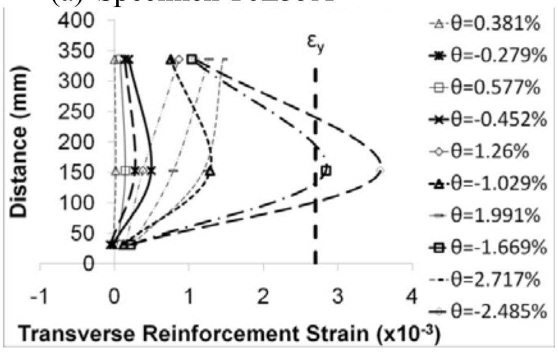

(c) Specimen T6L61B

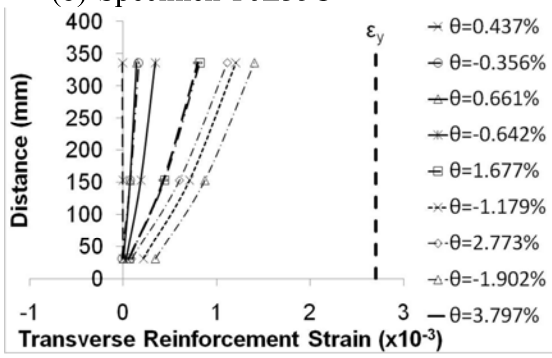

(d) Specimen T6L61C

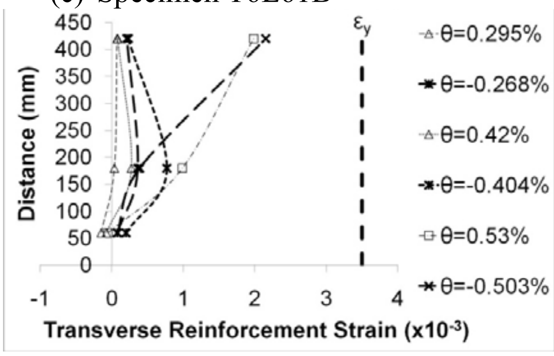

(e) Specimen T4L120A

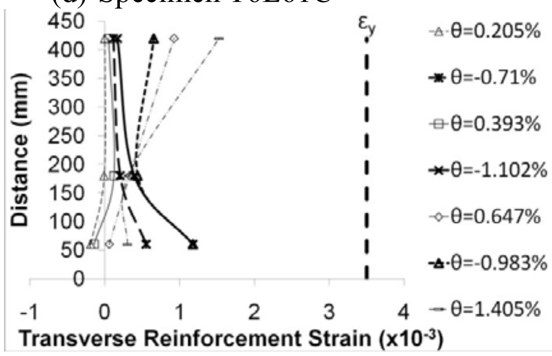

(f) Specimen T4L120C

Figure 6-30 Variation of Hoop Strain near Hook from Distances above Footing (Type L Detailing)

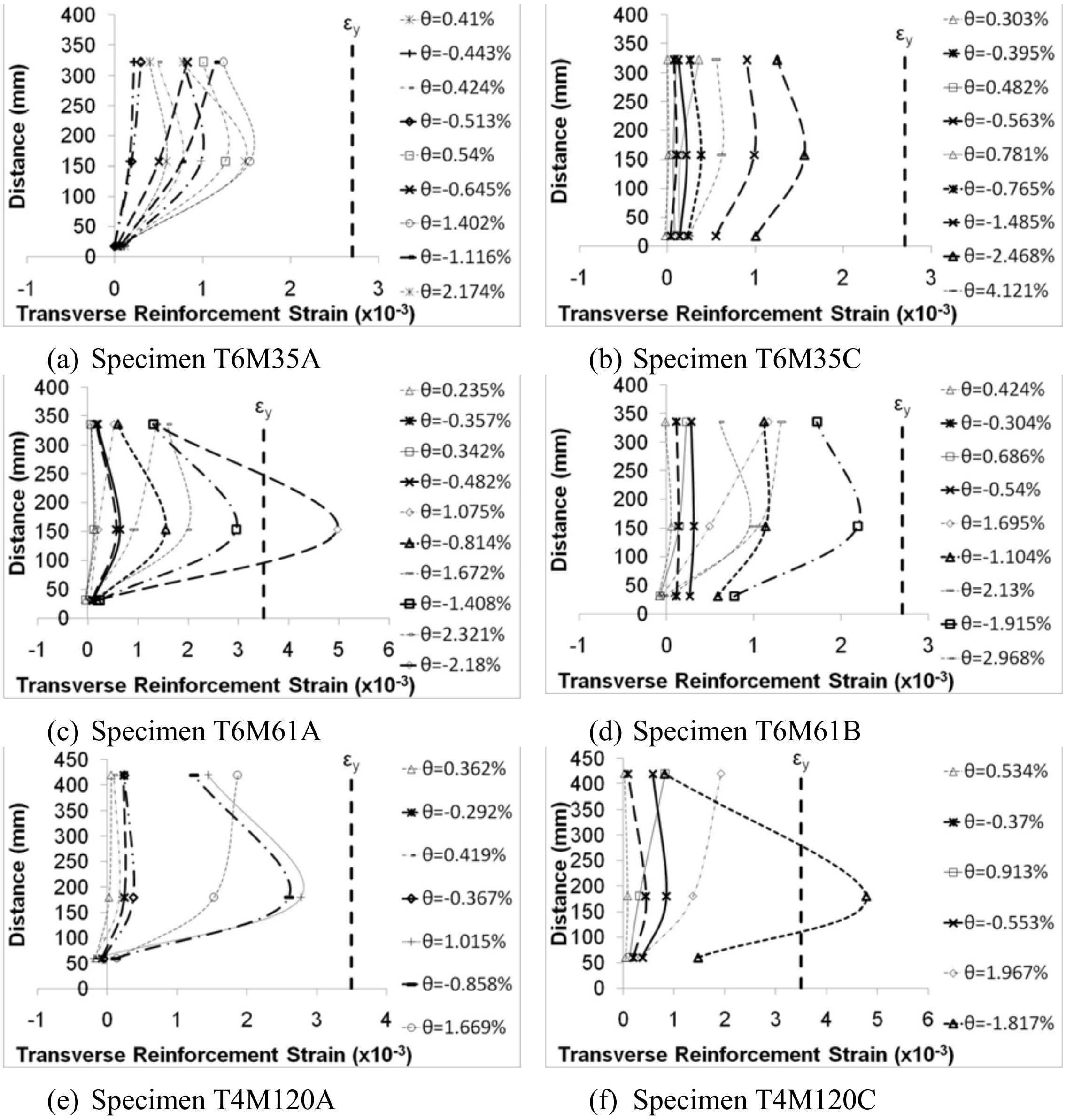

(a) Specimen T6M35A

(b) Specimen T6M35C

(c) Specimen T6M61A

(d) Specimen T6M61B

(e) Specimen T4M120A

(f) Specimen T4M120C

Figure 6-31 Variation of Hoop Strain near Hook from Distances above Footing (Type M Detailing)

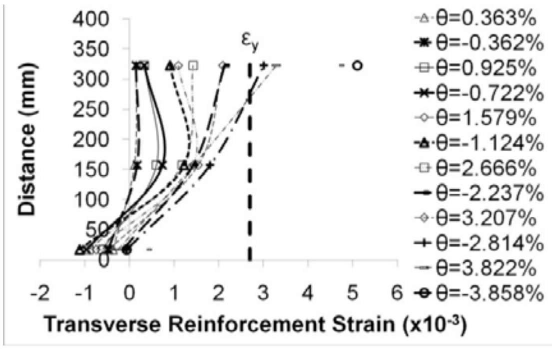

(a) Specimen T6L35A

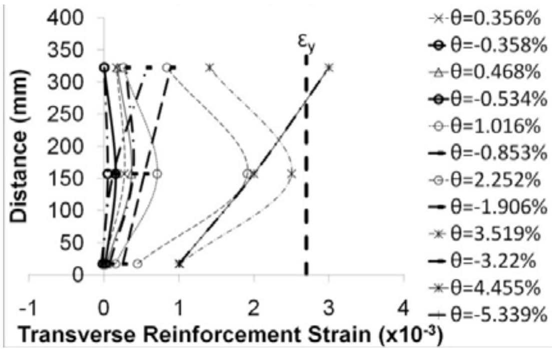

(b) Specimen T6L35C

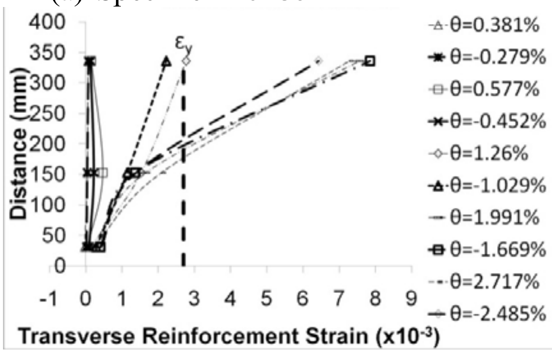

(c) Specimen T6L61B

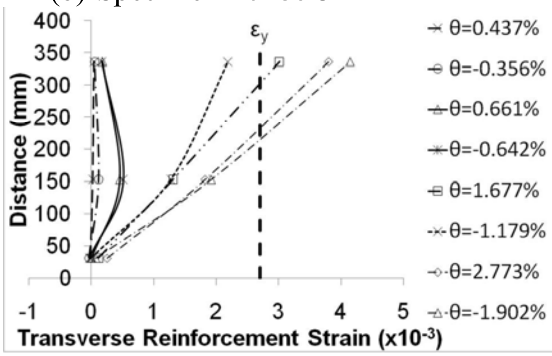

(d) Specimen T6L61C

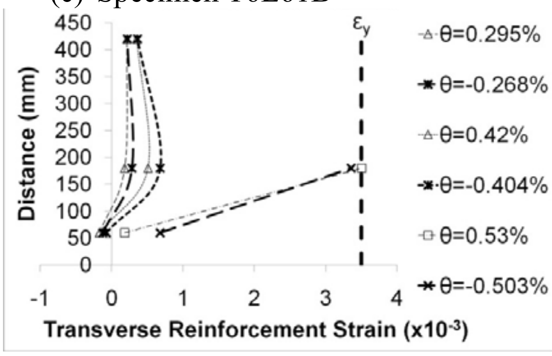

(e) Specimen T4L120A

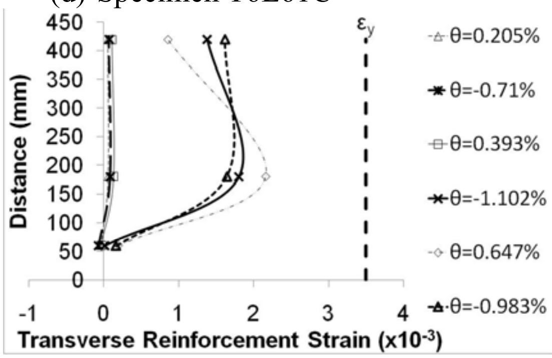

(f) Specimen T4L120C

Figure 6-32 Variation of Hoop Strain far from Hook from Distances above Footing (Type L Detailing)

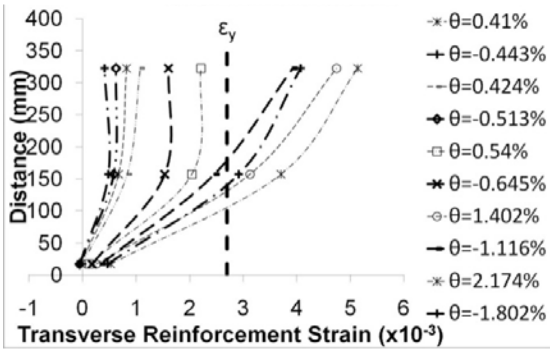

(a) Specimen T6M35A

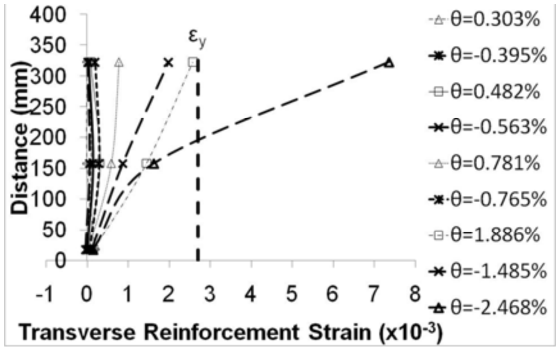

(b) Specimen T6M35C

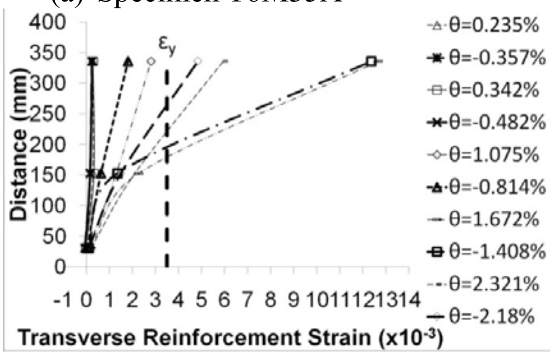

(c) Specimen T6M61A

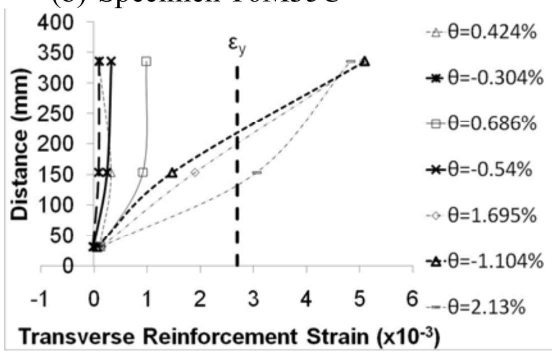

(d) Specimen T6M61B

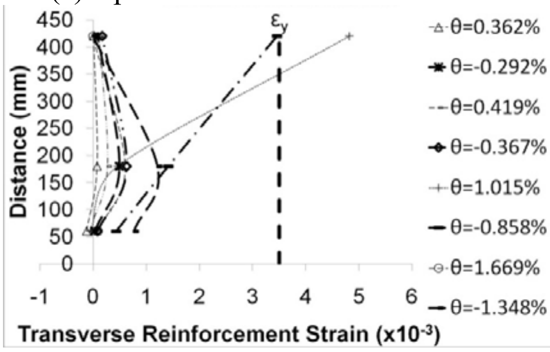

(e) Specimen T4M120A

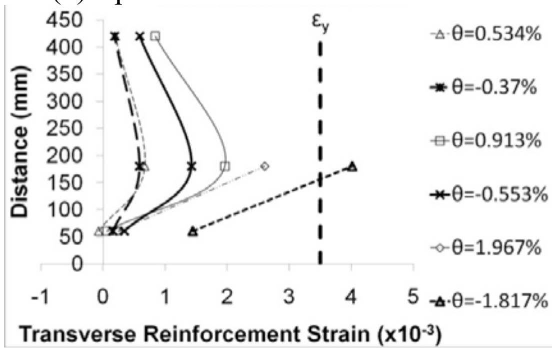

(f) Specimen T4M120C

Figure 6-33 Variation of Hoop Strain far from Hook from Distances above Footing (Type M Detailing)

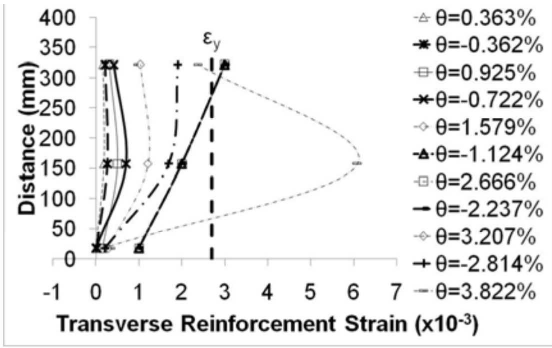

(a) Specimen T6L35A

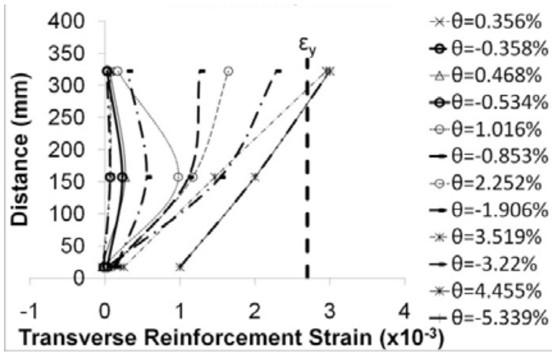

(b) Specimen T6L35C

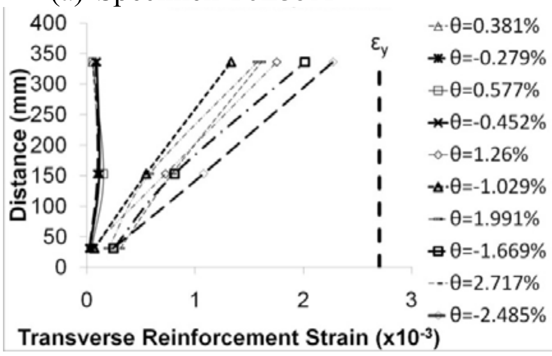

(c) Specimen T6L61B

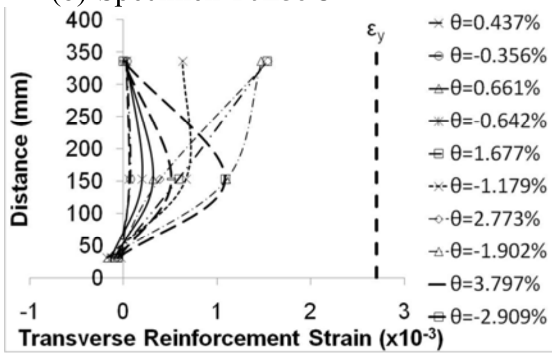

(d) Specimen T6L61C

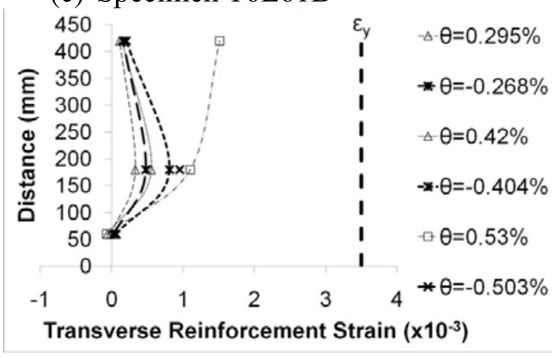

(e) Specimen T4L120A

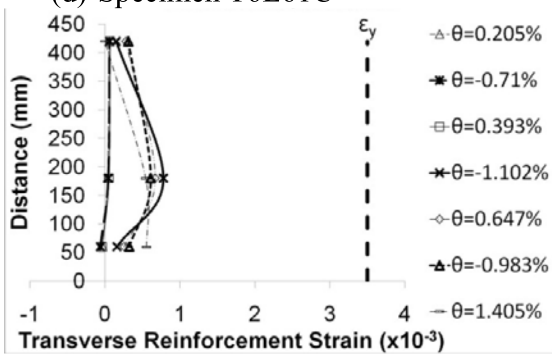

(f) Specimen T4L120C

Figure 6-34 Variation of Strains in Long Crossties Perpendicular to Loading Direction from Distances above Footing (Type L Detailing)

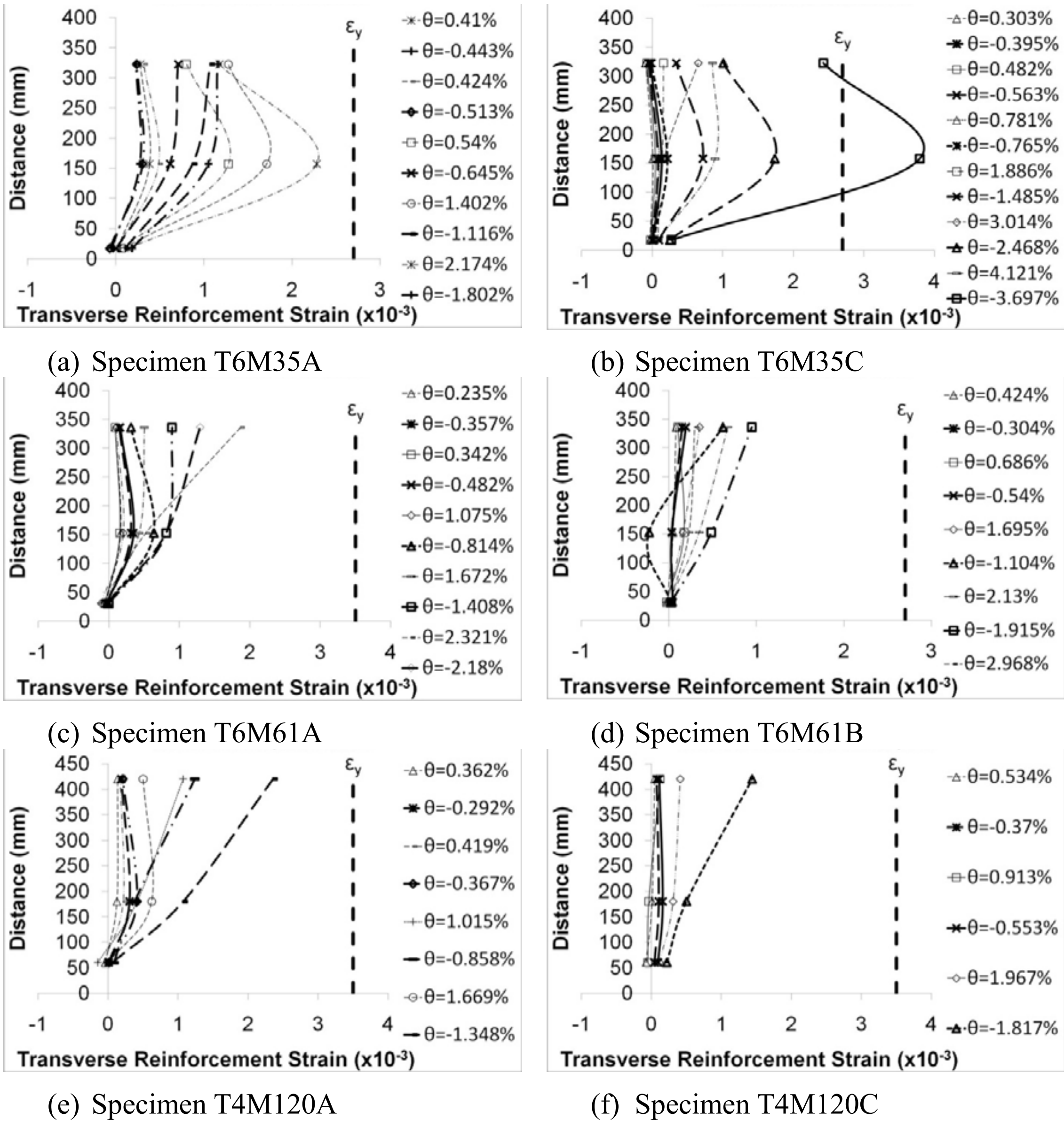

Figure 6-35 Variation of Strains in Long Crossties Perpendicular to Loading Direction from Distances above Footing (Type M Detailing)

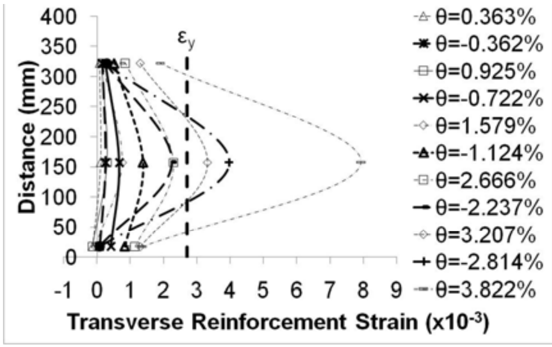

(a) Specimen T6L35A

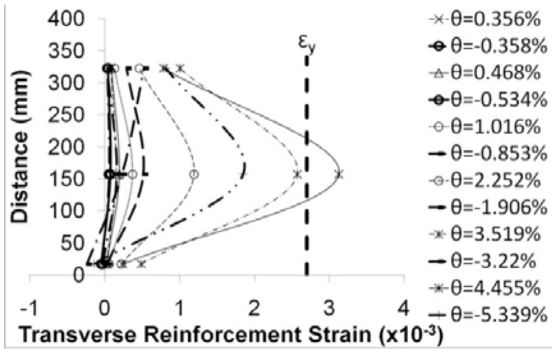

(b) Specimen T6L35C

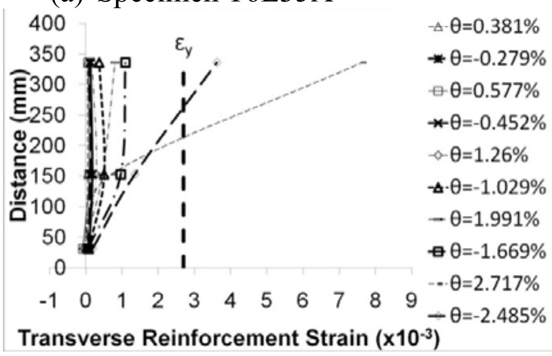

(c) Specimen T6L61B

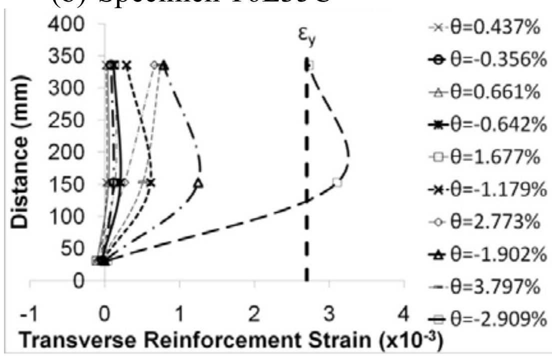

(d) Specimen T6L61C

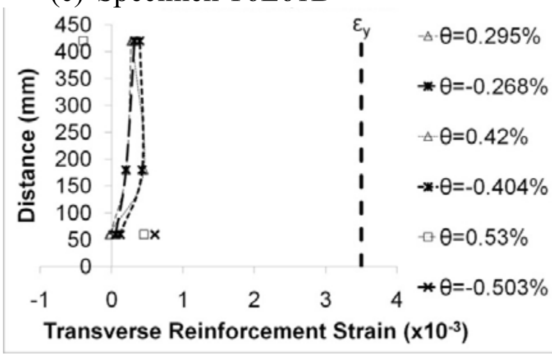

(e) Specimen T4L120A

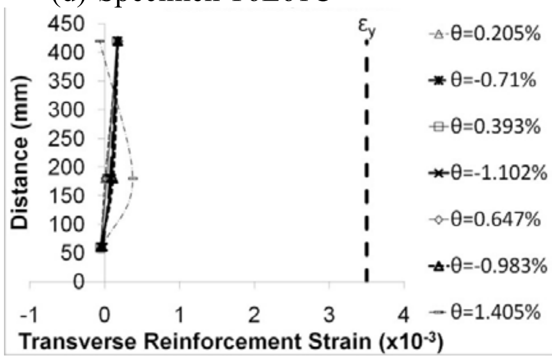

(f) Specimen T4L120C

Figure 6-36 Variation of Strains in Long Crossties Parallel to Loading Direction from Distances above Footing (Type L Detailing)

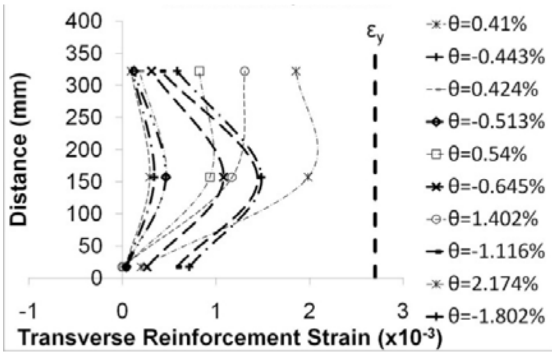

(a) Specimen T6M35A

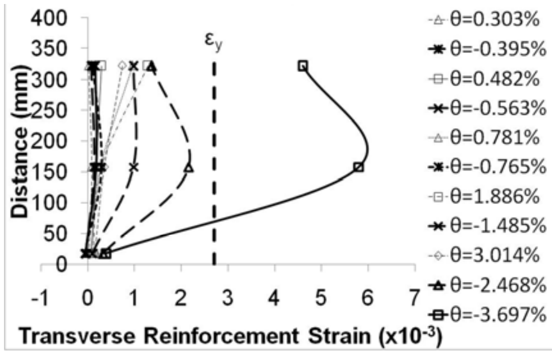

(b) Specimen T6M35C

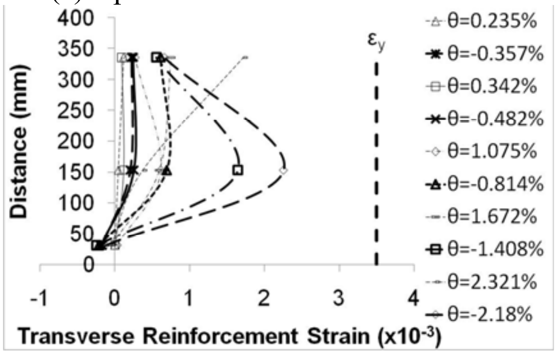

(c) Specimen T6M61A

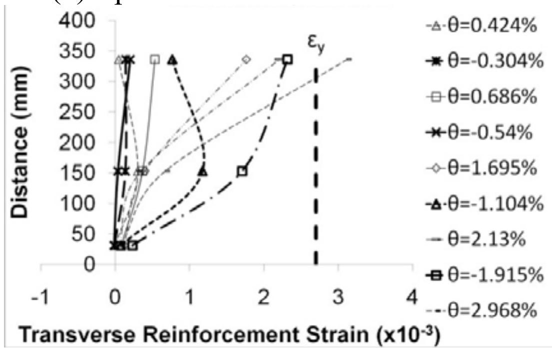

(d) Specimen T6M61B

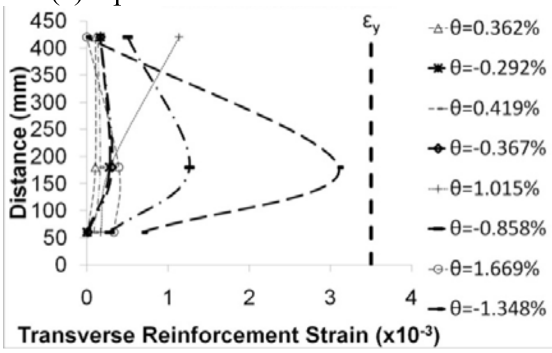

(e) Specimen T4M120A

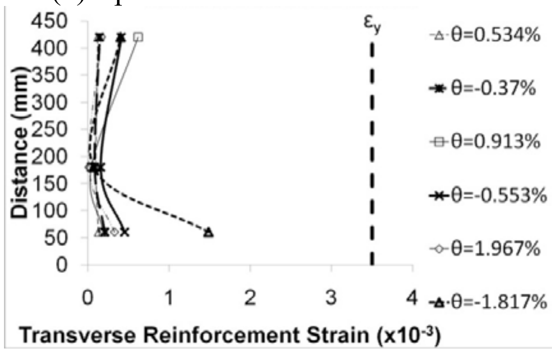

(f) Specimen T4M120C

Figure 6-37 Variation of Strains in Short Crossties Parallel to Loading Direction from Distances above Footing (Type M Detailing)

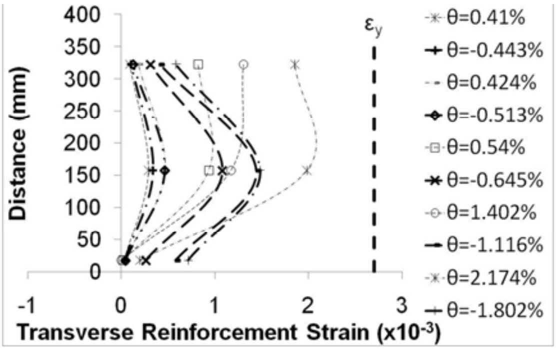

(a) Specimen T6M35A

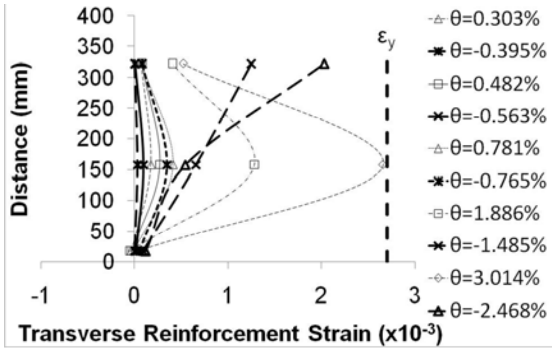

(b) Specimen T6M35C

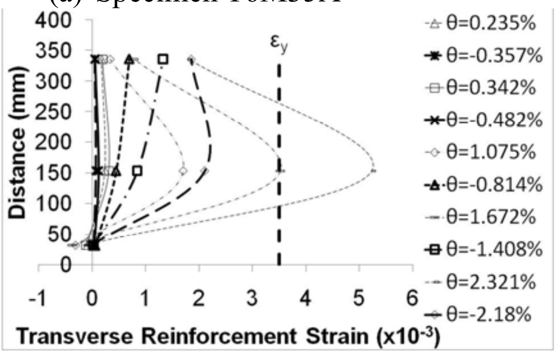

(c) Specimen T6M61A

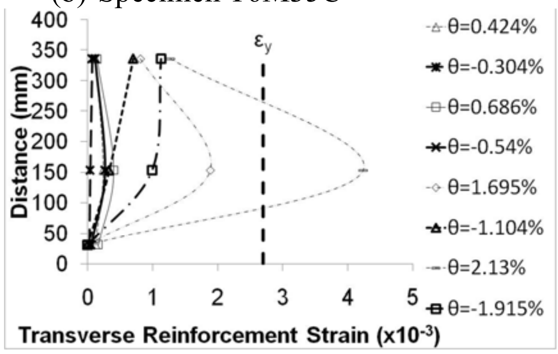

(d) Specimen T6M61B

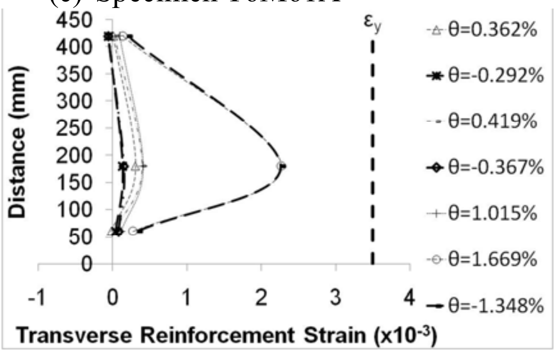

(e) Specimen T4M120A

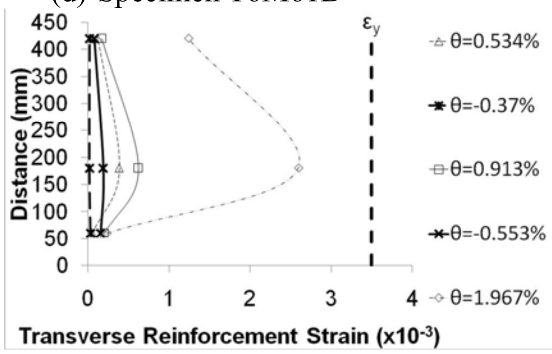

(f) Specimen T4M120C

Figure 6-38 Variation of Strains in Short Crossties Parallel to Loading Direction from Distances above Footing (Type M Detailing)

Table 6-1 Properties of Specimen

Specimen	ρ_s	n	Type	Mode of Failure
T6L35A	0.022756	0.6	L	Flexural-shear
T6L35B	0.022756	0.3	L	Flexural-shear
T6M35A	0.022756	0.6	M	Flexural-shear
T6M35B	0.022756	0.3	M	Flexural-shear
T6L61B	0.013057	0.3	L	Flexural-shear
T6L61C	0.013057	0.45	L	Flexural-shear
T6M61A	0.013057	0.6	M	Flexural-shear
T6M61C	0.013057	0.45	M	Flexural-shear
T4L120A	0.00295	0.6	L	Shear
T4L120B	0.00295	0.3	L	Shear
T4M120A	0.00295	0.6	M	Shear
T4M120B	0.00295	0.3	M	Shear

ρ_s: volumetric transverse reinforcement ratio

n: axial load capacity ratio

Type: type of configuration of transverse reinforcement

Table 6-2 Comparison of Shear Force with Design Codes

Specimen	Shear Force			Flexural Force			Experimental
	ACI 318	BS 8110	GB 50010	ACI 318	BS 8110	GB 50010	
T6L35A	684.33	1090.40	726.01	368.06	321.39	388.73	417.67
T6L35C	610.76	994.91	704.47	391.15	315.62	375.07	348.27
T6M35A	678.65	1077.91	720.28	355.42	310.72	375.94	305.47
T6M35C	606.77	985.56	703.05	384.01	314.06	371.39	319.9
T6L61B	456.19	842.43	487.13	376.77	339.90	402.74	330.94
T6L61C	420.26	752.41	469.90	384.01	314.06	371.39	329.1
T6M61A	492.13	844.76	487.13	355.42	310.72	375.94	348.5
T6M61B	456.19	842.43	487.13	376.77	339.90	402.74	308.25
T4L120A	326.61	643.26	278.86	368.06	321.39	388.73	296.97
T4L120C	253.04	547.77	257.33	391.15	315.62	375.07	260.32
T4M120A	326.61	643.26	278.86	368.06	321.39	388.73	249.19
T4M120C	253.04	547.77	257.33	391.15	315.62	375.07	267.49

Table 6-3 Force-deflection of Specimens

Specimen	Δ_y (mm)	F_y (kN)	Δ_{Fmax} (mm)	F_{max} (kN)	Δ_u (mm)	F_u (kN)
T6L35A	12.38	417.67	21.74	698.54	29.45	263.16
T6L35C	16.43	348.27	18.61	500.85	43.86	412.91
T6M35A	10.14	305.47	17.79	590.63	25.01	372.35
T6M35C	11.61	319.90	24.53	534.20	31.85	371.70
T6L61B	9.98	330.94	16.38	535.53	26.50	471.43
T6L61C	13.58	329.10	23.99	519.77	33.12	428.51
T6M61A	9.07	348.50	13.78	525.08	19.66	424.68
T6M61B	9.17	308.25	12.52	477.48	21.10	255.95
T4L120A	5.64	296.97	8.18	427.68	12.90	268.03
T4L120C	5.19	260.32	11.22	348.33	19.54	327.21
T4M120A	4.69	249.19	8.38	371.62	12.02	254.84
T4M120C	5.43	267.49	6.56	299.22	17.52	265.44

Δ_y: yield deflection

Δ_{max}: deflection at maximum strength

Δ_u: ultimate deflection

F_y: Lateral yield strength

F_{max}: Maximum lateral strength

F_u: Ultimate lateral strength

Table 6-4 Moment-curvature of Specimens

Specimen	φ_y (mm^{-1})	M_y (kNm)	φ_{max} (mm^{-1})	M_{max} (kNm)	φ_u (mm^{-1})	M_u (kNm)
T6L35A	0.0171	292.37	0.0690	488.98	0.1004	391.18
T6L35C	0.0186	243.79	0.0868	350.60	0.1172	280.48
T6M35A	0.0171	213.83	0.0415	413.45	0.0688	330.76
T6M35C	0.0187	223.93	0.0907	373.95	0.1126	299.16
T6L61B	0.0187	231.66	0.0607	374.88	0.0968	299.90
T6L61C	0.0200	230.37	0.0917	363.85	0.1061	291.08
T6M61A	0.0169	243.96	0.0524	367.56	0.0562	294.05
T6M61B	0.0199	215.78	0.0377	334.24	0.0335	267.39
T4L120A	0.0166	207.88				
T4L120C	0.0185	182.23				
T4M120A	0.0166	174.44				
T4M120C	0.0185	187.25				

φ_y: yield curvature

φ_{max}: curvature at maximum moment

φ_u: ultimate curvature

M_y: Lateral yield moment

M_{max}: Maximum moment

M_u: Ultimate moment

7. Lateral Force Deflection Relationship

7.1 Introduction

This chapter presents lateral force-deflection relationship of reinforced concrete column subjected to cyclic loading. Based on the test results shown in Chapter 6, specimens with high volumetric transverse reinforcement ratio failed in flexural-shear behavior whereas specimens with low volumetric reinforcement ratio failed in shear manner. As demonstrated by many researchers (e.g. Azizianamini et al 1992, Saatciglu and Razvi 2002 etc), for reinforced concrete columns failed in flexural manner, lateral force-deflection relationship were influenced by plastic hinge length and curvature ductility. For specimens failed in flexural-shear manner, lateral force-deflection relationship can be calculated based on curvature. The curvature is estimated based on stress-strain relationship of confined concrete. In this study, curvature was estimated from proposed stress-strain relationship of confined concrete, (see Chapter 4). For specimens failed in shear manner, lateral force-deflection relationship was not accurately predicted by moment-curvature relationship. A new lateral force-deflection relationship was developed by conducting non-linear regression analysis on specimens failed by shear deformation.

7.2 Specimens Failed in Flexural Shear Manner

Mechanism leading to failure in flexural shear manner consists of flexural deflection, bond slip and shear deflection, see Figure 7-1. Flexural deflection depends on moment curvature relationship. Bond slip affects the deflection by bond slip of main reinforcement. Shear deflection is lateral deflection contributed by shear behavior.

7.2.1 Moment-curvature Relationship

Flexural deflection is controlled by moment curvature profile along height of specimens. Based on the experimental results, there are two groups of specimens. The first group failed in flexural shear while the second group failed in shear. Flexural stiffness, flexural strength and yield deflection of specimens with high volumetric transverse reinforcement ratio were larger than the one with low volumetric transverse reinforcement ratio, see Table 7-1.

Moment curvature relationship is calculated by the following procedure. Firstly, strain profile across the section of specimen was determined by considering axial compressive load. Strain was linearly related to depth of section. Curvature of specimens was then obtained. Compressive stress of confined concrete and unconfined concrete and tensile stress of main reinforcement were computed. Corresponding moment was calculated. Meanwhile, moment at the base of specimen was calculated as lateral load times height of specimen. Curvature of specimens was computed from the vertical displacements recorded from electrical dial gauges. Detail calculation was complied by a computer program as shown in Appendix A.

Initial stiffness predicted analytically by moment curvature relationship agrees well with the experimental results for specimens with high volumetric transverse reinforcement ratio and subjected to high axial load ratio. This is attributed to flexural failure of those specimens. In addition, specimens subjected to high axial load ratio have better agreement than those with low axial load as the lateral load deflection relationship of the specimens depends on stress-strain relationship of confined concrete.

Stress-strain relationship of confined concrete is more accurately predicted than those in unconfined concrete. Therefore, the numerical results of specimens subjected to high axial load give a more accurate prediction than the one subjected to low axial load.

In short, the moment curvature curve provides an approximate solution for specimens subjected to flexural loading and assists in calculating the force deflection response, see Figures 7-2 and 7-3.

7.2.2 Flexural Deflection

Flexural deflection is calculated based on the curvature profile along height of specimens. During the initial stage, the curvature profile was assumed as linear along height of specimens. If the main reinforcement on the external side of specimens yield at the critical zone, then the curvature profile will be non-linearly varied along height of specimen. The plastic hinge length is then defined as moment ratio times height of specimen, see Figure 7-4 (Saatcioglu et al 2000). Moment ratio is defined as follows,

$$M_{ratio} = 1 - \frac{M_y}{M_{\max}} \tag{7-1}$$

$$L_p = M_{ratio} L \tag{7-2}$$

$$\Delta_{flex} = \frac{\varphi_y L^2}{3} + (\varphi_u - \varphi_y) L_p (L - \frac{L_p}{2}) \tag{7-3}$$

where M_{ratio} is the moment ratio, M_y is the moment corresponding to yielding of main reinforcement, M_{max} is the maximum moment throughout the loading history, Δ_{flex} is the flexural deflection, φ_y is the yield curvature, φ_u is the ultimate curvature, L_p is the plastic hinge length and L is height of reinforced concrete specimen.

Besides, stress-strain relationship of confined concrete for specimens with non-seismic detailing was different from that with seismic detailing due to ineffective of confinement action provided by different configuration of transverse reinforcement. A new non-linear regression model is proposed in this study to depict the stress-strain relationship of confined concrete in non-seismic detailing, see Chapter 4. This stress-strain relationship represents the stress across the section. Flexural strength and deflection of specimens with non-seismic detailing is then determined. The numerical predictions are close to the experimental results for reinforced concrete specimens with non-seismic detailing.

7.2.3 Bond Slip Deflection

Another issue related to lateral deflection is bond slip of main reinforcement during the tests. It was controlled according to Calderone's model (Calderone et al 2000), see Figure 7-5, and related to the slippage along the anchorage length. Based on the observation, there was slippage of main reinforcement when under tension. There was no bond slip on main reinforcement in the compressive side. As a result, this induced bond slip rotation on the base. Additionally, bond slip increased with cracking of cover concrete. Bond slip deflection is calculated as the bond slip rotation times height of specimen.

$$L_{ae} = \frac{f_s \phi_{main}}{4 f_{be}} \tag{7-4}$$

$$f_{be} = \sqrt{f_c} \tag{7-5}$$

$$u_t = \int \varepsilon_s dx = \frac{\varepsilon_s L_{ae}}{2} \tag{7-6}$$

$$\theta_{slip} = \frac{u_t}{d - c} \tag{7-7}$$

$$\Delta_{slip} = \theta_{slip} L \tag{7-8}$$

where f_s is main reinforcement stress in the end section, ϕ_{main} is diameter of main reinforcement, f_{be} is bond strength, f_c is concrete strength, ε_s is main reinforcement strain, u_t is bond slip of main reinforcement, d is effective depth of concrete section, c is the neutral axis of concrete section, L is height of reinforced concrete column, θ_{slip} is slippage rotation at the base and Δ_{slip} bond slip deflection due to bond slip of main reinforcement.

7.2.4 Shear Deflection

Shear deformation of concrete is attributed by shear strain of concrete and yield strain of transverse reinforcement (Paulay and Preistley 1992). It is estimated by the following expression,

$$\Delta_{shear} = \frac{VL}{A_g}\left(\frac{1}{\rho_s E_s} + \frac{4}{E_{con}}\right) \tag{7-9}$$

where Δ_{shear} is shear deflection, V is shear force, L is the height of reinforced concrete specimens, A_g is the gross sectional area of concrete, ρ_s is the volumetric transverse reinforcement of concrete, E_s is the Modulus of Elasticity of transverse reinforcement and E_{con} is the Young's Modulus of confined concrete.

7.2.5 Lateral Force Deflection Curve

Lateral deflection was calculated by summating the flexural deflection, bond slip deflection and shear deflection while lateral load was the action force. Lateral load deflection relationship calculated based on the above deflections are compared with the experimental results, see Figures 7-6 and 7-7. Specimens with high volumetric transverse reinforcement (ρ_s>0.66%) failed in flexural shear manner. Initial stiffness of lateral force-deflection curve calculated by numerical method is similar to the one obtained from the experiments. Maximum lateral forces calculated by numerical method are greater than the experimental results. Deflections at maximum lateral force calculated by numerical method are smaller than the one in experimental results. However, ultimate deflections calculated by numerical method are larger than those in experimental results. Based on the results, the numerical method may provide good estimate on lateral force deflection curve. Since lateral force deflection curve was based on stress-strain relationship of confined concrete, it also shows that the proposed stress-strain relationship of confined concrete is reliable.

For specimens with low volumetric transverse reinforcement ratio (ρ_s<0.15%), the initial stiffness, maximum lateral force and ultimate displacement calculated from numerical method are larger than the experimental results. Since specimens with low volumetric transverse reinforcement ratio failed in shear, lateral forces of these specimens are overestimated. Lateral displacements at maximum lateral load calculated from numerical method are close to the experimental results.

7.2.6 Plastic Hinge Length

Table 7-1 shows the parameters used in describing the plastic hinge length of specimens. Plastic hinge length increases with increasing axial load ratio but reduces with increasing volumetric transverse reinforcement ratio. For example, plastic hinge length of specimen T6L35B (229mm) is smaller than specimen T6L61B (240mm) and also smaller than specimen T6L35A (416mm). As plastic hinge length is related to plastic rotation, plastic rotation increases with reduction of volumetric transverse reinforcement ratio and poor confinement action of transverse reinforcement. When volumetric transverse reinforcement ratio increases, curvature ductility of specimens also increases. By the same reason, more cracks were observed on specimens with low volumetric transverse reinforcement ratio. As a result, bond slip rotation and shear deflection also increase.

Plastic hinge length is important in the design of transverse reinforcement detailing because spacing of transverse reinforcement outside this zone can be less stringent. Plastic rotation includes rotation induced by plastic flexural curvature, bond slip and shear deflection. A new empirical formula is formed in this study. Plastic hinge length in specimens with high volumetric transverse reinforcement was calculated by regression analysis. Experimental plastic hinge length is estimated from non-linear yield curvature, ultimate curvature, ultimate deflection and height of column. The quadratic equation Eq. (7-10) with unknown L_p is then solved by Eq. (7-11).

The expressions are as follows,

$$(\varphi_u - \varphi_y)\frac{{L_p}^2}{2} - (\varphi_u - \varphi_y)LL_p + \Delta_u - \frac{\varphi_y L^2}{3} = 0 \qquad (7\text{-}10)$$

$$L_p = \frac{(\varphi_u - \varphi_y)L \pm \sqrt{\left[(\varphi_u - \varphi_y)L\right]^2 - 4\frac{(\varphi_u - \varphi_y)}{2}L(\Delta_u - \frac{\varphi_y L^2}{3})}}{2\frac{(\varphi_u - \varphi_y)}{2}} \qquad (7\text{-}11)$$

where φ_u is ultimate curvature, φ_y is yield curvature, Δ_u is ultimate deflection, L is height of specimen and L_p is plastic hinge length.

The calculated L_p is correlated with axial load capacity ratio and volumetric transverse reinforcement ratio, see Eq. (7-12) and Eq. (7-13). The plastic hinge length estimated by the above equation is shown in Table 7.1. Comparison of experimental results and numerical data is shown in Figure 7-8. The correlation factor is about 99%.

The expressions are as follows,

For type L detailing,

$$\frac{L_p}{d_s} = 1.37n^{2.73}\left(\frac{\rho_S f_y}{f_c}\right)^{-0.45} + 0.6 \tag{7-12}$$

For type M detailing,

$$\frac{L_p}{d_s} = 0.30n^{0.44}\left(\frac{\rho_S f_y}{f_c}\right)^{-0.45} + 0.6 \tag{7-13}$$

where L_p is plastic hinge length, d_s is depth of specimen, n is axial load capacity ratio, ρ_s is volumetric transverse reinforcement ratio, f_y is yield strength of reinforcement and f_c is unconfined concrete strength.

As shown in the above equations, plastic hinge length of specimens with type M detailing is significantly affected by axial load capacity ratio as compared with type L detailing. As specimens with type M detailing provide poorer confinement action than those with type L detailing, confined concrete strength and ductility of confined concrete reduce. When specimens with type M detailing are subjected to high axial load, more cracks are generated as compared with those having type L detailing. Shear deflection and bond slip rotation in specimens with type M detailing would then be larger than those with type L detailing. Therefore, plastic hinge length for specimens with type M detailing is larger than those with type L detailing.

7.3 Specimens Failed in Shear

Specimens with high volumetric transverse reinforcement behave differently from those with low volumetric transverse reinforcement ratio. In order to ascertain the behavior of specimens with low volumetric transverse reinforcement, a new formula is formed by conducting non-linear regression analysis. Several parameters are formed by non-linear regression analysis. They are: 1) initial stiffness, 2) yield deflection, 3) strain-hardening stiffness, 4) displacement at maximum load and 5) ultimate deflection. All the formulas are correlated to volumetric transverse reinforcement ratio and axial load capacity ratio.

7.3.1 Flexural Stiffness

Initial stiffness is based on the flexural stiffness. The initial stiffness was smaller than flexural stiffness because the initial tangential stiffness of confined concrete is smaller than the secant stiffness of concrete at maximum stress, which is σ_c/ε_c where σ_c is confined concrete stress and ε_c is confined concrete strain, see Figure 6-4. Besides, flexural strength of confined concrete is related to confinement action of transverse reinforcement.

The initial stiffness of specimens with high volumetric transverse reinforcement ratio is stiffer than the one with low volumetric transverse reinforcement ratio, for example, stiffness of specimen T6L61C (82kN/m) is larger than that of specimen T6L35C (59kN/m). Flexural stiffness is also related to the axial load ratio. For specimens subjected to high axial load, of which the initial stiffness of specimen T6M61A (79kN/m) is larger than that of specimen T6M61B (76kN/m), the initial stiffness is stiffer than the one subjected to low axial load. When the axial load increases, confined concrete stress on the external side of specimen also increases. So, flexural stiffness (K_s) increases with increasing volumetric transverse reinforcement ratio (ρ_s) and axial load ratio (n). Equation for flexural stiffness is given in Eq. (7-14).

$$K_s = \frac{3E_{con}I}{L^3}\frac{1}{6.23(1-0.742n)(1+6.98C_{type}\frac{\rho_s f_y}{f_c})} \tag{7-14}$$

$$C_{type} = \begin{matrix} 1 & type & L \\ 0.8 & type & M \end{matrix} \tag{7-15}$$

where K_s is flexural stiffness, E_{con} is Modulus of Elasticity of confined concrete, I is second moment of area, L is height of specimens, ρ_s is volumetric transverse reinforcement ratio, f_y is yield strength of transverse reinforcement, f_c is unconfined concrete strength, C_{type} is coefficient of configuration of transverse reinforcement ratio and n is axial load ratio.

The correlation between experimental results and numerical data is about 93.1% for type L and M detailing respectively, see Figure 7-9.

7.3.2 Yield Deflection

Empirical formula for yield deflection (Δ_y) is given in Eq. (7-18). Yield curvature is defined as yield strain divided by neutral depth. Yield deflection includes flexural deflection, bond-slip rotation and shear deflection. Neutral depth is defined as depth of specimen under compression. Based on the regression analysis, neutral depth (c) was related to volumetric transverse reinforcement ratio (ρ_s) and axial load ratio (n). The neutral depth (c) increases with axial load ratio (n) because compressive stress of section was increased to balance the axial load. Hence, the yield deflection was reduced by increasing the axial load. For example, deflection of specimen T6L61C (5.02mm) is larger than that of specimen T6L61B (4.03mm).

Secondly, the neutral depth reduces with increasing volumetric transverse reinforcement ratio. When the volumetric transverse reinforcement ratio increases, the confined concrete stress increases. Hence the neutral depth is reduced. So the yield deflection increases with increasing volumetric transverse reinforcement ratio. For example, yield deflection of specimen T6L61C (5.02mm) is smaller than that of specimen T6L35C (5.88mm).

Another factor affecting the neutral depth is configuration of transverse reinforcement. Type L detailing provides better confinement action than type M detailing. Therefore, specimen with type L detailing has larger confined concrete strength. Hence, the compressive zone of specimen with type L detailing is smaller than the one with type M detailing and yield deflection of specimen with type M detailing is smaller than that with type L detailing.

Yield deflection

$$\Delta_{fy} = \frac{\varphi_y L^2}{3} \tag{7-16}$$

$$\varphi_y = \frac{\varepsilon_y}{c} \tag{7-17}$$

where Δ_{fy} is flexural yield deflection, ϕ_y is yield curvature, L is height of specimen, ε_y is yield strain and c is neutral depth.

$$\Delta_y = \frac{\varepsilon_y L^2}{3d_s\left(5.24 - 4.958n + 36.782C_{type}\dfrac{\rho_s f_y}{f_c}\right)} \qquad (7\text{-}18)$$

$$C_{type} = \begin{matrix} 1 & type \quad L \\ 0.8 & type \quad M \end{matrix} \qquad (7\text{-}19)$$

where Δ_y is the yield deflection, d_s is the depth of specimen, ε_y is yield strain of main reinforcement, L is height of specimen, ρ_s is volumetric transverse reinforcement ratio, f_y is the yield strength of transverse reinforcement, f_c is confined concrete strength and n is axial load capacity ratio. Yield strain of main reinforcement (ε_y) is 0.00255 in this study.

Yield deflection (Δ_y) of specimens is 94.8% for all types of configuration of transverse reinforcement, see Figure 7-10.

7.3.3 Strain Hardening Stiffness Ratio

Strain hardening stiffness ratio (χ) is defined as the ratio of strain hardening stiffness (K_{sh}) to the flexural stiffness (K_s) of confined concrete. Strain hardening stiffness ratio (χ) is related to axial load ratio (n) and volumetric transverse reinforcement ratio (ρ_s). Strain hardening ratio (χ) increases with increasing axial load ratio. As the axial load induces lateral crack, transverse reinforcement interacts with the confined concrete and increases the lateral resistance. Confined concrete strength is also increased. So, increasing the axial load would increase the strain hardening of specimens subjected to lateral load.

Another parameter considered in strain hardening stiffness ratio is volumetric transverse reinforcement ratio. The strain hardening stiffness ratio increases with increasing volumetric transverse reinforcement ratio. As the amount of transverse reinforcement is increased, the confined concrete strength increases. This would increase the compressive strength and lateral strength. So strain hardening increases with increasing transverse reinforcement ratio.

Effectiveness of transverse reinforcement configuration is related to strain hardening stiffness. Confined concrete strength and ductility of specimens are enhanced with effective configuration of transverse reinforcement. Based on the results, type L detailing is a better configuration providing higher confined concrete strength.

$$\chi = 0.270\left(1+1.185n\right)\left(1-1.319C_{type}\frac{\rho_s f_y}{f_c}\right) \tag{7-20}$$

$$C_{type} = \begin{matrix} 1 & type & L \\ 0.8 & type & M \end{matrix} \tag{7-21}$$

where χ is strain hardening stiffness ratio, n is axial load capacity ratio, C_{type} is coefficient of configuration of transverse reinforcement, ρ_s is volumetric transverse reinforcement ratio, f_y is yield strength of transverse reinforcement and f_c is confined concrete strength. The correlation of strain hardening stiffness ratio is 64.6%, see Figure 7-11.

7.3.4 Drift Ratio at Maximum Strength

Drift ratio at maximum strength (Δ_{max}) consists of flexural deflection, bond slip deflection and shear deflection. It is related to volumetric transverse reinforcement ratio (ρ_s) and axial load ratio (n). As mentioned in Section 7.3.3, transverse reinforcement ratio affects the confined concrete strength and strain at compressive strength. So the drift ratio at maximum strength is also related to the volumetric transverse reinforcement ratio.

Deflection at peak load increases with reducing axial load ratio because part of strain energy stored in transverse reinforcement was dissipated to resist high axial load. Meanwhile, when axial load is increased, lateral cracks formed on concrete cover increase. The strain energy in enhancing ductility or deflection at peak load is then reduced.

Specimens with type L detailing are effective in providing confined concrete strength. Confined concrete strength and strain in specimens with type L detailing are larger than the ones with type M detailing. The deflection at maximum strength increases with the effectiveness of transverse reinforcement.

$$\Delta_{\max} = 6.866 n^{-0.460} \left(\frac{\rho_s f_y}{f_c} \right)^{0.586} C_{type} \frac{L}{100} \qquad (7\text{-}22)$$

$$C_{type} = \begin{matrix} 1 & type & L \\ 0.8 & type & M \end{matrix} \qquad (7\text{-}23)$$

where Δ_{max} is the deflection at maximum strength, n is axial load ratio, ρ_s is volumetric transverse reinforcement ratio, f_y is yield strength of transverse reinforcement, f_c is confined concrete strength, C_{type} is coefficient of configuration of transverse reinforcement and L is height of specimen. The correlation is 98.6%, see Figure 7-12.

7.3.5 Ultimate Deflection

An empirical formula is formed to describe ultimate deflection (Δ_{ult}). Ultimate deflection is correlated to volumetric transverse reinforcement ratio (ρ_s) and axial load ratio (n). It is related to confined concrete strain and also ductility of confined concrete. Ductility of confined concrete increases with volumetric transverse reinforcement ratio because strain energy of transverse reinforcement increases the confinement action and provide resistance from lateral expansion.

Type L detailing

$$\Delta_{ult} = 9.448 n^{-0.213} \left(\frac{\rho_s f_y}{f_c} \right)^{0.497} \frac{L}{100} \tag{7-24}$$

Type M detailing

$$\Delta_{ult} = 9.448 * 0.856 n^{-0.213} \left(\frac{\rho_s f_y}{f_c} \right)^{0.497} \frac{L}{100} \tag{7-25}$$

where Δ_{ult} is the ultimate deflection, n is axial load capacity ratio, ρ_s is volumetric transverse reinforcement ratio, f_y is yield strength of transverse reinforcement, f_c is confined concrete strength and L is height of specimen. Correlation of ultimate deflection with specimens having type L detailing is 98.9% while those with type M detailing is 99.6%, see Figure 7-13.

7.4 Load Deflection Curve

As shown Figures 7-14 and 7-15, numerical predictions based on the proposed model with several parameters provide reasonable agreement with the experimental results. The empirical formula would provide reasonable prediction on lateral strength and deflection of specimens with low volumetric transverse reinforcement ratio and high axial load capacity ratio. Yield stiffness (K_s), yield deflection (Δ_y) and strain hardening parameter (χ) of specimen increase with increasing axial load ratio but reduce with increasing volumetric transverse reinforcement ratio (ρ_s). Deflections at peak lateral load (Δ_{max}) and ultimate deflection (Δ_{ult}) increase with increasing volumetric transverse reinforcement ratio (ρ_s) but reduce with increasing axial load ratio (n).

7.5 Summary

In short, there are two approaches in predicting lateral load deflection behavior under monotonic loading. The first one predicts the behavior based on moment curvature analysis. The method consists of flexural, bond slip and shear deflection of specimens and is only valid when reinforced concrete column fails under flexural or flexural shear. The second one is based on empirical formula. It is applicable to reinforced concrete columns failed that one in shear. Based on the results, the numerical model gives good prediction on lateral load deflection relationship for specimens fail by shear.

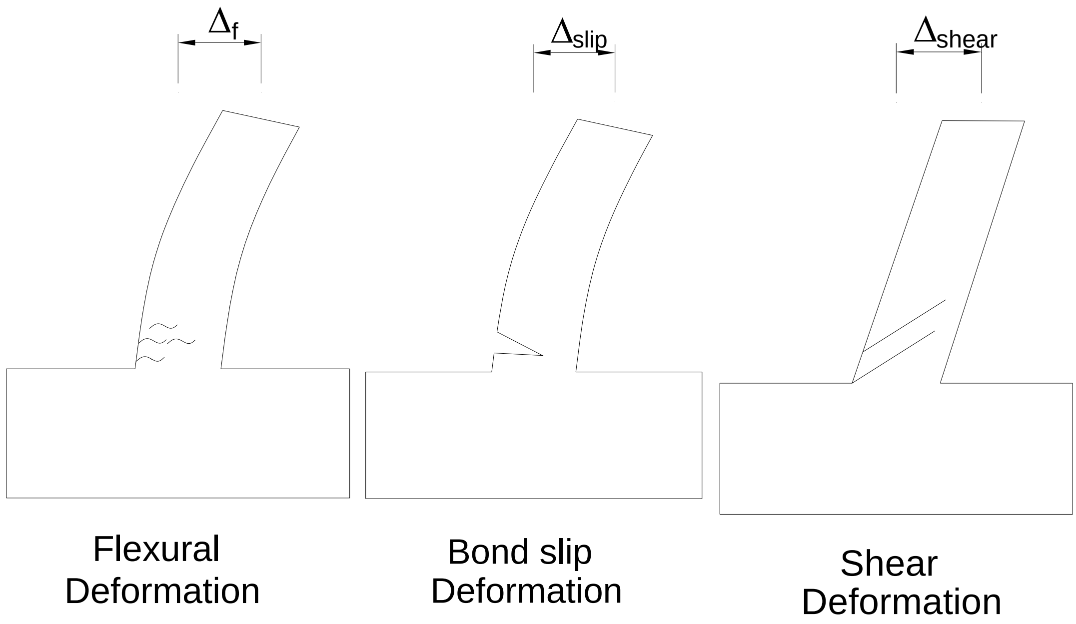

Figure 7-1 Mode of Deformation

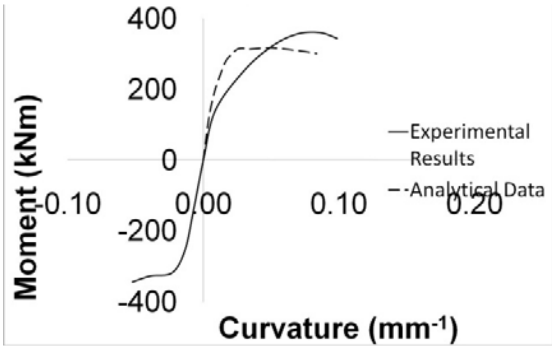

a) Specimen T6L35A

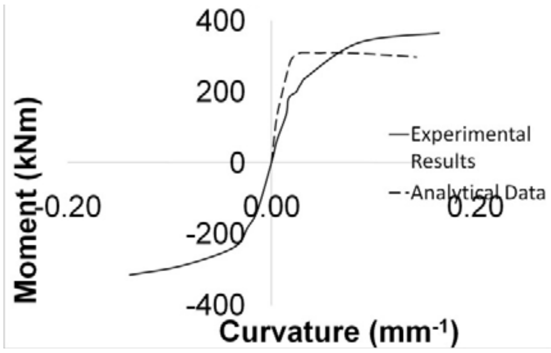

b) Specimen T6L35C

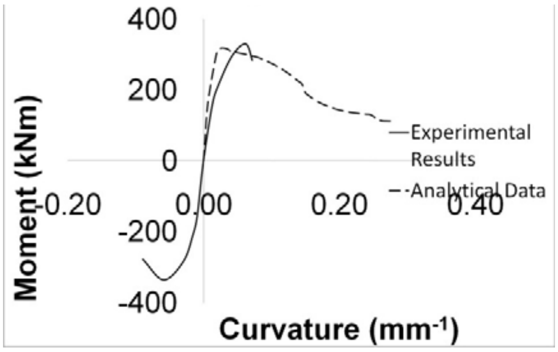

c) Specimen T6L61B

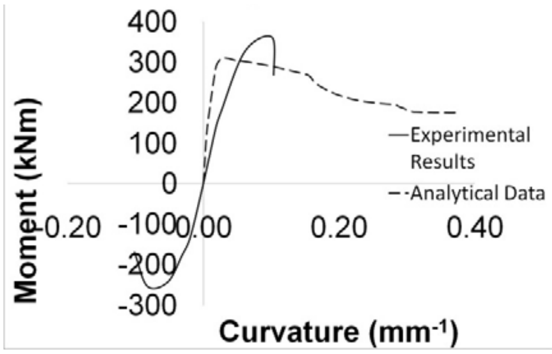

d) Specimen T6L61C

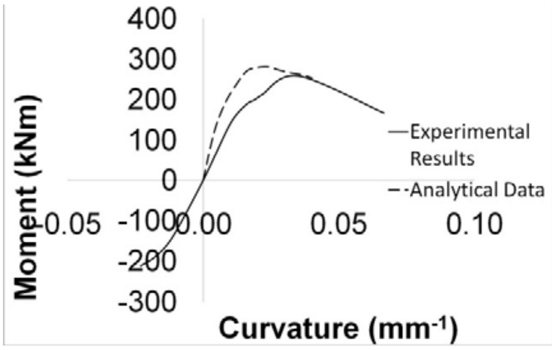

e) Specimen T4L120A

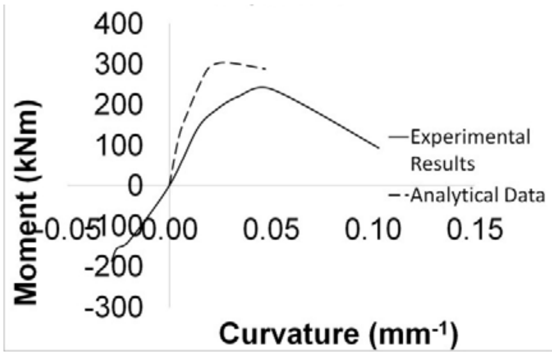

f) Specimen T4L120C

Figure 7-2 Moment Curvature Relationship (Type L Detailing)

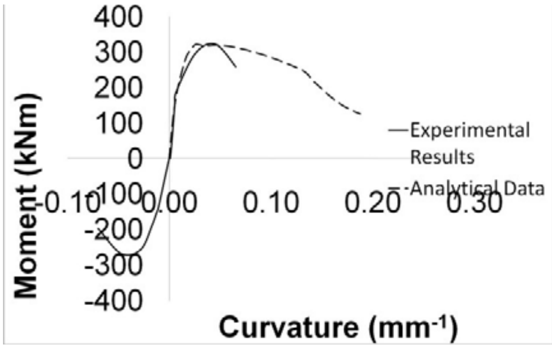

a) Specimen T6M35A

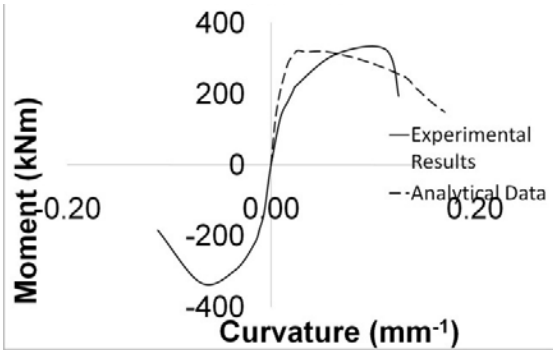

b) Specimen T6M35C

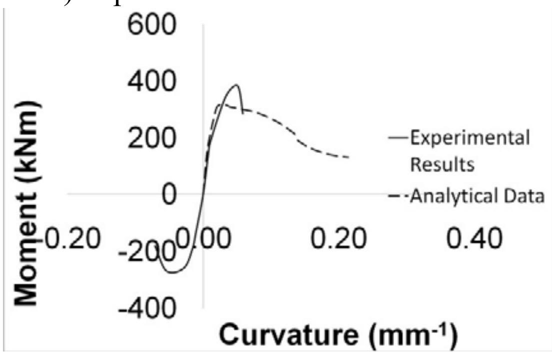

c) Specimen T6M61A

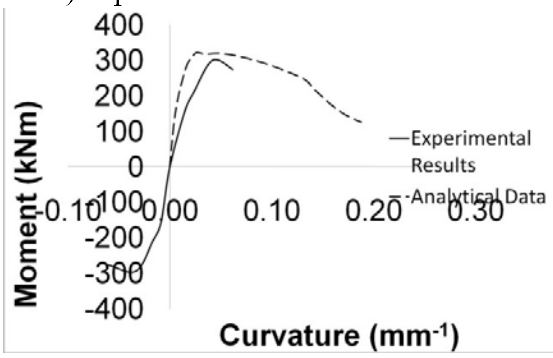

d) Specimen T6M61B

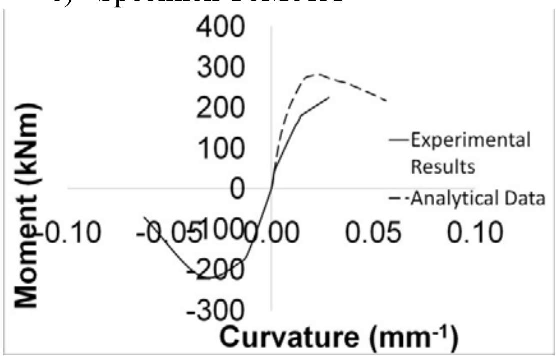

e) Specimen T4M120A

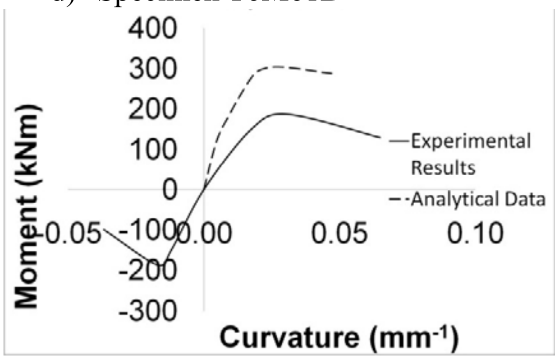

f) Specimen T4M120C

Figure 7-3 Moment Curvature Relationship (Type M Detailing)

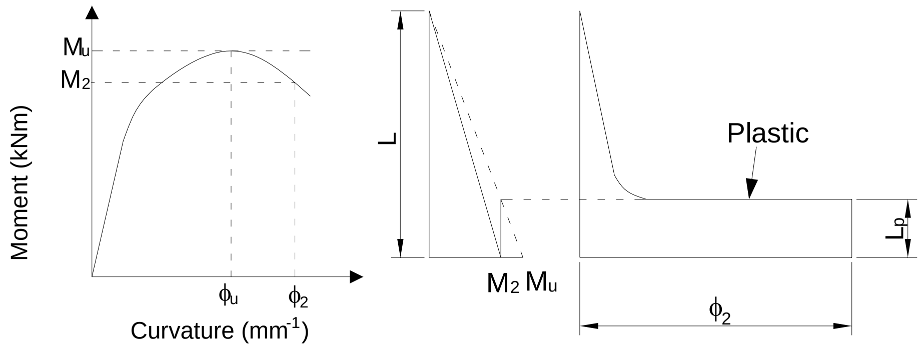

Figure 7-4 Formation of Plastic Hinge

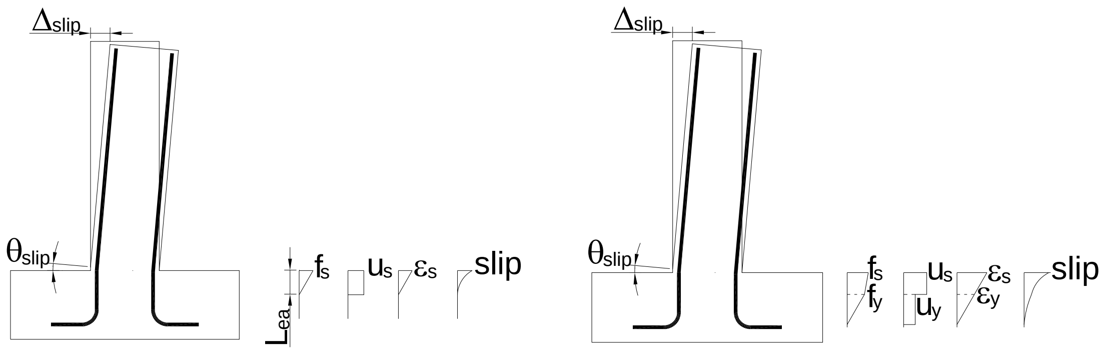

a) Elastic Stage

b) Plastic Stage

Figure 7-5 Bond Slip Deflection

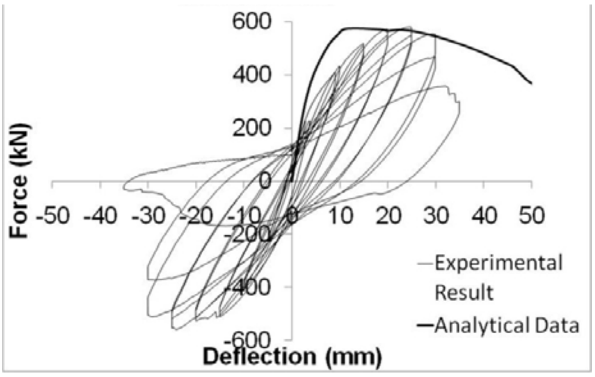

a) Specimen T6L35A

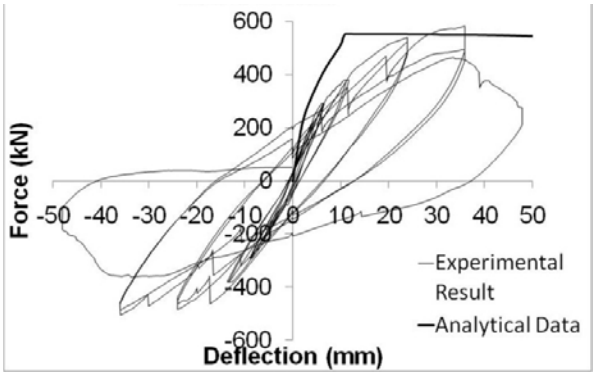

b) Specimen T6L35C

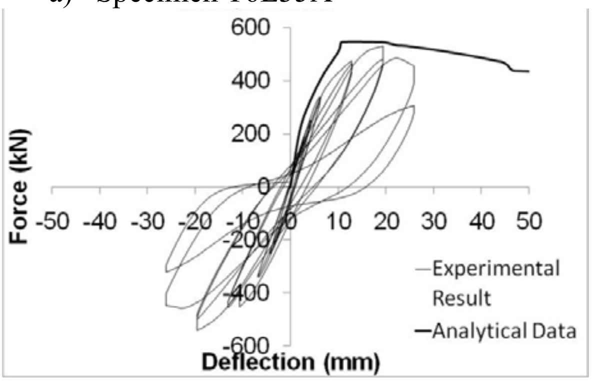

c) Specimen T6L61B

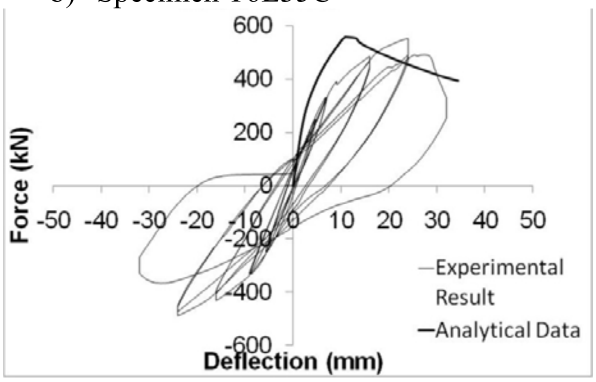

d) Specimen T6L61C

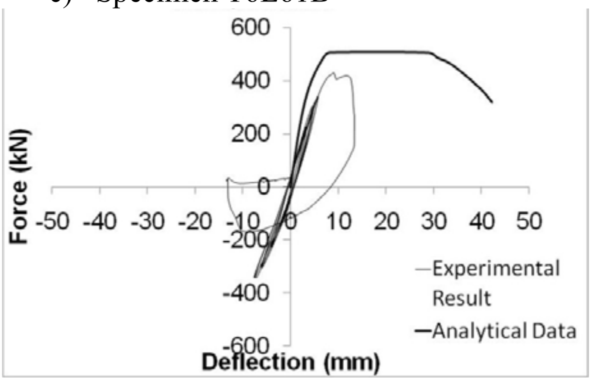

e) Specimen T4L120A

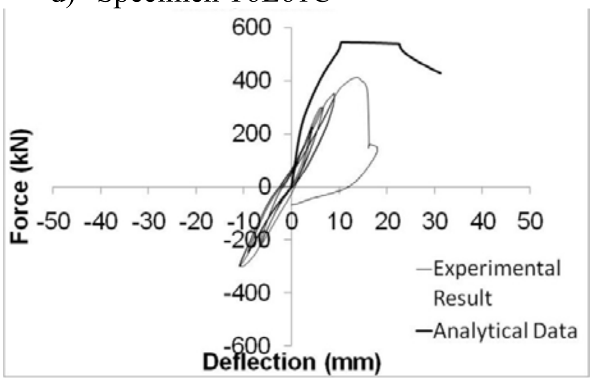

f) Specimen T4L120C

Figure 7-6 Force Deflection Curve (Type L Detailing)

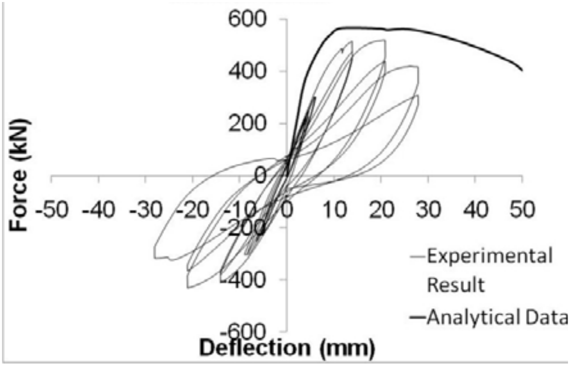

a) Specimen T6M35A

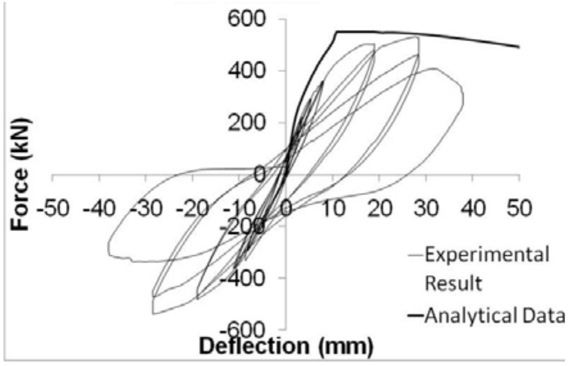

b) Specimen T6M35C

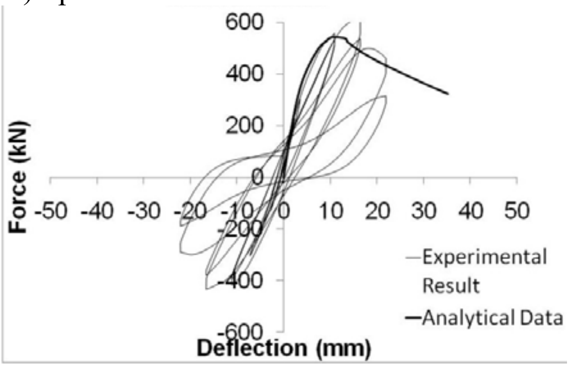

c) Specimen T6M61A

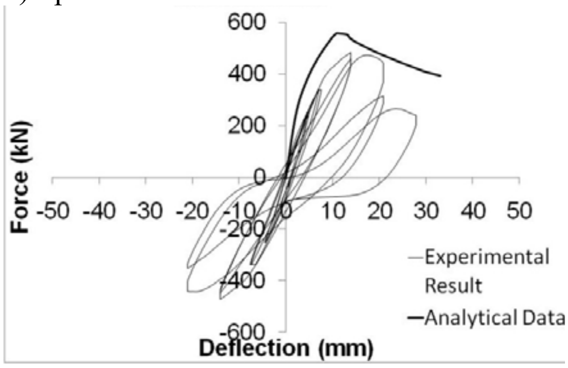

d) Specimen T6M61B

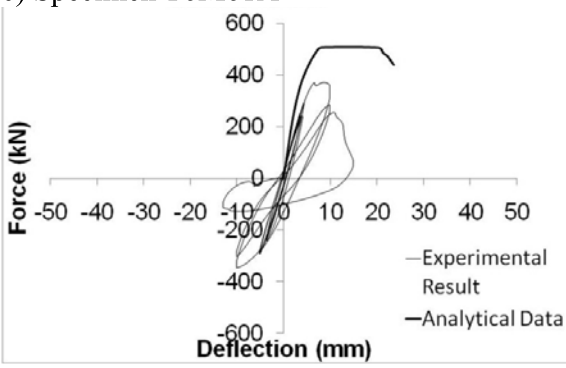

e) Specimen T4M120A

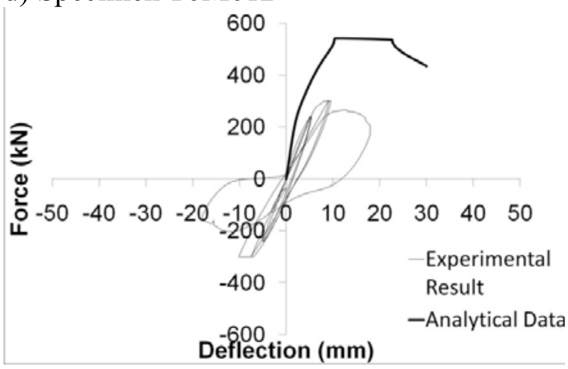

f) Specimen T4M120C

Figure 7-7 Force Deflection Curve (Type M Detailing)

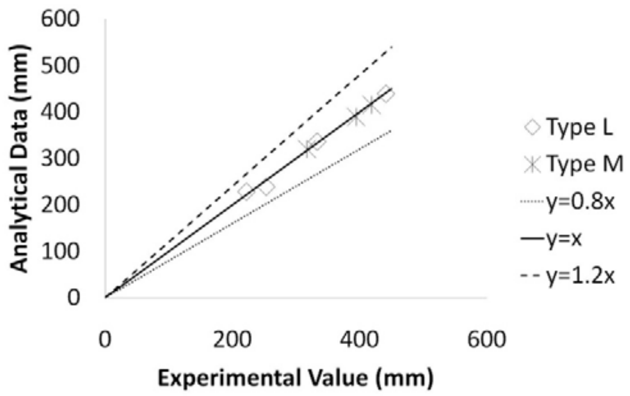

Figure 7-8 Comparison of Experimental Results and Numerical Data (Plastic Hinge Length) (L_p)

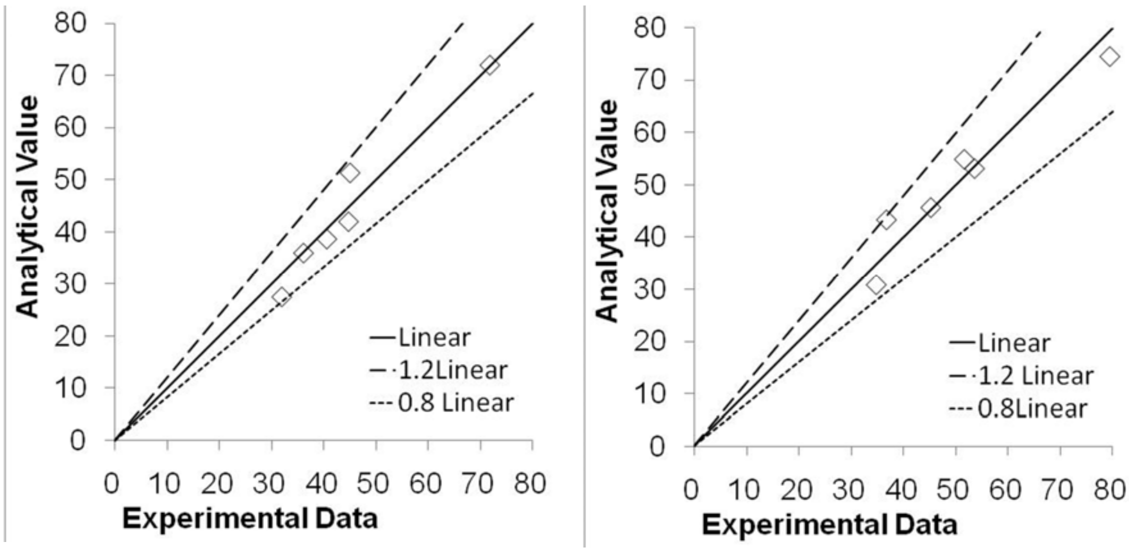

a) Type L Detailng

b) Type M Detailing

Figure 7-9 Comparison of Stiffness between Numerical Value and Experimental Data (K_s)

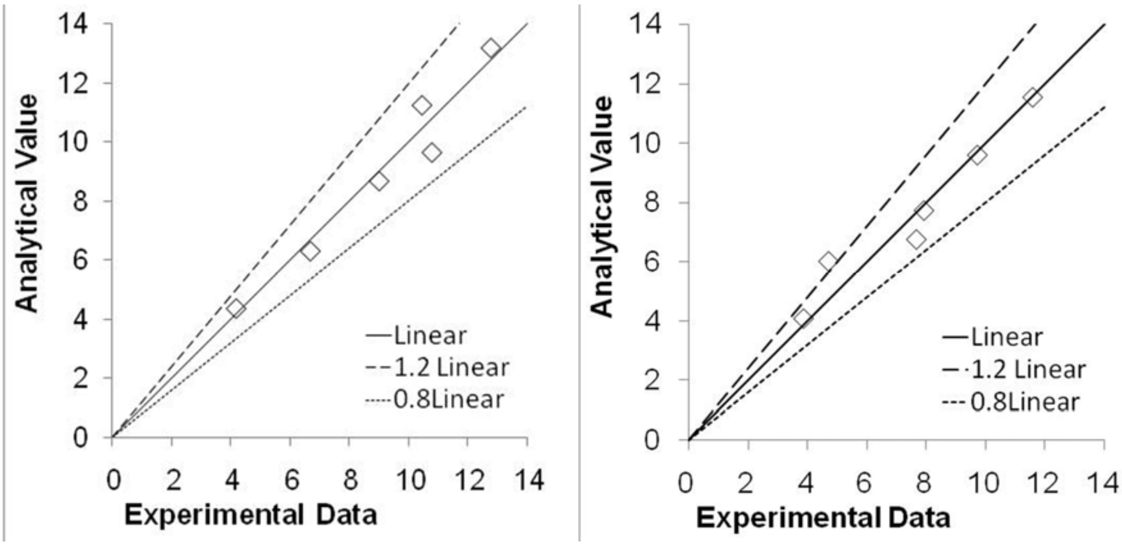

a) Type L Detailing

b) Type M Detailing

Figure 7-10 Comparison of Yield Deflection between Numerical Value and Experimental Data (Δ_y)

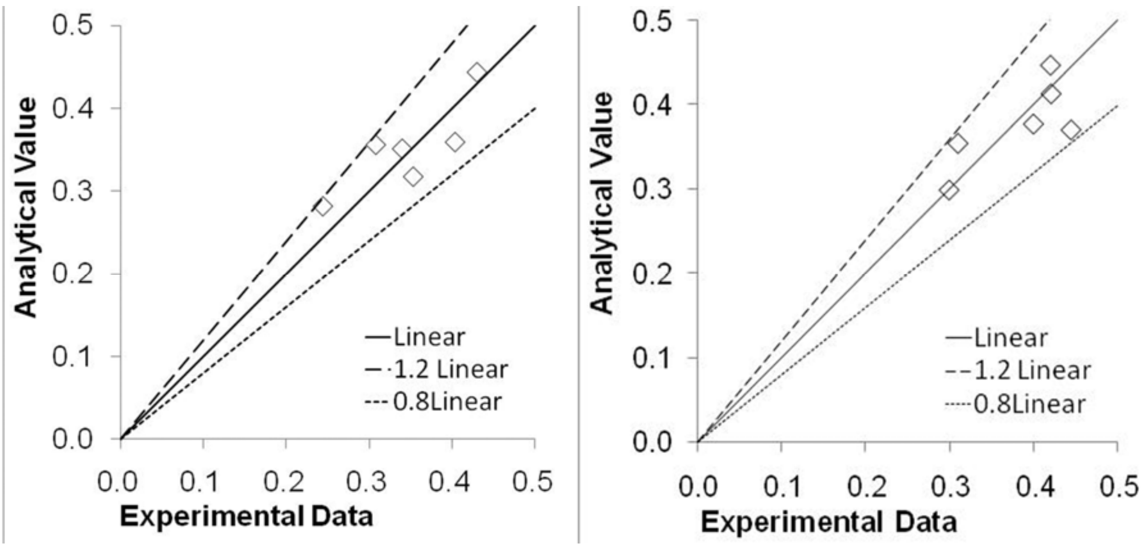

a) Type L Detailing

b) Type M Detailing

Figure 7-11 Comparison of Strain Hardening between Numerical Value and Experimental Data (χ)

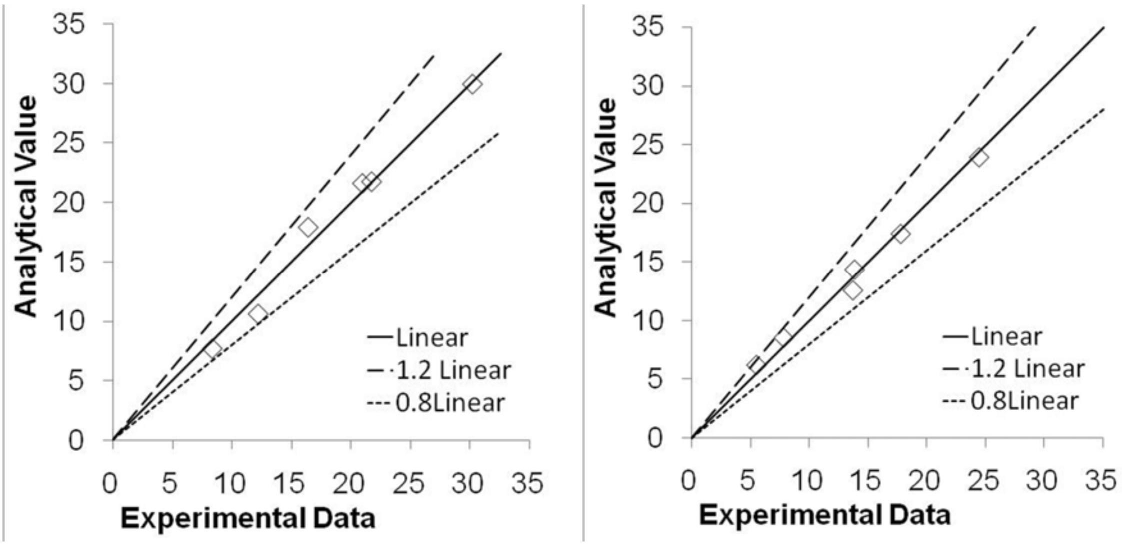

a) Type L Detailing

b) Type M Detailing

Figure 7-12 Comparison of Displacement at Maximum Strength between Numerical Value and Experimental Data (Δ_{max})

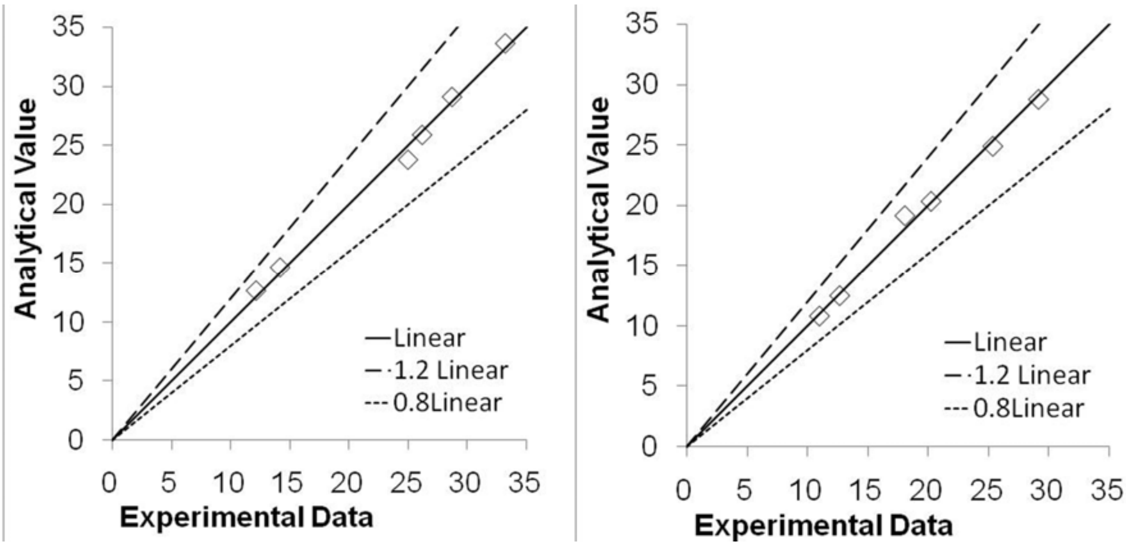

a) Type L Detailing

b) Type M Detailing

Figure 7-13 Comparison of Ultimate Displacement between Numerical Value and Experimental Data (Δ_{ult})

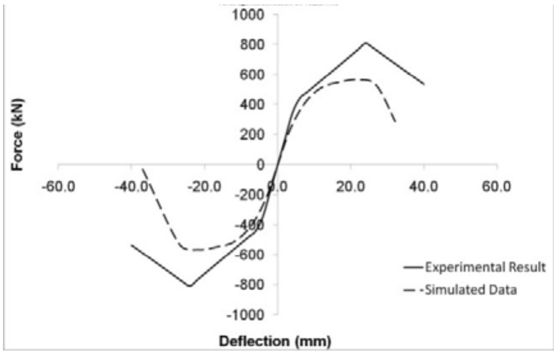

a) Specimen T6L35A

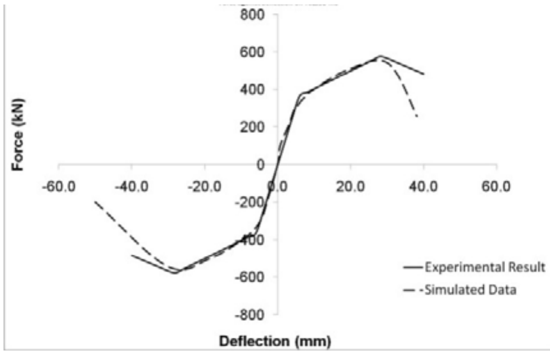

b) Specimen T6L35C

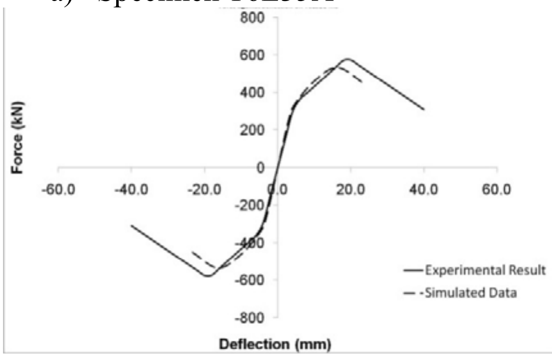

c) Specimen T6L61B

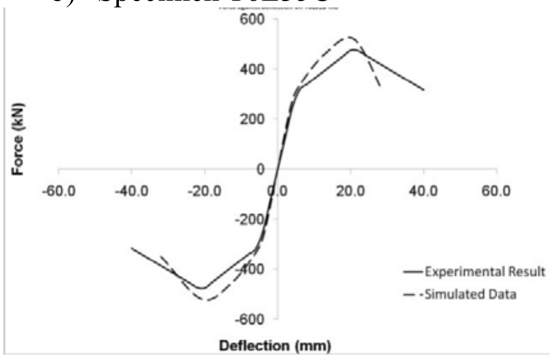

d) Specimen T6L61C

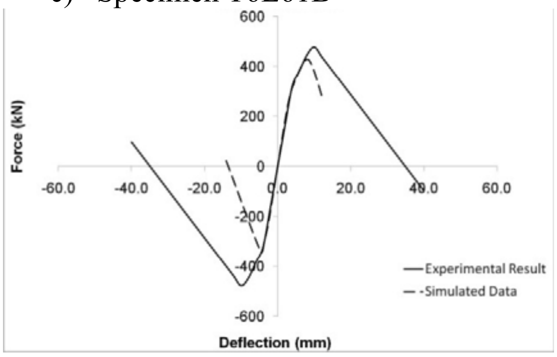

e) Specimen T4L120A

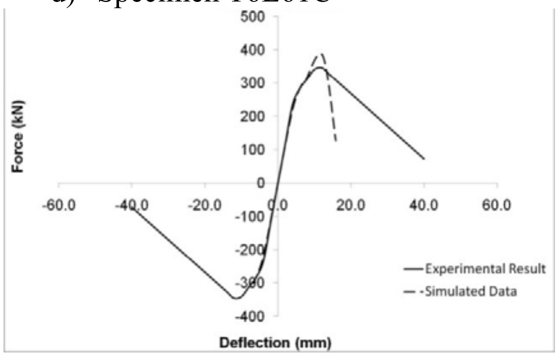

f) Specimen T4L120B

Figure 7-14 Comparison of Experimental Results and Simulated Data (Monotonic Loading) (Type L Detailing)

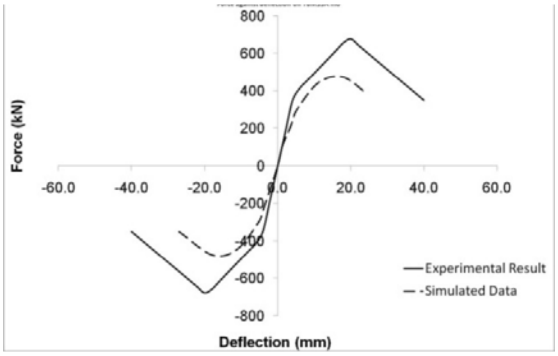

a) Specimen T6M35A

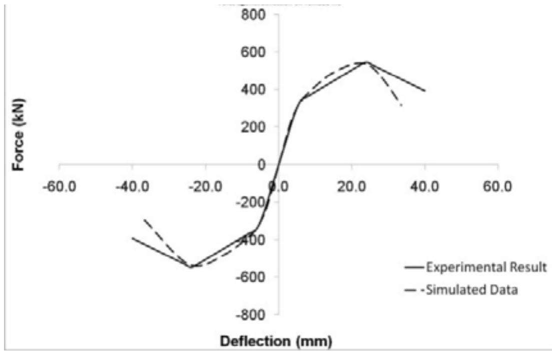

b) Specimen T6M35C

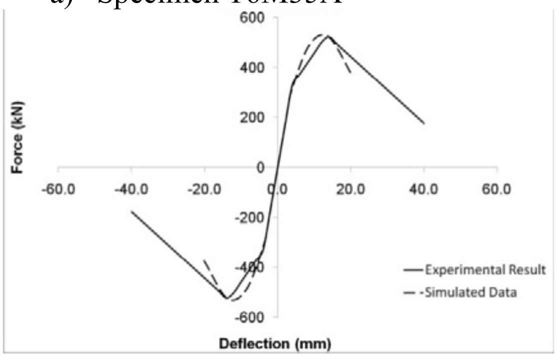

c) Specimen T6M61A

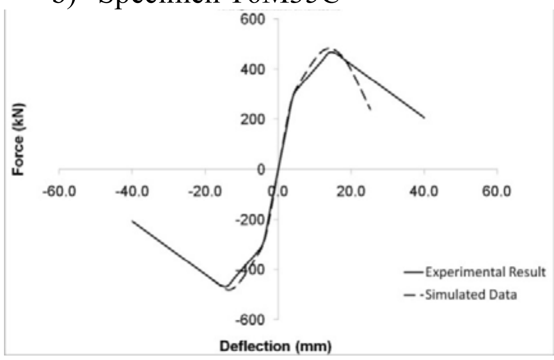

d) Specimen T6M61B

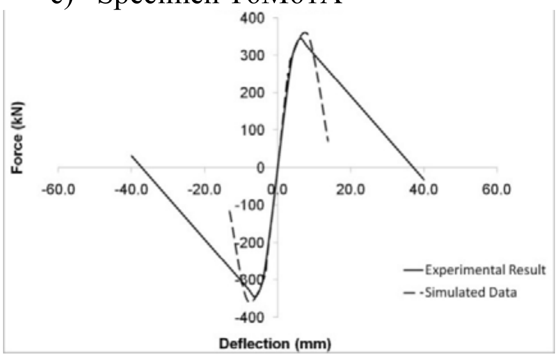

e) Specimen T4M120A

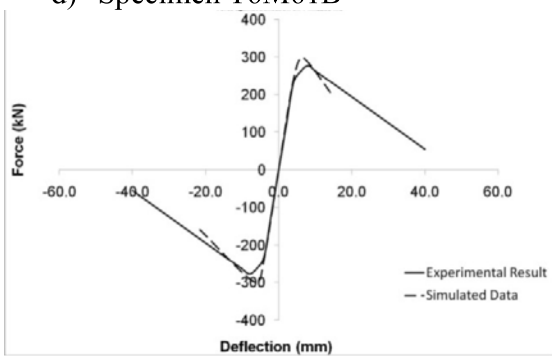

f) Specimen T4M120C

Figure 7-15 Comparison of Experimental Results and Simulated Data (Monotonic Loading) (Type M Detailing)

Table 7-1 Plastic Hinge Length

Label	$\phi_{transverse}$ (mm)	s (mm)	Type	n	$L_{p,exp}$ (mm)	$L_{p,anal}$ (mm)	φ_y (mm^{-1})	M_y (kNm)	φ_{max} (mm^{-1})	M_{max} (kNm)	φ_u (mm^{-1})	M_u (kNm)
T6L35A	6	35	L	0.6	441	439	0.0305	255.3	0.0857	361.3	0.0987	344.3
T6L35B	6	35	L	0.3	222	229	0.0327	238.2	0.1646	365.4		
T6M35A	6	35	M	0.6			0.0067	187.3	0.0452	323.2	0.0654	259.2
T6M35B	6	35	M	0.3	318	320	0.0243	222.3	0.1126	325.4	0.1255	193.8
T6L61C	6	61	L	0.45	333	336	0.0210	209.4	0.0621	330.1	0.0719	283.4
T6L61B	6	61	L	0.3	253	240	0.0526	243.3	0.1009	361.3	0.1034	268.3
T6M61A	6	61	M	0.6	419	416	0.0108	187.9	0.0508	384.0	0.0586	285.1
T6M61C	6	61	M	0.45	395	389	0.0233	209.8	0.0418	300.7	0.0617	275.0
T4L120A	4	120	L	0.6	197		0.0216	211.9	0.0350	259.0	0.0667	167.1
T4L120B	4	120	L	0.3	156		0.0339	220.6	0.0500	239.0	0.1027	93.9
T4M120A	4	120	M	0.6	203		0.0145	180.7	0.0281	224.8	0.0625	70.9
T4M120B	4	120	M	0.3	153		0.0305	187.5	0.0305	187.5	0.0650	129.3

Table 7-2 Parameters for Lateral Strength and Deflection Curve

Label	K_s (kN/mm)		Δ_y (mm)		α		θ_{max}		θ_u	
	Exp	Ana	Exp	Ana	Exp	Ana	Exp	Ana	Exp	Ana
T6L35A	61.10	85.19	6.84	4.89	0.31	0.24	21.74	24.16	34.37	33.43
T6L35B	59.23	62.47	5.88	5.81	0.20	0.15	18.61	28.36	43.83	42.20
T6M35A	65.46	86.29	4.67	4.42	0.33	0.24	17.79	19.46	25.67	27.81
T6M35B	61.05	62.69	5.24	5.29	0.18	0.19	24.53	23.77	34.98	35.10
T6L61C	59.62	61.31	5.52	4.98	0.17	0.19	23.99	20.79	31.98	31.83
T6L61B	82.12	73.31	4.03	4.59	0.20	0.24	16.38	18.93	23.28	27.78
T6M61A	79.75	83.87	4.37	3.91	0.24	0.25	13.78	13.41	19.36	21.37
T6M61C	76.68	72.07	4.02	4.22	0.26	0.23	12.52	14.57	25.12	23.54
T4L120A	76.54	81.76	3.88	3.90	0.40	0.38	8.18	9.39	12.03	14.49
T4L120B	60.26	58.66	4.32	4.46	0.21	0.24	11.22	11.02	19.74	18.30
T4M120A	78.86	80.37	3.16	3.58	0.30	0.29	8.38	6.07	13.52	12.28
T4M120B	61.92	57.66	4.32	4.10	0.23	0.23	6.56	7.41	14.21	15.51

8. Hysteresis behavior

8.1 Introduction

It is useful to formulate the hysteresis behavior of reinforced concrete column by an hysteresis model to ascertain its structural behavior when subjected to seismic loading. The model consists of the following parameters: (a) initial stiffness, (b) strain hardening model, (c) descending branch, (d) unloading stiffness and (e) reloading stiffness. The first three parameters are related to lateral force deformation behavior under monotonic loading and are presented in Chapter 7. The last two parameters are presented in this chapter.

In the past 40 years, many researchers, for example, Takeda et al (1970), Saiidi (1982), Chung et al (1987), Umemura et al (1998), Phan et al (2007), proposed different hysteresis models to predict the unloading and reloading stiffness of reinforced concrete columns. Parameters of unloading and reloading stiffness are related to the configuration of transverse reinforcement, volumetric transverse reinforcement ratio and axial load capacity ratio. As the transverse reinforcement details of reinforced concrete column with non-seismic detailing considered in this study is different from those with seismic detailing, a new hysteresis model is proposed by conducting non-linear regression analysis based on the experimental results of twelve specimens with different volumetric transverse reinforcement ratio, configuration of transverse reinforcement and axial load capacity ratio.

The hysteresis model consists of initial stiffness (K_s); strain hardening ratio (χ); descending branch (α); displacement at maximum force (Δ_{max}) and ultimate displacement (Δ_u) (at 80% of maximum force at the descending branch); unloading and reloading stiffness. The proposed hysteresis model is shown in Figure 8-1. The unloading and reloading stiffness are related to stress-strain relationship of confined concrete and depend on volumetric transverse reinforcement ratio and effectiveness of transverse reinforcement to provide confinement action. The unloading and reloading stiffness are presented as follows while the remaining parameters are given in Chapter 7.

8.2 Unloading Stiffness

When the specimens are under elastic response, unloading follows the elastic load deformation curve. The initial stiffness is the same as the unloading stiffness. When the specimens yield, the unloading stiffness becomes smaller than the initial stiffness. Hooks of transverse reinforcement hoops considered in Takeda et al (1970) and Saiidi (1982) are 135° end hook. In this study, 90° end hooks are used. Therefore, studies by others are not applicable to specimen with non-seismic detailing.

The unloading stiffness ratio (α) is defined as the ratio of unloading stiffness to yield stiffness, see Figure 8-1. It increases with volumetric transverse reinforcement ratio, see Figure 8.2(a) and (b), because confinement action induced from transverse reinforcement increases the confined concrete strength and ductility. The confinement action also reduces the formation and propagation of cracks. It can be quantified by the volumetric transverse reinforcement ratio, yield strength of transverse reinforcement and unconfined concrete strength of specimen. This is related to the amount of strain energy in resisting lateral expansion of concrete. The unloading stiffness factor is different from the one proposed by Saiidi (1982) because Saiidi's model was related to reinforced concrete column under flexural loading cycles as the shear span depth ratio of Saiidi's specimens and this study are about 3.1 and 2.1 respectively. The initial yield stiffness of specimens is assumed to be the same as the secant stiffness, being the ratio of yield force to yield displacement and is smaller than the initial tangent stiffness of the specimens.

In contrast, the unloading stiffness ratio (α) increases with reducing axial load capacity ratio, see Figures 8-2 (c) and (d). Specimens subjected to high axial load capacity ratio dissipated strain energy stored in transverse reinforcement to increase the strength of confined concrete. More lateral tensile cracks are induced in the core concrete when the axial load is increased. When the specimens are subjected to lateral load, specimens with high axial load will dissipate more strain energy than the one subjected to low axial load. The transverse reinforcement strain reflects the lateral strain movement in core concrete because the transverse reinforcement strain resists lateral expansion of core concrete. Since lateral expansion induced micro-crack in the core concrete, the unloading stiffness is reduced with increasing axial load capacity ratio.

Another factor is configuration of transverse reinforcement detailing. Type M detailing consists of reinforcement hoop, long crossties and short crossties. Short crossties dissipated less strain energy than long crossties. In Figure 8-2, unloading factor for specimens with type M detailing is smaller than the one with type L detailing. The effectiveness of type M detailing is reflected by a reduction factor (C_{type}) and is assumed to be 0.8 which is the ratio of length of two short crossties to the length of long crossties. It is because less strain energy is stored in type M detailing. When the specimen is subjected to lateral load, the transverse reinforcement deforms to resist the lateral expansion Specimens with type M detailing perform poorer than those with type L detailing. When specimens are subjected to the same lateral displacement, specimens with type L detailing resist higher lateral force than those with type M detailing.

Unloading stiffness of specimens reduces with increasing displacement at maximum excursion points, see Figure 8-2 (e) and (f). Lateral displacement and transverse reinforcement strains increase when the specimen is subjected to lateral load. After yielding of the transverse reinforcement, confined concrete strength deteriorates and surface cracks widen. Lateral displacement at maximum excursion point is a critical parameter because lateral displacement reflects condition of the specimens under different lateral load. Meanwhile, transverse reinforcement strains increase with lateral displacement.

Based on the above observations, mathematical model is developed by carrying out non-linear regression analysis on the experimental data. The equations are as follows,

$$K_{un} = \alpha \; * K_s \tag{8-1}$$

$$\alpha = 1.978 n^{-0.254} (C_{type} \frac{\rho_s f_{yt}}{f_c})^{0.123} \left(\frac{\Delta_y}{\Delta_m} \right)^{0.568} \tag{8-2}$$

$$C_{type} = \{ \begin{array}{ll} 0.8 & typeM \\ 1 & typeL \end{array} \tag{8-3}$$

where α is the unloading stiffness ratio, n is axial load capacity ratio, C_{type} is coefficient of transverse reinforcement configuration, ρ_s is volumetric transverse reinforcement ratio, f_{yt} is yield strength of transverse reinforcement, f_c is unconfined concrete strength, Δ_y is yield displacement, Δ_m is maximum displacement excursion point during the loading cycle, K_{un} is unloading stiffness and K_s is flexural yield stiffness.

Correlation factor of this empirical formula against the experimental results is about 61.6%. The error distribution is shown in Figure 8-3 which demonstrates that the model provides resonable prediction.

8.3 Reloading Displacement Factor

When the specimen is subjected to cyclic loading, the lateral strength of specimen is reduced after each cycle. Lateral expansion can be reflected by transverse reinforcement strain. As shown in Figures 8-4 to 8-6, the transverse reinforcement strain increases after each loading cycle. Meanwhile, the lateral load needed to reload the specimen to the same lateral displacement is smaller than that required in the previous loading cycle.

In the past, researchers such as Umemura et al (1998) proposed that reloading degradation of specimens is related to the delay on the response of the displacement in lateral load displacement curve, the so-called reloading target displacement. After reloading target displacement is larger than the maximum excursion point achieved in the previous loading cycle. The reloading stiffness would then be the ratio of lateral force at the target point to the sum of unloading displacement in the other direction and target displacement in this direction. Based on Umemura's results, the target displacement was related to volumetric transverse reinforcement ratio; axial load capacity ratio and displacement at maximum excursion point.

Based on Figures 8-7 (a) and (b), the axial load capacity ratio of specimens is not related to reloading displacement factor. Plastic deformation in the previous unloading cycle in the push direction affects the reloading displacement factor in the pull direction. The effect of axial load capacity ratio on reloading stiffness is reflected by the plastic deformation. Hence, the parameters used in defining reloading displacement factor do not include the axial load capacity ratio.

Based on the experimental results, the reloading displacement factor increases with reducing volumetric transverse reinforcement ratio, see Figures 8-7 (c) and (d). As specimens with higher volumetric transverse reinforcement contain higher strain energy to confine core concrete, confined concrete strength in these specimens is increased. Hence, micro-cracks on core concrete increase with reducing volumetric transverse reinforcement ratio. Therefore, the reloading displacement factor is reduced by increasing volumetric transverse reinforcement ratio.

Configuration of transverse reinforcement affects effectiveness of confinement action, see Figure 8-7. If the transverse reinforcement provides ineffective confinement action, the confined concrete strength reduces either progressively or suddenly with increasing lateral load or number of loading cycles. Consequently, the reloading stiffness is reduced. Hence, specimens with type M detailing have larger reloading displacement factor as compared with type L detailing.

Besides, the displacement at maximum excursion point is also an important factor to be considered because it reflects degradation of reloading stiffness of specimens at different loading stages, see Figures 8-7 (e) and (f). When lateral displacement increases, compressive stress of core concrete increases, meanwhile, the confined concrete strength is degraded in the descending branch of lateral load deformation curve. When more micro-cracks are induced after yielding of transverse reinforcement, the confined concrete strength will be further degraded. Degree of degradation of core concrete can be determined by lateral displacement at maximum excursion point. So, displacement at maximum excursion point is a critical parameter in defining the reloading displacement factor.

Last but not least, number of cycles is another parameter to be considered in the reloading displacement, as deterioration increases with number of cycles due to formation and propagation of cracks at each loading cycle, see Figures 8-7(g) and (h). During the post-peak loading cycle, the transverse reinforcement strains are related to lateral deflection because lateral deflection increases with increasing lateral load. As a result, the reloading stiffness reduces with number of cycles.

In this study, an empirical formula is proposed by conducting non-linear regression analysis on the experimental data. The empirical formula is in the form of,

$$\Delta_r = \beta_{re}\Delta_m \tag{8-4}$$

$$\beta_{re} = 0.58\left(C_{type}\frac{\rho_s f_y}{f_c}\right)^{-0.138}\left(\frac{\Delta_y}{\Delta_m}\right)^{-0.342} cycle^{0.371} \tag{8-5}$$

$$C_{type} = \begin{cases} 0.75 & typeM \\ 1 & typeL \end{cases} \tag{8-6}$$

where β_{re} is reloading displacement factor, C_{type} is type of detailing, ρ_s is volumetric transverse reinforcement ratio, f_y is yield strength of reinforcement, f_c is unconfined concrete strength, Δ_y is yield displacement, cycle is number of cycles, Δ_r is reloading target displacement and Δ_m is maximum excursion displacement.

Correlation factor of this empirical formula against the experimental results is about 63.4%. The error distribution is shown in Figure 8-8 which demonstrates reasonable prediction on the hysteretic behavior.

8.4 Hysteresis Model

The proposed hysteresis model provides a simple material non-linear model to represent the response of a reinforced concrete column under cyclic load, especially unloading and reloading stiffness, when subjected to cyclic loading. Comparisons of experimental results with prediction by hysteresis model are shown in Figures 8-9 and 8-10. The hysteretic model is able to estimate the hysteresis relationship of specimens with flexural shear or shear failure. Better correlation is obtained for specimens with low and high volumetric transverse reinforcement ratio. The flow chart of hysteresis model is shown in Figures 8-11 and 8-12.

8.5 Summary

A simple hysteresis model is proposed to predict the structural behavior of reinforced concrete column when subjected to cyclic loading. The unloading and reloading stiffness are related to volumetric transverse reinforcement ratio, configuration of transverse reinforcement, axial load capacity ratio, displacement at maximum excursion points and number of cycles. The unloading stiffness increases with increasing volumetric transverse reinforcement ratio but reduces with increasing axial load capacity ratio and displacement at maximum excursion points. Meanwhile, the reloading stiffness increases with increasing volumetric transverse reinforcement ratio, but reduces with increasing displacement of maximum excursion point and number of cycles.

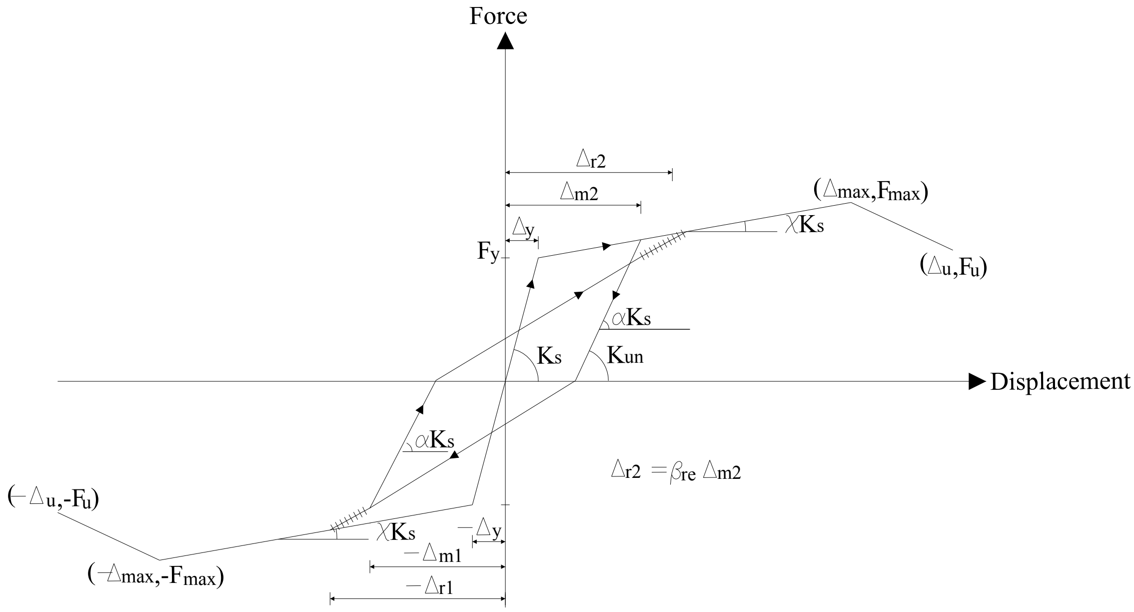

Figure 8-1 Proposed Hysteresis Model for Specimens with Non-seismic Detailing

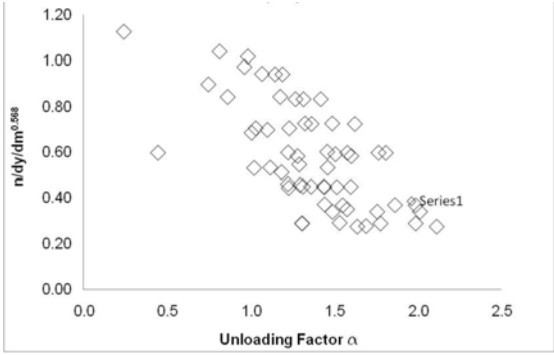

(a) Axial Load Capacity Factor (Type L Detailing)

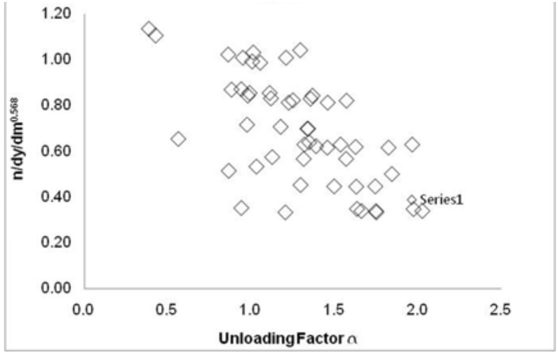

(b) Axial Load Capacity Factor (Type M Detailing)

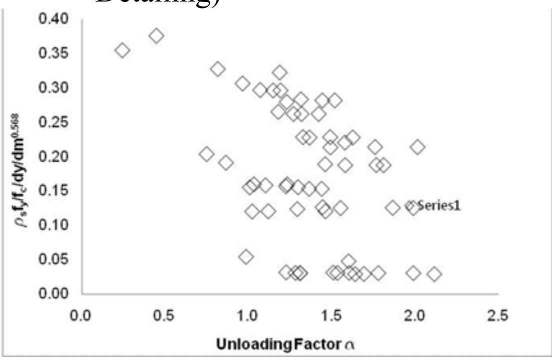

(c) Confinement Factor (Type L Detailing)

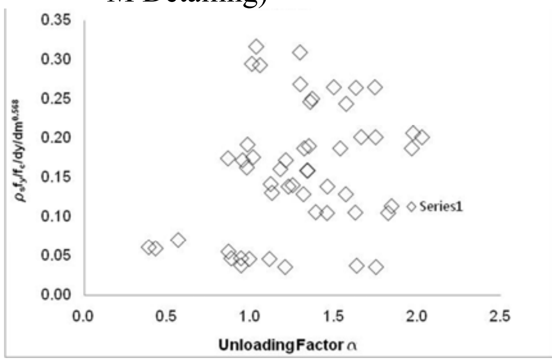

(d) Confinement Factor (Type M detailing)

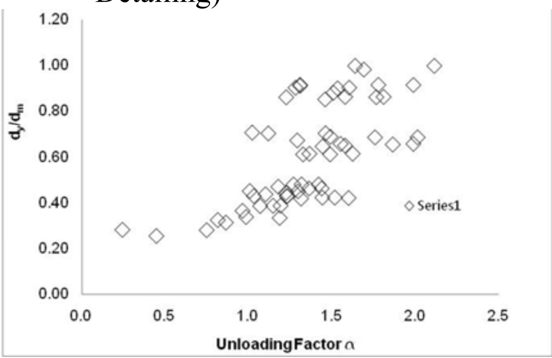

(e) Yield Displacement Factor (Type L Detailing)

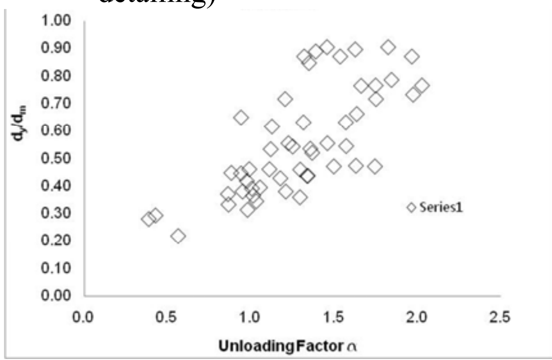

(f) Yield Displacement Factor (Type M Detailing)

Figure 8-2: The Variation of Various Parameters against Unloading Stiffness Factor (α)

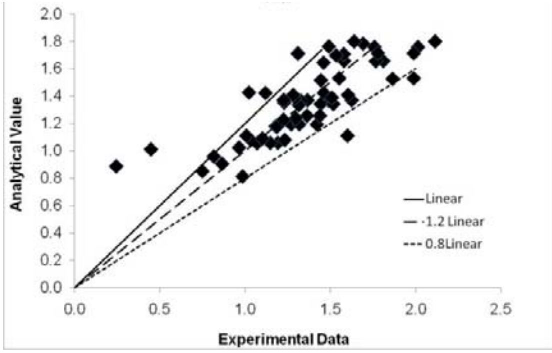

(a) Type L Detailing

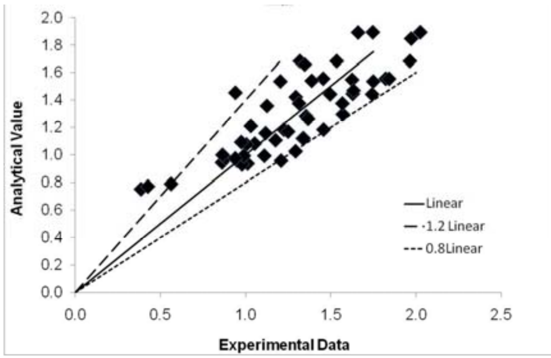

(b) Type M Detailing

Figure 8-3 Comparison of Numerical Value and Experimental Results on Unloading Stiffness factor (α)

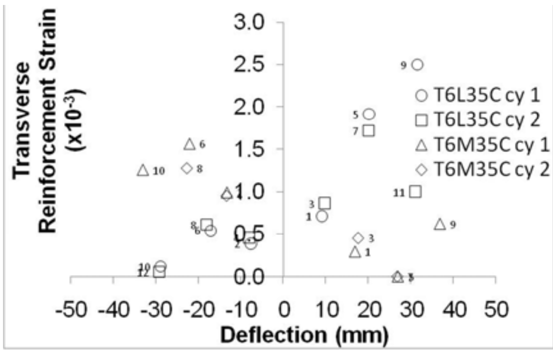

(a) Specimens with T6@35C (B1 shown in Fig 5-9)

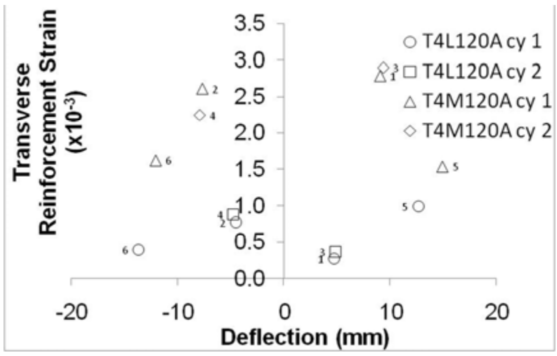

(b) Specimens withT4@120A (B1 shown in Fig 5-9)

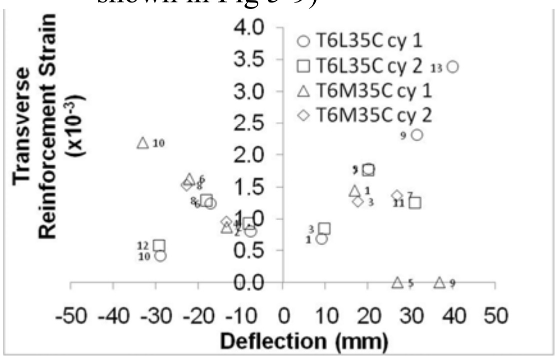

(c) Specimens with T6@35C (B2 shown in Fig 5-9)

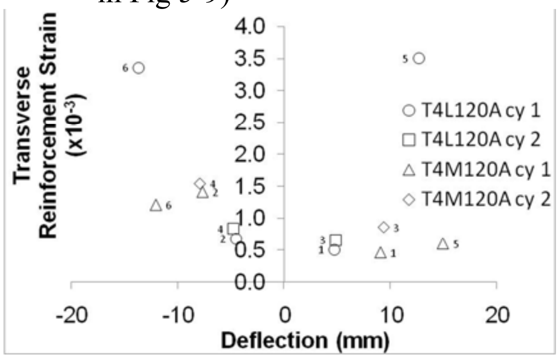

(d) Specimens with T4@120A (B2 shown in Fig 5-9)

Figure 8-4 Variation of Strains at Reinforcement Hoop against Deflection (Cyclic Loading)

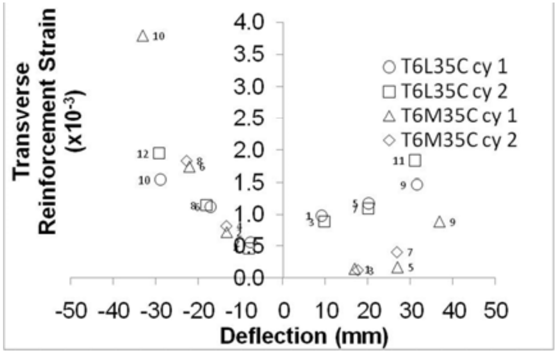

(a) Specimens with T6@35C (B3 shown in Fig 5-9)

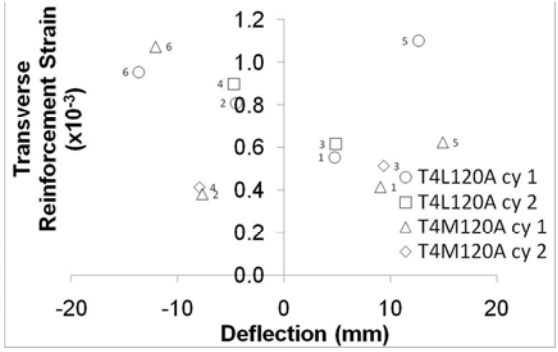

(b) Specimens with T4@120A (B3 shown in Fig 5-9)

Figure 8-5 Variation of Strains at Long Crossties against Deflection under Cyclic Loading

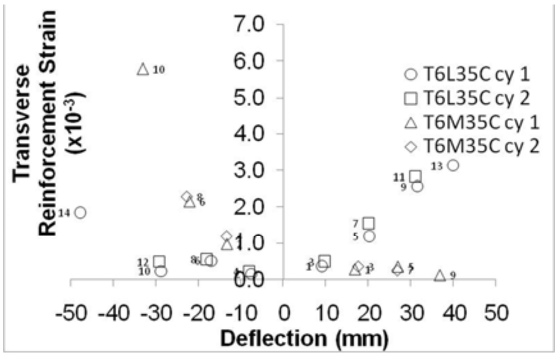

(a) Specimens with T6@35C (B4 shown in Fig 5-9)

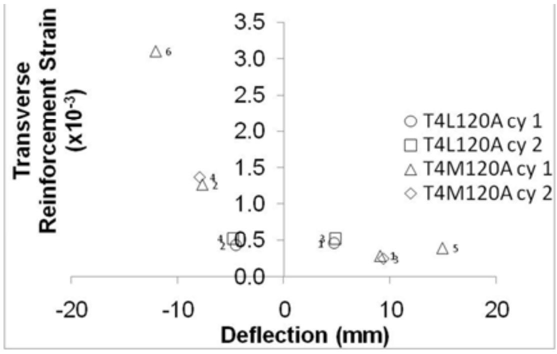

(b) Specimens with T4@120A (B4 shown in Fig 5-9)

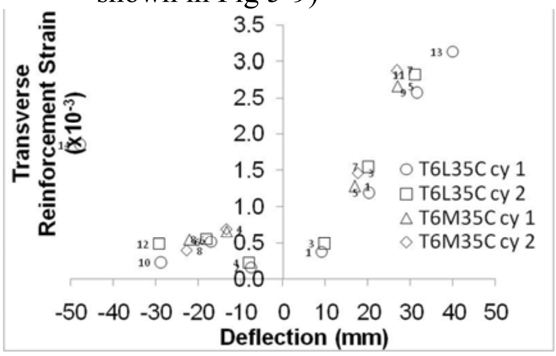

(c) Specimens with T6@35C (B5 shown in Fig 5-9)

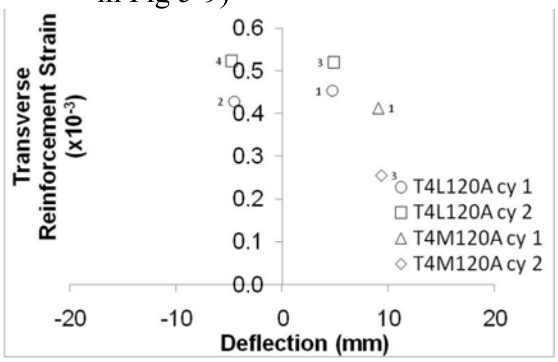

(d) Specimens with T4@120A (B5 shown in Fig 5-9)

Figure 8-6 Variation of Strains at Short Crossties against Deflection under Cyclic Loading

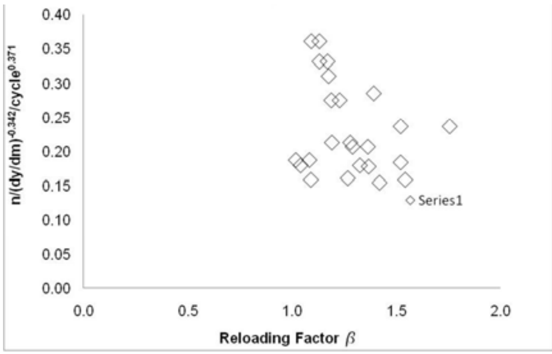

(a) Axial Load (Type L Detailing)

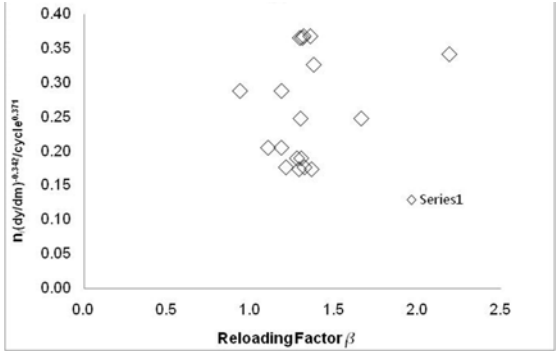

(b) Axial Load (Type M Detailing)

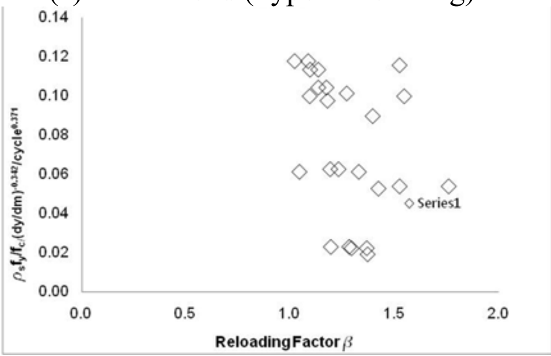

(c) Confinement Factor (Type L Detailing)

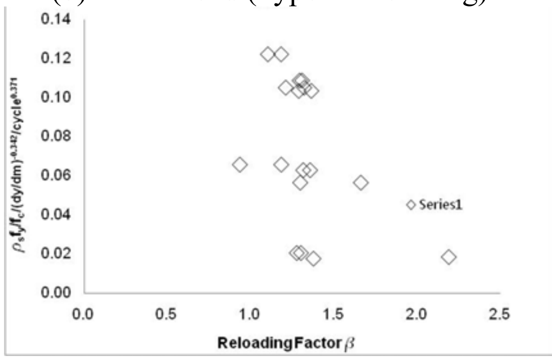

(d) Confinement Factor (Type M Detailing)

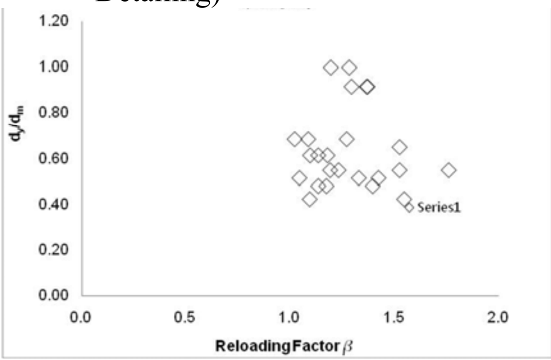

(e) Yield Displacement Factor (Type L Detailing)

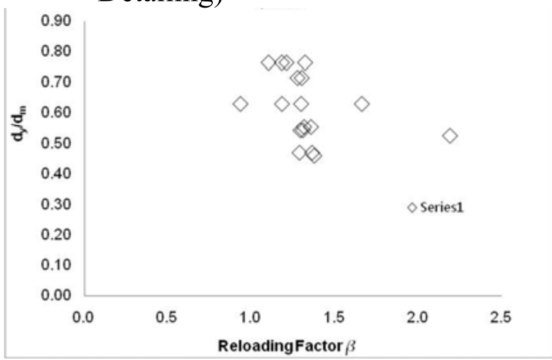

(f) Yield Displacement Factor (Type M Detailing)

Figure 8-7 Variation of Various of Parameters against Reloading Displacement Factor (β_{re}) (Cont'd)

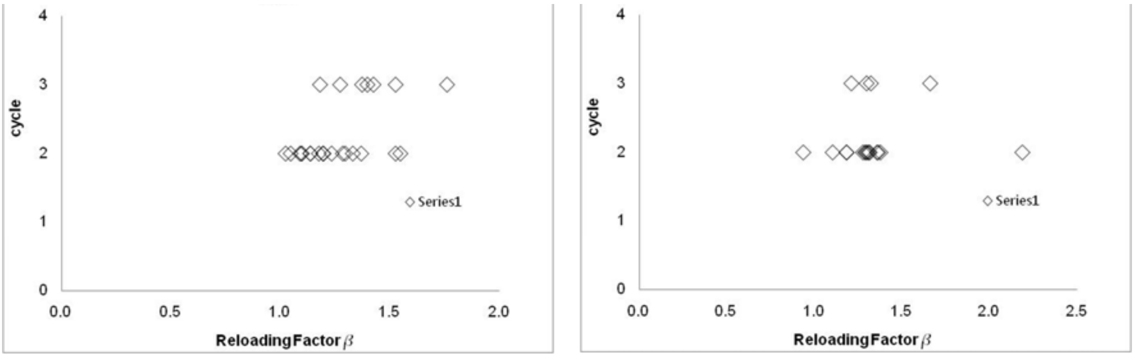

(g) Number of Cycle (Type L Detailing)

(h) Number of Cycle (Type M Detailing)

Figure 8-7 Variation of Various of Parameters against Reloading Displacement Factor (β_{re})

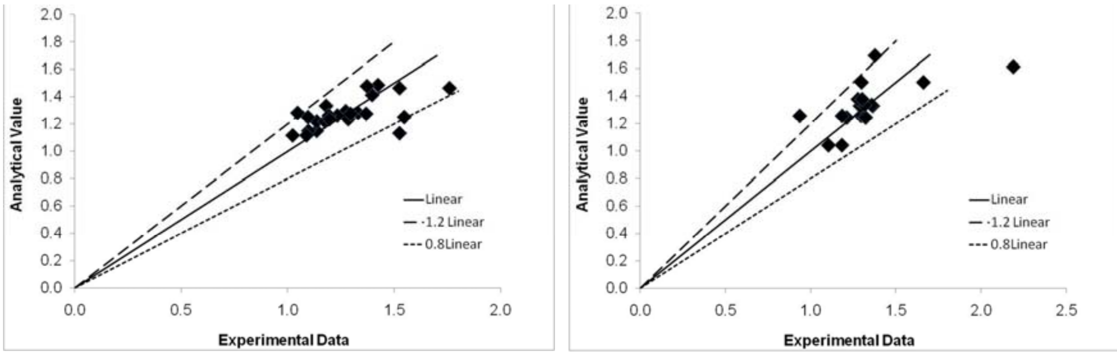

(a) Type L Detailing

(b) Type M Detailing

Figure 8-8 Comparison of Numerical Value and Experimental Results on Reloading Stiffness (β_{re})

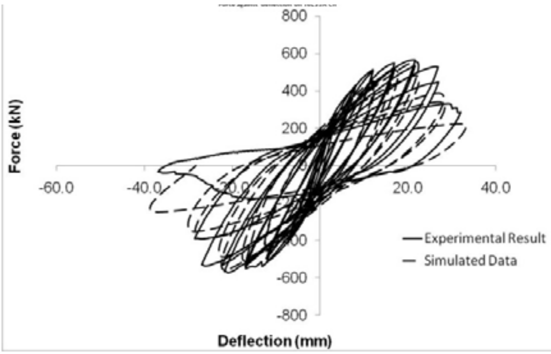

(a) Specimen T6L35A

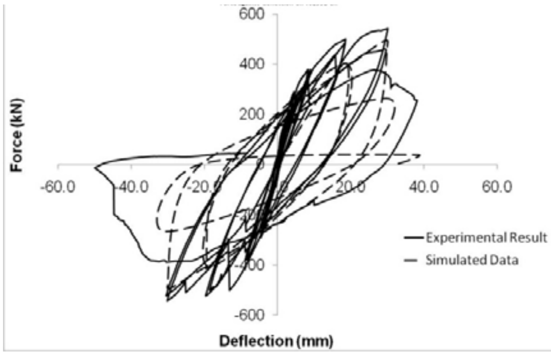

(b) Specimen T6L35C

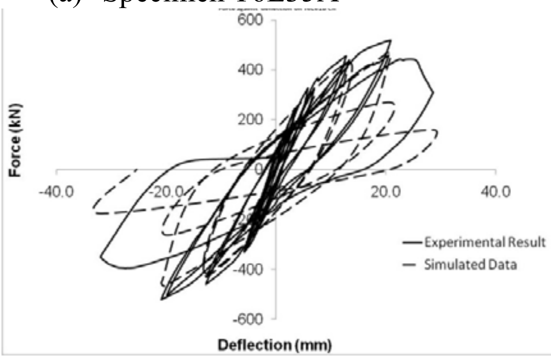

(c) Specimen T6L61B

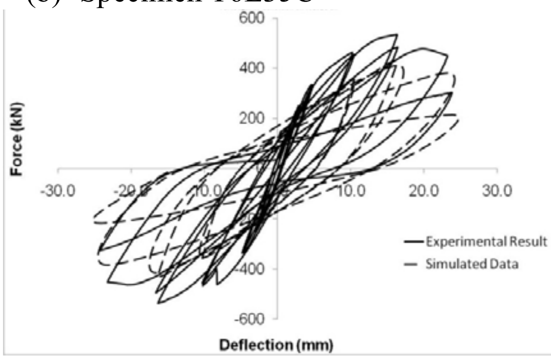

(d) Specimen T6L61C

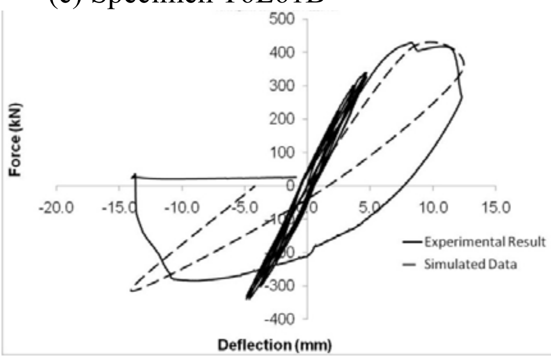

(e) Specimen T4L120A

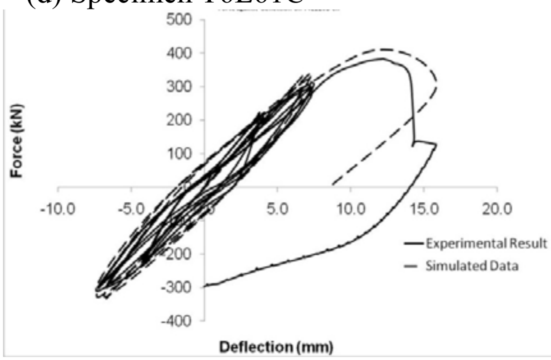

(f) Specimen T4L120C

Figure 8-9 Comparison of Prediction by Hysteresis Model with Experimental Results (Type L Detailing)

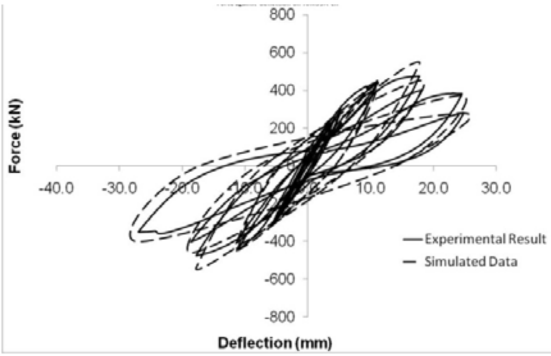

(a) Specimen T6M35A

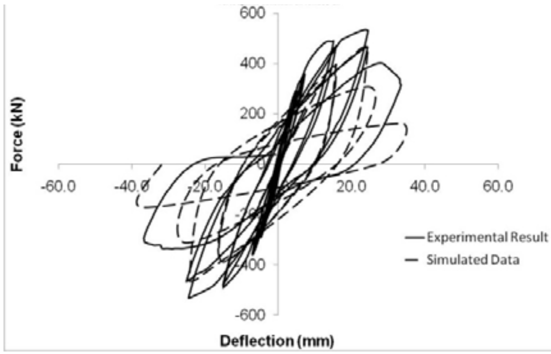

(b) Specimen T6M35C

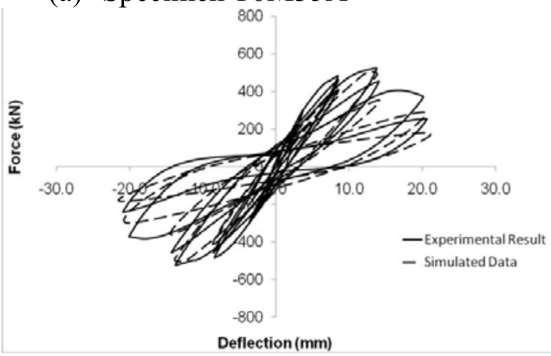

(c) Specimen T6M61A

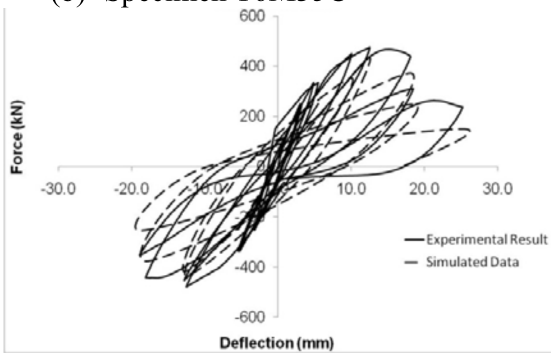

(d) Specimen T6M61B

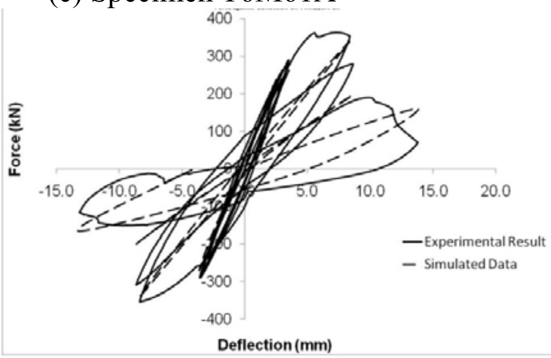

(e) Specimen T4M120A

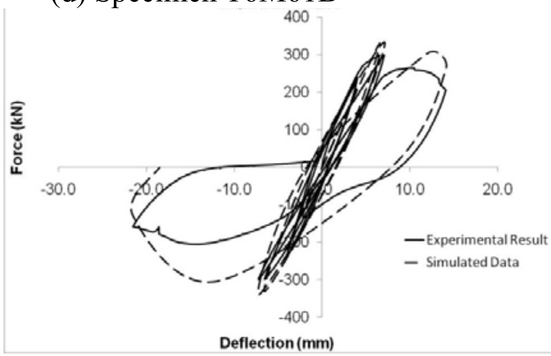

(f) Specimen T4M120C

Figure 8-10 Comparison of Prediction by Hysteresis Model with Experimental Results (Type M Detailing)

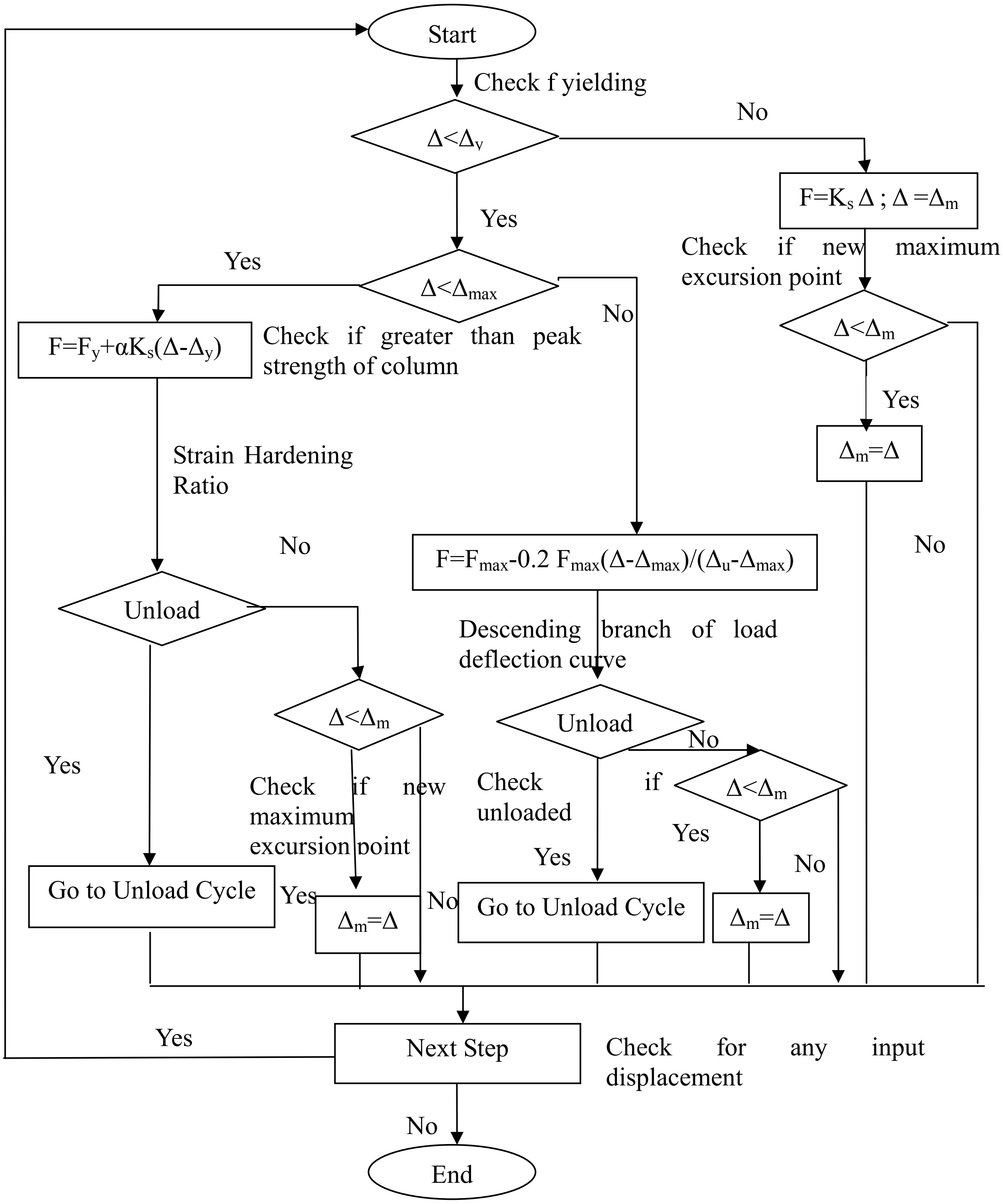

Figure 8-11 Flow Chart of Hysteresis Model

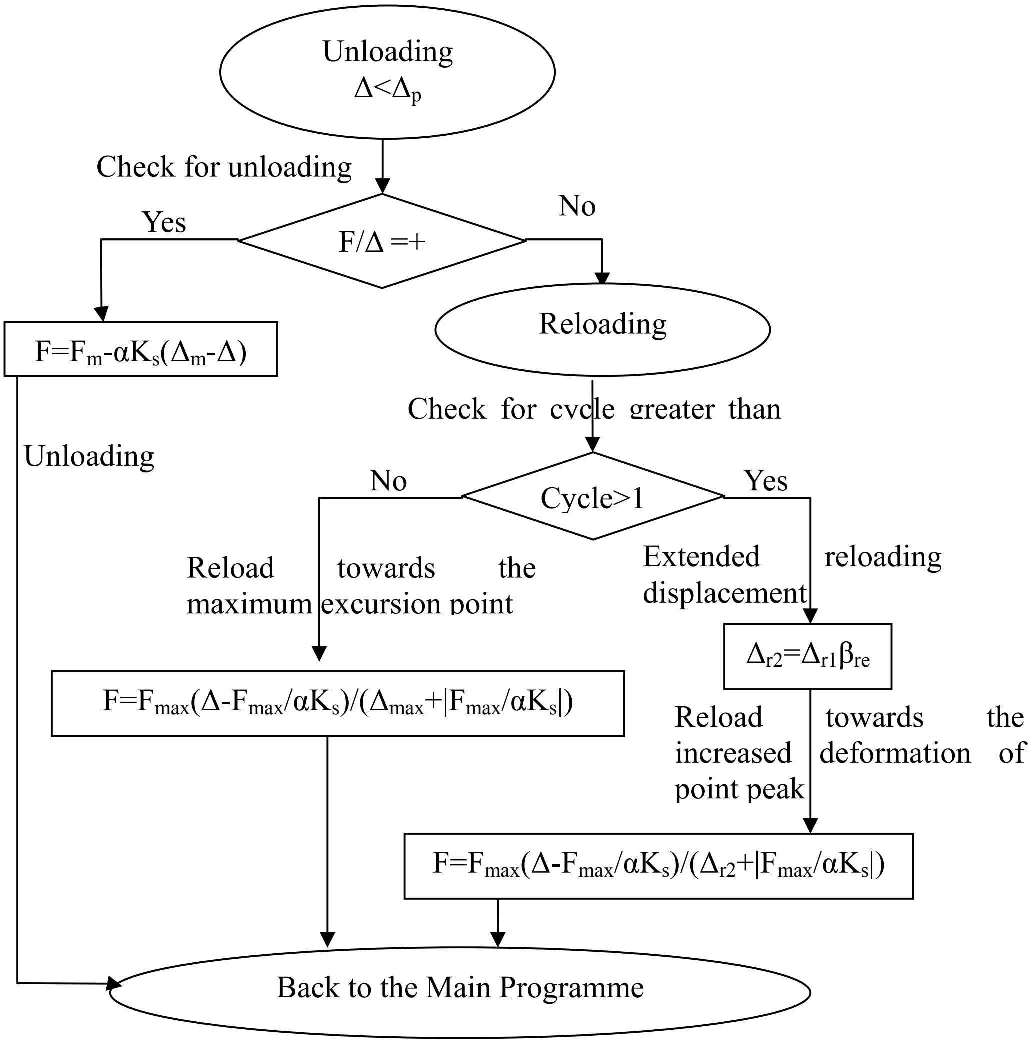

Figure 8-12 Flow Chart of Unloading and Reloading Model

Chapter 9 Damage Model

9.1 Introduction

In recent years, reinforced concrete structures were designed according to the performance based principle, for example, One Rincon Hill, San Francisco and St. Francis Tower, Manila etc. One key feature of performance based design is to assess the degree of damage of reinforced concrete structure after the occurrence of seismic activities. It is necessary to develop a damage model to quantify the damage. Besides, damage model may assist post-earthquake reconnaissance and disaster planning. In reinforced concrete structures, column is a critical element in the moment-frame. Although reinforced concrete columns are normally designed to fail in flexural mode, many were observed to have failed in flexural shear or shear in the post-earthquake investigation. Moreover, configurations of the transverse reinforcements in our reinforced concrete columns is different from that specified in resisting severe seismic hazard and different from those tested by the previous researchers. In this study, a damage model is proposed to quantify degree of degradation include shear of reinforced concrete columns.

In the past, researchers (Park and Ang 1985, Chung et al 1987, Kunnath at al 2001, Hindi and Sexsmith 2001, Berry and Eberhard 2004, Kim et al 2005, Khashee 2005 and Erdurant and Yakut 2007, etc) derived empirical formula to quantify the damage of reinforced concrete columns. There are different approaches on assessing the damage such as the use of degree of energy dissipation, stiffness degradation, displacement ductility and drift ratio.

9.2 Damage Model

A damage model of reinforced concrete columns can be categorized into two types. First type is related to the subjective damage, i.e. cracking of reinforced concrete columns or observation on structural behavior such as spalling of concrete, buckling of main reinforcements etc. Second type is related to strength and stiffness degradation similar to the reloading displacement model presented in Chapter 8. In this chapter, a damage model is proposed based on the damage index obtained from physical observation on cyclic loading tests conducted previously, see Chapter 6.

One of the most well-known damage models of reinforced concrete element was proposed by Park and Ang (1987). Park and Ang quantified damage by using a classification based on damage index (D) as shown in Table 9-1. Damage index based on the physical appearance of specimens observed after subjected to cyclic loading.

For specimens with volumetric transverse reinforcement ratio greater than 1%, cracks are induced after yielding of main reinforcements. The damage index (D) at this stage is classified as 0.1. The damage index (D) is increased to 0.25 when crack width widens. When the displacement and loading increase, crack width further widens to form large cracks and the damage index (D) is increased to 0.4. If the specimen fails by buckling of main reinforcements or fracture of transverse reinforcements, the damage index (D) is increased to 0.8. As some of the tests were terminated when lateral strength of specimens is dropped to 80% of its maximum value, damage index of those specimens does not reach 0.8. In this study, no specimen was tested to failure and the damage index does not equal to 1.

For specimens with low volumetric transverse reinforcement ratio, hairline cracks were observed prior to yielding of main reinforcements. The damage index (D) at this stage is classified as 0.1. Classification for other damage index in this class of specimens is similar to specimens with high volumetric transverse reinforcement ratio.

Park and Ang (1985) proposed a model to correlate damage index (D) of reinforced concrete column under cyclic loading with displacement ratio and energy dissipation ratio. Displacement ratio is maximum displacement during cyclic loading to the ultimate displacement under monotonic loading. The energy dissipation ratio is defined as a specimen characteristic index (β_{Park}) times energy dissipation during whole cyclic loading to plastic energy dissipated under monotonic loading. The characteristic index (β_{Park}) according to Park's model consists of volumetric transverse reinforcement ratio (ρ_s), shear-span depth ratio (L/d) and main reinforcement ratio (ρ_{main}). Total cyclic energy dissipation is the sum of energy dissipation in each loading cycle, that is the enclosed area (A1) of hysteresis loop in each cycle, see Figure 9-1. The enclosed area is calculated based on trapezoidal rule. Energy dissipated under monotonic loading is yield load times the ultimate displacement.

Park's model is based on specimens that are designed to fail in flexural mode under monotonic loading. Furthermore, Park's model assumes that bond slip failure occurs at large displacement. In this study, main reinforcements buckled at small lateral displacement after subjected to lateral load in a small number of cycles. As the specimens considered in this study have very different characteristic as compared with the specimens used in formulating Park's model, Park's model is modified to quantify the damage of reinforced concrete columns with non-seismic detailing.

As shown Table 9-3, the damage index (D) increases with reduction of volumetric transverse reinforcement ratio (ρ_s). As the volumetric transverse reinforcement ratio increases, the strain energy stored in transverse reinforcements being used to resist the lateral expansion increases. This reduces damage to core concrete from lateral expansion and number of cracks induced on concrete cover.

Besides, configurations of transverse reinforcements affect the degree of damage. When the confinement action provided by transverse reinforcements is low, compressive strength of core concrete and ultimate displacement are reduced

Moreover, increasing axial load increases the damage index (D). When the axial load is increased, strain energy in transverse reinforcements is dissipated to resist the axial load. When a reinforced concrete column is subjected to high axial load ratio, lateral expansion increases. The transverse reinforcements offer less strain energy to resist lateral load than the one subjected to low axial load ratio.

Based on the observation on the specimens, damage index of all the specimens is summarized in Table 9-3. Damage index (D) is proposed as a linear contribution by displacement index (D_d) and energy dissipation index (D_e). The displacement coefficient (α_{Dd}) and energy dissipation coefficient (β_{De}) are related to volumetric transverse reinforcement ratio (ρ_s), axial load ratio (n) and configurations of transverse reinforcements (C_{type}), see Table 9-2. By carrying out nonlinear regression analysis, the proposed damage model is as follows,

$$D = D_d + D_e \tag{9-1}$$

$$D_d = \alpha_{Dd} \frac{\Delta_m}{\Delta_u} \tag{9-2}$$

$$D_e = \beta_{De} \frac{\int dE}{F_y \Delta_u} \tag{9-3}$$

$$\alpha_{Dd} = 0.474 - 1.61 C_{type} \frac{\rho_s f_{yt}}{f_c} + 0.13n \tag{9-4}$$

$$\beta_{De} = 0.316 C_{type} \frac{\rho_s f_{yt}}{f_c} \tag{9-5}$$

$$C_{type} = \begin{matrix} 0.512 & \quad for \quad type \quad L \quad Detailing \\ 1 & \quad for \quad type \quad M \quad Detailing \end{matrix} \tag{9-6}$$

where D is damage index, D_d is displacement index, D_e is energy dissipation index, α_{Dd} is displacement coefficient, Δ_m is lateral displacement at maximum excursion points, Δ_u is ultimate deflection, β_{De} is energy dissipation coefficient, E is strain energy, F_y is yield load, C_{type} is factor of configurations of transverse reinforcements, ρ_s is volumetric transverse reinforcement ratio, f_{yt} is yield strength of transverse reinforcements, f_c is confined concrete strength and n is axial load capacity ratio. Correlation of damage model is about 88%, see Figure 9-2.

The displacement index (D_d) dominates the damage model. As shown in Table 9-4, it can reflect shear failure because it is based on the ultimate deflection of specimens subjected to lateral load under monotonic loading. For specimens with small volumetric transverse reinforcement ratio, energy dissipated by hysteretic behavior is smaller than the energy dissipated by specimens with large volumetric transverse reinforcement ratio. It follows that the specimens will fail in shear mode under monotonic loading and contribution to energy dissipation by hysteresis loops is very small. On the other hand, the energy dissipation index (D_e) can reflect flexural failure because energy dissipation is related to strain energy stored in the transverse reinforcements to resist lateral load. For specimens with high volumetric transverse reinforcement ratio, the specimens fail in flexural mode. Energy dissipation index (D_e) shows increasing contribution of energy dissipation in the damage model, see Table 9-4.

9.3 Verification of the Damage Model

The proposed damage model is compared with Park and Ang's model as shown in Figure 9-2 and Table 9-5. Based on Figure 9-2, correlation of experimental results and analytical data is about 88% while the correlation between experimental results and Park and Ang's model is about 80%, see Figure 9-2. The proposed damage model provides better prediction on specimens with type M detailing which was not considered in Park and Ang's model. Also, Park and Ang's model is not appropriate for predicting the damage of columns considered in this study.

9.4 Conclusion

A new damage model is proposed. It is modified from Park and Ang's model (1985) which contains two parts, namely displacement index (D_d) and energy dissipation index (D_e). The major difference between these two models is that there are additional characteristic parameters on the displacement index. The characteristic parameters include configurations of transverse reinforcements, volumetric transverse reinforcement ratio and axial load capacity ratio whereas the characteristic parameters of energy dissipation index include volumetric transverse reinforcement ratio and configurations of transverse reinforcements. The energy dissipation factor is related to the degree of flexural degradation or strain energy stored in transverse reinforcements to provide confinement action of core concrete.

Based on the experimental results, correlation factor of the proposed damage model is about 88%. It provides a method to quantify damage of reinforced concrete columns subjected to seismic loading. Besides, the model can also ascertain as to whether it is necessary to strengthen reinforced concrete column in order to resist the seismic loading.

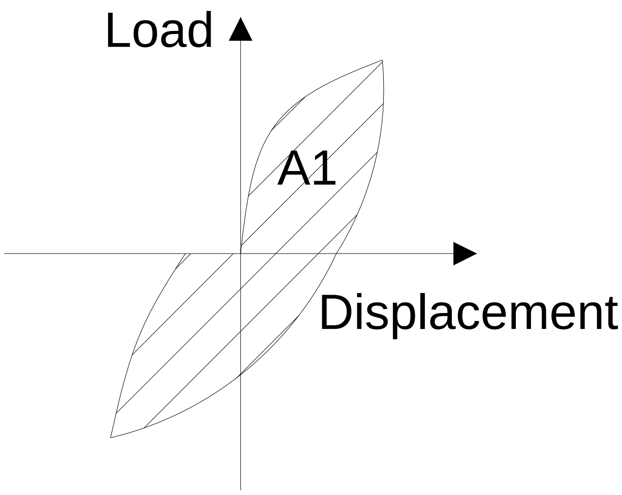

Figure 9-1: Enclosed Hysteresis Area

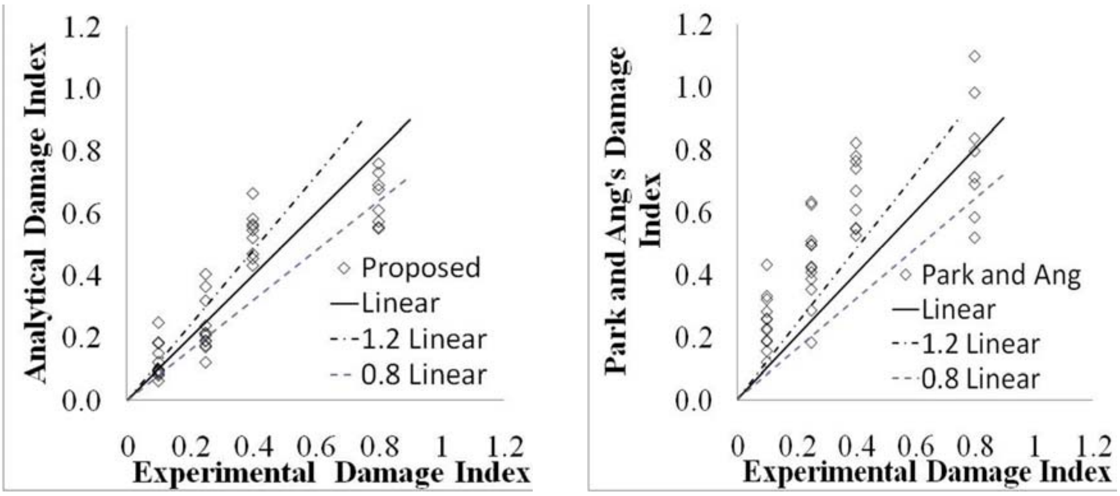

(a) Modified Park and Ang's Model

(b) Park and Ang's Model

Figure 9-2 Comparison of Proposed Damage and Experimental Model

Table 9-1 Classification of Damage Index (Park and Ang 1985)

Damage Index	Degree of Damage	Physical Appearance
0<D<0.1	Slight	Sporadic Occurrence of Cracking
0.1<D<0.25	Minor	Minor Cracks throughout Building. Partial Crashing of Concrete in Columns
0.25<D<0.4	Moderate	Extensive large cracks. Spalling of Concrete in Weak Elements
0.4<D<0.8	Severe	Extensive Crashing of Concrete. Disclosure of Buckled Reinforcements
0.8<D<1	Collapse	Total or Partial Collapse

Table 9-2 Parameters of Specimen in Damage Model

Label	n	$\Phi_{transverse}$ (mm)	s (mm)	Type	$\rho_s f_y/f_c$	Δ_y (mm)	Δ_u (mm)	F_y kN
T6L35A	0.6	6	35	L	0.173	10.43	28.70	423.76
T6L35B	0.3	6	35	L	0.173	12.75	33.18	408.18
T6L61B	0.45	6	61	L	0.099	8.99	24.99	402.35
T6L61C	0.3	6	61	L	0.099	10.77	26.18	389.35
T4L120A	0.6	4	120	L	0.030	4.17	12.18	299.49
T4L120B	0.3	4	120	L	0.030	6.67	14.21	300.62
T6M35A	0.6	6	35	M	0.173	9.70	25.34	356.97
T6M35B	0.3	6	35	M	0.173	11.56	29.12	402.83
T6M61A	0.6	6	61	M	0.099	7.65	18.06	395.26
T6M61C	0.45	6	61	M	0.099	7.91	20.23	358.01
T4M120A	0.6	4	120	M	0.030	3.86	10.99	306.48
T4M120B	0.3	4	120	M	0.030	4.70	12.67	251.97

Table 9-3 Data for Determination of Damage Index

Specimen	D	Δ_m (mm)	Δ_m/Δ_u	$\int dE$ (Nm)	$\int dE/F_y\Delta_{ult}$
T6L35A	0.1	8.01	0.28	2889	0.24
	0.25	13.86	0.48	8455	0.70
	0.4	28.43	0.99	59334	4.88
	0.8	33.94	1.18	88599	7.29
T6L35B	0.1	10.01	0.30	4519	0.33
	0.25	20.37	0.61	10460	0.77
	0.4	40.09	1.21	66551	4.91
	0.8	47.56	1.43	82791	6.11
T6L61B	0.1	5.23	0.21	1603	0.16
	0.25	11.35	0.45	5098	0.51
	0.4	24.39	0.98	27102	2.70
T6L61C	0.1	6.15	0.23	3120	0.31
	0.25	14.07	0.54	6967	0.68
	0.4	33.04	1.26	36588	3.59
T4L120A	0.1	2.83	0.23	324	0.09
	0.25	3.95	0.32	1130	0.31
	0.8	12.84	1.05	6116	1.68
T4L120B	0.1	1.83	0.13	223	0.05
	0.25	3.51	0.25	1419	0.33
	0.4	12.57	0.88	7238	1.69
T6M35A	0.1	4.41	0.17	2024	0.22
	0.25	11.80	0.47	5861	0.65
	0.4	26.42	1.04	27719	3.06
	0.8	26.69	1.05	36050	3.99
T6M35B	0.1	7.16	0.25	1668	0.14
	0.25	17.05	0.59	7512	0.64
	0.8	37.05	1.27	40212	3.43
T6M61A	0.1	8.98	0.50	4394	0.62
	0.25	14.32	0.79	11078	1.55
	0.4	20.13	1.11	22069	3.09
	0.8	20.64	1.14	28379	3.98
T6M61C	0.1	6.39	0.32	1894	0.26
	0.25	15.42	0.76	6878	0.95
	0.4	26.81	1.33	26611	3.67
T4M120A	0.1	3.69	0.34	426	0.13
	0.25	4.20	0.38	805	0.24
	0.4	9.53	0.87	3296	0.98
	0.8	15.39	1.40	7824	2.32
T4M120B	0.1	4.69	0.37	654	0.20
	0.25	8.08	0.64	2326	0.73
	0.8	17.51	1.38	6451	2.02

Table 9-4 Distribution of Displacement and Energy Distribution of Damage Model

Specimen	D_{exp}	D_{ana}	D_d	D_e	D_d/D_{ana}	D_e/D_{ana}
T6L35A	0.1	0.09	0.078	0.013	86%	14%
	0.25	0.17	0.135	0.038	78%	22%
	0.4	0.54	0.277	0.267	51%	49%
	0.8	0.73	0.331	0.399	45%	55%
T6L35B	0.1	0.09	0.072	0.018	80%	20%
	0.25	0.19	0.146	0.042	78%	22%
	0.4	0.56	0.287	0.269	52%	48%
	0.8	0.68	0.341	0.335	50%	50%
T6L61B	0.1	0.08	0.079	0.005	94%	6%
	0.25	0.19	0.171	0.016	91%	9%
	0.4	0.45	0.368	0.085	81%	19%
T6L61C	0.1	0.09	0.084	0.010	90%	10%
	0.25	0.21	0.192	0.021	90%	10%
	0.4	0.56	0.450	0.113	80%	20%
T4L120A	0.1	0.12	0.119	0.001	99%	1%
	0.25	0.17	0.166	0.003	98%	2%
	0.8	0.55	0.538	0.016	97%	3%
T4L120B	0.1	0.06	0.060	0.000	99%	1%
	0.25	0.12	0.116	0.003	97%	3%
	0.4	0.43	0.415	0.016	96%	4%
T6M35A	0.1	0.08	0.072	0.006	92%	8%
	0.25	0.21	0.194	0.018	91%	9%
	0.4	0.52	0.433	0.086	83%	17%
	0.8	0.55	0.438	0.112	80%	20%
T6M35B	0.1	0.10	0.092	0.004	96%	4%
	0.25	0.24	0.219	0.018	92%	8%
	0.8	0.57	0.475	0.096	83%	17%
T6M61A	0.1	0.25	0.237	0.010	96%	4%
	0.25	0.40	0.378	0.025	94%	6%
	0.4	0.58	0.531	0.050	91%	9%
	0.8	0.61	0.544	0.064	89%	11%
T6M61C	0.1	0.15	0.144	0.004	97%	3%
	0.25	0.36	0.347	0.015	96%	4%
	0.4	0.66	0.604	0.059	91%	9%
T4M120A	0.1	0.18	0.179	0.001	100%	0%
	0.25	0.21	0.204	0.001	99%	1%
	0.4	0.47	0.463	0.005	99%	1%
	0.8	0.76	0.747	0.011	99%	1%
T4M120B	0.1	0.18	0.182	0.001	99%	1%
	0.25	0.32	0.314	0.004	99%	1%
	0.8	0.69	0.680	0.010	99%	1%

Table 9-5 Comparison between Experimental Damage and Park and Ang Model

Specimen	D_{exp}	D_{ana}	D_{ana}/D_{exp}	D_{PARK}	D_{PARK}/D_{exp}
T6L35A	0.1	0.078	-9%	0.257	157%
	0.25	0.135	-31%	0.419	68%
	0.4	0.277	36%	0.545	36%
	0.8	0.331	-9%	0.518	-35%
T6L35B	0.1	0.072	-10%	0.255	155%
	0.25	0.146	-25%	0.507	103%
	0.4	0.287	39%	0.525	31%
	0.8	0.341	-16%	0.583	-27%
T6L61B	0.1	0.079	-16%	0.187	87%
	0.25	0.171	-25%	0.385	54%
	0.4	0.368	13%	0.607	52%
T6L61C	0.1	0.084	-7%	0.184	84%
	0.25	0.192	-15%	0.424	70%
	0.4	0.450	41%	0.668	67%
T4L120A	0.1	0.119	19%	0.221	121%
	0.25	0.166	-33%	0.284	14%
	0.8	0.538	-31%	0.836	4%
T4L120B	0.1	0.060	-39%	0.118	18%
	0.25	0.116	-52%	0.181	-28%
	0.4	0.415	8%	0.548	37%
T6M35A	0.1	0.072	-21%	0.154	54%
	0.25	0.194	-15%	0.407	63%
	0.4	0.433	30%	0.763	91%
	0.8	0.438	-31%	0.690	-14%
T6M35B	0.1	0.092	-4%	0.226	126%
	0.25	0.219	-5%	0.496	99%
	0.8	0.475	-29%	0.796	-1%
T6M61A	0.1	0.237	147%	0.430	330%
	0.25	0.378	61%	0.624	150%
	0.4	0.531	45%	0.779	95%
	0.8	0.544	-24%	0.711	-11%
T6M61C	0.1	0.144	48%	0.280	180%
	0.25	0.347	45%	0.632	153%
	0.4	0.604	66%	0.822	105%
T4M120A	0.1	0.179	80%	0.319	219%
	0.25	0.204	-18%	0.351	40%
	0.4	0.463	17%	0.740	85%
	0.8	0.747	-5%	1.098	37%
T4M120B	0.1	0.182	83%	0.330	230%
	0.25	0.314	27%	0.493	97%
	0.8	0.680	-14%	0.981	23%

D_{exp}: Damage in experiment

D_{ana}: Damage index of modified model
D_{PARK}: Damage index calculated in Park and Ang's model

10. Conclusion and Future Recommendation

10.1 Conclusion

10.1.1 Local Transverse Reinforcement Detailing

Hong Kong is located in a moderate seismic hazard zone. Reinforced concrete buildings were not designed to resist any seismic attack. One of the common transverse reinforcement detailing in Hong Kong consists of reinforcement hoops with 90º end hooks, long crossties and short crossties. Long crossties are crossties fixed between main reinforcements while short crossties are crossties fixed to main reinforcements at one end while the other end fixed to long crossties being perpendicular to the short crossties.

Effectiveness of transverse reinforcements in providing confinement action is examined. Two configurations of transverse reinforcements are considered in this study. One is type L detailing being reinforcement hoops with 90º and long crossties. Another one is type M detailing being reinforcement hoops with 90º, long crossties and short crossties.

10.1.2 Stress-strain Relationship of Reinforced Concrete Column

In this study, 12 quarter-scaled reinforced concrete specimens were axially loaded to failure. The test parameters include volumetric transverse reinforcement ratio and configurations of transverse reinforcements. Spacing of transverse reinforcements was between 25mm and 120mm. Volumetric transverse reinforcement ratio ranged between 0.0018-0.023. Specimens with high volumetric transverse reinforcement ratio failed in ductile manner. Specimens with low volumetric transverse reinforcement ratio failed in a brittle mode because spacing of transverse reinforcements was too large and cannot resist expansion of core concrete.

Type L detailing is more effective than type M detailing in providing confinement to core concrete. Short crossties in type M detailing are less effective in confinement as compared with long crossties in type L detailing. In addition, effectiveness of transverse reinforcements in specimens with type M detailing is improved when spacing of transverse reinforcements is reduced. Transverse reinforcement strains in type L detailing are more evenly distributed as compared to those in type M detailing.

Strain on reinforcement hoop at one side near a 90º hook was larger than the one far away from the hook. This indicates that stiffness of reinforcement hoop depends on the anchorage provided by hook and influences the confinement action.

A stress-strain relationship is proposed for this type of detailing by conducting non-linear regression analysis on the test data. By comparing with the experimental results, the stress-strain relationship provides very good agreement with the test data.

10.1.3 Hysteresis Behavior of Reinforced Concrete Column

It is necessary to predict the cyclic behavior of reinforced concrete column when subjected to lateral load. Twelve 0.4-scale reinforced concrete specimens with non-seismic detailing were subjected to cyclic loading. Parameters of the tests include volumetric transverse reinforcement ratio (0.114%-2.2%), configurations of transverse reinforcements (type L and M detailing) and axial load capacity ratio (0.3-0.6). Based on the test results, lateral strength and ultimate displacement of specimens with short crossties (Type M detailing) were smaller than that with long crossties (Type L detailing) because less effective confinement action is provided by short crossties. Strain energy in type M detailing was less than that in type L detailing as strain energy of short crossties in tensile zone of the column section is negligible. Pinching was observed when the axial load increased as cracks were formed in the compressive zone during cyclic loading.

When the specimens were subjected to high axial load, lateral strength was increased but ultimate deflection was reduced. Specimens with low volumetric transverse reinforcement ratio failed in shear and it is necessary to increase shear capacity of these columns.

A new lateral force deflection relationship was proposed by conducting non-linear regression analysis on the test data. It consists of five parameters, including yield stiffness, yield deflection, strain hardening, deflection at maximum force and ultimate deflection. The relationship has correlated reasonably well with the experimental data.

10.1.4 Damage Model of Reinforced Concrete Column

A damage model is developed by modifying the damage index proposed by Park and Ang (1985). It contains displacement index and energy dissipated index. Reinforced concrete columns with low transverse reinforcement ratio and poor configurations of transverse reinforcements fail in shear and the displacement index dominates the damage. The hysteretic energy dissipated throughout the loading cycles was very small as compared with those with larger volumetric transverse reinforcement ratio.

10.2 Future Development

In this study, reinforced concrete columns with non-seismic detailing were subjected to axial load as well as cyclic loading. Future works to be investigated would include the following:

1) It would be desirable to test reinforced concrete columns with different height to breath ratios to include the effect of shear span depth ratio.
2) The experimental results should be verified by 3D finite element analysis, especially on bond slip and confinement.

3) A computer program should be developed based on the proposed mathematical models to predict the cyclic behavior of reinforced concrete columns and to quantify the damage under moderate earthquake action.

Appendix 1 Computer Programme

A1.1 Moment Curvature Relationship

A matlab programme is formulate to simulate the moment curvature analysis of reinforced concrete column with non-seismic detailing.

For Calculating Moment Curvature Relationship

```
% Basic Variable
% To verify the yield strain of curvature is defined by the tension side of
% reinforcement, this can be done by neutral_Axis2.m line278&279in this page
fcu=-35;
buc=320;
duc=320;
cover=16;
diashear=6; %%
Spac=35;%%
fct=1.4*(abs(fcu)/10)^(2/3);
straincra=fct/2/abs(fcu)*0.002;
diamain=16;
phor=pi()*diashear^2/4*4/Spac/buc;
bcc=buc-cover*2-diashear;
dcc=duc-cover*2-diashear;
bcov=cover+diashear/2;
dcov=cover+diashear/2;
nrow=5;
Loadadd=-2088;
loadrat=Loadadd/fcu/buc/duc*1000; %Load ratio 0.55 for
Fc=loadrat*fcu*buc*duc;
Ast=pi()*nrow*(nrow-1)/4*diamain^2;
Asti=pi()/4*diamain^2;
Ac=bcc*dcc-Ast;
Auc=2*(buc-bcov)*dcov+2*(duc-dcov)*bcov;
epsilonsty=0.0027;
nointcur=20; %%L35A 330 L61A 190 L120B Use Moment4_06Pu
Length=570;
Mealength=700;
Este=200*10^3;
noyiediv=4;

ndiameter(1,1)=nrow+1;
for i=2:nrow;
   ndiameter(i,1)=2;
```

```
end
ndiameter((nrow+1),1)=nrow+1;
intdismain=(dcc-diamain-diashear)/nrow;

for i=1:(nrow+1);
   ddiamain(i,1)=cover+diashear+diamain/2+intdismain*(i-1);
end

% To divide the confined concrete section into n by m
n=140; % 560 is the best grid
wic=dcc/n;
for i=1:n+1;
   dic(i,1)=(i-1)*dcc/n+dcov;
   bic(i,1)=wic;
end

% To divide the unconfined concrete section on compressive side () and tension (2)
into n by m
m=10; % 40 is the best grid
wicov=dcov/m;
for i=1:m+1;
   dicov(i,1)=(i-1)*dcov/m;
   dicov2(i,1)=dcov+dcc+(i-1)*dcov/m;
   bicov(i,1)=wicov;
end

% To find the strain in zero curvature
Strain=-0.006;
esp=(CCon(Strain,fcu)*Ac+Steel(Strain)*Ast+Uncon(Strain,fcu)*Auc)-Fc;
Strain1=0;
Strain2=Strain;
while abs(esp)>0.000001;
   if esp>0
      Strain=(Strain1+Strain2)/2;
      esp=(CCon(Strain,fcu)*Ac+Steel(Strain)*Ast+Uncon(Strain,fcu)*Auc)-Fc;
      if esp>0
        Strain1=Strain;
      else
         Strain2=Strain;
      end
   elseif esp<0
      Strain=(Strain1+Strain2)/2;
      esp=(CCon(Strain,fcu)*Ac+Steel(Strain)*Ast+Uncon(Strain,fcu)*Auc)-Fc;
      if esp<0
        Strain2= Strain;
      else
```

```
      Strain1=Strain;
    end
  end
end
F=(CCon(Strain,fcu)*Ac+Steel(Strain)*Ast+Uncon(Strain,fcu)*Auc);

% To calculate the yield curvature
% To calculate the neutral axis from the compressive side
% To find the strain in zero curvature
neutdcy=ddiamain(1,1);
curvatyc=epsilonsty/neutdcy;
concy=-1*epsilonsty-ddiamain(1,1)*curvatyc;
  for i=1:m+1;
    Strainiuaccy(i,1)=curvatyc*dicov(i,1)+concy;
    fucaicy(i,1)=Uncon(Strainiuaccy(i,1),fcu);
    Fuconacy(i,1)=fucaicy(i,1)*duc;
  end
  Fuconcracy=Fuconacy(1,1);
  for i=2:2:m
    Fuconcracy=Fuconcracy+4*Fuconacy(i,1);
  end
  for i=3:2:m-1
    Fuconcracy=Fuconcracy+2*Fuconacy(i,1);
  end
  Fuconcracy=Fuconcracy+Fuconacy(m+1,1);
  Fuconcracy=dcov/3/m*Fuconcracy;

  for i=1:m+1;
    Strainiubccy(i,1)=curvatyc*dicov2(i,1)+concy;
    fucbicy(i,1)=Uncon(Strainiubccy(i,1),fcu);
    Fuconbcy(i,1)=fucbicy(i,1)*duc;
  end
  Fuconcrbcy=Fuconbcy(1,1);
  for i=2:2:m
    Fuconcrbcy=Fuconcrbcy+4*Fuconbcy(i,1);
  end
  for i=3:2:m-1
    Fuconcrbcy=Fuconcrbcy+2*Fuconbcy(i,1);
  end
  Fuconcrbcy=Fuconcrbcy+Fuconbcy(m+1,1);
  Fuconcrbcy=dcov/3/m*Fuconcrbcy;

  for i=1:n+1;
    Strainiccy(i,1)=curvatyc*dic(i,1)+concy;
    fcicy(i,1)=CCon(Strainiccy(i,1),fcu);
    funconicy(i,1)=Uncon(Strainiccy(i,1),fcu);
```

```
      Fconcy(i,1)=fcicy(i,1)*bcc+funconicy(i,1)*bcov*2;
    end
    Fconcrcy=Fconcy(1,1);
    for i=2:2:n
      Fconcrcy=Fconcrcy+4*Fconcy(i,1);
    end
    for i=3:2:n-1
      Fconcrcy=Fconcrcy+2*Fconcy(i,1);
    end
    Fconcrcy=Fconcrcy+Fconcy(n+1,1);
    Fconcrcy=dcc/3/n*Fconcrcy;

    for i=1:(nrow+1)
      Strainiscy(i,1)=curvatyc*ddiamain(i,1)+concy;
      fsicy(i,1)=Steel(Strainiscy(i,1))-CCon(Strainiscy(i,1),fcu);
      Fstecy(i,1)=fsicy(i,1)*ndiameter(i,1)*Asti;
    end
    Fsteecy=Fstecy(1,1);
    for i=2:(nrow+1)
      Fsteecy=Fsteecy+Fstecy(i,1);
    end
    espcurcy=Fconcrcy+Fsteecy+Fuconcracy+Fuconcrbcy-Fc;
    neutdcy1=ddiamain(1,1); %'+'
    neutdcy2=ddiamain((nrow+1),1); %'-'
while abs(espcurcy)>0.000001;
   neutdcy=(neutdcy1+neutdcy2)/2;
   curvatyc=epsilonsty/neutdcy;
   concy=-1*epsilonsty-ddiamain(1,1)*curvatyc;
     for i=1:m+1;
        Strainiuaccy(i,1)=curvatyc*dicov(i,1)+concy;
        fucaicy(i,1)=Uncon(Strainiuaccy(i,1),fcu);
        Fuconacy(i,1)=fucaicy(i,1)*duc;
     end
      Fuconcracy=Fuconacy(1,1);
      for i=2:2:m
        Fuconcracy=Fuconcracy+4*Fuconacy(i,1);
      end
      for i=3:2:m-1
        Fuconcracy=Fuconcracy+2*Fuconacy(i,1);
      end
      Fuconcracy=Fuconcracy+Fuconacy(m+1,1);
      Fuconcracy=dcov/3/m*Fuconcracy;

      for i=1:m+1;
        Strainiubccy(i,1)=curvatyc*dicov2(i,1)+concy;
        fucbicy(i,1)=Uncon(Strainiubccy(i,1),fcu);
```

```
        Fuconbcy(i,1)=fucbicy(i,1)*duc;
    end
    Fuconcrbcy=Fuconbcy(1,1);
    for i=2:2:m
        Fuconcrbcy=Fuconcrbcy+4*Fuconbcy(i,1);
    end
    for i=3:2:m-1
        Fuconcrbcy=Fuconcrbcy+2*Fuconbcy(i,1);
    end
    Fuconcrbcy=Fuconcrbcy+Fuconbcy(m+1,1);
    Fuconcrbcy=dcov/3/m*Fuconcrbcy;

    for i=1:n+1;
        Strainiccy(i,1)=curvatyc*dic(i,1)+concy;
        fcicy(i,1)=CCon(Strainiccy(i,1),fcu);
        funconicy(i,1)=Uncon(Strainiccy(i,1),fcu);
        Fconcy(i,1)=fcicy(i,1)*bcc+funconicy(i,1)*bcov*2;
    end
    Fconcrcy=Fconcy(1,1);
    for i=2:2:n
        Fconcrcy=Fconcrcy+4*Fconcy(i,1);
    end
    for i=3:2:n-1
        Fconcrcy=Fconcrcy+2*Fconcy(i,1);
    end
    Fconcrcy=Fconcrcy+Fconcy(n+1,1);
    Fconcrcy=dcc/3/n*Fconcrcy;

    for i=1:(nrow+1)
        Strainiscy(i,1)=curvatyc*ddiamain(i,1)+concy;
        fsicy(i,1)=Steel(Strainiscy(i,1))-CCon(Strainiscy(i,1),fcu);
        Fstecy(i,1)=fsicy(i,1)*ndiameter(i,1)*Asti;
    end
    Fsteecy=Fstecy(1,1);
    for i=2:(nrow+1)
        Fsteecy=Fsteecy+Fstecy(i,1);
    end
    espcurcy=Fconcrcy+Fsteecy+Fuconcracy+Fuconcrbcy-Fc;

    if espcurcy>0
        neutdcy1=neutdcy;
    else
        neutdcy2=neutdcy;
    end
end
```

```
curvatyc=(Strainiscy((nrow+1),1)-Strainiscy(1,1))/(ddiamain((nrow+1))-
ddiamain(1,1));
%curvatyc=epsilonsty/neutdcy;
neutdty=ddiamain(nrow+1,1);
curvatyt=epsilonsty/neutdty;
conty=epsilonsty-ddiamain(nrow+1,1)*curvatyt;
   for i=1:m+1
      Strainiuacty(i,1)=curvatyt*dicov(i,1)+conty;
      fucaity(i,1)=Uncon(Strainiuacty(i,1),fcu);
      Fuconaty(i,1)=fucaity(i,1)*duc;
   end
   Fuconcraty=Fuconaty(1,1);
   for i=2:2:m
      Fuconcraty=Fuconcraty+4*Fuconaty(i,1);
    end
    for i=3:2:m-1
       Fuconcraty=Fuconcraty+2*Fuconaty(i,1);
    end
    Fuconcraty=Fuconcraty+Fuconaty(m+1,1);
    Fuconcraty=dcov/3/m*Fuconcraty;

   for i=1:m+1;
      Strainiubcty(i,1)=curvatyt*dicov2(i,1)+conty;
      fucbity(i,1)=Uncon(Strainiubcty(i,1),fcu);
      Fuconbty(i,1)=fucbity(i,1)*duc;
   end
   Fuconcrbty=Fuconbty(1,1);
   for i=2:2:m
      Fuconcrbty=Fuconcrbty+4*Fuconbty(i,1);
    end
    for i=3:2:m-1
       Fuconcrbty=Fuconcrbty+2*Fuconbty(i,1);
    end
    Fuconcrbty=Fuconcrbty+Fuconbty(m+1,1);
    Fuconcrbty=dcov/3/m*Fuconcrbty;

   for i=1:n+1;
      Strainicty(i,1)=curvatyt*dic(i,1)+conty;
      fcity(i,1)=CCon(Strainicty(i,1),fcu);
      funconity(i,1)=Uncon(Strainicty(i,1),fcu);
      Fconty(i,1)=fcity(i,1)*bcc+funconity(i,1)*bcov*2;
   end
   Fconcrty=Fconty(1,1);
   for i=2:2:n
      Fconcrty=Fconcrty+4*Fconty(i,1);
    end
```

```
 for i=3:2:n-1
    Fconcrty=Fconcrty+2*Fconty(i,1);
 end
 Fconcrty=Fconcrty+Fconty(n+1,1);
 Fconcrty=dcc/3/n*Fconcrty;


for i=1:(nrow+1)
    Strainisty(i,1)=curvatyt*ddiamain(i,1)+conty;
    fsity(i,1)=Steel(Strainisty(i,1))-CCon(Strainisty(i,1),fcu);
    Fstety(i,1)=fsity(i,1)*ndiameter(i,1)*Asti;
end
Fsteety=Fstety(1,1);
for i=2:(nrow+1)
    Fsteety=Fsteety+Fstety(i,1);
end
espcurty=Fconcrty+Fsteety+Fuconcraty+Fuconcrbty-Fc;


neutdty1=290; %'+' for 0.6 plaease try initial value 64 from Neutral_Axis 2 others use 290
neutdty2=30; %'-' for 0.3 please try initial value 62 from Neutral_Axis 2 others use 30

while abs(espcurty)>0.000001
neutdty=(neutdty1+neutdty2)/2;
curvatyt=epsilonsty/neutdty;
conty=epsilonsty-ddiamain((nrow+1),1)*curvatyt;
for i=1:m+1
    Strainiuacty(i,1)=curvatyt*dicov(i,1)+conty;
    fucaity(i,1)=Uncon(Strainiuacty(i,1),fcu);
    Fuconaty(i,1)=fucaity(i,1)*duc;
end
Fuconcraty=Fuconaty(1,1);
for i=2:2:m
    Fuconcraty=Fuconcraty+4*Fuconaty(i,1);
 end
 for i=3:2:m-1
    Fuconcraty=Fuconcraty+2*Fuconaty(i,1);
 end
 Fuconcraty=Fuconcraty+Fuconaty(m+1,1);
 Fuconcraty=dcov/3/m*Fuconcraty;

for i=1:m+1;
    Strainiubcty(i,1)=curvatyt*dicov2(i,1)+conty;
    fucbity(i,1)=Uncon(Strainiubcty(i,1),fcu);
```

```
    Fuconbty(i,1)=fucbity(i,1)*duc;
  end
  Fuconcrbty=Fuconbty(1,1);
  for i=2:2:m
    Fuconcrbty=Fuconcrbty+4*Fuconbty(i,1);
   end
   for i=3:2:m-1
     Fuconcrbty=Fuconcrbty+2*Fuconbty(i,1);
   end
   Fuconcrbty=Fuconcrbty+Fuconbty(m+1,1);
   Fuconcrbty=dcov/3/m*Fuconcrbty;

  for i=1:n+1;
    Strainicty(i,1)=curvatyt*dic(i,1)+conty;
    fcity(i,1)=CCon(Strainicty(i,1),fcu);
    funconity(i,1)=Uncon(Strainicty(i,1),fcu);
    Fconty(i,1)=fcity(i,1)*bcc+funconity(i,1)*bcov*2;
  end
  Fconcrty=Fconty(1,1);
  for i=2:2:n
    Fconcrty=Fconcrty+4*Fconty(i,1);
   end
   for i=3:2:n-1
     Fconcrty=Fconcrty+2*Fconty(i,1);
   end
   Fconcrty=Fconcrty+Fconty(n+1,1);
   Fconcrty=dcc/3/n*Fconcrty;
    for i=1:(nrow+1)
      Strainisty(i,1)=curvatyt*ddiamain(i,1)+conty;
      fsity(i,1)=Steel(Strainisty(i,1))-CCon(Strainisty(i,1),fcu);
      Fstety(i,1)=fsity(i,1)*ndiameter(i,1)*Asti;
    end
    Fsteety=Fstety(1,1);
    for i=2:(nrow+1)
      Fsteety=Fsteety+Fstety(i,1);
    end
    espcurty=Fconcrty+Fsteety+Fuconcraty+Fuconcrbty-Fc;

    if espcurty>0
      neutdty1=neutdty;
    else
      neutdty2=neutdty;
    end
end
```

```
curvatyt=(Strainisty((nrow+1),1)-Strainisty(1,1))/(ddiamain((nrow+1),1)-
ddiamain(1,1));
%curvatyt=epsilonsty/neutdty;

if curvatyt<curvatyc;
  curvaty=curvatyt;
else
  curvaty=curvatyc;
end

for j=1:nointcur
  curvat(1,j)=curvaty*j/noyiediv;
% To calculate the neutral axis from the compressive side
% To find the strain in zero curvature
  neutd(1,j)=buc;
  for i=1:m+1;
    Strainiuac(i,j)=Strain+curvat(1,j)*(dicov(i,1)-neutd(1,j));
    fucai(i,j)=Uncon(Strainiuac(i,j),fcu);
    Fucona(i,j)=fucai(i,j)*duc;
  end
  Fuconcra(1,j)=Fucona(1,j);
  for i=2:2:m
    Fuconcra(1,j)=Fuconcra(1,j)+4*Fucona(i,j);
   end
   for i=3:2:m-1
    Fuconcra(1,j)=Fuconcra(1,j)+2*Fucona(i,j);
   end
   Fuconcra(1,j)=Fuconcra(1,j)+Fucona(m+1,j);
   Fuconcra(1,j)=dcov/3/m*Fuconcra(1,j);

  for i=1:m+1;
    Strainiubc(i,j)=Strain+curvat(1,j)*(dicov2(i,1)-neutd(1,j));
    fucbi(i,j)=Uncon(Strainiubc(i,j),fcu);
    Fuconb(i,j)=fucbi(i,j)*duc;
  end
  Fuconcrb(1,j)=Fuconb(1,j);
  for i=2:2:m
    Fuconcrb(1,j)=Fuconcrb(1,j)+4*Fuconb(i,j);
  end
  for i=3:2:m-1
    Fuconcrb(1,j)=Fuconcrb(1,j)+2*Fuconb(i,j);
  end
  Fuconcrb(1,j)=Fuconcrb(1,j)+Fuconb(m+1,j);
  Fuconcrb(1,j)=dcov/3/m*Fuconcrb(1,j);

  for i=1:n+1;
```

```
   Strainic(i,j)=Strain+curvat(1,j)*(dic(i,1)-neutd(1,j));
   fci(i,j)=CCon(Strainic(i,j),fcu);
   funconi(i,j)=Uncon(Strainic(i,j),fcu);
   Fcon(i,j)=fci(i,j)*bcc+funconi(i,j)*bcov*2;
end
Fconcr(1,j)=Fcon(1,j);
for i=2:2:n
   Fconcr(1,j)=Fconcr(1,j)+4*Fcon(i,j);
end
for i=3:2:n-1
   Fconcr(1,j)=Fconcr(1,j)+2*Fcon(i,j);
end
Fconcr(1,j)=Fconcr(1,j)+Fcon(n+1,j);
Fconcr(1,j)=dcc/3/n*Fconcr(1,j);

for i=1:(nrow+1)
   Strainis(i,j)=Strain+curvat(1,j)*(ddiamain(i,1)-neutd(1,j));
   fsi(i,j)=Steel(Strainis(i,j))-CCon(Strainis(i,j),fcu);
   Fste(i,j)=fsi(i,j)*ndiameter(i,1)*Asti;
end
Fstee(1,j)=Fste(1,j);
for i=2:(nrow+1)
   Fstee(1,j)=Fstee(1,j)+Fste(i,j);
end
espcur(1,j)=Fconcr(1,j)+Fstee(1,j)+Fuconcra(1,j)+Fuconcrb(1,j)-Fc;

neutd1=0;
neutd2=buc;
while abs(espcur(1,j))>0.000001;
     neutd(1,j)=(neutd1+neutd2)/2;

   for i=1:m+1;
      Strainiuac(i,j)=Strain+curvat(1,j)*(dicov(i,1)-neutd(1,j));
      fucai(i,j)=Uncon(Strainiuac(i,j),fcu);
      Fucona(i,j)=fucai(i,j)*duc;
   end
   Fuconcra(1,j)=Fucona(1,j);
   for i=2:2:m
      Fuconcra(1,j)=Fuconcra(1,j)+4*Fucona(i,j);
   end
   for i=3:2:m-1
      Fuconcra(1,j)=Fuconcra(1,j)+2*Fucona(i,j);
   end
   Fuconcra(1,j)=Fuconcra(1,j)+Fucona(m+1,j);
   Fuconcra(1,j)=dcov/3/m*Fuconcra(1,j);
   for i=1:m+1;
```

```
        Strainiubc(i,j)=Strain+curvat(1,j)*(dicov2(i,1)-neutd(1,j));
        fucbi(i,j)=Uncon(Strainiubc(i,j),fcu);
        Fuconb(i,j)=fucbi(i,j)*duc;
      end
      Fuconcrb(1,j)=Fuconb(1,j);
      for i=2:2:m
        Fuconcrb(1,j)=Fuconcrb(1,j)+4*Fuconb(i,j);
      end
      for i=3:2:m-1
        Fuconcrb(1,j)=Fuconcrb(1,j)+2*Fuconb(i,j);
      end
      Fuconcrb(1,j)=Fuconcrb(1,j)+Fuconb(m+1,j);
      Fuconcrb(1,j)=dcov/3/m*Fuconcrb(1,j);
      for i=1:n+1;
        Strainic(i,j)=Strain+curvat(1,j)*(dic(i,1)-neutd(1,j));
        fci(i,j)=CCon(Strainic(i,j),fcu);
        funconi(i,j)=Uncon(Strainic(i,j),fcu);
        Fcon(i,j)=fci(i,j)*bcc+funconi(i,j)*bcov*2;
      end
      Fconcr(1,j)=Fcon(1,j);
      for i=2:2:n
        Fconcr(1,j)=Fconcr(1,j)+4*Fcon(i,j);
      end
      for i=3:2:n-1
        Fconcr(1,j)=Fconcr(1,j)+2*Fcon(i,j);
      end
      Fconcr(1,j)=Fconcr(1,j)+Fcon(n+1,j);
      Fconcr(1,j)=dcc/3/n*Fconcr(1,j);
      for i=1:(nrow+1)
        Strainis(i,j)=Strain+curvat(1,j)*(ddiamain(i,1)-neutd(1,j));
        fsi(i,j)=Steel(Strainis(i,j))-CCon(Strainis(i,j),fcu);
        Fste(i,j)=fsi(i,j)*ndiameter(i,1)*Asti;
      end
      Fstee(1,j)=Fste(1,j);
      for i=2:(nrow+1)
        Fstee(1,j)=Fstee(1,j)+Fste(i,j);
      end
      espcur(1,j)=Fconcr(1,j)+Fstee(1,j)+Fuconcra(1,j)+Fuconcrb(1,j)-Fc;

      if espcur(1,j)>0
       neutd1=neutd(1,j);
      else
       neutd2=neutd(1,j);
      end
    end
  end
```

```
%To calculate the moment of the concrete and steel
for j=1:nointcur
   for i=1:n+1;
      MomentC(i,j)=fci(i,j)*bcc*(dic(i,1)-duc/2)+funconi(i,j)*bcov*2*(dic(i,1)-
duc/2);
   end
      Momentconc(1,j)=MomentC(1,j);
   for i=2:2:n
      Momentconc(1,j)=Momentconc(1,j)+4*MomentC(i,j);
   end
   for i=3:2:n-1
      Momentconc(1,j)=Momentconc(1,j)+2*MomentC(i,j);
   end
   Momentconc(1,j)=Momentconc(1,j)+MomentC(n+1,j);
   Momentconc(1,j)=dcc/3/n*Momentconc(1,j);

   for i=1:m+1;
      MomentUC1(i,j)=fucai(i,j)*buc*(dicov(i,1)-duc/2);
   end
   MomentUconc1(1,j)=MomentUC1(1,j);
   for i=2:2:m
      MomentUconc1(1,j)=MomentUconc1(1,j)+4*MomentUC1(i,j);
   end
   for i=3:2:m-1
      MomentUconc1(1,j)=MomentUconc1(1,j)+2*MomentUC1(i,j);
   end
   MomentUconc1(1,j)=MomentUconc1(1,j)+MomentUC1(m+1,j);
   MomentUconc1(1,j)=dcov/3/m*MomentUconc1(1,j);

   for i=1:m+1;
      MomentUC2(i,j)=fucbi(i,j)*buc*(dicov2(i,1)-duc/2);
   end
   MomentUconc2(1,j)=MomentUC2(1,j);
   for i=2:2:m
      MomentUconc2(1,j)=MomentUconc2(1,j)+4*MomentUC2(i,j);
   end
   for i=3:2:m-1
      MomentUconc2(1,j)=MomentUconc2(1,j)+2*MomentUC2(i,j);
   end
   MomentUconc2(1,j)=MomentUconc2(1,j)+MomentUC2(m+1,j);
   MomentUconc2(1,j)=dcov/3/m*MomentUconc2(1,j);

   for i=1:(nrow+1)
      MomentS(i,j)=fsi(i,j)*ndiameter(i,1)*Asti*(ddiamain(i,1)-duc/2);
   end
```

```
      Momentstee(1,j)=MomentS(1,j);
    for i=2:(nrow+1);
       Momentstee(1,j)=Momentstee(1,j)+MomentS(i,j);
    end

Moment(1,j)=Momentconc(1,j)+Momentstee(1,j)+MomentUconc1(1,j)+Moment
Uconc2(1,j);
end

%plot(curvat,Moment);
%For calculation of Force Deflection Curve
%For calculation of the Deflection curve

Momentj(1,1)=0;
curvatj(1,1)=0;
for j=1:nointcur;
   Momentj(1,j+1)=Moment(1,j);
   curvatj(1,j+1)=curvat(1,j);
end

Moment=Momentj;
curvat=curvatj;
[MaxMoment,locmaxmom]=max(Moment);
curvatmax3=curvat(1,locmaxmom);

figure(1)
plot(curvat*10^3,Moment/10^6),title('Moment against curvature 0.6P T6@35
f_{c}=37 Type L','FontSize',16),xlabel('curvature (m^{-
1})','FontSize',16),ylabel('Moment (kNm)','FontSize',16);
set(gca,'FontSize',14);
set(gcf,'color','w');
%text(curvat(1,21)*10^3,Moment(1,21)/10^6,sprintf('(%2.4f,%2.0f)',[curvat(1,2
1)*10^3 Moment(1,21)/10^6]),'FontSize',10);
%text(curvat(1,21)*MaxMoment/Moment(1,21)*10^3,MaxMoment/10^6,sprintf('
(%2.4f,%2.0f)',[curvat(1,21)*MaxMoment/Moment(1,21)*10^3
MaxMoment/10^6]),'FontSize',10);
%print('-f1','-dmeta','Moment vs Cur 06P0635 fcu 37 Type Lc')
ForceStorage06P0635fcu37(:,1)=curvat';
ForceStorage06P0635fcu37(:,2)=Moment';
xlswrite('T6L35A 564 moment cur.xls',ForceStorage06P0635fcu37);
```

A1.1.1 Material Model

Steel

```
function Sstress = Steel(Strain)
E=188.889*10^3;
if abs(Strain)<=0.0027;
Sstress=E*Strain;
elseif abs(Strain)<=0.0234;
%elseif abs(Strain)<=0.0234  ;
   Sstress=510*sign(Strain);
elseif abs(Strain)<=0.12;
   Sstress=(510+(630-510)*(abs(Strain)-0.0234)/(0.12-0.0234))*sign(Strain);
else
   Sstress=0;
End
```

Confined Concrete with Type L Detailing

```
function CCstress = CCon(Strain,fc)
fy=510; % Type L
fyh=75 fs0; % 6mm=530 4mm=750
b=320;
d=320;
diamain=16;
diashear=4; %%
spashear=120; %%
spaa=36;
spab=88;
Ashear=pi()*diashear^2/4;
Amain=pi()*diamain^2/4;
nomain=20;
spashear2=spashear-diashear;
cover=16;
bc=b-2*cover-diashear;
dc=d-2*cover-diashear;
phocc=nomain*pi()*diamain^2/4/bc/dc;
phox=4*pi()*diashear^2/4/bc/spashear;
phoy=4*pi()*diashear^2/4/bc/spashear;
Sumwi=(spaa^2*4+spab^2*8)/6;
Areae=bc*dc*(1-Sumwi/bc/dc)*(1-0.5*spashear2/bc)*(1-0.5*spashear2/dc);
Ke=Areae/bc/dc/(1-phocc);
flx=Ke*phox*fy;
fly=Ke*phoy*fy;
phos=phox+phoy;
fl=(flx+fly)/2;
K=1+2.61*phox*fyh*Ke/abs(fc);
fcc=fc*K;
epssilocc=-0.002*(1+5.1*(K-1));
```

```
epssilosm=-0.09;
epssilocu=-0.004+0.25*phos*fyh*epssilosm/abs(fc);
Ec=2*fc/-0.002;
Esec=fcc/epssilocc;
r=Ec/(Ec-Esec);
epssilocp0=5*(epssilocu-epssilocc)+epssilocc;


if Strain>0
   CCstress=0;
elseif abs(Strain)<=abs(epssilocc);
   CCstress=fcc*(abs(Strain)/abs(epssilocc))*r/(r-
1+((abs(Strain)/abs(epssilocc))^r));
elseif abs(Strain)<=abs(epssilocp0);
   CCstress=fcc-0.2*fcc/(abs(epssilocu)-abs(epssilocc))*(abs(Strain)-
abs(epssilocc));
else
   CCstress=0;
 End
```

Unconfined Concrete

```
function UCstress = Uncon(Strain,fc)
strainucmax=0.0005*(abs(fc)^0.4);
if Strain>0
   UCstress=0;
elseif abs(Strain)<=0.002;
   UCstress=fc*(2*abs(Strain)/strainucmax-(Strain)^2/strainucmax^2);
elseif abs(Strain)<=0.006;
   UCstress=fc*(1-(abs(Strain)-strainucmax)/(0.006-strainucmax));
else
   UCstress=0;
End
```

A1.2 Yield Deflection

In order to obtain yield deflection by the energy balance method with reference to BS1998-3 (2005).

```
function [DeltaForyield MaxForce DeltaForyieldapp]=YieldChi(A)
delta=A(:,1);
Force=A(:,2);

[MaxForce locMaxForce]=max(Force);
[MinForce locMinForce]=min(Force);
```

```
n=length(A);
j=1;
for i=2:n;
   if A(i,2)<0;
      j=i+1;
   else
      j=j;
   end
end

delForRelb4max=spaps(delta(j:locMaxForce),Force(j:locMaxForce),10^-20);   %   to
correlate the curve with cubic spline
delForRelb4max=fn2fm(delForRelb4max,'pp');
Forarea=gaussQuadn(delForRelb4max,0,delta(locMaxForce,1),40);
DeltaForyield=2*(delta(locMaxForce,1)-Forarea/MaxForce);
FordelRelb4max=spaps(Force(j:locMaxForce-1),delta(j:locMaxForce-1),10^-20);   %
to correlate the curve with cubic spline
FordelRelb4max=fn2fm(FordelRelb4max,'pp');
DeltaForyieldapp=fnval(FordelRelb4max,0.75*Force(locMaxForce,1))/0.75;
```

A1.3 Force Deflection Curve

```
% Basic Variable
% To verify the yield strain of curvature is defined by the tension side of
% reinforcement, this can be done by neutral_Axis2.m line278&279in this page
fcu=-37;
buc=320;
duc=320;
cover=16;
diashear=6;
diamain=16;
bcc=buc-cover*2-diashear*2;
dcc=duc-cover*2-diashear*2;
bcov=cover+diashear;
dcov=cover+diashear;
nrow=5;
loadrat=0.6;
Fc=loadrat*fcu*buc*duc;
Ast=pi()*nrow*(nrow-1)/4*diamain^2;
Asti=pi()/4*diamain^2;
Ac=bcc*dcc-Ast;
Auc=2*(buc-bcov)*dcov+2*(duc-dcov)*bcov;
epsilonsty=0.0027;
nointcur=500;
Length=895;
```

```
ndiameter(1,1)=nrow+1;
for i=2:nrow;
   ndiameter(i,1)=2;
end
ndiameter((nrow+1),1)=nrow+1;
intdismain=(dcc-diamain)/nrow;

for i=1:(nrow+1);
   ddiamain(i,1)=cover+diashear+diamain/2+intdismain*(i-1);
end

% To divide the confined concrete section into n by m
n=240;
wic=dcc/n;
for i=1:n;
   dic(i,1)=i*dcc/n-dcc/2/n+dcov;
   bic(i,1)=wic;
end

% To divide the unconfined concrete section on compressive side () and tension (2)
into n by m
m=20;
wicov=dcov/m;
for i=1:m;
   dicov(i,1)=i*dcov/m-dcov/m/2;
   dicov2(i,1)=dcov+dcc+i*dcov/m-dcov/m/2;
   bicov(i,1)=wicov;
end

% To find the strain in zero curvature
Strain=-0.006;
esp=(CCon(Strain,fcu)*Ac+Steel(Strain)*Ast+Uncon(Strain,fcu)*Auc)-Fc;
Strain1=0;
Strain2=Strain;
while abs(esp)>0.000001;
   if esp>0
      Strain=(Strain1+Strain2)/2;
      esp=(CCon(Strain,fcu)*Ac+Steel(Strain)*Ast+Uncon(Strain,fcu)*Auc)-Fc;
      if esp>0
        Strain1=Strain;
      else
         Strain2=Strain;
      end
```

```
   elseif esp<0
      Strain=(Strain1+Strain2)/2;
      esp=(CCon(Strain,fcu)*Ac+Steel(Strain)*Ast+Uncon(Strain,fcu)*Auc)-Fc;
      if esp<0
        Strain2= Strain;
      else
         Strain1=Strain;
      end
   end
end
F=(CCon(Strain,fcu)*Ac+Steel(Strain)*Ast+Uncon(Strain,fcu)*Auc);

% To calculate the yield curvature
% To calculate the neutral axis from the compressive side
% To find the strain in zero curvature
neutdcy=30;
curvatyc=epsilonsty/neutdcy;
concy=epsilonsty*-1-30*curvatyc;
   for i=1:m
      Strainiuaccy(i,1)=curvatyc*dicov(i,1)+concy;
      dicucovcy(i,1)=dicov(i,1)-neutdcy;
      fucaicy(i,1)=Uncon(Strainiuaccy(i,1),fcu);

      Fuconacy(i,1)=fucaicy(i,1)*bicov(i,1)*duc;
   end
   Fuconcracy=Fuconacy(1,1);
   for i=2:m
      Fuconcracy1=Fuconcracy+Fuconacy(i,1);
   end

   for i=1:m;
      Strainiubccy(i,1)=curvatyc*dicov2(i,1)+concy;
      fucbicy(i,1)=Uncon(Strainiubccy(i,1),fcu);
      Fuconbcy(i,1)=fucbicy(i,1)*bicov(i,1)*duc;
   end
   Fuconcrbcy=Fuconbcy(1,1);
   for i=2:m
      Fuconcrbcy=Fuconcrbcy+Fuconbcy(i,1);
   end

   for i=1:n;
      Strainiccy(i,1)=curvatyc*dic(i,1)+concy;
      fcicy(i,1)=CCon(Strainiccy(i,1),fcu);
      funconicy(i,1)=Uncon(Strainiccy(i,1),fcu);
      Fconcy(i,1)=fcicy(i,1)*bic(i,1)*bcc+funconicy(i,1)*bcov*2*bic(i,1);
   end
```

```
    Fconcrcy=Fconcy(1,1);
    for i=2:n
        Fconcrcy=Fconcrcy+Fconcy(i,1);
    end
    for i=1:(nrow+1)
        Strainiscy(i,1)=curvatyc*ddiamain(i,1)+concy;
        fsicy(i,1)=Steel(Strainiscy(i,1));
        Fstecy(i,1)=fsicy(i,1)*ndiameter(i,1)*Asti;
    end
    Fsteecy=Fstecy(1,1);
    for i=2:(nrow+1)
        Fsteecy=Fsteecy+Fstecy(i,1);
    end
    espcurcy=Fconcrcy+Fsteecy+Fuconcracy+Fuconcrbcy-Fc;
    neutdcy1=30; %'+'
neutdcy2=260; %'-'
while abs(espcurcy)>0.000001;

   if espcurcy>0
   neutdcy=(neutdcy1+neutdcy2)/2;
   curvatyc=epsilonsty/neutdcy;
   concy=epsilonsty*-1-30*curvatyc;
        for i=1:m
            Strainiuaccy(i,1)=curvatyc*dicov(i,1)+concy;
            fucaicy(i,1)=Uncon(Strainiuaccy(i,1),fcu);
            Fuconacy(i,1)=fucaicy(i,1)*bicov(i,1)*duc;
        end
        Fuconcracy=Fuconacy(1,1);
        for i=2:m
            Fuconcracy1=Fuconcracy+Fuconacy(i,1);
        end

        for i=1:m;
            Strainiubccy(i,1)=curvatyc*dicov2(i,1)+concy;
            fucbicy(i,1)=Uncon(Strainiubccy(i,1),fcu);
            Fuconbcy(i,1)=fucbicy(i,1)*bicov(i,1)*duc;
        end
        Fuconcrbcy=Fuconbcy(1,1);
        for i=2:m
            Fuconcrbcy=Fuconcrbcy+Fuconbcy(i,1);
        end

        for i=1:n;
            Strainiccy(i,1)=curvatyc*dic(i,1)+concy;
            fcicy(i,1)=CCon(Strainiccy(i,1),fcu);
            funconicy(i,1)=Uncon(Strainiccy(i,1),fcu);
```

```
    Fconcy(i,1)=fcicy(i,1)*bic(i,1)*bcc+funconicy(i,1)*bcov*2*bic(i,1);
  end
  Fconcrcy=Fconcy(1,1);
  for i=2:n
    Fconcrcy=Fconcrcy+Fconcy(i,1);
  end
  for i=1:(nrow+1)
    Strainiscy(i,1)=curvatyc*ddiamain(i,1)+concy;
    fsicy(i,1)=Steel(Strainiscy(i,1));
    Fstecy(i,1)=fsicy(i,1)*ndiameter(i,1)*Asti;
  end
  Fsteecy=Fstecy(1,1);
  for i=2:(nrow+1)
    Fsteecy=Fsteecy+Fstecy(i,1);
  end
  espcurcy=Fconcrcy+Fsteecy+Fuconcracy+Fuconcrbcy-Fc;

  if espcurcy>0
    neutdcy1=neutdcy;
  else
    neutdcy2=neutdcy;
  end
elseif espcurcy<0
neutdcy=(neutdcy1+neutdcy2)/2;
curvatyc=epsilonsty/neutdcy;
concy=epsilonsty*-1-30*curvatyc;

  for i=1:m
    Strainiuaccy(i,1)=curvatyc*dicov(i,1)+concy;
    fucaicy(i,1)=Uncon(Strainiuaccy(i,1),fcu);
    Fuconacy(i,1)=fucaicy(i,1)*bicov(i,1)*duc;
  end
  Fuconcracy=Fuconacy(1,1);
  for i=2:m
    Fuconcracy1=Fuconcracy+Fuconacy(i,1);
  end

  for i=1:m;
    Strainiubccy(i,1)=curvatyc*dicov2(i,1)+concy;
    fucbicy(i,1)=Uncon(Strainiubccy(i,1),fcu);
    Fuconbcy(i,1)=fucbicy(i,1)*bicov(i,1)*duc;
  end
  Fuconcrbcy=Fuconbcy(1,1);
  for i=2:m
    Fuconcrbcy=Fuconcrbcy+Fuconbcy(i,1);
  end
```

```
    for i=1:n;
      Strainiccy(i,1)=curvatyc*dic(i,1)+concy;
      fcicy(i,1)=CCon(Strainiccy(i,1),fcu);
      funconicy(i,1)=Uncon(Strainiccy(i,1),fcu);
      Fconcy(i,1)=fcicy(i,1)*bic(i,1)*bcc+funconicy(i,1)*bcov*2*bic(i,1);
    end
    Fconcrcy=Fconcy(1,1);
    for i=2:n
      Fconcrcy=Fconcrcy+Fconcy(i,1);
    end
    for i=1:(nrow+1)
      Strainiscy(i,1)=curvatyc*ddiamain(i,1)+concy;
      fsicy(i,1)=Steel(Strainiscy(i,1));
      Fstecy(i,1)=fsicy(i,1)*ndiameter(i,1)*Asti;
    end
    Fsteecy=Fstecy(1,1);
    for i=2:(nrow+1)
      Fsteecy=Fsteecy+Fstecy(i,1);
    end
    espcurcy=Fconcrcy+Fsteecy+Fuconcracy+Fuconcrbcy-Fc;

    if espcurcy<0
      neutdcy2= neutdcy;
    else
      neutdcy1=neutdcy;
    end
  end
end
curvatyc=epsilonsty/neutdcy;
neutdty=30;


curvatyt=epsilonsty/neutdty;
conty=epsilonsty-290*curvatyt;
  for i=1:m
    Strainiuacty(i,1)=curvatyt*dicov(i,1)+conty;
    fucaity(i,1)=Uncon(Strainiuacty(i,1),fcu);

    Fuconaty(i,1)=fucaity(i,1)*bicov(i,1)*duc;
  end
  Fuconcraty=Fuconaty(1,1);
  for i=2:m
    Fuconcraty1=Fuconcraty+Fuconaty(i,1);
  end
```

```
  for i=1:m;
    Strainiubcty(i,1)=curvatyt*dicov2(i,1)+conty;
    fucbity(i,1)=Uncon(Strainiubcty(i,1),fcu);
    Fuconbty(i,1)=fucbity(i,1)*bicov(i,1)*duc;
  end
  Fuconcrbty=Fuconbty(1,1);
  for i=2:m
    Fuconcrbty=Fuconcrbty+Fuconbty(i,1);
  end

  for i=1:n;
    Strainicty(i,1)=curvatyt*dic(i,1)+conty;
    fcity(i,1)=CCon(Strainicty(i,1),fcu);
    funconity(i,1)=Uncon(Strainicty(i,1),fcu);
    Fconty(i,1)=fcity(i,1)*bic(i,1)*bcc+funconity(i,1)*bcov*2*bic(i,1);
  end
  Fconcrty=Fconty(1,1);
  for i=2:n
    Fconcrty=Fconcrty+Fconty(i,1);
  end
  for i=1:(nrow+1)
    Strainisty(i,1)=curvatyt*ddiamain(i,1)+conty;
    fsity(i,1)=Steel(Strainisty(i,1));
    Fstety(i,1)=fsity(i,1)*ndiameter(i,1)*Asti;
  end
  Fsteety=Fstety(1,1);
  for i=2:(nrow+1)
    Fsteety=Fsteety+Fstety(i,1);
  end
  espcurty=Fconcrty+Fsteety+Fuconcraty+Fuconcrbty-Fc;


  neutdty1=290; %'+' for 0.6 plaease try initial value 64 from Neutral_Axis 2 others use 290
  neutdty2=30; %'-' for 0.3 please try initial value 62 from Neutral_Axis 2 others use 30
while abs(espcurty)>0.000001

 if espcurty>0
  neutdty=(neutdty1+neutdty2)/2;
  curvatyt=epsilonsty/neutdty;
  conty=epsilonsty-290*curvatyt;
    for i=1:m
      Strainiuacty(i,1)=curvatyt*dicov(i,1)+conty;
      fucaity(i,1)=Uncon(Strainiuacty(i,1),fcu);
      Fuconaty(i,1)=fucaity(i,1)*bicov(i,1)*duc;
```

```
    end
    Fuconcraty=Fuconaty(1,1);
    for i=2:m
        Fuconcraty1=Fuconcraty+Fuconaty(i,1);
    end

    for i=1:m;
        Strainiubcty(i,1)=curvatyt*dicov2(i,1)+conty;
        fucbity(i,1)=Uncon(Strainiubcty(i,1),fcu);
        Fuconbty(i,1)=fucbity(i,1)*bicov(i,1)*duc;
    end
    Fuconcrbty=Fuconbty(1,1);
    for i=2:m
        Fuconcrbty=Fuconcrbty+Fuconbty(i,1);
    end

    for i=1:n;
        Strainicty(i,1)=curvatyt*dic(i,1)+conty;
        fcity(i,1)=CCon(Strainicty(i,1),fcu);
        funconity(i,1)=Uncon(Strainicty(i,1),fcu);
        Fconty(i,1)=fcity(i,1)*bic(i,1)*bcc+funconity(i,1)*bcov*2*bic(i,1);
    end
    Fconcrty=Fconty(1,1);
    for i=2:n
        Fconcrty=Fconcrty+Fconty(i,1);
    end
    for i=1:(nrow+1)
        Strainisty(i,1)=curvatyt*ddiamain(i,1)+conty;
        fsity(i,1)=Steel(Strainisty(i,1));
        Fstety(i,1)=fsity(i,1)*ndiameter(i,1)*Asti;
    end
    Fsteety=Fstety(1,1);
    for i=2:(nrow+1)
        Fsteety=Fsteety+Fstety(i,1);
    end
    espcurty=Fconcrty+Fsteety+Fuconcraty+Fuconcrbty-Fc;

    if espcurty>0
        neutdty1=neutdty;
    else
        neutdty2=neutdty;
    end
elseif espcurty<0
 neutdty=(neutdty1+neutdty2)/2;
 curvatyt=epsilonsty/neutdty;
 conty=epsilonsty-290*curvatyt;
```

```
for i=1:m
   Strainiuacty(i,1)=curvatyt*dicov(i,1)+conty;
   fucaity(i,1)=Uncon(Strainiuacty(i,1),fcu);
   Fuconaty(i,1)=fucaity(i,1)*bicov(i,1)*duc;
end
Fuconcraty=Fuconaty(1,1);
for i=2:m
   Fuconcraty1=Fuconcraty+Fuconaty(i,1);
end

for i=1:m;
   Strainiubcty(i,1)=curvatyt*dicov2(i,1)+conty;
   fucbity(i,1)=Uncon(Strainiubcty(i,1),fcu);
   Fuconbty(i,1)=fucbity(i,1)*bicov(i,1)*duc;
end
Fuconcrbty=Fuconbty(1,1);
for i=2:m
   Fuconcrbty=Fuconcrbty+Fuconbty(i,1);
end

for i=1:n;
   Strainicty(i,1)=curvatyt*dic(i,1)+conty;
   fcity(i,1)=CCon(Strainicty(i,1),fcu);
   funconity(i,1)=Uncon(Strainicty(i,1),fcu);
   Fconty(i,1)=fcity(i,1)*bic(i,1)*bcc+funconity(i,1)*bcov*2*bic(i,1);
end
Fconcrty=Fconty(1,1);
for i=2:n
   Fconcrty=Fconcrty+Fconty(i,1);
end
for i=1:(nrow+1)
   Strainisty(i,1)=curvatyt*ddiamain(i,1)+conty;
   fsity(i,1)=Steel(Strainisty(i,1));
   Fstety(i,1)=fsity(i,1)*ndiameter(i,1)*Asti;
end
Fsteety=Fstety(1,1);
for i=2:(nrow+1)
   Fsteety=Fsteety+Fstety(i,1);
end
espcurty=Fconcrty+Fsteety+Fuconcraty+Fuconcrbty-Fc;

if espcurty<0
   neutdty2= neutdty;
else
   neutdty1=neutdty;
```

```
      end
    end
end

curvatyt=epsilonsty/neutdty;

if curvatyt<curvatyc;
    curvaty=curvatyt;
else
    curvaty=curvatyc;
end



for j=1:nointcur
    curvat(1,j)=curvaty*j/20;
% To calculate the neutral axis from the compressive side
% To find the strain in zero curvature
    neutd(1,j)=320;
    for i=1:m
        Strainiuac(i,j)=Strain+curvat(1,j)*(dicov(i,1)-neutd(1,j));
        fucai(i,j)=Uncon(Strainiuac(i,j),fcu);
        Fucona(i,j)=fucai(i,j)*bicov(i,1)*duc;
    end
    Fuconcra(1,j)=Fucona(1,j);
    for i=2:m
        Fuconcra(1,j)=Fuconcra(1,j)+Fucona(i,j);
    end

    for i=1:m;
        Strainiubc(i,j)=Strain+curvat(1,j)*(dicov2(i,1)-neutd(1,j));
        fucbi(i,j)=Uncon(Strainiubc(i,j),fcu);
        Fuconb(i,j)=fucbi(i,j)*bicov(i,1)*duc;
    end
    Fuconcrb(1,j)=Fuconb(1,j);
    for i=2:m
        Fuconcrb(1,j)=Fuconcrb(1,j)+Fuconb(i,j);
    end

    for i=1:n;
        Strainic(i,j)=Strain+curvat(1,j)*(dic(i,1)-neutd(1,j));
        fci(i,j)=CCon(Strainic(i,j),fcu);
        funconi(i,j)=Uncon(Strainic(i,j),fcu);
        Fcon(i,j)=fci(i,j)*bic(i,1)*bcc+funconi(i,j)*bcov*2*bic(i,1);
    end
    Fconcr(1,j)=Fcon(1,j);
```

```
  for i=2:n
    Fconcr(1,j)=Fconcr(1,j)+Fcon(i,j);
  end
  for i=1:(nrow+1)
    Strainis(i,j)=Strain+curvat(1,j)*(ddiamain(i,1)-neutd(1,j));
    fsi(i,j)=Steel(Strainis(i,j));
    Fste(i,j)=fsi(i,j)*ndiameter(i,1)*Asti;
  end
  Fstee(1,j)=Fste(1,j);
  for i=2:(nrow+1)
    Fstee(1,j)=Fstee(1,j)+Fste(i,j);
  end
  espcur(1,j)=Fconcr(1,j)+Fstee(1,j)+Fuconcra(1,j)+Fuconcrb(1,j)-Fc;

  neutd1=0;
  neutd2=320;
% while (abs(espcur(1,j))>0.000001) && (Fconcr(1,j)==0);
  while abs(espcur(1,j))>0.000001;

    if espcur(1,j)>0
      neutd(1,j)=(neutd1+neutd2)/2;

      for i=1:m
        Strainiuac(i,j)=Strain+curvat(1,j)*(dicov(i,1)-neutd(1,j));
        fucai(i,j)=Uncon(Strainiuac(i,j),fcu);
        Fucona(i,j)=fucai(i,j)*bicov(i,1)*duc;
      end
      Fuconcra(1,j)=Fucona(1,j);
      for i=2:m
        Fuconcra(1,j)=Fuconcra(1,j)+Fucona(i,j);
      end

      for i=1:m;
        Strainiubc(i,j)=Strain+curvat(1,j)*(dicov2(i,1)-neutd(1,j));
        fucbi(i,j)=Uncon(Strainiubc(i,j),fcu);
        Fuconb(i,j)=fucbi(i,j)*bicov(i,1)*duc;
      end
      Fuconcrb(1,j)=Fuconb(1,j);
      for i=2:m
        Fuconcrb(1,j)=Fuconcrb(1,j)+Fuconb(i,j);
      end

      for i=1:n;
        Strainic(i,j)=Strain+curvat(1,j)*(dic(i,1)-neutd(1,j));
        fci(i,j)=CCon(Strainic(i,j),fcu);
        funconi(i,j)=Uncon(Strainic(i,j),fcu);
```

```
      Fcon(i,j)=fci(i,j)*bic(i,1)*bcc+funconi(i,j)*bcov*2*bic(i,1);
    end
    Fconcr(1,j)=Fcon(1,j);
    for i=2:n
      Fconcr(1,j)=Fconcr(1,j)+Fcon(i,j);
    end
    for i=1:(nrow+1)
      Strainis(i,j)=Strain+curvat(1,j)*(ddiamain(i,1)-neutd(1,j));
      fsi(i,j)=Steel(Strainis(i,j));
      Fste(i,j)=fsi(i,j)*ndiameter(i,1)*Asti;
    end
    Fstee(1,j)=Fste(1,j);
    for i=2:(nrow+1)
      Fstee(1,j)=Fstee(1,j)+Fste(i,j);
    end
    espcur(1,j)=Fconcr(1,j)+Fstee(1,j)+Fuconcra(1,j)+Fuconcrb(1,j)-Fc;

    if espcur(1,j)>0
      neutd1=neutd(1,j);
    else
      neutd2=neutd(1,j);
    end
  elseif espcur(1,j)<0
     neutd(1,j)=(neutd1+neutd2)/2;

    for i=1:m
      Strainiuac(i,j)=Strain+curvat(1,j)*(dicov(i,1)-neutd(1,j));
      fucai(i,j)=Uncon(Strainiuac(i,j),fcu);
      Fucona(i,j)=fucai(i,j)*bicov(i,1)*duc;
    end
    Fuconcra(1,j)=Fucona(1,j);
    for i=2:m
      Fuconcra(1,j)=Fuconcra(1,j)+Fucona(i,j);
    end

    for i=1:m;
      Strainiubc(i,j)=Strain+curvat(1,j)*(dicov2(i,1)-neutd(1,j));
      fucbi(i,j)=Uncon(Strainiubc(i,j),fcu);
      Fuconb(i,j)=fucbi(i,j)*bicov(i,1)*duc;
    end
    Fuconcrb(1,j)=Fuconb(1,j);
    for i=2:m
      Fuconcrb(1,j)=Fuconcrb(1,j)+Fuconb(i,j);
    end

    for i=1:n;
```

```
          Strainic(i,j)=Strain+curvat(1,j)*(dic(i,1)-neutd(1,j));
          fci(i,j)=CCon(Strainic(i,j),fcu);
          funconi(i,j)=Uncon(Strainic(i,j),fcu);
          Fcon(i,j)=fci(i,j)*bic(i,1)*bcc+funconi(i,j)*bcov*2*bic(i,1);
        end
        Fconcr(1,j)=Fcon(1,j);
        for i=2:n
          Fconcr(1,j)=Fconcr(1,j)+Fcon(i,j);
        end
        for i=1:(nrow+1)
          Strainis(i,j)=Strain+curvat(1,j)*(ddiamain(i,1)-neutd(1,j));
          fsi(i,j)=Steel(Strainis(i,j));
          Fste(i,j)=fsi(i,j)*ndiameter(i,1)*Asti;
        end
        Fstee(1,j)=Fste(1,j);
        for i=2:(nrow+1)
          Fstee(1,j)=Fstee(1,j)+Fste(i,j);
        end
        espcur(1,j)=Fconcr(1,j)+Fstee(1,j)+Fuconcra(1,j)+Fuconcrb(1,j)-Fc;

        if espcur(1,j)<0
          neutd2= neutd(1,j);
        else
          neutd1=neutd(1,j);
        end
      end
    end
end

%To calculate the moment of the concrete and steel
for j=1:nointcur
   for i=1:n;
      MomentC(i,j)=fci(i,j)*bic(i,1)*buc*(dic(i,1)-neutd(1,j));
   end
   Momentconc(1,j)=MomentC(1,j);
   for i=2:n;
     Momentconc(1,j)=Momentconc(1,j)+MomentC(i,j);
   end
   for i=1:(nrow+1)
       MomentS(i,j)=fsi(i,j)*ndiameter(i,1)*Asti*(ddiamain(i,1)-neutd(1,j));
   end
      Momentstee(1,j)=MomentS(1,j);
   for i=2:(nrow+1);
     Momentstee(1,j)=Momentstee(1,j)+MomentS(i,j);
   end
  Moment(1,j)=Momentconc(1,j)+Momentstee(1,j);
```

```
end



%plot(curvat,Moment);

%For calculation of Force Deflection Curve
% For calculation of the Deflection curve

Momentj(1,1)=0;
curvatj(1,1)=0;
for j=1:nointcur;
   Momentj(1,j+1)=Moment(1,j);
   curvatj(1,j+1)=curvat(1,j);
end

Moment=Momentj;
curvat=curvatj;

[MaxMoment,locmaxmom]=max(Moment);


MomCurRel=csapi(Moment(1:locmaxmom),curvat(1:locmaxmom));


deltaflex(1,1)=0;
deltaslip(1,1)=0;
deltashear(1,1)=0;
Force(1,1)=0;
delta(1,1)=0;
Forcedelta(1,1)=0;
for j=2:nointcur+1


% Location of the Gauss point
   factor_gauss(1,1,1)=1-0.861136311594053;
   factor_gauss(1,1,2)=1-0.339981043584856;
   factor_gauss(1,1,3)=1+0.339981043584856;
   factor_gauss(1,1,4)=1+0.861136311594053;

   weight_gauss(1,1,1)=0.347854845137454*0.5*Length;
   weight_gauss(1,1,2)=0.652145154862546*0.5*Length;
   weight_gauss(1,1,3)=0.652145154862546*0.5*Length;
   weight_gauss(1,1,4)=0.347854845137454*0.5*Length;

   for f=1:4;
```

```
        if (Moment(1,j)*0.5*factor_gauss(1,1,f))<Moment(1,2);

curvat_gauss(1,j,f)=curvat(1,2)/Moment(1,2)*(Moment(1,j)*0.5*factor_gauss(1,1,
f));
        else

curvat_gauss(1,j,f)=fnval(MomCurRel,(Moment(1,j)*0.5*factor_gauss(1,1,f)));
        end
    end



deltaflex(1,j)=curvat_gauss(1,j)*weight_gauss(1,1,1)*Length*0.5*factor_gauss(1,1,1
);
    for f=2:4;

deltaflex(1,j)=deltaflex(1,j)+curvat_gauss(1,j,f)*weight_gauss(1,1,f)*0.5*Length*fac
tor_gauss(1,1,f);
    end

    deltaslip(1,j)=abs(bondslip(Strainis(1,j-1),fcu)-bondslip(Strainis((nrow+1),j-
1),fcu))*Length/(dcc-diamain);

    Force(1,j)=Moment(1,j)/Length;
    if fci(1,j-1)==0;
        deltashear(1,j)=delsh;
    else
        Ec(1,j)=fci(1,j-1)/Strainic(1,j-1);
        deltashear(1,j)=Force(1,j)/0.4/0.8/buc/duc/Ec(1,j);
        delsh=deltashear(1,j);
    end
    delta(1,j)=deltaflex(1,j)+deltaslip(1,j)+deltashear(1,j);
    Forcedelta(1,j)=(Moment(1,j)-abs(Fc)*delta(1,j))/Length;

end
[MaxForce locMaxForce]=max(Force);
[MaxForcedel locMaxForcedel]=max(Forcedelta);

appyiedelta=MaxForce/Force(1,21)*delta(1,21); % To locate the apparent yield
deflection
appyiedelta75=0.75*appyiedelta;

MaxForcedel80=0.8*MaxForcedel;

delForRelb4max=csapi(delta(1:locMaxForce),Force(1:locMaxForce)); % to correlate
the curve with cubic spline
```

```
FordeldelRelaftmax=csapi(Forcedelta(locMaxForcedel:nointcur+1),delta(locMaxForcedel:nointcur+1));

appyieForce75=fnval(delForRelb4max,appyiedelta75);
deltault=fnval(FordeldelRelaftmax,MaxForcedel80);


figure(1);
plot(curvat,Moment/10^6),title('Moment against curvature 0.6P T6@61 f_{c}=37','FontSize',14),xlabel('curvature (mm^{-1})','FontSize',16),ylabel('Moment (kNm)','FontSize',16);
set(gca,'FontSize',14);
print('-f1','-dmeta','Moment vs Cur 06P0661 fcu 37 b')
figure(2)
plot(delta,Force/10^3),title('Force against deflection 0.6P T6@61 f_{c}=37','FontSize',14),xlabel('deflection (mm)','FontSize',16),ylabel('Force (kN)','FontSize',16);
text(delta(1,2),Force(1,2)/10^3,'\Leftarrow','FontSize',12);
text(delta(1,21)+5,Force(1,21)/10^3,sprintf('(%2.4f,%2.0f)',[delta(1,21) Force(1,21)/10^3]),'FontSize',10);
text(appyiedelta75,appyieForce75/10^3,sprintf('(%2.4f,%2.0f)',[appyiedelta75 appyieForce75/10^3]),'FontSize',10);
hold on;
set(gca,'YLim',[0 max(Force/10^3)*1.1]);
set(gca,'FontSize',14);
set(gca,'XLim',[0 60]);
plot(delta,Forcedelta/10^3,'r--');legend('without P-delta effect','with P-delta effect',4);
text(deltault,MaxForcedel80/10^3,sprintf('(%2.4f,%2.0f)',[deltault MaxForcedel80/10^3]),'FontSize',10);
print('-f2','-dmeta','F vs d 06P0661 fcu 37 b');
hold off;

ForceStorage06P0661fcu37b(:,1)=curvat';
ForceStorage06P0661fcu37b(:,2)=Moment';
ForceStorage06P0661fcu37b(:,3)=delta';
ForceStorage06P0661fcu37b(:,4)=Force';
ForceStorage06P0661fcu37b(:,5)=Forcedelta';
xlswrite('Force Storage 06P0661 fcu 37 b.xls',ForceStorage06P0661fcu37b);
```

Function of Moment Curvature

```
function [curvatresult neutd3 Ecia]=Mom(Strain,InpMom,curvatmax,Mommax)
clear curvatresult neutd3 Ecia;
fcu=-35;
buc=320;
duc=320;
```

```
cover=16;
diashear=4; %%
Spac=120;%%
fct=1.4*(abs(fcu)/10)^(2/3);
straincra=fct/2/abs(fcu)*0.002;
diamain=16;
phor=pi()*diashear^2/4*4/Spac/buc;
bcc=buc-cover*2-diashear;
dcc=duc-cover*2-diashear;
bcov=cover+diashear/2;
dcov=cover+diashear/2;
nrow=5;
Loadadd=-1044;
loadrat=Loadadd/fcu/buc/duc*1000; %Load ratio 0.55 for
Fc=loadrat*fcu*buc*duc;
Ast=pi()*nrow*(nrow-1)/4*diamain^2;
Asti=pi()/4*diamain^2;
Ac=bcc*dcc-Ast;
Auc=2*(buc-bcov)*dcov+2*(duc-dcov)*bcov;
epsilonsty=0.0027;
nointcur=8; %%L35A 330 L61A 190 L120B Use Moment4_06Pu
Length=570;
Mealength=815;
Este=200*10^3;
noyiediv=4;

ndiameter(1,1)=nrow+1;
parfor i=2:nrow;
   ndiameter(i,1)=2;
end
ndiameter((nrow+1),1)=nrow+1;
intdismain=(dcc-diamain-diashear)/nrow;

parfor i=1:(nrow+1);
   ddiamain(i,1)=cover+diashear+diamain/2+intdismain*(i-1);
end

% To divide the confined concrete section into n by m
n=140; % 560 is the best grid
wic=dcc/n;
parfor i=1:n+1;
   dic(i,1)=(i-1)*dcc/n+dcov;
   bic(i,1)=wic;
end
```

```
% To divide the unconfined concrete section on compressive side () and tension (2)
into n by m
m=10; % 40 is the best grid
wicov=dcov/m;
parfor i=1:m+1;
   dicov(i,1)=(i-1)*dcov/m;
   dicov2(i,1)=dcov+dcc+(i-1)*dcov/m;
   bicov(i,1)=wicov;
end

%Strain=-5.348237515540860*10^-4;
%InpMom=3*10^8; %0.06
%curvatmax=4.761414408614897*10^-5; %4.251262864834729*10^-7;
%Mommax=3.24*10^8;

Momenta(1,1)=0;
Momenta(1,2)=Mommax;

curvatt(1,1)=0;
curvatt(1,2)=curvatmax;

parfor j=1:2;
   errMom(1,j)=Momenta(1,j)-InpMom;
end;

if abs(errMom(1,1))<abs(errMom(1,2));
   errMom3(1,1)=errMom(1,1);
else
   errMom3(1,1)=errMom(1,2);
end

while abs(errMom3(1,1))>0.000001
   curvattrial=(curvatt(1,1)+curvatt(1,2))/2;
   if InpMom>=3*10^6
     neutd3=buc;
   elseif InpMom>=2.82*10^5
     neutd3=buc*50;
   else
     neutd3=buc*5*10^2;
   end
   parfor i=1:m+1;
      Strainiuaca(i,1)=Strain+curvattrial*(dicov(i,1)-neutd3);
      fucaia(i,1)=Uncon(Strainiuaca(i,1),fcu);
      Fuconaa(i,1)=fucaia(i,1)*duc;
   end
   Fuconcraa(1,1)=Fuconaa(1,1);
```

```
for i=2:2:m
   Fuconcraa(1,1)=Fuconcraa(1,1)+4*Fuconaa(i,1);
end
for i=3:2:m-1
   Fuconcraa(1,1)=Fuconcraa(1,1)+2*Fuconaa(i,1);
end
Fuconcraa(1,1)=Fuconcraa(1,1)+Fuconaa(m+1,1);
Fuconcraa(1,1)=dcov/3/m*Fuconcraa(1,1);

parfor i=1:m+1;
   Strainiubca(i,1)=Strain+curvattrial*(dicov2(i,1)-neutd3);
   fucbia(i,1)=Uncon(Strainiubca(i,1),fcu);
   Fuconba(i,1)=fucbia(i,1)*duc;
end
Fuconcrba(1,1)=Fuconba(1,1);
for i=2:2:m
   Fuconcrba(1,1)=Fuconcrba(1,1)+4*Fuconba(i,1);
end
for i=3:2:m-1
   Fuconcrba(1,1)=Fuconcrba(1,1)+2*Fuconba(i,1);
end
Fuconcrba(1,1)=Fuconcrba(1,1)+Fuconba(m+1,1);
Fuconcrba(1,1)=dcov/3/m*Fuconcrba(1,1);

parfor i=1:n+1;
   Strainica(i,1)=Strain+curvattrial*(dic(i,1)-neutd3);
   fcia(i,1)=CCon(Strainica(i,1),fcu);
   funconia(i,1)=Uncon(Strainica(i,1),fcu);
   Fcona(i,1)=fcia(i,1)*bcc+funconia(i,1)*bcov*2*bic(i,1);
end
Fconacra(1,1)=Fcona(1,1);
for i=2:2:n
   Fconacra(1,1)=Fconacra(1,1)+4*Fcona(i,1);
end
for i=3:2:n-1
   Fconacra(1,1)=Fconacra(1,1)+2*Fcona(i,1);
end
Fconacra(1,1)=Fconacra(1,1)+Fcona(n+1,1);
Fconacra(1,1)=dcc/3/n*Fconacra(1,1);

parfor i=1:(nrow+1)
   Strainisa(i,1)=Strain+curvattrial*(ddiamain(i,1)-neutd3);
   fsia(i,1)=Steel(Strainisa(i,1))-CCon(Strainisa(i,1),fcu);
   Fstea(i,1)=fsia(i,1)*ndiameter(i,1)*Asti;
end
Fsteae(1,1)=Fstea(1,1);
```

```
for i=2:(nrow+1)
   Fsteae(1,1)=Fsteae(1,1)+Fstea(i,1);
end
espcurtta(1,1)=Fconacra(1,1)+Fsteae(1,1)+Fuconcraa(1,1)+Fuconcrba(1,1)-Fc;

neutd1=0;
if InpMom>=3*10^6
   neutd2=buc;
elseif InpMom>=2.82*10^5
   neutd2=buc*50;
else
   neutd2=buc*5*10^3;
end
while abs(espcurtta(1,1))>0.00000001;
     neutd3=(neutd1+neutd2)/2;

   parfor i=1:m+1;
      Strainiuaca(i,1)=Strain+curvattrial*(dicov(i,1)-neutd3);
      fucaia(i,1)=Uncon(Strainiuaca(i,1),fcu);
      Fuconaa(i,1)=fucaia(i,1)*duc;
   end
   Fuconcraa(1,1)=Fuconaa(1,1);
   for i=2:2:m
      Fuconcraa(1,1)=Fuconcraa(1,1)+4*Fuconaa(i,1);
   end
   for i=3:2:m-1
      Fuconcraa(1,1)=Fuconcraa(1,1)+2*Fuconaa(i,1);
   end
    Fuconcraa(1,1)=Fuconcraa(1,1)+Fuconaa(m+1,1);
    Fuconcraa(1,1)=dcov/3/m*Fuconcraa(1,1);

   parfor i=1:m+1;
      Strainiubca(i,1)=Strain+curvattrial*(dicov2(i,1)-neutd3);
      fucbia(i,1)=Uncon(Strainiubca(i,1),fcu);
      Fuconba(i,1)=fucbia(i,1)*duc;
   end
   Fuconcrba(1,1)=Fuconba(1,1);
   for i=2:2:m
      Fuconcrba(1,1)=Fuconcrba(1,1)+4*Fuconba(i,1);
   end
   for i=3:2:m-1
      Fuconcrba(1,1)=Fuconcrba(1,1)+2*Fuconba(i,1);
   end
   Fuconcrba(1,1)=Fuconcrba(1,1)+Fuconba(m+1,1);
   Fuconcrba(1,1)=dcov/3/m*Fuconcrba(1,1);
```

```
    parfor i=1:n+1;
      Strainica(i,1)=Strain+curvattrial*(dic(i,1)-neutd3);
      fcia(i,1)=CCon(Strainica(i,1),fcu);
      funconia(i,1)=Uncon(Strainica(i,1),fcu);
      Fcona(i,1)=fcia(i,1)*bcc+funconia(i,1)*bcov*2;
    end
    Fconacra(1,1)=Fcona(1,1);
    for i=2:2:n
      Fconacra(1,1)=Fconacra(1,1)+4*Fcona(i,1);
    end
    for i=3:2:n-1
      Fconacra(1,1)=Fconacra(1,1)+2*Fcona(i,1);
    end
    Fconacra(1,1)=Fconacra(1,1)+Fcona(n+1,1);
    Fconacra(1,1)=dcc/3/n*Fconacra(1,1);

    parfor i=1:(nrow+1)
      Strainisa(i,1)=Strain+curvattrial*(ddiamain(i,1)-neutd3);
      fsia(i,1)=Steel(Strainisa(i,1))-CCon(Strainisa(i,1),fcu);
      Fstea(i,1)=fsia(i,1)*ndiameter(i,1)*Asti;
    end
      Fsteae(1,1)=Fstea(1,1);
      for i=2:(nrow+1)
        Fsteae(1,1)=Fsteae(1,1)+Fstea(i,1);
      end

espcurtta(1,1)=Fconacra(1,1)+Fsteae(1,1)+Fuconcraa(1,1)+Fuconcrba(1,1)-Fc;

    if espcurtta(1,1)>0
      neutd1=neutd3;
    else
      neutd2=neutd3;
    end
  end

%To calculate the Momenta of the concrete and steel

   parfor i=1:n+1;
       MomentaC(i,1)=fcia(i,1)*bcc*(dic(i,1)-
duc/2)+funconia(i,1)*bcov*2*(dic(i,1)-duc/2);
   end
   Momentaconc(1,1)=MomentaC(1,1);
   for i=2:2:n
     Momentaconc(1,1)=Momentaconc(1,1)+4*MomentaC(i,1);
   end
   for i=3:2:n-1
```

```
    Momentaconc(1,1)=Momentaconc(1,1)+2*MomentaC(i,1);
  end
  Momentaconc(1,1)=Momentaconc(1,1)+MomentaC(n+1,1);
  Momentaconc(1,1)=dcc/3/n*Momentaconc(1,1);

  parfor i=1:m+1;
     MomentaUC1(i,1)=fucaia(i,1)*buc*(dicov(i,1)-duc/2);
  end
  MomentaUconc1(1,1)=MomentaUC1(1,1);
  for i=2:2:m
    MomentaUconc1(1,1)=MomentaUconc1(1,1)+4*MomentaUC1(i,1);
  end
  for i=3:2:m-1
    MomentaUconc1(1,1)=MomentaUconc1(1,1)+2*MomentaUC1(i,1);
  end
  MomentaUconc1(1,1)=MomentaUconc1(1,1)+MomentaUC1(m+1,1);
  MomentaUconc1(1,1)=dcov/3/m*MomentaUconc1(1,1);

  parfor i=1:m+1;
     MomentaUC2(i,1)=fucbia(i,1)*buc*(dicov2(i,1)-duc/2);
  end
  MomentaUconc2(1,1)=MomentaUC2(1,1);
  for i=2:2:m
    MomentaUconc2(1,1)=MomentaUconc2(1,1)+4*MomentaUC2(i,1);
  end
  for i=3:2:m-1
    MomentaUconc2(1,1)=MomentaUconc2(1,1)+2*MomentaUC2(i,1);
  end
  MomentaUconc2(1,1)=MomentaUconc2(1,1)+MomentaUC2(m+1,1);
  MomentaUconc2(1,1)=dcov/3/m*MomentaUconc2(1,1);

  parfor i=1:(nrow+1)
     MomentaS(i,1)=fsia(i,1)*ndiameter(i,1)*Asti*(ddiamain(i,1)-duc/2);
  end
     Momentastee(1,1)=MomentaS(1,1);
  for i=2:(nrow+1);
    Momentastee(1,1)=Momentastee(1,1)+MomentaS(i,1);
  end

Momenta(1,1)=Momentaconc(1,1)+Momentastee(1,1)+MomentaUconc1(1,1)+M
omentaUconc2(1,1);

  errMom3(1,1)=Momenta(1,1)-InpMom;
  if errMom3(1,1)==0;
    curvatresult=curvattrial; return
  end
```

```
    if errMom3(1,1)<0;
        curvatt(1,1)=curvattrial;
        errMom(1,1)=errMom3(1,1);
    else
        curvatt(1,2)=curvattrial;
        errMom(1,2)=errMom3(1,1);
    end
end
if Strainica(1,1)==0;
    Ecia(1,1)=0;
else
   Ecia(1,1)=fcia(1,1)/Strainica(1,1);
end
curvatresult(1,1)=(curvatt(1,1)+curvatt(1,2))/2;
```

Bond Slip

```
function u=bondslip(Strain,fcu)
Strainhardenrat=0.0027;
E=200*10^3;
diabar=16;
Strainy=0.0027;
fcu=abs(fcu);
if abs(Strain)<=0.0027;
    Ldb=E*abs(Strain)*diabar/4/sqrt(fcu);
    u=0.5*Strain*Ldb;
else
    Ldi=Strainhardenrat*E*diabar*(abs(Strain)-Strainy)/4/0.5/sqrt(fcu);
    Ldy=E*Strainy*diabar/4/sqrt(fcu);
    u=(0.5*(abs(Strain)+Strainy)*Ldi+0.5*Strainy*Ldy)*Strain/abs(Strain);
end
```

Appendix 2 Reference Picture

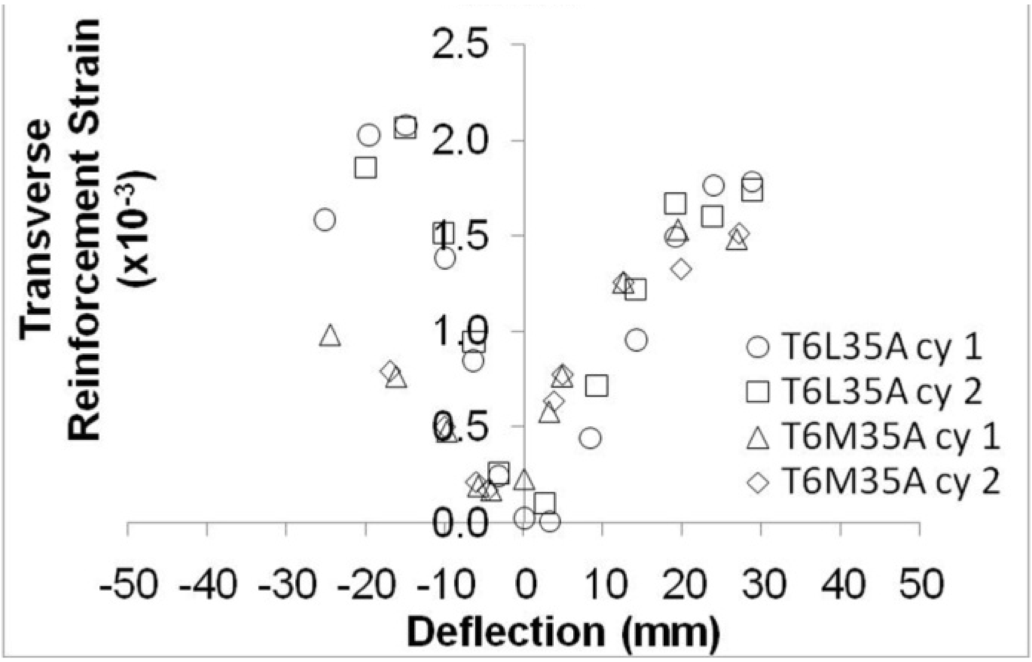

Figure A2-1 Transverse Reinforcement Strain against Deflection under Cyclic Loading at B1 for T6@35A

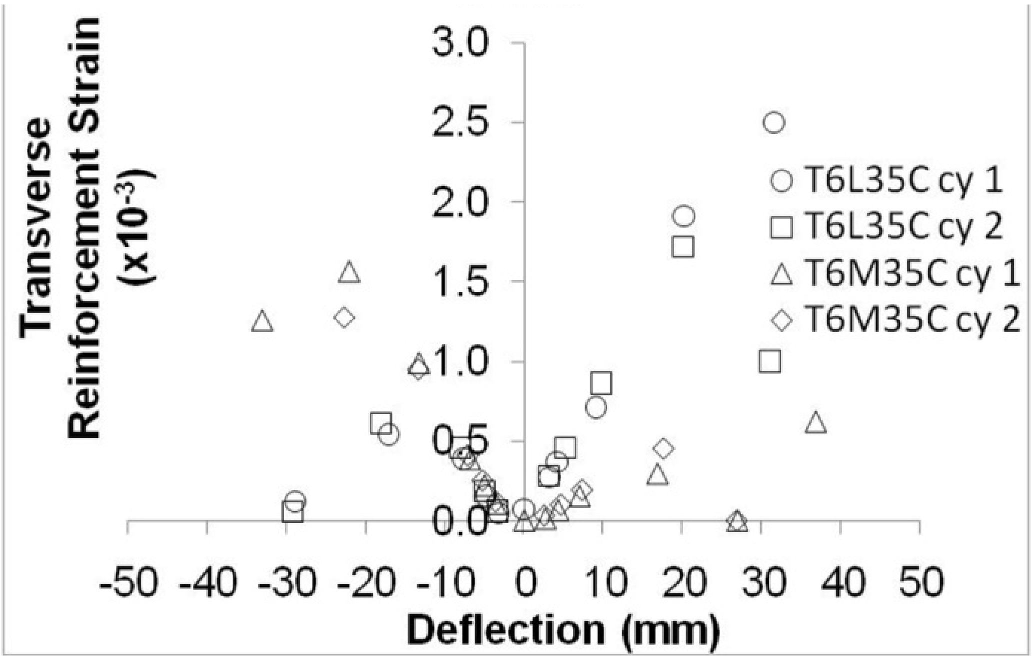

Figure A2-2 Transverse Reinforcement Strain against Deflection under Cyclic Loading at B1 for T6@35C

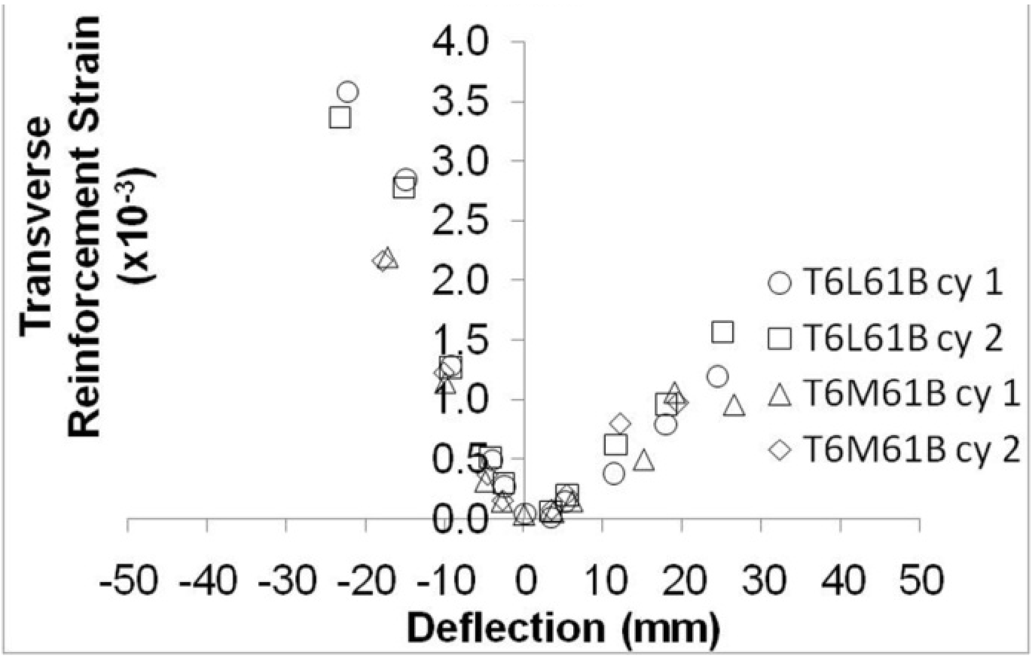

Figure A2-3 Transverse Reinforcement Strain against Deflection under Cyclic Loading at B1 for T6@61B

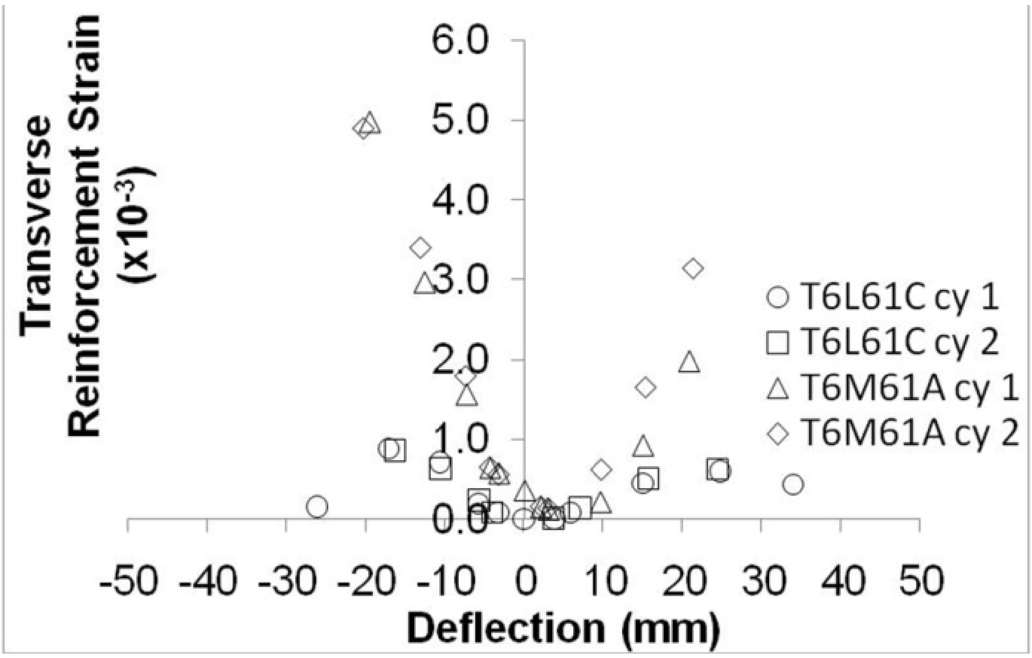

Figure A2-4 Transverse Reinforcement Strain against Deflection under Cyclic Loading at B1 for T6L61C and T6M61A

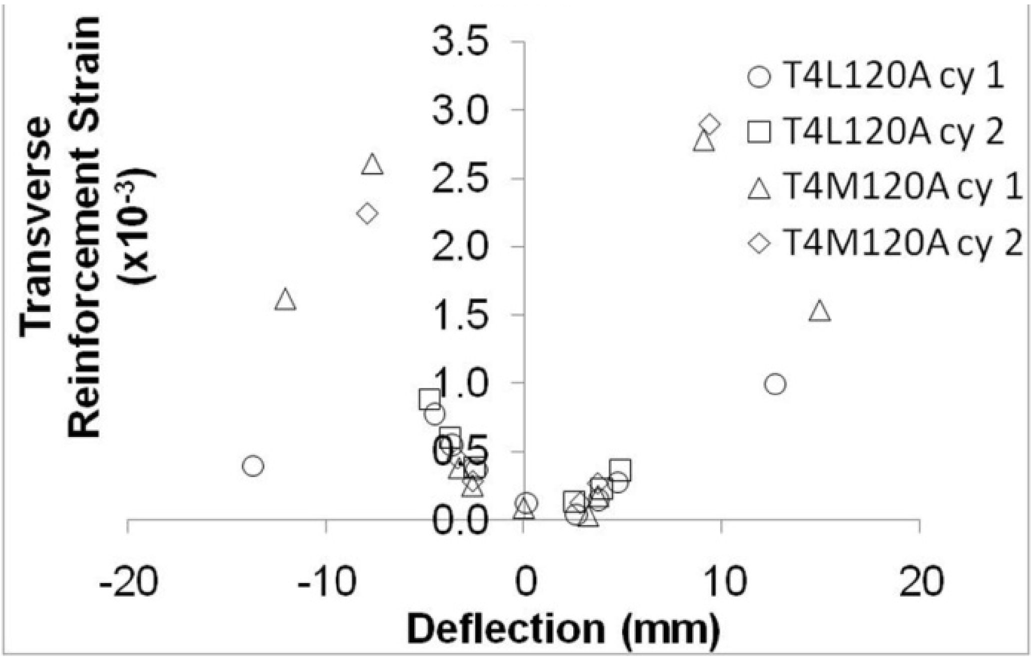

Figure A2-5 Transverse Reinforcement Strain against Deflection under Cyclic Loading at B1 for T4@120A

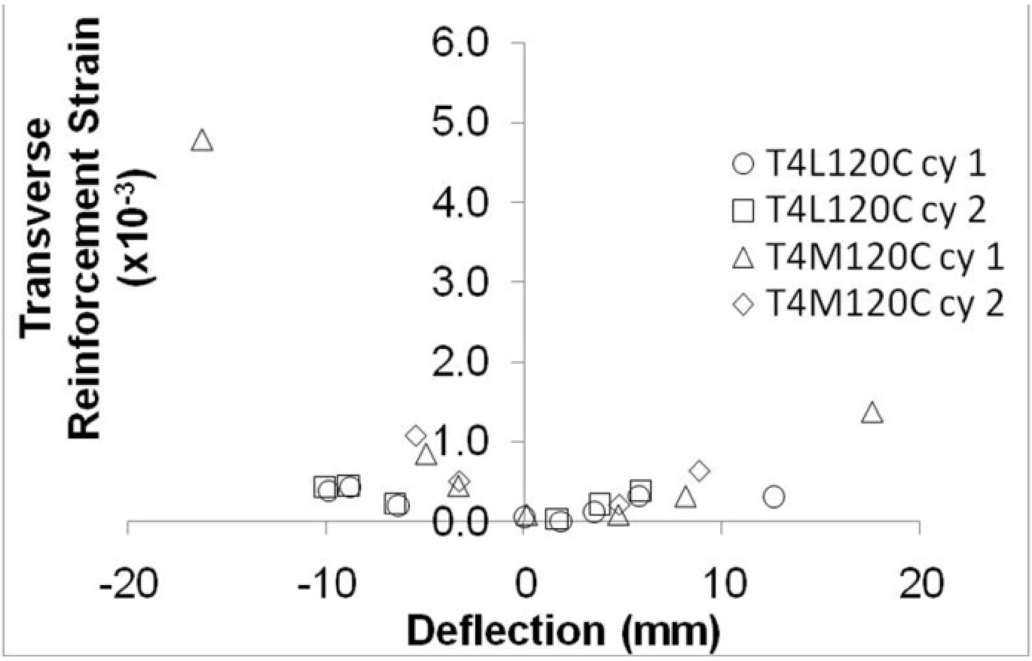

Figure A2-6 Transverse Reinforcement Strain against Deflection under Cyclic Loading at B1 for T4@120C

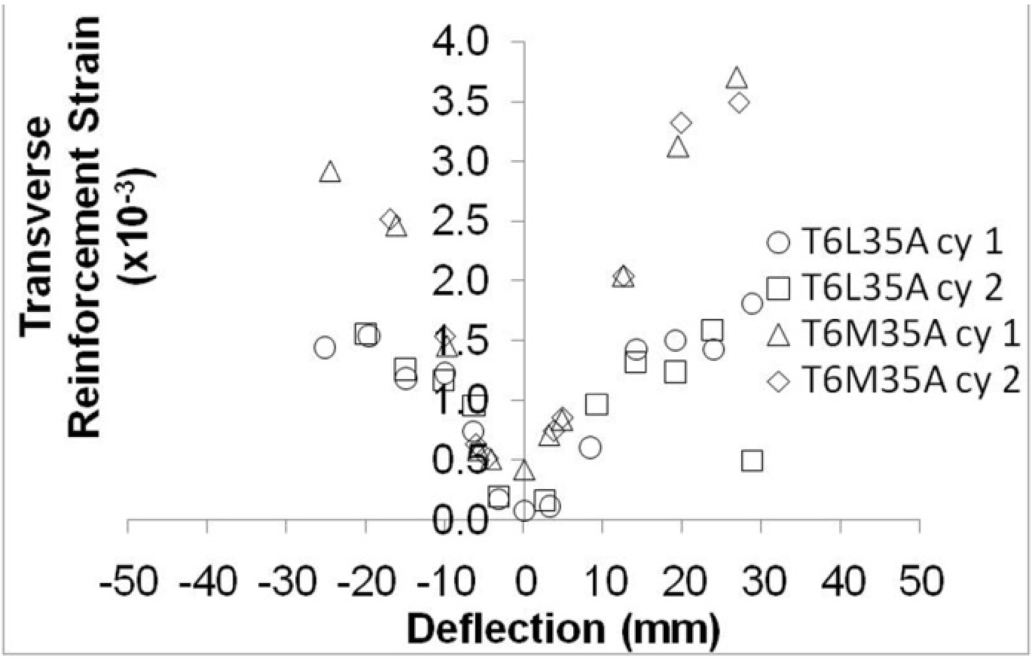

Figure A2-7 Transverse Reinforcement Strain against Deflection under Cyclic Loading at B2 for T6@35A

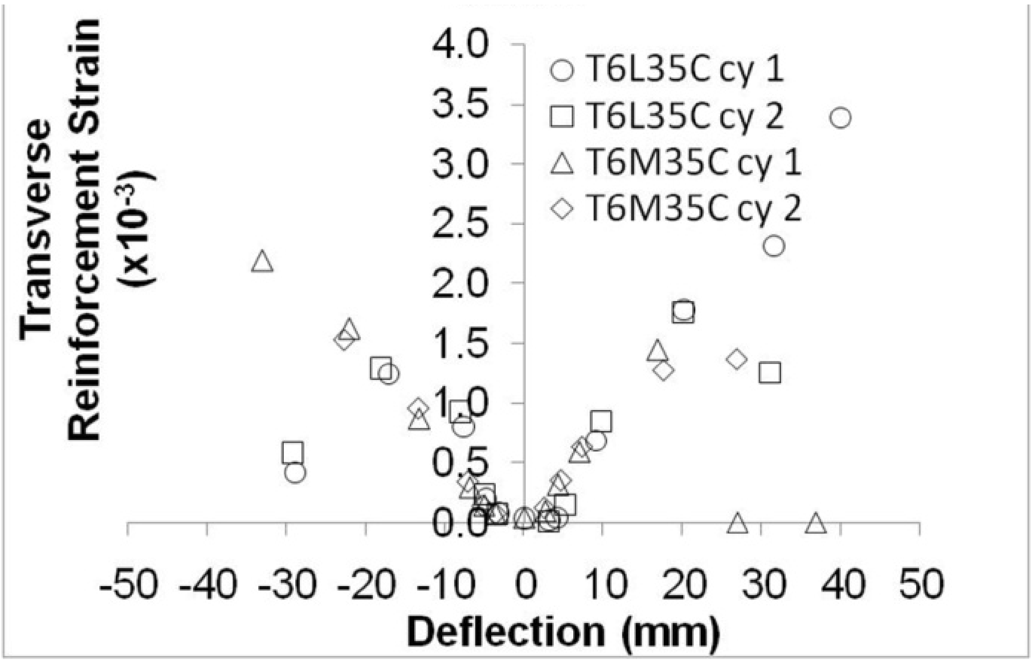

Figure A2-8 Transverse Reinforcement Strain against Deflection under Cyclic Loading at B2 for T6@35C

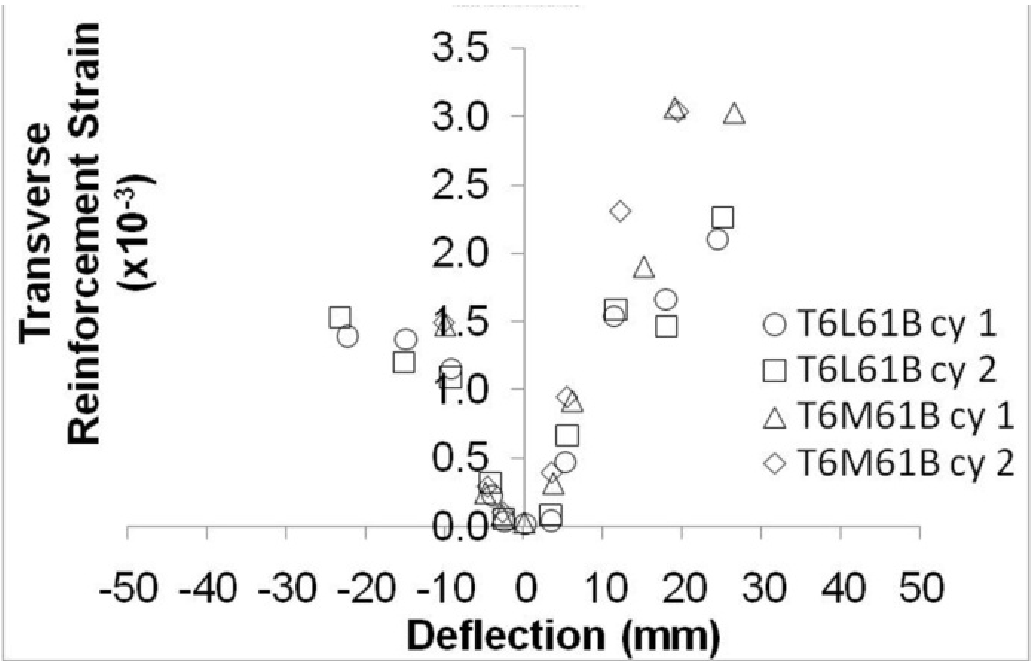

Figure A2-9 Transverse Reinforcement Strain against Deflection under Cyclic Loading at B2 for T6@61B

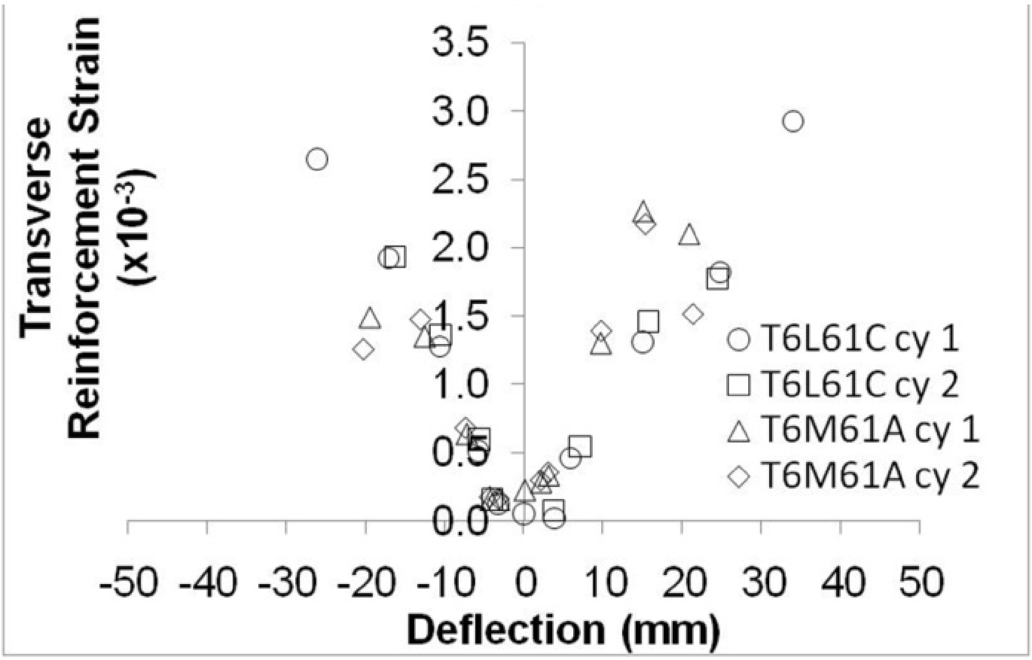

Figure A2-10 Transverse Reinforcement Strain against Deflection under Cyclic Loading at B2 for T6L61C and T6M61A

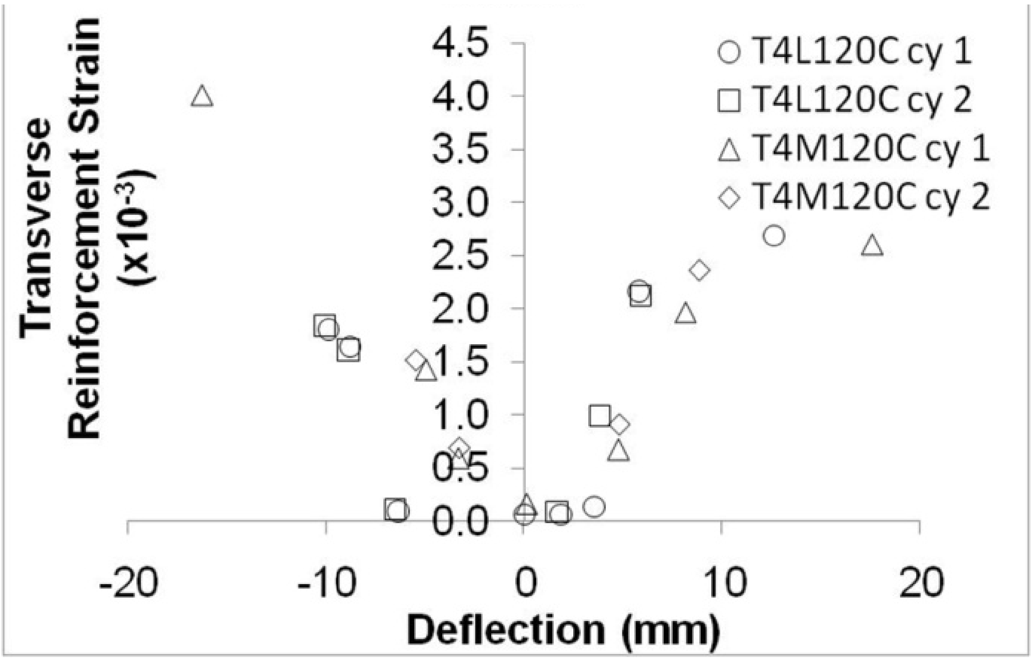

Figure A2-11 Transverse Reinforcement Strain against Deflection under Cyclic Loading at B2 for T4@120A

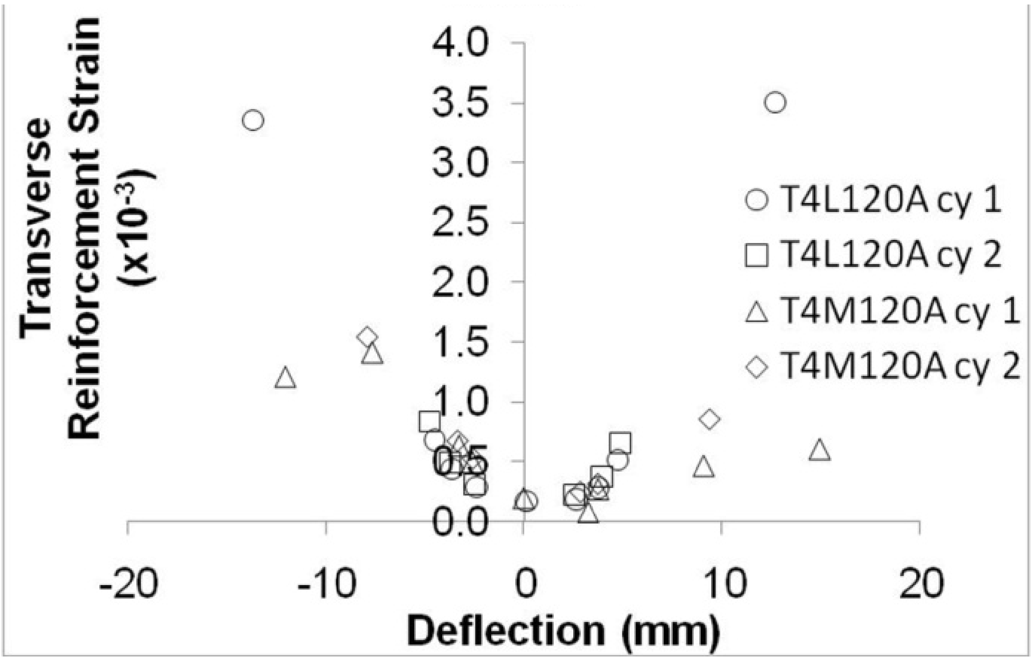

Figure A2-12 Transverse Reinforcement Strain against Deflection under Cyclic Loading at B2 for T4@120C

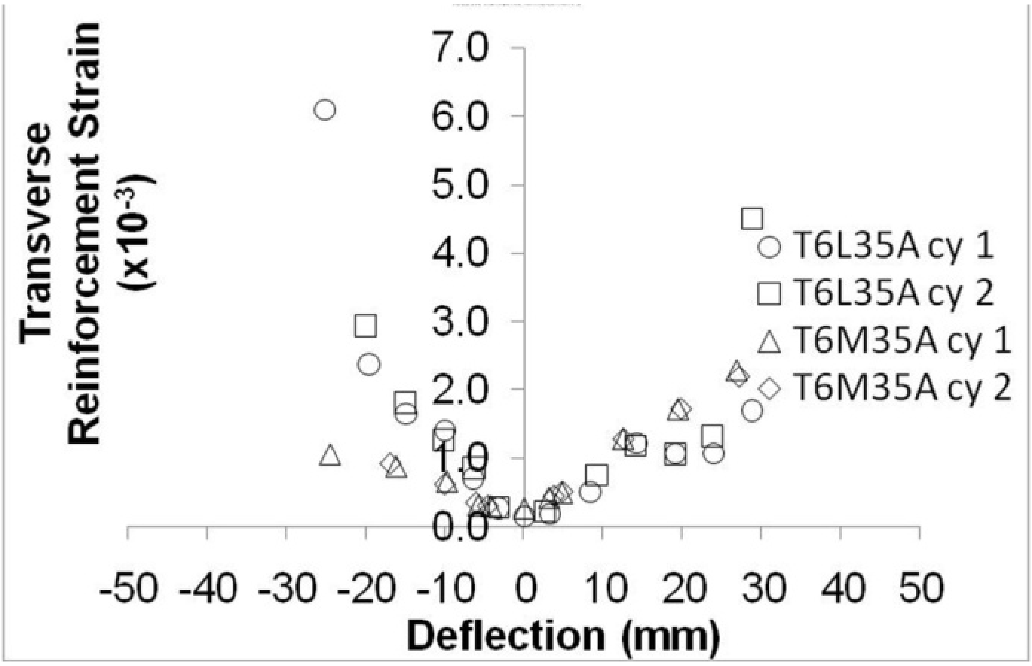

Figure A2-13 Transverse Reinforcement Strain against Deflection under Cyclic Loading at B3 for T6@35A

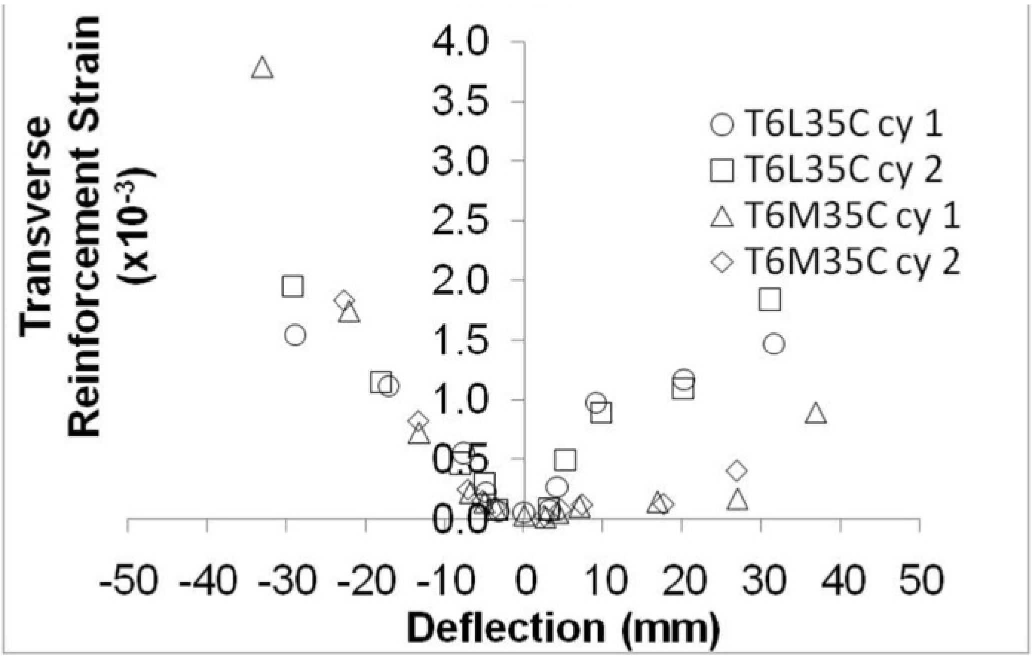

Figure A2-14 Transverse Reinforcement Strain against Deflection under Cyclic Loading at B3 for T6@35C

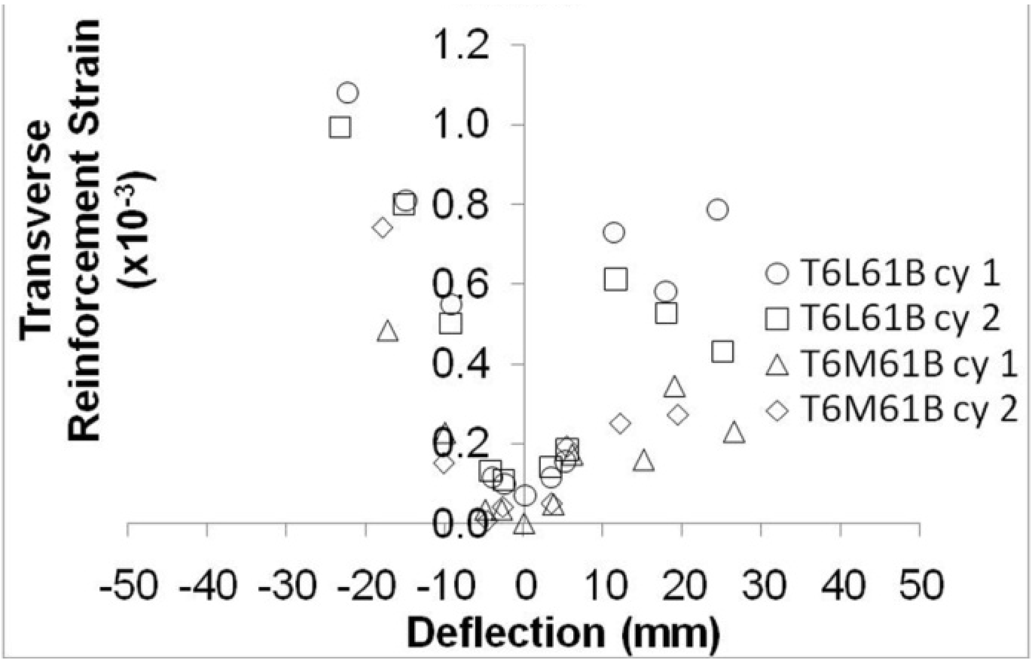

Figure A2-15 Transverse Reinforcement Strain against Deflection under Cyclic Loading at B3 for T6@61B

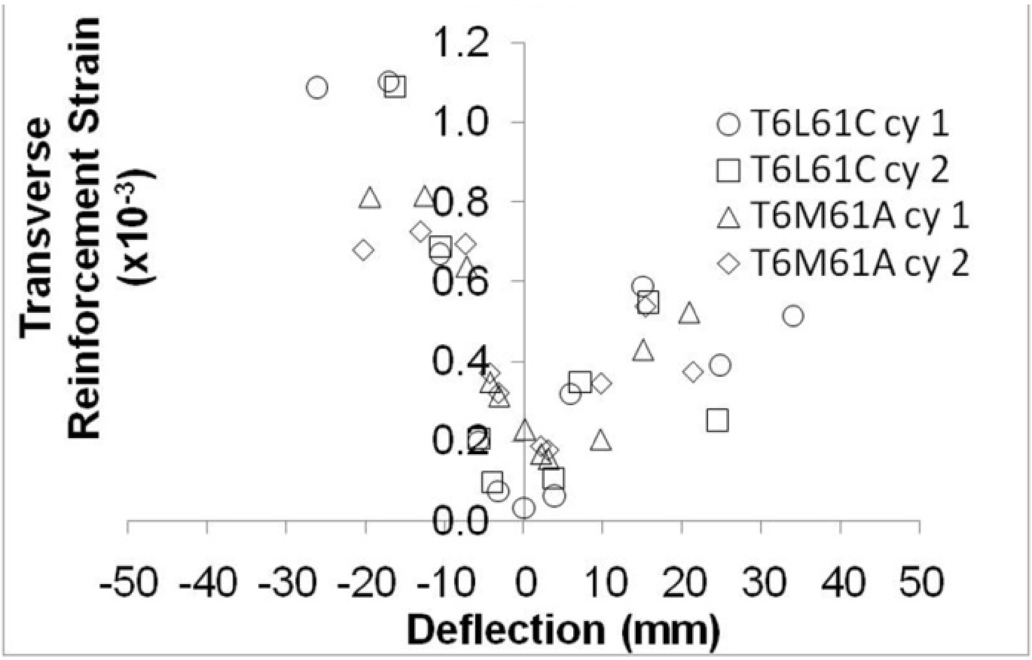

Figure A2-16 Transverse Reinforcement Strain against Deflection under Cyclic Loading at B3 for T6L61C and T6M61A

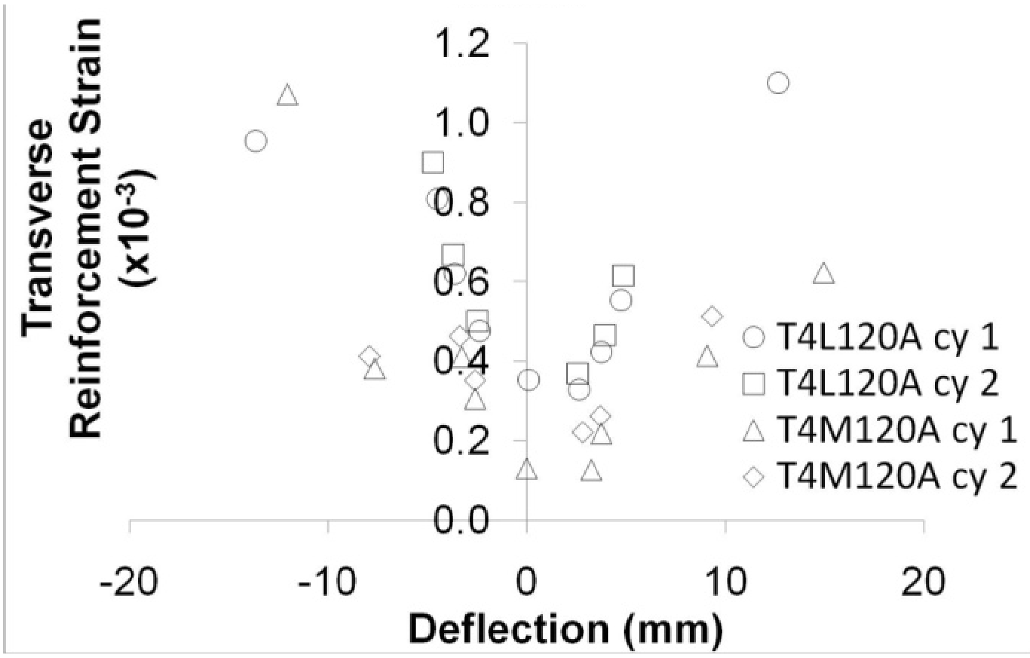

Figure A2-17 Transverse Reinforcement Strain against Deflection under Cyclic Loading at B3 for T4@120A

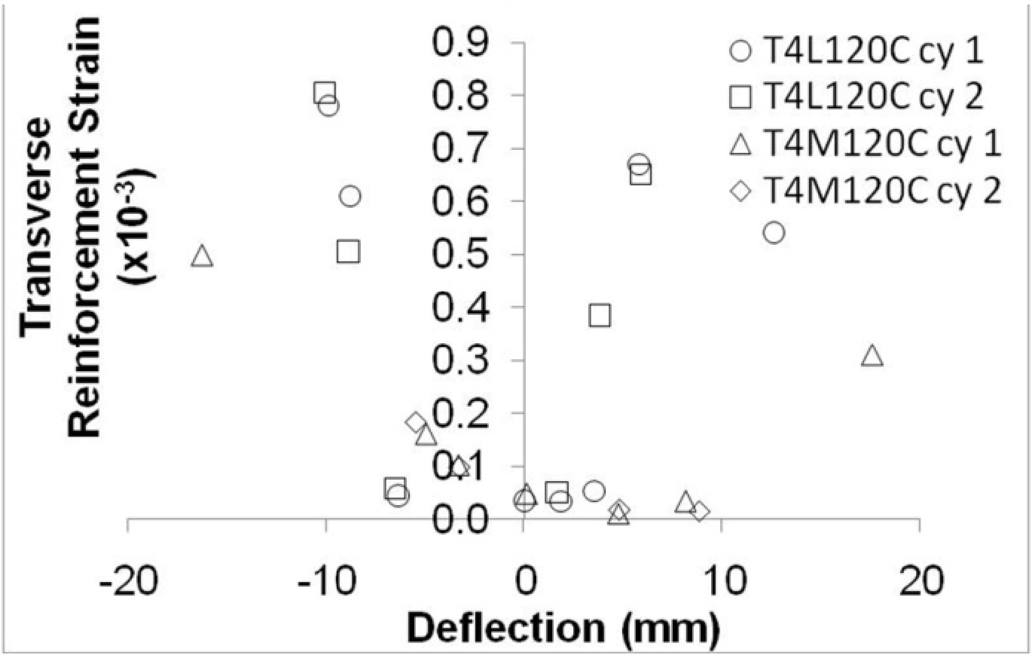

Figure A2-18 Transverse Reinforcement Strain against Deflection under Cyclic Loading at B3 for T4@120C

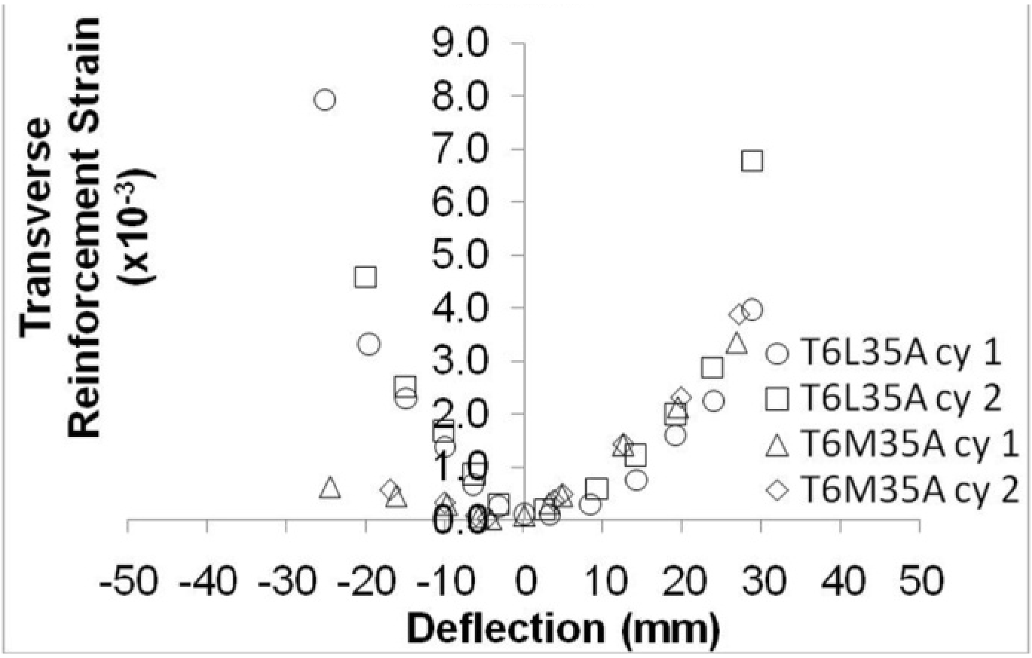

Figure A2-19 Transverse Reinforcement Strain against Deflection under Cyclic Loading at B4 for T6@35A

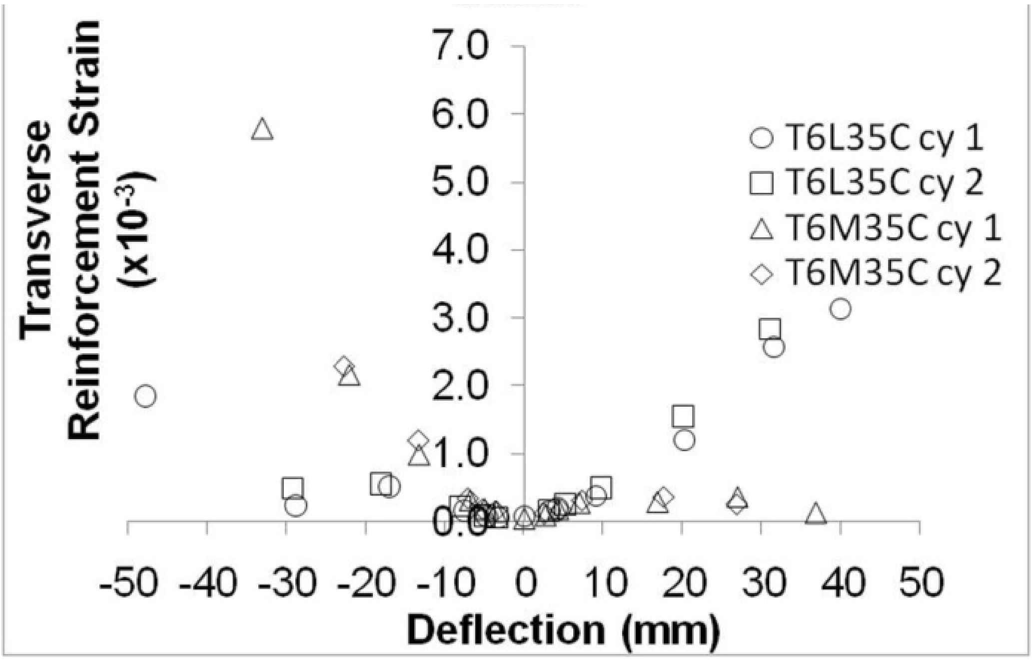

Figure A2-20 Transverse Reinforcement Strain against Deflection under Cyclic Loading at B4 for T6@35C

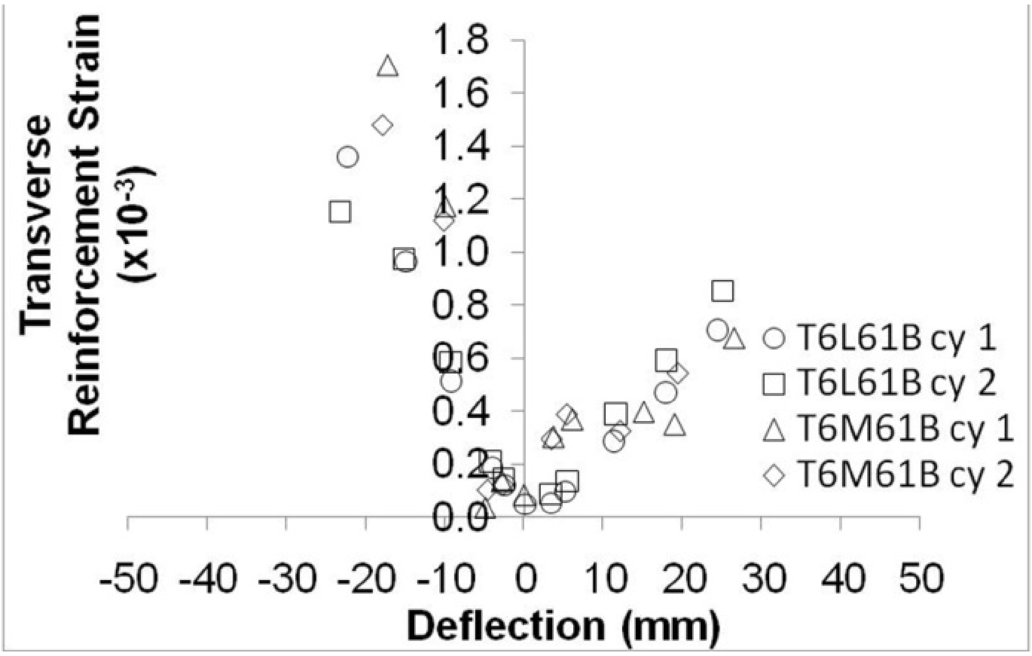

Figure A2-21 Transverse Reinforcement Strain against Deflection under Cyclic Loading at B4 for T6@61B

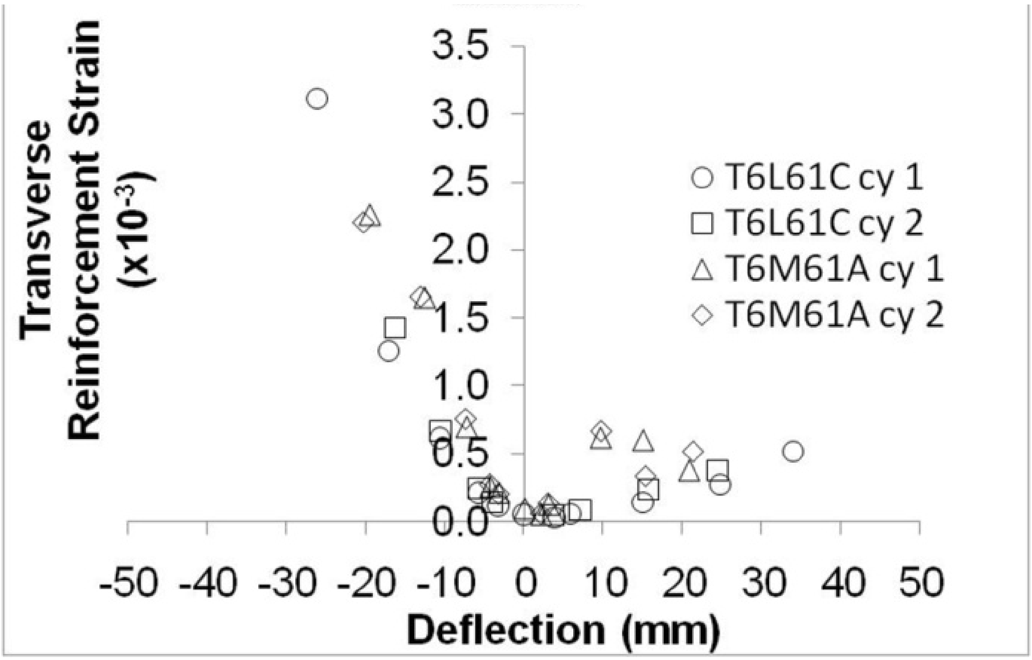

Figure A2-22 Transverse Reinforcement Strain against Deflection under Cyclic Loading at B4 for T6L61C and T6M61A

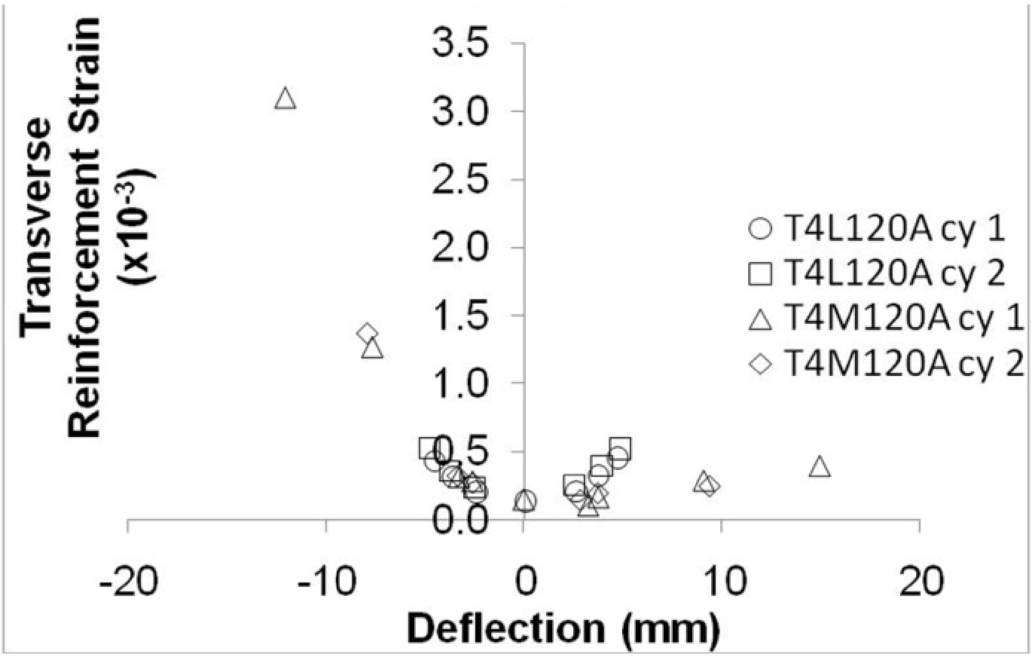

Figure A2-23 Transverse Reinforcement Strain against Deflection under Cyclic Loading at B4 for T4@120A

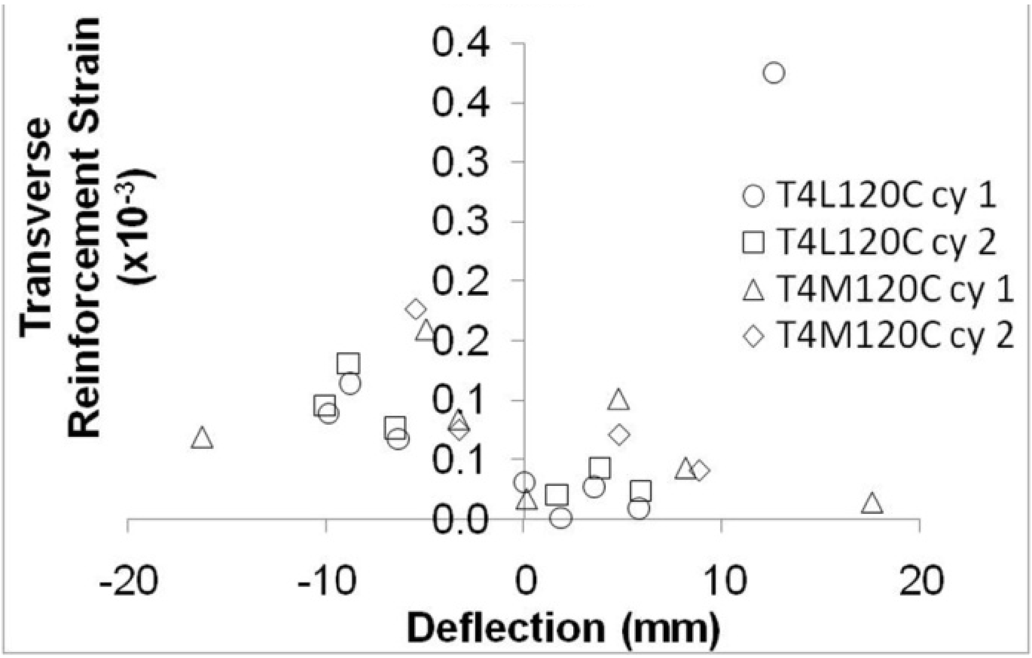

Figure A2-24 Transverse Reinforcement Strain against Deflection under Cyclic Loading at B4 for T4@120C

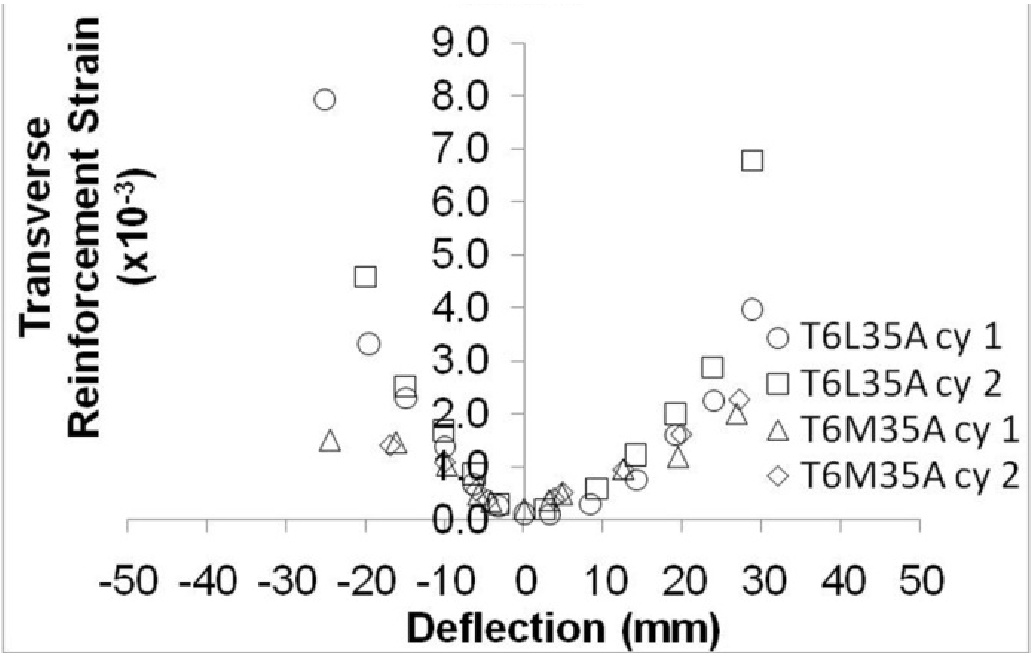

Figure A2-25 Transverse Reinforcement Strain against Deflection under Cyclic Loading at B5 at type M and B4 at type L for T6@35A

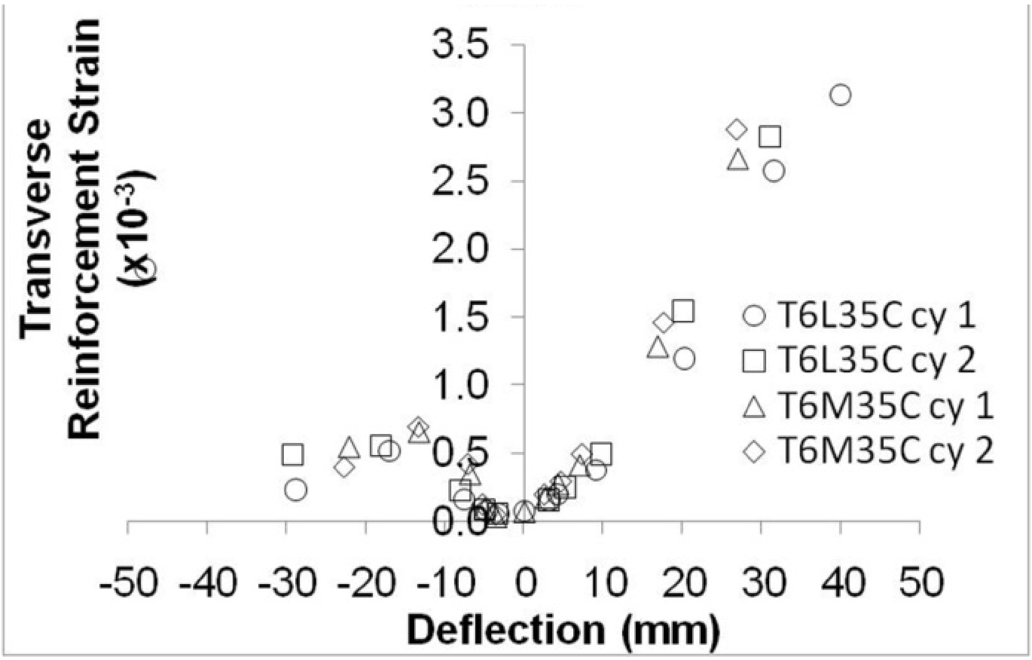

Figure A2-26 Transverse Reinforcement Strain against Deflection under Cyclic Loading at B5 at type M and B4 at type L for T6@35C

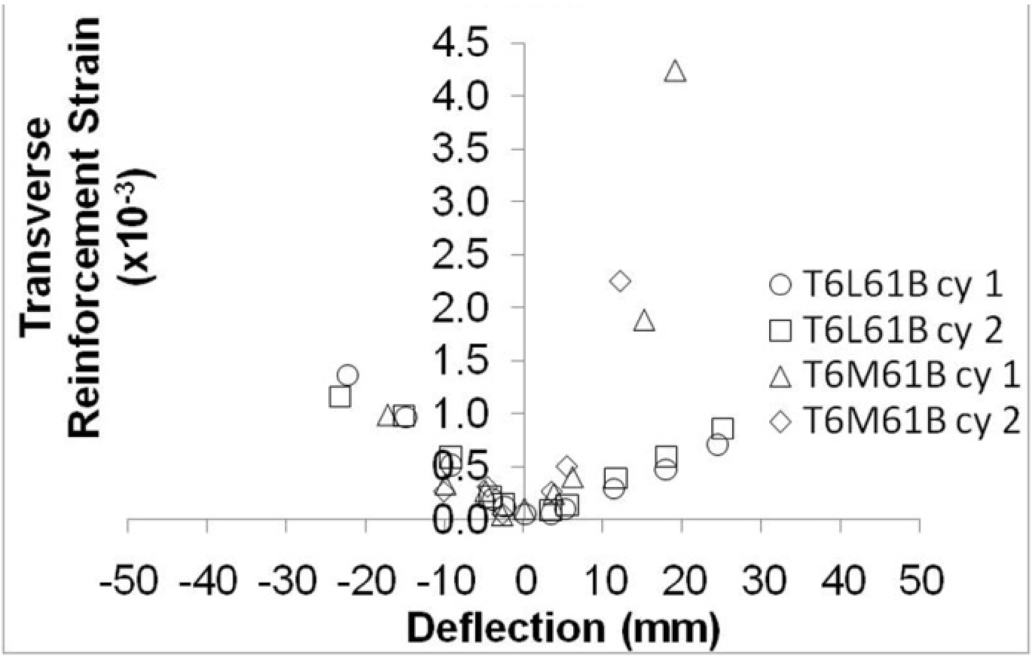

Figure A2-27 Transverse Reinforcement Strain against Deflection under Cyclic Loading at B5 at type M and B4 at type L for T6@61B

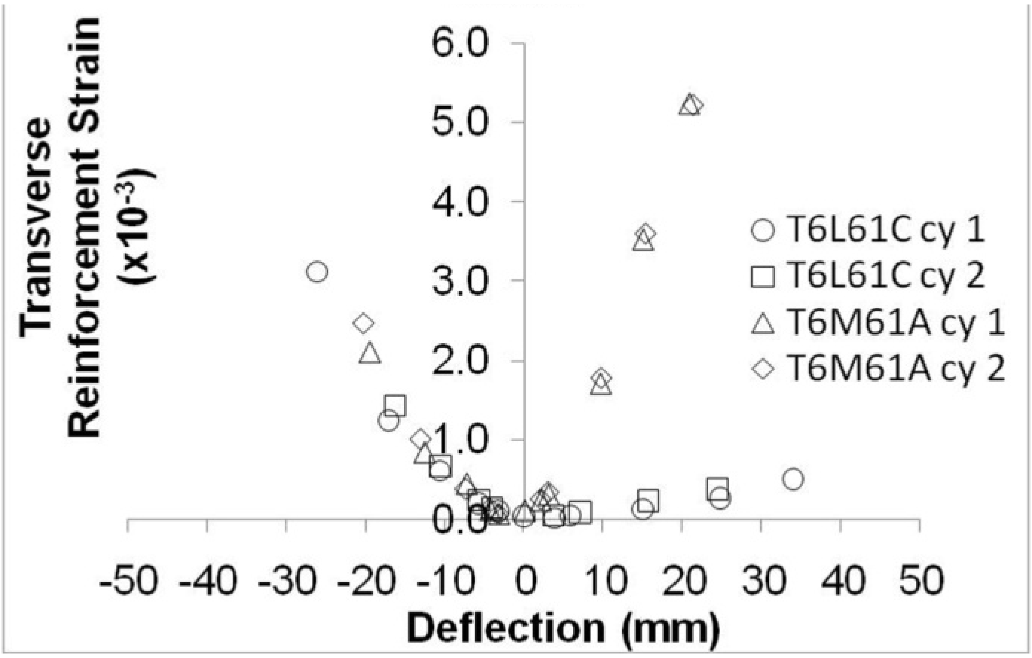

Figure A2-28 Transverse Reinforcement Strain against Deflection under Cyclic Loading at B5 at type M and B4 at type L for T6L61C and T6M61A

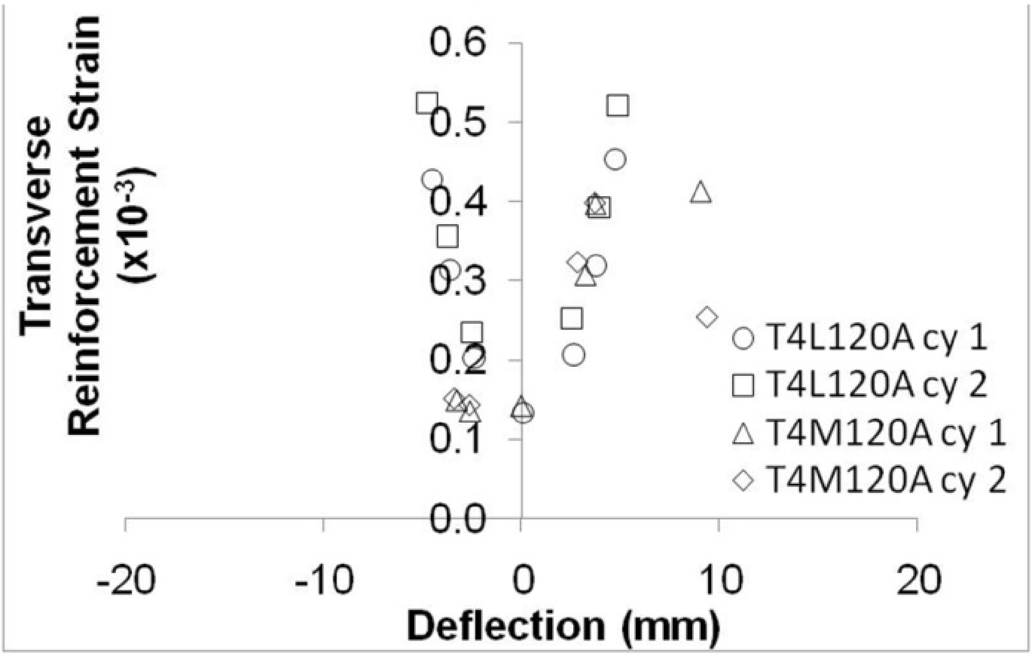

Figure A2-29 Transverse Reinforcement Strain against Deflection under Cyclic Loading at B5 at type M and B4 at type L for T4@120A

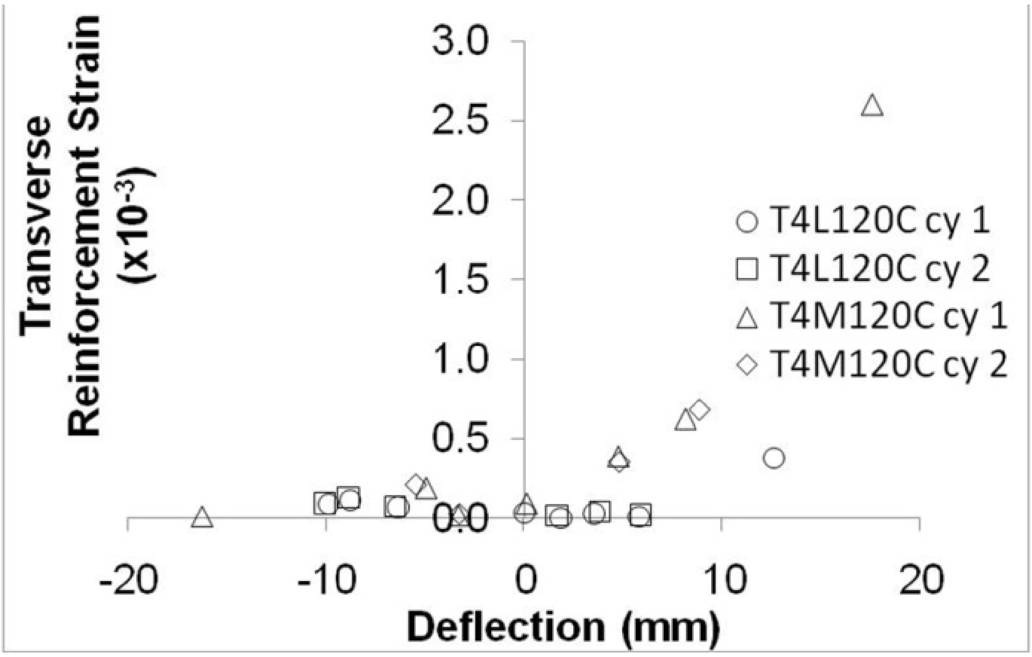

Figure A2-30 Transverse Reinforcement Strain against Deflection under Cyclic Loading at B5 at type M and B4 at type L for T4@120C

References

ACI 318-02 (2002), *Building Code Requirements for Structural Concrete (ACI 318-02) and Commentary (ACI 318R-02),* American Concrete Institute, Ch 10 & 21

AIJ Structural Design Guidelines for Reinforced Concrete Buildings (1994), Architectural Institute of Japan

Alsiwat J. and Saatcioglu M. (1992), "Reinforcement Anchorage Slip under Monotonic Loading", *Journal of Structural Engineering,* ASCE, Vol. 118, No 9, pp 2421-2438

Ang B. G., Priestley M.J.N. and Park R. (1981), *Ductility of Reinforced Concrete Bridge Piers under Seismic Loading, Report 81-3,* Department of Civil Engineering, University of Canterbury, Christchurch, New Zealand, February 1981, 109 pages

Atanda A. I. and Kuang J. S. (2004), "Inherent Ductility of Non-Seismically Designed and Detailed Reinforced Concrete Frame Buildings", *Transactions- Hong Kong Institution of Engineers,* Vol. 11, No. 3, pp 1-4

Au, F.T.K., Bai, B.Z.Z., and Kwan, A.K.H. (2005), "Complete Moment-Curvature Relationship of Reinforced Normal- and High-Strength Concrete Beams

Experiencing Complex Load History" *Computers and Concrete*, Vol.2 No.4, pp 309-324

Au F.T.K. and Bai Z.Z. (2007), “Two-dimensional Nonlinear Finite Element Analysis of Monotonically and Non-reversed Cyclically Loaded RC Beams”, *Engineering Structures*, Vol. 29,No. 11, pp2921-2934

Azizinamini A., Corley W.G. and Johal L.S.P. (1992), “Effects of Transverse Reinforcement on Seismic Performance of Columns”, *ACI Structural Journal,* Vol. 89, No. 4, pp 442-450

Bae S. and Bayrak O. (2008) “Plastic Hinge Length of Reinforced Concrete Columns”, *ACI Structural Journal,* Vol. 105, No. 3, pp 290-300

Bai Z.Z. and Au F.T.K. (2007), “Two-dimensional Nonlinear Finite Element Analysis of Monotonically and Non-reversed Cyclically Loaded RC Beams”, *Engineering Structures*, Vol. 29, No. 11, pp2921-2934

Bazant Z.P. and Bhat P.D. (1977), “Prediction on Hysteresis of Reinforced Concrete Members”, *Journal of Structural Division, ASCE,* Vol. 103 pp153-166

Baker A.L.L. and Amarkone A. M. N., (1964), “Inelastic Hyper-static Frames Analysis”, *Proceedings of the International Symposium on the Flexural Mechanics of Reinforced Concrete*, ASCE-ACI, Miami, November, pp 85-142

Bangash (2001) *Manual of Numerical Methods in Concrete*, Thomas Telford

Bousalem B. and Chikh N. (2007) "Development of a Confined Model for Rectangular Ordinary Reinforced Concrete Columns", *Materials and Structures*, Vol. 40, No. 6, pp 605-613

BS8110-1985 *British Standard Structural Use of Concrete (1985)*, British Standards Institution

BS EN 1998-1 (2004), *Eurocode 8: Design of Structures for Earthquake Resistance-Part 1: General Rules, Seismic Action and Rules for Buildings*, European Committee for Standardization

BS EN 1998-2 (2005), *Eurocode 8: Design of Structures for Earthquake Resistance-Part 2: Bridges*, European Committee for Standardization

BS EN 1998-3 (2005), *Eurocode 8: Design of Structures for Earthquake Resistance-Part 3: Assessment and Retrofitting of Buildings*, European Committee for Standardization

BS EN 10002-1 (2001), *Metallic Materials-Tensile Testing-Part 1: Methods of test at ambient temperature*, European Committee for Standardization

Calderone A.J., Lehmen D.E., Moehle J.P. (2000) *Behavior of Reinforced Concrete Bridge Columns Having Varying Aspect Ratios and Varying Lengths of Confinement*, Pacific Earthquake Engineering Research Center,

Code for Design of Concrete Structures GB50010-2001, (2002), China Architecture and Building Press, PRC

Code for Seismic Design of Buildings GB50011-2001, (2002), China Architecture and Building Press, PRC

Code of Practice for the Structural Use of Concrete-1987, Building Authority of Hong Kong, Cl.3.3.1 (2)a, pp27

Code of Practice for the Structural Use of Concrete-2004, Building Authority of Hong Kong, pp199

Chan C.M. and Zou X.K. (2004), "Elastic and Inelastic Drift Performance Optimization for Reinforced Concrete Buildings under Earthquake Loads", *Earthquake Engineering and Structural Dynamics*, Vol. 33, No 8, July, 2004, pp 929-950

Chan K.M. (2001), *Ultimate Strength of Reinforced Concrete Columns with Different Arrangement of Transverse reinforcement,* BEng Thesis, Department of Civil and Structural Engineering, The Hong Kong Polytechnic University

Chandler A.M. and Lam N.T.K. (2002), "Scenario Predictions for Potential Near-Field and Far-Field Earthquakes Affecting Hong Kong: soil sites", *Journal of Soil Dynamics & Earthquake Engineering*, Vol. 22, No. 6, pp 419-440

Chau K.T., Wong Y.L., Lam E.S.S. and Lee C.M. (1998), *Seismic Risk Assessment for Hong Kong,* CIDARC, The Hong Kong Polytechnic University

Chen A, Li CS, Lam E.S.S., Wong YL, "Testing of a Transfer Plate by Pseudo-Dynamic Test Method with Substructure Technique", Advances in Building Technology, Vols. I and II, Proceedings, pp 731-738

Chung Y.S., Meyer C. and Shinozuka M. (1987), *Seismic Damage Assessment of Reinforced Concrete Members,* Department of Civil and Engineering Mechanics, Columbia University, New York, NCEER 87-0022

El-Dash K.M. and El-Mahdy (2004), "Modeling the Stress-Strain Behavior of Confined Concrete Columns", *International Symposium on Confined Concrete, SP238,* American Concrete Institute

Erduran E. and Yakut A. (2007), "Component Damage Functions for Reinforced Concrete Frame Structures", *Engineering Structures*, Vol. 29, No. 9, pp 2242-2253

Eligehausen R., Popov E.P. and Bertero V.V. (1983), *Local Bond Stress-Slip Relationships of Deformed Bars under Generalized Excitations,* Report No. UCB/EERC-83/23, Earthquake Engineering Research Center, University of California, Berkeley, Oct. 1983. 169 pages

Fafitis A. and Shah S.P. (1985),"Prediction of Ultimate Behavior of Confined Columns Subjected to Large Deformations", *ACI Journal*, Vol. 82 pp423-433

Harris H.G, and Sahnis G.M. (1999), *Structural Modeling and Experimental Techniques*

Hindi R.A. and Sexsmith R.G. (2001) "A Proposed Damage Model for RC Bridge Column under Cyclic Loading", *Earthquake Spectra*, Vol. 17, No 2, pp 261-290

Ho J.C.M., Pam H.J. and Li J. (2000), "Strength Enhancement of Confined High-strength Reinforced Concrete Sections for Code Consideration", *Proceedings* *of the International Conference on Advances in Structural Dynamics*, Hong Kong, pp 651-658

Ho C.M.J. (2003), *Inelastic Design of Reinforced Concrete Beams and Limited Ductile High-Strength Concrete Columns*, PhD Thesis, Department of Civil Engineering, The University of Hong Kong

Ho J.C.M., and Pam H.J. (2003), "Influence of Transverse Steel Configuration on Post-Elastic Behaviour of High-Strength Reinforced Concrete Columns" *Transactions of the Hong Kong Institution of Engineers*, Vol. 10, No.2, pp 1-9

Ho J.C.M., Au F.T.K., and Kwan A.K.H. (2005), "Effects of Strain Hardening of Steel Reinforcement on Flexural Strength and Ductility of Concrete Beams" *Structural Engineering and Mechanics*, Vol. 19, No. 2, pp 185-19

Hognestad E. (1951), *Study of combined bending and axial load in reinforced concrete members*, University of Illinois at Urbana Champaign

Hoshikuma J, Kawashima K., Nagaya K and Taylor (1997), “Stress-Strain Model for Confined Reinforced Concrete in Bridge Piers”, *Journal of the Structural Division, ASCE*, Vol. 123, No 5, pp 624-633

Ibarra L.F., Medina R.A. and Krawinkler H. (2005),”Hysteretic Model That Incorporate Strength and Stiffness Deterioration” *Earthquake Engineering and Structural Dynamics,* Vol. 34, pp 1489-1511

Kakuta Y., Okamura H. and Kohno M. (1982), "New Concepts for Concrete Fatigue Design Procedures in Japan" *IABSE Colloquium of Fatigue of Steel and Concrete Structures*, Lausanne, pp 51–58

Kent D.C. and Park R. (1971), "Flexural Members with Confined Concrete", *Journal of Structural Division*, ASCE, Vol. 97 No 7, pp1969-1990

Khashaee P. (2005), "Damage-Based Seismic Design of Structures", *Earthquake Spectra,* Vol.21, No.2, pp 371-387

Kim T.H., Lee K.M., Chung Y.S. and Shin H.M. (2005), "Seismic Damage Assessment of Reinforced Concrete Bridge Columns", *Engineering Structures,* Vol. 27, No. 4, pp 576-592

King J.W.H. (1946), "The Effect of Transverse Reinforcement in Reinforced Concrete Columns", *The Structural Engineer* (London), Vol. 24, No. 7, pp 355-388

Kinugasa H., Xiao Y., and Martirossyan A. (2006), "Modeling of Stress-Strain Relationship and Deformability for Confined High-Strength Concrete", *ACI Special Publication 238,* pp 111-126

Kuang J.S. and Atanda A.I. (2005a), "Enhancing the Ductility of Reinforced Concrete Frame Buildings", *Journal of Structures and Buildings, ICE,* Vol. 158, No.4, pp 253-265

Kuang J.S. and Atanda A.I. (2005b), "Predicting the Ductility Demands on Reinforced Concrete Moment Resisting Frames for Moderate Seismicity", *Journal of the Structural Design of Tall and Special Buildings*, Vol.14, No.4, pp 369-378

Kuang J. S. and Wong H. F. (2001), *Enhancing the Ductility of Non-Seismically Detailed Reinforced Concrete Columns.* Research Report, Department of Civil Engineering, Hong Kong University of Science & Technology

Kuang J.S. and Wong H.F. (2005), “Ductility Enhancement of Non-Seismically Designed Reinforced Concrete Columns for Low to Moderate Seismicity”, *Journal of Structures and Buildings, ICE,* Vol. 158, No.1, pp 13-20

Kunnath S.K. and Jenne C. (1994), “Seismic Damage Assessment of Inelastic RC Structures”, *Proceeding of 5th U.S. National Conference on Earthquake Engineering*, EERI, Oakland, CA, Vol. 1, pp55-64

Kunnath S.K., El-Bahy A., Taylor A.W. and Stone W.C. (1997), *Cumulative Seismic Damage of Reinforced Concrete Bridge Piers*, NISTIR 6075, National Institute of Standards and Technology, 133 pages

Kwan A. K. H. (2006), *Concrete Code Handbook – An Explanatory Handbook to the Code of Practice for Structural Use of Concrete 2004, Structural Division, Hong Kong Institution of Engineers, Hong Kong*

Kwan A.K.H., Chau S.L., and Au F.T.K. (2006), "Design of High-Strength Concrete Beams Subjected to Small Axial Loads." *Magazine of Concrete Research*, Vol. 58 No. 6, pp333-341

Lam S.S.E, Xu Y.L., Chau K.T., Wong Y.L. and Ko J.M. (2002), Progress in

Earthquake Resistant Design of Buildings in Hong Kong, *Structural Engineering World Congress (SEWC 2002)*, Oct 9-12, 2002, Yokohama, Japan.

Lam S.S.E., Wu B., Wong Y.L., Wang Z.Y., Liu Z.Q. and Li C.S. (2003), "Drift Capacity of Rectangular Reinforced Concrete Columns with Low Lateral Confinement", *ASCE, Journal of Structural Engineering*, Vol. 129, No. 6, pp 733-742

Lam S.S.E., Wu B., Liu Z.Q. and Wong Y.L., "Experimental Study on Seismic Performance of Non-Ductile Coupling Beams", *Structural Engineering and Mechanics*, Vol. 28, No.3, pp 317-334, 2008

Lau W.C. (1999), "*Strength of Axially Loaded Reinforced Concrete Column*", BEng Thesis, Department of Civil and Structural Engineering, The Hong Kong Polytechnic University

Lee C.F., Ding Y.Z., Huanng R.H., Yu Y.B., Guo G.A., Chen P.L. and Huanng X.H. (1996), *Seismic Hazard Analysis of the Hong Kong Region*, GEO Report No. 65, Geotechnical Engineering Office, Civil Engineering Department, HKSAR

Legeron F. and Paultre P (2003), "Uniaxial Confinement Model for Normal and High Strength Concrete Columns", *Journal of Structural Engineering, ASCE*, Vol. 129, No 2, pp241-252

Lehman D.E. and Moehle J.P. (2000), *Seismic Performance of Well Confined Concrete Bridge Columns*, Pacific Earthquake Engineering Research Center, PEER 1998/01, December

Li C.S., Lam S.S.E., Zhang M.Z. and Wong Y.L. (2006), "Shaking Table Test of a 1:20 Scale High-Rise Building with Transfer Plate System", *ASCE, Journal of Structural Engineering*, Vol. 132, No. 11, pp 1732-1744

Li C.S., Lam S. S.E., Chen A. and Wong Y.L. (2008), "Seismic Performance of a Transfer Plate Structure", *ASCE, Journal of Structural Engineering*, Vol. 134, No.11, pp 1705-1716

Lynn A.C., Moehle J.P., Mahin S.A. and Holmes W.T. (1996), "Seismic Evaluation of Existing Reinforced Concrete Building Columns", *Earthquake Spectra,* Vol. 12, No. 4, November, pp715-739

Mander J.B., Priestley M. J. N., and Park R. (1988), "Theoretical Stress – Strain Behaviour of Confined Concrete," *ASCE Journal of Structural Engineering*, Vol. 114, No. 8, pp 1804-1826 and "Observed Stress – Strain Behaviour of Confined Concrete", *ASCE Journal of Structural Engineering*, Vol. 114, No. 8, pp 1827-1849

Mander J.B., Panthaki F.D. and Kasalanati K. (1994), "Low-Cycle Fatigue Behaviour of Reinforcing Steel", *Journal of Materials in Civil Engineering,* ASCE, Vol. 6, No. 4, pp 453-468

Mandis P.A., Kovacic D., and Setunge S. (2000), "Basis for the Design of Transverse Reinforcement for High-Strength Concrete Columns", *Structural Engineering and Mechanics,* Vol. 9, No 6, 2000, pp 589-600

Meyer C., Roufaiel M.S.L. and Arzoumanidis S. G. (1983), “Analysis of Damaged Concrete Frames for Cyclic Loads”, *International Journal of Earthquake Engineering and Structural Dynamic*, Vol. 11 No. 3, pp 207-228

Miner M.A. (1945), “Cumulative Damage in Fatigue”, *Journal of Applied Mechanics*, Vol. 12, pp 159-164

Neveille A.M., (1987), *Properties of Concrete,* Addison Wesley Longman Limited

NZS 3101: Part 1: 1995 (1995), *Concrete Structures Standards,* Standards New Zealand

Pam H.J. and Ho J.C.M. (2001), "Flexural Strength Enhancement of Confined Reinforced Concrete Columns" *Structures and Buildings*, Proceedings of the Institution of Civil Engineers, Vol. 146, No.4, pp 363-370

Pam H.J., Kwan A.K.H., and Islam M.S. (2001a), "Flexural Strength and Ductility of Reinforced Normal- and High-Strength Concrete Beams" *Structures and Buildings*, Proceedings of the Institution of Civil Engineers, Vol. 146, No.4, pp381-389

Pam H.J., Kwan A.K.H., and Ho J.C.M. (2001b) "Post-peak behavior and flexural ductility of doubly reinforced normal- and high-strength concrete beams" *Structural Engineering and Mechanics*, Vol. 12, No. 5, pp 459-474

Pam H.J. and Ho J.C.M., "Flexural Strength Enhancement of Confined High-strength Reinforced Concrete Columns", *Proceedings of the Structural Engineers World Congress (SEWC2002)*, 9-12 Oct 2002, Yokohama, Japan, paper no. P3-5-4, 8pp (full manuscript published in CD Rom and abstract published in pp 363)

Park R. (1975), *Reinforced Concrete Structures,* Wiley Interscience

Park R. and Paulay T. (1990), "Use of Interlocking Spirals for Transverse Reinforcement in Bridge Columns", *Strength and Ductility of Concrete Substructures of Bridges,* PRU (Road Research Unit) Bulletin 84, Vol. 1, 1990, pp 77-92

Park R., Priestley M.J.N. and Gill W.D. (1982), "Ductility of Square-Confined Concrete Columns", *ASCE, Journal of Structural Division,* Vol. 108, No. 4, pp 929-950

Park Y.J. and Ang A. H.S. (1985), "Mechanistic Seismic Damage Model for Reinforced Concrete", *Journal of Structural Engineering,* Vol. 111, No. 4, pp 722-739

Paulay T. and Priestley M.J.N. (1992), *Seismic design of Reinforced Concrete and Masonry Buildings,* Wiley Interscience

Phan V., Saiidi M.S., Anderson J. and Ghasemi H. (2007), "Near-Fault Ground Motion Effects on Reinforced Concrete Bridge Columns", *Journal of Structural Engineering,* Vol. 133, No 7, pp 982-989

Palermo D. and Vecchio F.J. (2007), "Simulation of Cyclically Loaded Concrete Structures Based on the Finite-Element Method", *Journal of Structural Engineering*, Vol. 133, No. 5, pp 728-738

Popovics S. (1973), "A Review of Stress-Strain Relationships for Concrete", *ACI Journal*, Vol. 67, No 3, pp 243-248

Priestley M.J.N. and Park R. (1987), “Strength and Ductility of Concrete Bridge Columns under Seismic Loading”, *ACI Structural Journal*, Vol. 84, No. 1, pp 61-76

Priestley M.J.N. (1996), *Seismic Design and Retrofit of Bridges***,** John Wiley

Priestley M.J.N., Verma R. and Xiao Y. (1994), “Seismic Shear Strength of RC Columns”, *Journal of Structural Engineering*, Vol. 120, No. 8, pp 2310-2329

Pujol S., Sözen M. and Ramirez J. (2000), “Transverse Reinforcement for Columns of RC Frames to Resist Earthquakes”, *Journal of Structural Engineering,* Vol. 126, No. 4, pp 461-466

Richart F. E, Brandtzaeg A. And Brown R.L. (1928), *A study of the Failure of Concrete Under Combined Compressive Stress*, University of Illinois Engineering Experimental Station, Bulletin No. 185

Roufaiel M.S.L. and Meyer C. (1983), *Analysis of damaged concrete frame buildings*, *Report No. NSF-CEE81-21359-1*, Department of Civil Engineering and Engineering Mechanics, Columbia University, New York

Ranf R.T., Nelson J.M., Price Z., Eberhard M.O., Stanton J.F. (2006), *Damage Accumulation in Lightly Confined Reinforced Concrete Bridge Columns,* Pacific Earthquake Engineering Research Center, PEER 2005/08

Razvi S.R. and Saatcioglu M. (1999), “Analysis and Design of Concrete Columns for Confinement”, *Earthquake Spectra*, Vol. 15 No 4, November, pp 791-811

Razvi S.R. and Saatcioglu M. (1999), "Stress-Strain Relationship for Confined High-Strength Concrete," *ASCE Journal of Structural Engineering*, Vol. 125, No.3, pp.

281-289

Rossetto T. and Elnanshai A. (2003), "Derivation of Vulnerability Function for European-Type RC Structural Based on Observation Data", *Engineering Structures*, Vol. 25, No 10, pp 1241-1263

Saatcioglu M. And Ozcebe G. (1989), "Response of Reinforced Concrete Columns to Simulated Seismic Loading," *ACI Journal*, Vol. 86, No. 1, pp 3-12

Saatcioglu M., and Razvi S.R. (1992), "Strength and Ductility of Confined Concrete", *Journal of the Structural Division, ASCE,* Vol. 118, No. 6, pp 1590-1607

Saatcioglu M. And Razvi S.R. (2002), "Displacement –Based Design of Reinforced Concrete Columns for Confinement", *ACI Structural Journal,* Vol. 99, No. 2 pp 3-11

Sakai K. and Sheikh S.A. (1989), "What Do We Know about Confinement in Reinforced Concrete Column?" (A Critical Review of Previous Work and Code Provision), *ACI Structural Journal*, Vol. 86, No.2, pp 192-207

Saiidi M. (1982), "Hysteresis Models for Reinforced Concrete", *Journal of the Structural Division, ASCE,* Vol. 108, No. 5, pp1077-1087

Sargin M., Ghosh S.K. and Handa V.K. (1971), "Effects of Lateral Reinforcement Upon the Strength and Deformation Properties of Concrete", Magazine of Concrete Research, Vol. 23, No. 75, pp 99

Scott B.D., Park R. And Priestley M.J.N. (1982), "Stress-Strain Behavior of Concrete Confined by Overlapping Hoops at Low and High Strain Rates", *ACI Journal*, Vol. 79, No. 1, pp13-27

Sezen H. (2000) *Evaluation and Testing of Existing Reinforced Concrete Columns*, *CE 299 Report*, Department of Civil and Environmental Engineering, UC Berkeley

Sezen H. and Moehle J.P. (2004), "Shear Strength Model for Lightly Reinforced Concrete Columns", *Journal of Structural Engineering,* Vol. 130, No.11, pp1692-1703

Skeikh S.A. and Khoury S.S. (1993), "Confined Concrete Columns with Stubs", *ACI Structural Journal,* Vol. 90, No. 4, pp 414-431

Skeikh S.A., Shah D.V. and Khoury S.S. (1994), "Confinement of High Strength Concrete Columns" , *ACI Structural Journal*, Vol. 91, No. 1, pp 100-111

Skeikh S.A. and Khoury S.S. (1997), "A Performance-Based Approach for the Design of Configuration Steel in Tied Columns", *ACI Structural Journal*, Vol. 94, No. 4, pp 421-431

Skeikh S.A. and Yeh C.C. (1990), "Tied Concrete Columns under Axial Load and Flexure", *ASCE, Journal of Structural Engineering,* Vol. 116, No. 10, pp 2780-2800

Sheikh S.A. and Uzumeri S.M. (1982), "Analytical Model for Concrete Confinement in Tied Columns", *ASCE*, *Journal of Structural Engineering,* Vol. 108, No. 12, pp 2703-2722

Soesianawati M.T., Park R. and Priestley M.J.N. (1986), *Limited Ductility Design of Reinforced Concrete Columns*, *Report 86-10,*Department of Civil

Engineering, University of Canterbury, Christchurch, New Zealand, March 1986, 208pages

Su R.K.L., Lam N.T.K. and Tsang H.H. (2008), "Seismic Drift Demand and Capacity of Non-seismically Designed Buildings in Hong Kong", *Electronic Journal of Structural Engineering*, Vol. 8, pp110-120

Su R.K.L. (2008), "Seismic Behaviour of Buildings with Transfer Structures in Low-to-Moderate Seismicity Regions", *Electronic Journal of Structural Engineering*, Vol. 8, p 99-109

Takeda T. and Sozen M.A. and Nielsen N.N. (1970),"Reinforced Concrete Response to Simulated Earthquakes", *Journal of the Structural Division, ASCE,* Vol. 96, pp 2557-2573

Tanka H. and Prak R. (1990), *Effect of Lateral Confining Reinforcement on the Ductility Behaviour of Reinforced Concrete Columns, Report 90-2*, Department of Civil Engineering, University of Canterbury, June 1990, 458 pages

Tassio T.P. (1998), "Modelling for Design", *Modelling and Analysis of Reinforced Concrete Structures for Dynamic Loading,* pp 137-172

UGCS webpage http://earthquake.usgs.gov/

Umbehara H. and Jirsa J.O. (1982), "Shear Strength and Deterioration of Short Reinforced Concrete Columns under Cyclic Deformations", *PMFSEL Report No 82-3,* Department of Civil Engineering, University of Texas at Austin, Austin, Texas, July 1982, 256 pages

Umemura H., Sakai Y. Minami T. and Kabeyasawa T. (1998), "Modelling of Reinforced Concrete Member Hysteresis Characteristics Considering Strength Degradation Caused by Cyclic Loading", *Transactions of the Japan Concrete Institute*, Vol. 20, pp 137-142

Vintzileou E. and Stathatos A. (2007), "Assessment of the Seismic Behaviour of RC Columns", *Engineering Structures*, Vol. 29, pp 1296-1311

Wehbe N.I., Saiidi M.S. and Sanders D.H. (1999), "Seismic Performance of Rectangular Bridge Columns with Moderate Confinement", *ACI Structural* Journal, Vol. 96, No. 2, pp 248-259

Wong Y.L., Zhao J.X., Chau K.T. and Lee C.M. (1998a), "Assessment of Seismicity Model for Hong Kong Region", *HKIE Transactions*, Vol. 5(1), *pp50-62*

Wong Y.L., Zhao J.X., Lam S.E.E. and Chau K.T. (1998b), "Assessing Seismic Response of Soft Soil Sites in Hong Kong Using Microtremor Records", *HKIE Transactions*, Vol. 5(3), *pp70-79*

William K.J. and Warnke E.P. (1975), "Constitutive Model for the Triaxial Behavior of Concrete", *International Association Bridge Structural Engineering Proceeding*, Vol. 19, pp. 1-30

Xiao J. and Zhang C. (2008), "Seismic Behaviour of RC Columns with Circular, Square and Diamond Sections", *Construction and Building Materials*, Vol. 22, No. 5, pp 801-810

Xiong Z. (2001), *Reinforced Concrete Behaviour under Cyclic Loading*, PhD Thesis, The University of Hong Kong, 317 pages

Zhu Y., Zhou Y. and Su R.K.L. (2009), "Experimental Study of Strengthened RC Coupling Beams for Earthquake Resistance", *Sichuan Building Science*, Vol. 35, No. 3, pp 59-64

Zhu Y. and Su R.K.L. (2008), "Displacement Based Seismic Assessment and Design for Buildings in Low-to-Moderate Seismicity Regions", *Proceedings of the tenth International Symposium on Structural Engineering for Young Experts*, (1 & 2), Oct 19-21, 2008, Hunan University, Changsha, PRC, pp 1929-1934